Studies of hydroxybutyrate oligomers crystallization behaviour

Thesis

UNRESTRICTED

Studies of Hydroxybutyrate Oligomers Crystallization Behaviour

by

Junhui Li, B.Eng

A thesis submitted in partial fulfillment of the University's requirements

for the degree of Doctor of Philosophy

Faculty of Technology

The Open University

July 2005

DATE OF SUBMISSION 16 MAY 2005

DATE OF AWARD 01 AUGUST 2005

Abstract

Monodisperse long chain oligomers such as n-alkanes provide excellent model systems for fundamental studies of polymer crystallization and annealing. Previous studies revealed important results, including a preference for discrete crystal thicknesses corresponding to integer folded chain forms, minima in growth and nucleation rates as the system changes from one chain conformation to another, and clear unfolding transitions during melting.

The work presented here extends previous studies to oligomers of hydroxybutyrate (OHB), which serve as models for the polymer poly(3-R-hydroxybutyrate) (PHB). A range of exact length hydroxybutyrate oligomers have been synthesized and their crystallization behaviour and morphology studied using optical and electron microscopy, together with small and wide angle X-ray scattering, including dynamic measurements at the ESRF Grenoble.

The oligomers form crystals from dilute solution and from the melt, exhibiting similar overall morphologies and structure to PHB. Growth rate data for HB 24-mer and 32-mer spherulites grown from the melt and crystallization rate data from solution reveal discontinuities in the rate gradient which can be linked to changes in chain conformation. These features could arise from a 'self-poisoning' effect previously postulated for the growth minima in long n-alkanes. Crystals grown at the lower temperatures contain folded chains, which transform during heating through a process of partial melting/dissolution and re-crystallization to form extended chain crystals. These unfolding transitions were accompanied by changes in crystallinity and lattice parameter. Crystals grown at higher temperatures contain extended chains that do not rearrange further.

Preferred crystal thicknesses are those which result in relatively high proportions of chain ends in the surface. For the 24-mer, they correspond to the extended chain length (E), and to E/2, 2/3E, 3/4E and 5/6E. This wide range of thicknesses is in contrast to results from long n-alkanes, possibly due to hydrogen bonding between chain ends, which effectively links chains together into longer units.

The current work reveals a great deal about the way in which HB oligomer chains fold and how they re-arrange themselves from one folded form to another which, combined with previous results on PHB, will contribute towards a more complete view of the whole polymer crystallization process.

Acknowledgements

I will not ever be able to express enough appreciation to my internal advisor Dr Sally Organ from the Open University. Her generosity with ideas, time, responsibility, enthusiasm, patience, care and supervision, has been incredible to me during these three years. Sally has always been extremely supportive on all aspects of this work. She has also influenced me strongly with her own research interests throughout this project. Also, my special thanks go to her whole family:- John, Cathlyn and Evan for all the happy time we spent together.

I would like particularly to give my huge thanks to Dr Peter Barham. As my external advisor from the University of Bristol, he has been outstandingly inspiring, supportive and generous with sparkling ideas and advice. I wouldn't finish my work on time without his supervision and encouragement.

My special thanks go to Professor Dieter Seebach, Dr Matthias Albert and the whole Organic Chemistry group at ETH in Zurich for providing me with the HB oligomer materials and also for training me to be familiar with the synthesis process at the very beginning of this project in February 2002. I also thank Professor Tim Gallagher at Chemistry Dept. from University of Bristol for always welcoming me to use the facilities in his group to complete my own synthesis reactions.

I also wish to thank Dr Jamie Hobbs and Dr Ann Terry for their constant discussions and advice on some of the AFM and X-ray experiments, also the data processing thereafter. I really appreciate their extremely creative suggestions and all kinds of help. Thanks for all the support, advice and all the work we have done together at the ESRF, Grenoble.

Thanks are also addressed to Professor Rob Richardson, Dr Kevin Jack and Dr Cecile Dreiss for training me in using the SAXS machine in the Department of Chemistry in Bristol. I also thank Dr Mary Hill and Mr Jerry Hart for their help on the electron microscope. Mrs Anna Halter in the polymer group has provided relentless help and technical support throughout my three years, thanks. I would also like to thank the

whole Physics Department in Bristol University where I have happily spent a few years. All the people here are remarkably friendly and supportive to me.

I am grateful for the general guidance and suggestions from Professor Nick Braithwaite at the Faculty of Technology of the Open University. The friendly staff at the Research School of OU are also acknowledged. I also wish to thank the Open University and the EPSRC for financial support all through my studies.

Finally, a huge 'thank-you' goes to my husband, and all my family in China, for their endless encouragement, support, care and love.

Author's Declaration

This thesis is submitted to the Open University as a requirement for admission to the degree of Doctor of Philosophy. The work described in this thesis was carried out under the joint supervision of Dr S.J. Organ (the Open University) and Dr P.J. Barham (University of Bristol) at the H. H. Wills Physics Laboratory, University of Bristol between October 2001 and March 2005.

No part of the work in this thesis has been submitted previously to this or any other university for the award of a degree. All of the work described here is solely the result of my own research except where otherwise stated in the text.

Junhui Li

Department of Materials Engineering

Faculty of Technology

The Open University

July 2005

Table of Contents

Chapter 1 Introduction

1.1 Introduction

The main objective of this work is to gain a better understanding of the crystallization behaviour, in particular the chain folding, crystal growth and morphological changes at certain crystallization conditions, in hydroxybutyrate (HB) oligomers with up to 96 repeat units both from melt and solution crystallization.

The HB oligomer, in short OHB, is the short chain analogue of the polymer – poly(3-R-hydroxybutyrate), in short PHB. A good knowledge of PHB would be beneficial to the study of the crystallization behaviour of OHB. The following sections provide some background information on the production, history and physical properties of this polymer. An overview of the structure of the thesis and contents of each chapter is given at the end of chapter 1.

1.2 Introduction to PHB – An Environmental Biological Degradable Plastic

Concerns over environmental protection and natural resources conservation make it necessary to reduce our reliance on oil based products and at the same time improve the safe disposal of domestic wastes, in particular, commodity plastics. Polyolefins and polyesters are the traditionally used plastics. They are oil based, very difficult to recycle, and take a very long time to degrade in the environment. However, naturally occurring materials have emerged as better alternatives that could be used to replace these oil based materials in many applications. One of the leading candidate materials is a group of polymers known as poly(hydroxyalkanoates), PHAs. The most commonly found member of the PHA family is poly(3-R-hydroxybutyrate), P(3-HB), and its co-polymers with 3-R-hydroxyvalerate P(3-HB/3-HV) [Holmes, 1985 and 1987].

Poly(3-R-hydroxybutyrate), P(3-HB), is produced by a number of bacteria as an energy storage material [Doi, 1990]. It plays a similar role to mammalian fat. When

the bacteria are starved of some essential nutrient, such as nitrogen, oxygen, phosphorous or sulphur, they accumulate carbon within their cells in discrete granules of P(3-HB), which can be broken down at a later stage [Holmes, 1987]. P(3-HB) was first described by Lemoigne in 1925 [Lemoigne, 1925], who later isolated and identified the material from Bacillus megaterium [Lemoigne, 1927]. Since then, P(3-HB) has been identified in a large number of different micro-organisms [Doi, 1990; Brandl *et al.*, 1991]. Figure 1.1 shows the chemical structures of PHAs and P(3-HB). For simplification, the polymer P(3-HB) and oligomer 3-HB synthesized by the starting materials from direct degradation of P(3-HB) in this work are referred to as PHB and HB respectively in the whole thesis.

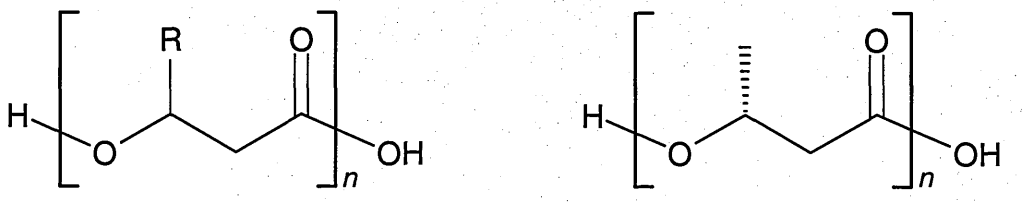

(a) (b)

Figure1.1 Chemical structure of (a) poly(hydroxyalkanoates), PHAs. 'R' group varies from methyl (C_1) to tridecyl (C_{13}); (b) poly(3-R-hydroxybutyrate), P(3-HB).

PHB homopolymer is a semi-crystalline thermoplastic material, i.e. it is a resin that becomes highly viscous and mouldable at temperature close to or above the melting point. In general its properties are similar to those of polypropylene, as both polymers have similar melting points, degrees of crystallinity and glass transition temperatures. As PHB is produced by bacterial fermentation, its advantage is that, on disposal, it will degrade in the environment back to water and carbon dioxide without leaving toxic by-products [Barak *et al.*, 1991; Gilmore, 1992; Krupp and Jewell, 1992]. A breakthrough in the potential commercialization of PHB was the development of a family of copolyesters by Imperial Chemical Industries (ICI) [Holmes *et al.*, 1981 and 1985]. These random copolymers, referred to as PHB/HV, were developed based on 3-hydroxybutyric and 3-hydroxyvaleric acids. Their properties could be tailored to fit a wide range of material needs with improved mechanical properties over the PHB homopolymer. Systems already exist to produce the polymer in bulk quantities. Zeneca, the pharmaceutical off-shoot of ICI, manufactured PHB along with its

copolymer polyhydroxyvalerate (PHV), known as BIOPOL™ on a commercial scale for almost twenty years by bacterial fermentation [King, 1982; Lafferty, 1988]. In 1996, Zeneca sold the BIOPOL™ business to the American company Monsanto, who carried out some work on producing PHB in plants through genetic engineering.

Besides the use as a biodegradable plastic for mass consumers, PHB is also discussed as a substitute for implants in reconstructive surgery or as a biologically degradable drug carrier that would slowly release medicines in the body at the exact certain point where they are required [Holland *et al.*, 1987]. PHB could be used for bone-implants, and it has been shown that such an implant actually stimulates natural bone growth [Knowles *et al.*, 1991]. Other possible medical applications of PHAs/PHB may be surgical swabs and sutures, wound dressing, as lubricant for surgeon's gloves or as artificial vascular grafts and blood vessels acting as temporary scaffolds for new tissue growth.

Another interesting aspect of PHB is its ubiquitous nature: Hydryxobutyrate (HB) oligomers have been found in trace amounts in every cell that has been studied carefully enough to detect such quantities [Reusch *et al.*, 1989 and 1992]. The precise function of HB within the living cell is still unclear, although many speculations have already been made. These include the suggestion that OHB could act as a channel for DNA or for ions in the lipid membranes of the cell [Reusch and Sadoff, 1988]. Reusch *et al.* even claim that PHB could be as important as proteins for living cells [Reusch, 1995 and 1996]. More details of the HB oligomers will be presented in chapter 3.

There are many extensive reviews on PHB in the open literatures, such as Holmes (1987), Doi (1990), Liggat (1996), Sykes (1996) and Sudesh (2000) etc.

1.3 Physical Properties of PHB

PHB is a semi-crystalline polymer with a glass transition temperature of ~0°C and an equilibrium melting temperature of ~195°C [Barham *et al.*, 1984]. There is a wide variation in melting temperature with the molecular weight. Molecular weights (M_w)

below 200,000 give an equilibrium melting point of 180–185°C, which could rapidly rise to a value of ~195°C on increasing the molecular weight [Organ and Barham, 1993]. The heat of fusion of PHB crystals is $146Jg^{-1}$ [Barham *et al.*, 1984]. The bacterial origins and solvent-based extraction procedures involved in the production of PHB result in a very pure polymer. Unlike conventional thermoplastics, there are no catalyst residues present. As a consequence of this purity, the level of heterogeneous nuclei present in PHB is very low. Due to its uncommon stereo-regularity, PHB can reach a relatively high level of crystallinity, even at high supercoolings, typically from 65% to 80%. The crystal lamellae are typically ~5 nm thick, and can reach ~10 nm thick even at low supercoolings. Thus, PHB is a very interesting material for studies of polymer crystallization. Table 1.1 lists some of the important physical properties of PHB.

Some Physical Properties of PHB		
Melting temperature, T_m (°C)	~ 180	[Ellar *et al.*, 1968]
Glass transition temperature, T_g (°C)	~ 0	[Barham *et al.*, 1984]
Crystallinity (%)	60 – 90	[Holmes, 1982]
Density (g cm^{-3})	1.23 – 1.25	[Okamura *et al.*, 1967]
Water uptake (w_t%)	0.2	[Barham and Keller, 1986]
Extension to break (%)	6	[Holmes, 1982]
Young's modulus (GPa)	3.5 – 4	[Otun, 1985]
Tensile strength (MPa)	~ 40	[Otun, 1985]

Table 1.1 Some physical properties of PHB.

1.3.1 Crystallographic structure

The crystal structure of PHB was first studied in the late sixties and early seventies in last century [Okamura and Marchessault, 1967]. It was later refined by X-ray diffraction [Yokouchi *et al.*, 1973; Brückner *et al.*, 1988] and molecular modelling [Cornibert and Marchessault, 1972]. On crystallization PHB adopts a compact 2_1 left-handed helical conformation in the crystalline state [Cornibert and Marchessault, 1972]. Figure 1.2 shows the crystallographic structure of PHB. The unit cell of PHB

is orthorhombic with dimensions of a=0.576 nm, b=1.32 nm, c=0.596 nm (fibre axis). The lattice contains two left-handed helical molecules in anti-parallel orientation, with the oxygen atoms of the carbonyl groups located nearly at the same level [Yokouchi *et al.*, 1973].

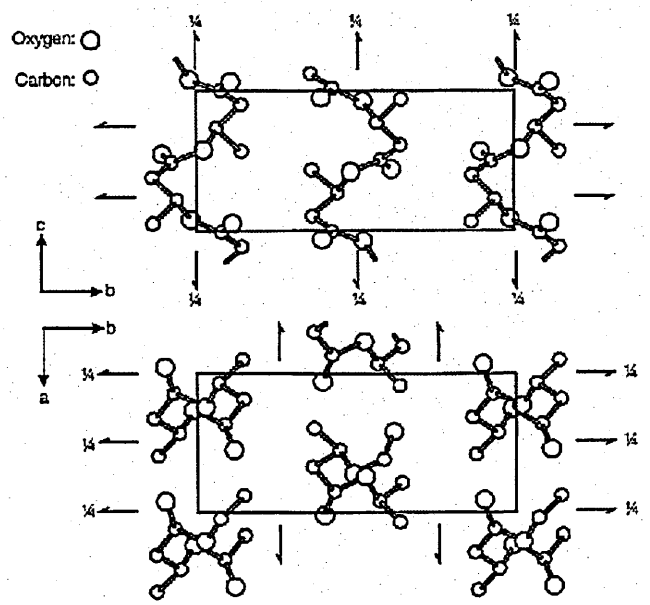

Figure 1.2 Unit cell of PHB, a=0.576 nm, b=1.32 nm, c=0.596 nm (fibre axis), after Cornibert and Marchessault, 1972 and Yokouchi, 1973.

1.3.2 Crystal morphology and growth of PHB

1.3.2.1 Spherulitic crystals grown from the melt

PHB crystallizes from the melt commonly to form banded spherulites, the morphology, growth and nucleation of which have been extensively studied [Barham *et al.*, 1984; Barham, 1984; Black *et al.*, 1990; Organ *et al.*, 1991; Akhtar, *et al.*, 1992]. The nucleation is generally homogeneous. In cells PHB does not appear to nucleate at all [de Koning *et al.*, 1992], as there are very few impurities due to its natural origin. After it is extracted, it is still difficult to nucleate even when impurities are deliberately added [Organ and Barham, 1991]. Nucleation is also random and rare, which allows crystallization to be performed at very high supercoolings. Low level of nucleation also leads to exceptionally large spherulites, sometimes up to several millimetres, which makes it ideal for morphological study. Crystal growth rates have

been obtained over a range of more than 100°C, covering both sides of the growth rate curve [Barham *et al.*, 1984; Otun, 1985; Hobbs, 1996; Hobbs *et al.*, 2000]. Nucleation rates have also been obtained over a similar range of temperatures [Organ *et al.*, 1991]. More details of the growth rates and spherulite morphology of HB oligomers grown from the melt will be reported in chapter 4.

1.3.2.2 Single crystals grown from solution

On crystallization from dilute solution, like most other polymers, PHB can form micron-sized chain-folded lamellar single crystals. These crystals are generally lath shaped, as shown in Figure 1.3. PHB single crystals are relatively thin compared to those grown in other polymer systems, with a typical thickness between 4–6 nm (depending on annealing or crystallization temperatures) as measured from small angle X-ray diffraction and other methods [Barham *et al.*, 1984; Sykes, 1996]. An electron diffraction pattern on a selected area within a PHB single crystal grown from dilute propylene carbonate solution is also given in Figure 1.3. This electron diffraction pattern corresponds to the *a* and *b* lattice dimensions of a PHB single crystal, suggesting the helix axis *c*, is perpendicular to the crystal surface [Barham *et al.*, 1984]. This indexing is consistent with the orthorhombic unit cell already characterized by X-ray diffraction analysis, and also confirms that the 'up' and 'down' anti-parallel chains are contiguous in the PHB unit cell [Birley, *et al.*, 1995].

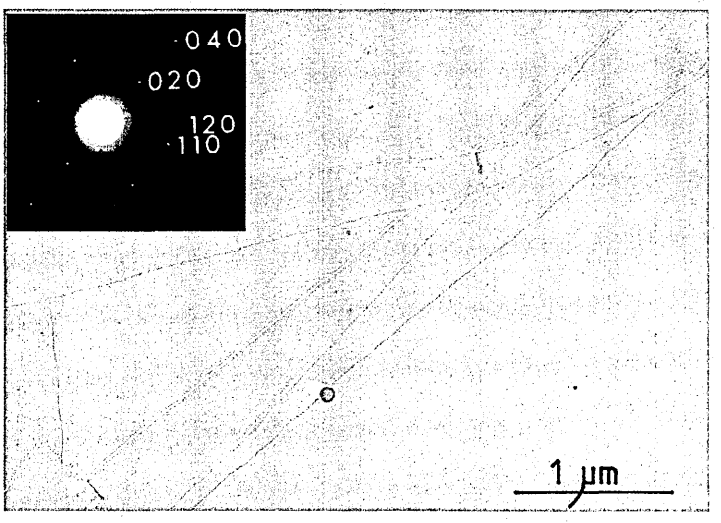

Figure 1.3 Electron micrograph of PHB single crystals grown from propylene carbonate at 69°C, together with the selected area diffraction pattern [from Otun, 1985].

The *c* axis value of the unit cell corresponds to the molecular length of helical PHB dimer in the unit cell, which is 0.596 nm. The chains fold parallel to the *a* axis of the schematic folded chain, given in Figure 1.4. This regular folding is called 'adjacent re-entry' after Keller 1957, and has been demonstrated by electron microscopy observation of fractured single crystals [Barham *et al.*, 1984]. On the basis of the orthorhombic unit cell, it is apparent that the fold must 'zig-zag' backwards and forwards, alternately, approximately +45° and –45° to the *a* axis. This is also in keeping with the $P2_12_12_1$ space group which requires two 'anti-parallel' chains per unit cell, and requires description of chain-folding in terms of an 'average chain-folding' plane parallel to the *a* axis. The schematic drawing is shown in Figure 1.5, and illustrates this morphological feature [Birley *et al.*, 1995] which implies tight folding and allows for 80% or more crystallinity in the single crystals. This chain-folding was first suggested by Holmes [1987].

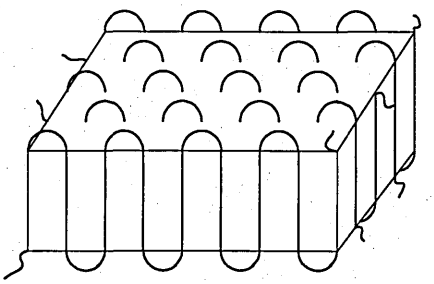

Figure 1.4 Schematic drawing of PHB folded chain lamellar crystal. The *a* axis of the unit cell is parallel to the horizontal direction.

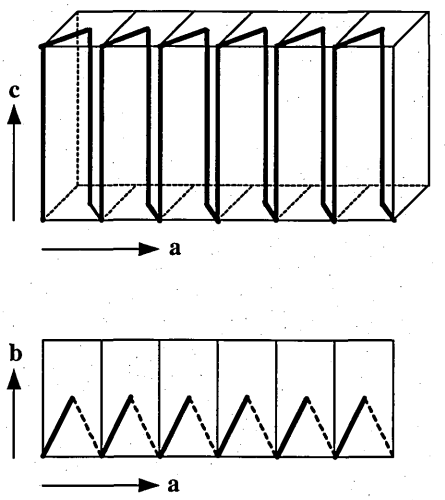

Figure 1.5 Schematic diagram showing the zig-zag conformation of the folds direction within PHB is along the [100] direction, while successive folds are in the [110] and [1$\bar{1}$0] directions [from Birley, 1995].

1.3.3 Mechanical properties

1.3.3.1 Ageing of PHB

In early studies on PHB [Barham *et al.*, 1986], it was suggested that the polymer was brittle due to the presence of cracks in the spherulites. These cracks were formed on cooling from the crystallization temperature to room temperature, due to the strain induced by differential thermal expansion [Martinez-Salazar *et al.*, 1989]. Later studies by Hobbs [Hobbs *et al.*, 1996] found that the freshly crystallized PHB is not so brittle. However over a period of 2–3 weeks, the impact strength halves [de Koning, 1992 and 1993] and the extension to break reduces. This is known as mechanical ageing. The effect of ageing can be reduced, and the mechanical properties almost restored to their original values by cold rolling the sample [Barham and Keller, 1986] or thermal treatment, but heat treatment can cause permanent structure change [de Koning and Lemstra, 1992b]. For more discussions on this see other references [e.g. de Koning, 1993].

1.3.3.2 Degradation of PHB

The PHB polymer chains can be hydrolyzed in water, without enzymes, at a very slow rate [Doi *et al.*, 1990]. Unlike enzymatic degradation, water uptake and subsequent chemical hydrolysis occur throughout the whole polymer matrix, giving a general decrease in molecular weight. The hydrolysis process can be very slow and it takes years for any significant change to take place. But it may become quicker in biological environments when PHB may be acting as an implant. Also the rate of hydrolysis can be increased if the polymer is in solution, or in alkaline environment, or at high temperatures [Riis, 1989].

PHB can be completely degraded into harmless and naturally occurring molecules in natural environments. A number of bacteria and fungi can digest PHB [Chowdhury, 1963; Delafield *et al.*, 1965]. More interestingly, some micro-organisms, such as fungi, although incapable of accumulating PHB, can excrete enzymes that degrade PHB. The enzymes are extra-cellular depolymerises that degrade and solubilize the polymer in the vicinity of the cell. The degradation products are then absorbed

through the cell wall and metabolised [Merrick and Doudoroff, 1961; Anderson and Dawes, 1990].

The ester link in polyesters is reactive to alcohols and amines. The reaction with methylamine is selective to amorphous materials and has been used to reveal the morphology of bulk PHB/HV [Organ and Barham, 1989] and of single crystals [Welland *et al.*, 1989]. More work on chemical degradation of PHB has been made previously by Sykes [Sykes, 1996].

Finally PHB is particularly prone to thermal degradation. It melts at ~180°C, but at temperatures ~170°C random chain scission reduces the molecular weight. From 200°C upwards a chain 'unzipping' reaction has been suggested [Grassie *et al.*, 1984 a,b,c; Billingham *et al.*, 1987; Doi *et al.*, 1989 and 1990]. Therefore, the minimum possible melting temperature, and shortest time at high temperatures should be chosen when melting PHB. As for HB short chain oligomers, the melting temperature is about 20°C lower, the thermal degradation is less a problem, but it still occurs to some extent. Hence fresh samples should be used after heating for several times.

1.4 Scope of the Thesis

The aim of this project is to gain a more complete understanding of the crystallization and annealing behaviour for poly(3-R-hydroxybutyrate), by means of studying short chain monodisperse model materials of 3-hydroxybutyrate oligomers (3-HB) with well defined chain lengths produced using a special chemical synthesis strategy.

The work mainly focuses on HB oligomer crystallization studies. This chapter provides a brief introduction to the polymer, PHB. Chapter 2 gives some general information on polymer crystallization and two widely used theoretical models for polymer crystal growth. Chapter 3 summarizes the previous work done in other oligomer systems such as n-alkanes and PEO fractions, which is very relevant to this work. Also included in chapter 3 are the biological functions (other than energy storage) of PHB and HB oligomers found in living cells and the chemical synthesis strategy to produce the entirely monodisperse HB oligomers used all through this

study. All the experimental results found in this project, and associated with detailed discussions, are reported in chapters 4 to 8:

- Chapter 4: a detailed study of the shperulitic morphologies, melt growth rates of HB oligomers with 24 and 32 repeat units.
- Chapter 5: HB oligomer crystallization studies from solution, the single crystal morphologies of HB 24-mer and 32-mer compared to those of the polymer. Measurement of the crystallization rates with HB 32-mer and 24mer by in-situ synchrotron X-rays.
- Chapter 6: comprehensive full sets data of crystal thicknesses with HB oligomers grown from both the melt and solution. Crystal chain conformation models are also proposed.
- Chapter 7: the unfolding transition behaviours followed by real time SAXS and WAXS of melt grown HB oligomer samples.
- Chapter 8: the growth and thickening of solution grown HB oligomer crystals observed in-situ using synchrotron radiation.

The overall conclusions and recommendations for future work are given in the final chapter, chapter 9.

Chapter 2 Polymer Crystallization

Understanding the principles of polymer physics will help in appreciating the experimental results and discussions presented in chapters 4–8 in this thesis. In this chapter some background to polymer physics and polymer crystallization is introduced first, followed by two frequently used theoretical models to interpret the crystal growth and chain folding behaviour. For a more thorough grounding in polymer physics, the reader is referred to a standard textbook, e.g. by Young and Lovell [Young and Lovell, 1991] or Gedde [Gedde, 1995].

2.1 Polymer Physics

2.1.1 What are polymers and oligomers?

Polymers consist of large molecules, i.e. macromolecules. A *polymer* is a substance composed of molecules characterized by the multiple repetition of one or more species of atoms or groups of atoms (constitutional repeating units) linked to each other in amounts sufficient to provide a set of properties that do not vary markedly with the addition of one or a few of the constitutional repeating units [Gedde,1995].

The word *polymer* originates from the Greek words 'poly' meaning many and 'mer' meaning part. The constitutional repeating units, which are also simply called 'repeat units', are linked by covalent bonds. Compared to the polymer, a molecule with only a few repeat units is defined as an *oligomer*. 'Oligo' is also derived from the Greek, meaning few. The polymer molecules can by synthesized from monomers (single units). In the case of polypropylene the monomer is propylene (propene). Similarly in the case of poly(3-R-hydroxybutyrate), PHB, the monomer is 3-hydroxybutyric acid, the model material used throughout this project.

2.1.2 A brief history of polymer science

The first polymers used were all obtained from natural products, e.g., natural rubber from *Hevea* trees, starch and collagen in leather etc. Modification of native polymers

started in the mid-nineteenth century and the first wholly synthetic polymer *Bakelite* made from formaldehyde resins was made at the beginning of the twentieth century. The science of polymers commenced in the 1920s, and the past 70–80 years have seen rapid development of polymer technology. With the advancement of the understanding of the physical and chemical nature of the polymers, the commercial production techniques and the range of the synthetic polymers available increased dramatically.

2.2 Polymer Crystallization

It is widely accepted that polymers can crystallize as thin lamellae with chain folding when grown from dilute solution, as shown by Figure 1.3–1.5 (see chapter 1). For most polymers crystallized from the melt, a crystalline lamella is also the basic morphological unit serving as the basic building block of larger structures, e.g. spherulites, row-structures and trans-crystalline layers. It has been a mystery why polymer chains fold into thin crystals rather than grow thermodynamically more stable thicker ones. The answer lies in that a thin crystal can grow faster than a thick one. This is because the reduction in entropy involved in laying down a short segment of the chain is lower than it would be for a long extended chain. Chain folding is necessary to form a crystalline lamellar morphology, therefore it is considered to be kinetically driven. The schematic drawing in Figure 1.4 is a simplified case of chain folding. The exact nature of the fold surface is far more complicated and is still a subject under continuous research. More information in this area can be found in [Wunderlich, 1976; Keller, 1991; Armitstead and Goldbeck-Wood, 1992; Gedde, 1995 etc].

2.2.1 Single crystals and chain folding

The crystalline nature of some polymers was first recognized in the early part of the twentieth century. X-ray diffraction studies of polymers revealed the existence of both small areas of regular crystal structure and a sizeable fraction of random amorphous material. A 'fringed micelle' model was then proposed, which consists of small crystalline regions with regularly aligned chains, surrounded by an amorphous matrix

[Bunn, 1953]. This model was accepted for many years and was successful in explaining such properties as the variable densities and melting points of crystallized polymers. However with the availability of more chemically and sterically regular polymers which could be crystallized to a much higher extent than previously, some observed structural features could not be easily explained by the traditional fringed micelle model. For example, spherulite crystals were observed in bulk crystallized materials using polarising microscopy [Bunn and Alcock, 1945; Hay and Keller, 1968], and single crystals were recognized from polyethylene crystals grown in dilute solution, with typically very high crystallinities of 80–90% [Till 1957; Keller 1957; Fischer, 1957]. The fringed micelle model struggled to explain the formation of such structures and there was clearly a need for an improved model to explain polymer crystallization.

When Keller [Keller, 1957] investigated thin platelet polyethylene crystals grown from dilute solution, the electron diffraction patterns indicated that the chain direction is perpendicular to the surface of the platelets. Figure 2.1 shows some typical polyethylene single crystals crystallized from dilute solution. Since the molecules were on average about 2,500 nm in length and the platelets were typically 10–20 nm thick, Keller concluded that the molecules must be folding back on themselves many times in order for them to be incorporated in the system. This phenomenon is known as chain folding and is illustrated schematically in Figure 1.4. It is worth pointing out that, although a planar lamella is depicted in this figure, not all crystals grow in this shape. Polyethylene single crystals, for example, can grow in the shape of hollow pyramids, bounded by four (110) faces. Truncating (100) faces may also appear at higher crystallization temperatures. When these crystals are dried down onto a substrate for microscopy, they collapse and often cause pleats or tears in the crystals. The pyramids may collapse to form rhombohedral platelets, while the crystals with truncating (100) faces may appear hexagonal after drying down [Keller and Goldbeck-Wood, 1996].

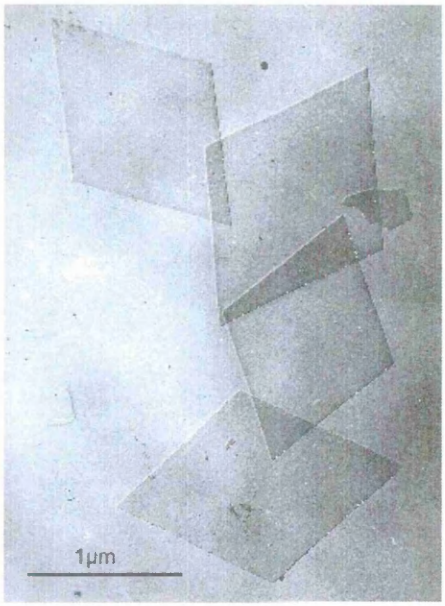

Figure 2.1 Electron micrograph of polyethylene single crystals crystallized from dilute solution (Courtesy of SJ Organ).

When the principles of chain folded crystallization were first introduced, it was assumed that all the folds were regular, like a hair-pin, so that the molecule always re-entered the crystalline lattice at the site adjacent to where it left. This is known as tight adjacent re-entrant folding. Later studies, however, suggested that this was an over simplification. In fact, these folds are often far from sharp. There may be many sections in the chain that are not a part of the crystalline phase, and there is a noticeable amorphous region in the whole system.

It has been controversial whether the chains are always adjacent re-entrant or whether they re-enter into the crystals more randomly, with chains crossing many other chain folds before re-entering the crystal (often referred to as the 'switchboard' model). Now it is widely accepted that polymer crystals will exhibit a mixture of both adjacent re-entrant and switchboard type folds. Sir Charles Frank gave a limit to the number of random re-entries [Frank, 1979]. He used density arguments to limit this to thirty percent, leaving at least seventy percent adjacent re-entries. Figure 2.2 illustrates such a mixture of different chain folding types in a crystal lamella.

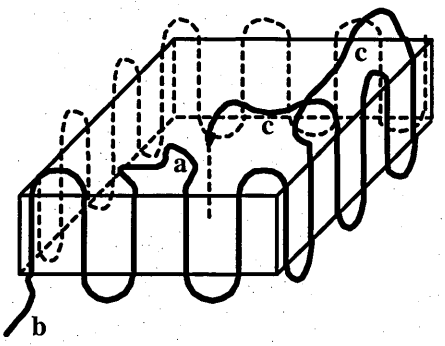

Figure 2.2 Schematic diagram showing a mixture of different types of chain-folding in a polymer crystal lamella. Most of the chains exhibit sharp hairpin folds, while some others do not. Fold marked with ***a*** represents a loose fold, label ***b*** indicates a chain end which is not totally folded into the crystal lamella structure, and ***c*** are non adjacent re-entrant folds (switchboard folds). Only the outermost chains have been drawn here for simplicity, all the folds in this lamella should be extrapolated back to the centre of the crystal.

Evidence for polymer chain folding crystallized from the melt was more difficult to obtain, but it was recognized that folding will be less regular and complete than that in solution grown crystals. Nevertheless small angle X-ray diffraction revealed the existence of a regular periodicity in melt crystallized polymers [Keller and O'Connor, 1957], which reflects a lamellar thickness. As for single crystals, this periodicity increases with crystallization temperature and on annealing [Keller and O'Connor, 1957 and 1958; Fischer and Schmidt, 1962]. This suggests that the underlying structure of solution grown crystals is the same as that of crystals grown from the melt, although neutron scattering studies [Sadler and Keller, 1977] indicated a more random re-entry at the fold surface in the case of melt crystallized material.

2.2.2 Crystal aggregates and spherulites

Perfect single crystals as described above will only be obtained in very dilute solutions. When more material is present (either in less dilute solutions or in melt crystallization grown processes) it is more than likely that larger aggregates will occur as individual chains are involved in more than one crystal at different sections along the chain. From solution crystallization under such conditions, multi-layered crystals or lamellae with spiral overgrowths, or twinned or dendritic structures might be observed.

When polymers are crystallized from the melt, the lamellar crystals usually appear as certain forms of aggregate. The most common such aggregate is known as a spherulite. Spherulites occur when crystallization commences at a 'point' nucleus and continues radially in all directions at a rate which is constant at a given radius, resulting in a spherically symmetric crystal. Figure 2.3 shows optical micrographs of spherulites from PHB and HB oligomer with 24 repeat units (referred to as HB 24-mer). There are no fundamental differences between the PHB and HB 24-mer spherulite morphologies, as they both clearly show nice banding. The band spacing and size of the spherulites depend on the crystallization temperatures and time. More micrographs of HB oligomer spherulite morphologies crystallized from the melt will be presented and discussed in chapter 4, together with the growth behaviour from melt crystallization.

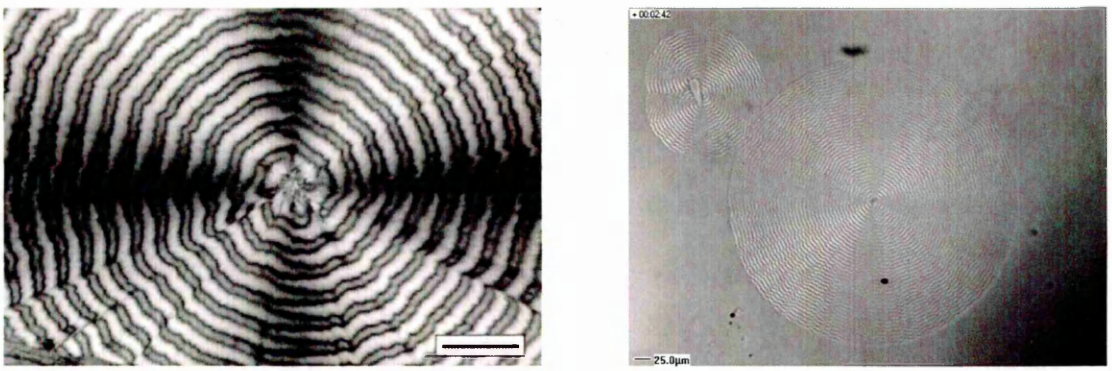

(a) (b)

Figure 2.3 Optical micrographs showing (a) PHB spherulite grown at 80°C, scale bar represents 100 µm; and (b) HB 24-mer spherulites grown at 70°C. Both spherulites show clear banding.

Also, both spherulites in Figure 2.3 display the 'Maltese Cross': a characteristic pattern when observed between crossed polarizers in optical microscope. The Maltese Cross arises from the coincidence of the principal axis of the crystal indicatrix with the extinction direction of the polarizer of analyzer. The lamellae are arranged radially within the spherulite. The regular concentric bands arise from a regular twist in the radiating lamellae. Extinction occurs when the lamellae are observed down an optic axis. Figure 2.4 is a schematic illustration of the orientation of molecules and lamellae in a polymer spherulite. In most polymer systems the radial growth rate is a constant which is dependent on supercooling. Spherulites are not unique to synthetic polymers

or long chain molecules, they can also occur in minerals, vitamins, ice and some other elements such as selenium [Ryschenkow *et al.*, 1988].

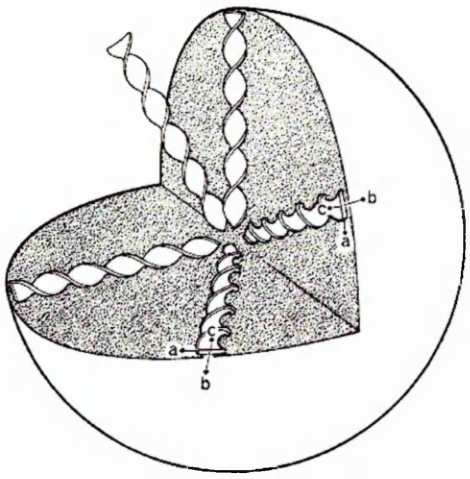

Figure 2.4 Schematic illustration of a polymer spherulite with crystal orientation [Barham and Keller, 1977].

2.3 Theories of Polymer Crystallization

It is an intriguing phenomenon that polymers tend not to crystallize in the form with lowest free energy (which would be in the fully extended state), but rather form a folded structure as described in section 2.2 at a higher free energy. This section will, from a theoretical point of view, address the question briefly: why do chains fold?

2.3.1 Introduction

The crystallization of polymers consists of two consecutive stages: (1) nucleation – the creation of a nucleus around which the crystal can grow, and (2) subsequent growth – the addition of material to the nucleus. The initial nucleation is not critical to the final shape and particularly the crystal thickness (or fold length). It is the crystal growth that is the more important stage. The temperature at which the growth occurs, as well as the availability of materials to be incorporated into the crystal lattice, has a marked effect on the morphology of the final crystal, and also the crystal thickness.

There are two frequently used competing theories to explain the method of crystal growth:

- **Secondary nucleation theory** suggests a model of a secondary nucleus forming on a crystallographically flat substrate of the crystallizing material. Since the time taken to form such a secondary nucleus is the important issue, the barrier to growth is essentially enthalpic.
- However, growth on atomically rough surfaces is another way for the stems of folded material to be added. Since the barrier to be overcome in this case is entropic in nature, this model is frequently referred to as **the rough surface entropic barrier model.**

In the rest of this section, the main approaches to these two theories of polymer crystallization will be described, followed by a brief comparison between the two. For more detailed description and review of the theories, see [Armistead and Goldbeck-Wood, 1992] and [Keller and Goldbeck-Wood, 1996].

2.3.2 Secondary nucleation theory

The original application of secondary nucleation theory to polymers was by Lauritzen and Hoffman (1960), and then Frank and Tosi (1961). A secondary nucleation model was suggested by the existence of only low index crystallographic planes in all the single crystals, and by the dependency of crystal thickness on supercoolings.

The Gibbs free energy G, is used in the secondary nucleation model, its definition in terms of enthalpy, H, temperature T and entropy S, are given in equation 2.1.

$$\Delta G = \Delta H - T\Delta S \qquad (2.1)$$

where T is the thermodynamic temperature. The system is in equilibrium when G has a minimum value '0'. The equilibrium melting temperature, at the point where the system is in equilibrium between melting and crystallization, is often denoted as T_m^0. This is the temperature at which a crystal of infinite dimensions would melt, and is also known as the equilibrium melting point. The significance of the crystal being

infinitely large is that the contribution to the free energy from the surface will be infinitesimally small. In any real crystal the influence of the surface free energy would tend to depress the melting temperature.

From equation 2.1, at the equilibrium melting temperature (where ΔG is of minimum value 0), $\Delta S = \Delta H/T_m^0$, which is then assumed not to be very temperature dependant. The temperature T_c, at which crystallization occurs, often appears in equations relative to the equilibrium melting temperature as $T_m^0 - T_c$. This is referred to as ΔT and also called *supercooling*.

2.3.2.1 Secondary nucleation models

The secondary nucleation model considers the growth of a layer of crystal on an infinite flat substrate of perfect crystal. It assumes that the lateral growth of crystal lamella of thickness l proceeds by deposition of layer upon layer of stems (straight chain segments) of length l, each layer being nucleated by the deposition of the first stem. Figure 2.5 gives a schematic drawing of chain deposition on the side surface of a polymer crystal.

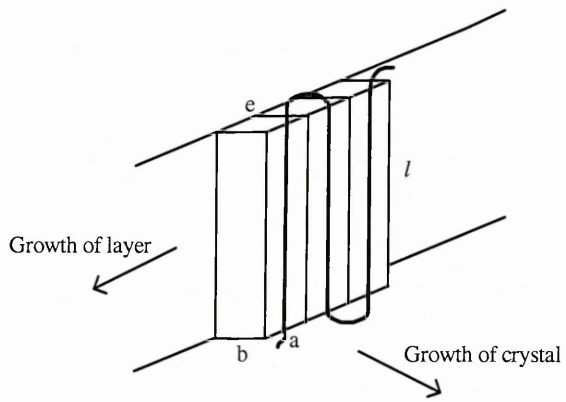

Figure 2.5 Schematic diagram showing the surface energies important for secondary nucleation theory: chain deposition on the side surface of a polymer crystal, σ and σ_e are side and end (fold) surface free energies, b is the width of the chain (after Hoffman, 1976).

For the first stem there is a net energy gain of $2b\sigma l - \psi abl\Delta F$, where σ is the lateral side surface free energy, ΔF is the bulk free energy of crystallization per unit volume, $\Delta F = \Delta H\Delta T/T_m^0$, and ψ is the factor determining what fraction of the crystallization

energy had been released at the peak of the barrier during the attachment of a stem [Hoffman *et al.*, 1976]. As the next stem arrives, two new fold ends are created with an energy gain of $2ab\sigma_e$ (σ_e is the end surface energy). Since there are no new sides are formed and a fraction of free energy of crystallization, $\psi abl\Delta F$, is released, the net energy barrier for the new stem is $2ab\sigma_e - \psi abl\Delta F$. According to this surface energy based theory, the barrier for deposition of the first stem is the highest of all due to the large surface area bl. Provided that the condition in equation 2.2 is satisfied, the overall free energy will decrease as more stems are added. Eventually, when the free energy is negative, a stable secondary nucleus is formed.

$$l > 2\sigma_e T_m^0 / \Delta H \Delta T \qquad (2.2)$$

$2\sigma_e T_m^0 / \Delta H \Delta T$ is the minimum thickness of crystals stable at a given crystallization temperature T_c.

It is important to note the dependence of the crystal thickness on the supercooling. The higher the supercooling, the thinner the crystal grows. For crystals grown at a certain supercooling (ΔT), then heated from room temperature to a lower ΔT (i.e., a higher temperature, but lower than the melting point), they may begin to thicken. The condition in equation 2.2 is then no longer satisfied. This process, also known as lamellar thickening, will be discussed in detail in chapters 6 and 7, which describes the experiments carried out on the thickening behaviour of HB oligomers.

The melting temperature (T_m) of a crystal of thickness l is related to the fold surface free energy and its thickness and is given in equation 2.3, according to the Gibbs-Thompson relation. T_m is dependant on the lamellar thickness l. The relationship between annealing, melting and crystallization temperature is complex, and polymers do not melt at the same temperature at which they were crystallized.

$$T_m = T_m^0 (1 - 2\sigma_e / l\Delta H) \qquad (2.3)$$

The elementary steps in the secondary nucleation theory are the deposition of the first stem and the subsequent stems forward and backward respectively. The whole process

is treated as a series of consecutive reactions. By integrating the steady-state constant flux of segments, the average thickness for the crystal can be known, equation 2.4. The derivation process is not performed here, for more information see e.g. [Frank *et al.*, 1961; Hoffman and Lauritzen, 1961].

$$\langle l \rangle = (2\sigma_e/\Delta F) + \delta l \qquad (2.4)$$

where $2\sigma_e/\Delta F$ is the thickness at which the crystal melting point is the same as the crystallization temperature, and δl is approximately $kT/2b\sigma$ (constant) for small ΔF.

The secondary nucleation theory is a simplification by treating the stem deposition as a single event. The most conspicuous consequence of this in the application to polymers is the erroneous prediction of δl increasing and diverging at large ΔT, this problem is called the 'δl catastrophe' and is avoided by adjusting ψ in such a way as to keep δl small at all practical supercoolings [Hoffman, 1976]. Some other criticisms and modification have been made, e.g. Frank and Tosi (1961), Point (1979) and recently Armistead and Goldbeck-Wood (1992), but the general form of the theory is still retained.

The initial model was developed to describe crystallization from dilute solution and was not expected to be applicable to crystallization from the melt. However, it was noted that the linear growth rate in melt crystallization varied in the way that might be expected for secondary nucleation. The theory was then extended to give linear growth rates and found to be in good agreement with experimental data [Lauritzen *et al.*, 1973; Hoffman *et al.*, 1975] for many different polymers.

2.3.2.2 Growth rates and the three regimes

To calculate the growth rates for a given crystal grown at the particular crystallization temperature, two important processes need to be considered: the rate g, at which a nucleus once formed, spreads across the surface, and the rate i, at which new nuclei are formed on the substrate. In the case where $g >> i$, and only one nucleus is active on the surface at a time, this is called regime *I*. The growth rate is dominated by the formation of new nuclei and is given by

$$G_I = b\, i\, L \qquad (2.5)$$

where L is the length of the substrate. It should be made clear that L is not the length of the crystal face in most cases, and must be small compared to the resolution of the technique used to measure G, if G is to be constant with crystal size.

If there are several nuclei active on the substrate at the same time, the crystal growth rate is given by

$$G_{II} = (b\, i\, g)^{1/2} \qquad (2.6)$$

This is known as regime *II* crystallization. If the rate of formation of new nuclei is sufficiently high that there is little chance for a nucleus to spread before a new nucleus is formed next to it, the growth rate is given by

$$G_{III} = a\, i\, b \qquad (2.7)$$

and the crystallization is said to occur in regime *III*.

The calculation of growth rate then becomes the calculation of i and g, which has effectively already been done in the calculation of l. The result is that

$$\begin{aligned} G_I &= G_{I0}\beta \exp\left(-\frac{4b\sigma\sigma_e}{\Delta FkT}\right) \\ G_{II} &= G_{II0}\beta \exp\left(-\frac{2b\sigma\sigma_e}{\Delta FkT}\right) \\ G_{III} &= G_{III0}\beta \exp\left(-\frac{4b\sigma\sigma_e}{\Delta FkT}\right) \end{aligned} \qquad (2.8)$$

Where β is given by

$$\beta = \beta_0 \frac{kT}{h} \exp\left(-\frac{U^*}{R(T - T_\infty)}\right) \qquad (2.9)$$

and $\Delta F = \Delta H \Delta T / T_m^0$, here β_0 is the transport term representing the rate at which molecules arrive at the surface, and h represents Planck's constant.

From equations (2.8) and (2.9), Hoffman (1983) gives the linear growth rate of polymer spherulties as:

$$G = G_0 \exp\left(-\frac{U^*}{R(T-T_\infty)}\right) \times \exp\left(-\frac{Kb\sigma\sigma_e T_m^{\,0}}{\Delta H \Delta T k T}\right) \qquad (2.10)$$

Where G_0 is the constant of the absolute value of the growth rate, U^* is an activation energy for transport of molecules to the growth front, R is the gas constant, T is the crytallization temperature, T_∞ is the temperature below which molecules become immobile, ΔT is the supercooling, k is Boltzmann's constant, σ is the side surface free energy, σ_e is the end free energy, and K may have the value 2 or 4 depending on the growth mechanism. Hoffman proposes that there are three distinct regimes of growth of polymer crystals, depending on the relative rates of formation of new secondary nuclei on the growth front and the rate at which the nuclei once formed spread along the growth front. The three regimes may be distinguished by the value of the constant K in equation (2.10): in Regimes *I* and *III* it takes the value 4, and in Regime *II* it takes the value 2. This theory introduces the third regime (Regime *III*) at high supercoolings.

A large amount of experimental evidence has been obtained in support of the existence of regime transitions in the growth of polymers, and a number of examples are also listed in Hoffman and Miller [1983 and 1989]. By plotting $lnG + U^*/R(T-T_\infty)$ vs $1/T\Delta T$, relationships have been seen for a number of polymers with approximately a factor of two difference in slope at each transition, as predicted. In some instances only one regime transition is obtainable, possibly due to the constraint on sufficiently high supercoolings. In many cases the transitions observed are sharp, and further analysis gives physically reasonable values for the polymer surface energies.

Previous work by Barham *et al.* [Barham *et al.*, 1984] provides strong evidence that there is a change in the growth mechanism of PHB spherulites at ~130°C. This corresponding to a transition from what is know as regime *II* growth to regime *III* as predicted by Hoffman. Regime *I* occurs at low supercoolings and had not yet been observed in PHB, the rate of secondary nucleation is low compared with the rate of spreading of a nucleus across the growth front. As the supercooling increases, regime *II* comes into being, the nucleation rate increases and several nucleated patches spread simultaneously across the growth front. The number of such patches increases with the supercooling until eventually the separation between nuclei is of the order of the molecular width at which stage regime *III* growth begins.

2.3.2.3 Further development

There have been many different approaches to develop the theory further, some of these may be found in: [Lauritzen and Hoffman, 1973; Point, 1978, 1979; Hoffman *et al.*, 1979; Point and Kovacs, 1980; DiMarzio and Guttman, 1982; Hoffman, 1983; Cheng and Wunderlich, 1986a, b; and Hoffman and Miller, 1988 and 1989]. All these people have made some modifications to remove the assumptions in the basic model which are considered to be incorrect or too simplistic. In general these modifications affect the way in which the rates i and g are calculated. All the authors agree that the secondary nucleation model gives an excellent agreement with the available experimental results on crystal thickness and growth rates.

The strong support for secondary nucleation theory was in part due to the fact that the materials studied exhibited crystal habits with planar surfaces. However, the crystals of polyethylene grown from the melt have exhibited curved surfaces, and many single crystals grown from dilute solution at low supercoolings have curved or high index surfaces too [Organ, 1983]. When such crystals with curved surfaces were observed, there was clearly a need for a new model which could explain this different phenomenon.

2.3.3 The rough surface entropy barrier model

The rough surface growth model was devised by Sadler and Gilmer after the observation of curved crystals at low supercoolings [Sadler, 1983; Sadler and Gilmer, 1984]. The new model was based on the idea of rough surfaces and nucleation-free growth. A surface possesses a configurational entropy so that a perfectly flat surface is extremely unlikely. A crystal surface should be expected to contain defects such as missing atoms and absorbed atoms. In the case of small molecule crystals, there is a temperature above which the surface entropy becomes so important that the surface can be described as rough. This temperature is called the roughening transition temperature, T_R. Also, at a temperature above T_R, high equilibrium roughness removes the necessity of surface nucleation as there is no additional free energy associated with a step. It had been assumed that in the case of large molecule crystals, T_R would be very close to the melting point that this type of growth will not occur. Sadler

[1987, a, b, c], however, showed that it was possible that the roughening transition temperature for polyethylene could lie in the range of temperatures used in crystallization studies, and this was in good agreement with the observed crystal morphologies [Sadler and Gilmer, 1984 and 1988].

Sadler's model is also referred to as the 'roughness pinning' model [Sadler, 1987]. Roughness refers to equilibrium and kinetic surface roughness, resulting from splitting stems into segments and negating the need for nucleation. Pinning refers to the adopted rule that a buried segment can not move unless the stems that covers it is detached. Thus, a stem is immobilized or pinned down, even if covered by only temporary unstable attachments. The free energy barrier for crystal growth is thus entropic rather than enthalpic.

The model usually relies on computer simulations and predicts typical lamellar thickness and growth rate behaviour fairly well, giving very similar results to secondary nucleation theories although the different growth regimes are not required with the model. Furthermore, the model can be applied to more complex situations such as copolymer crystallization [Goldbeck-Wood, 1993], where the units represent the chemically different sections of the chain. More specific experimental growth rates and lamellar thickness data have been fitted more satisfactorily [Goldbeck-Wood, 1994].

2.3.4 Comparison between the two models

It is surprising to note that despite the conceptual differences in these two models, their predictions are comparable for most experimental observations on polymer crystallization. Fundamentally, they are both based on the statistical dynamics of the growth process. Also they allow only lateral growth and do not allow thickening during the initial stage of the growth. In principle, the entropic barrier model is only a generalization of the nucleation approach [Binsbergen, 1972]. The nucleation models treat the chain as a smooth, structureless object, or to consist of units which all have the same heat of fusion and surface energy. Both models predict a reciprocal relationship between the crystal thickness l and the supercooling ΔT. This is also in good agreement with experiments. The secondary nucleation model has been more

frequently used up to now, maybe in part due to the relative simplicity of the model itself. Further comparison between the two models can be found in [Barham, 1993; Keller and Goldbeck-Wood, 1996].

2.3.5 Further development in polymer crystallization theories

Several significant developments in polymer crystallization theory studies have been made more recently, such as the two dimensional nucleation and sliding diffusion theory of Hikosaka [Hikosaka, 1990], the two stage crystallization model by Strobl [Heck and Strobl, 2000]. In addition, a number of computing simulation studies have been carried out and are making good progress.

Experimental results on monodisperse model polymers provided a much needed further test for the two theories. Particularly, the self-poisoning minima found in the short chain oligomer crystallization can be regarded as one of the key points. It would appear that a synthesis of Sadler's model and the secondary nucleation theory could come close to explaining most experimental observations in polymers as well as in monodisperse oligomer model materials. The relevant key findings from pervious studies on crystallization behaviour with oligomer materials, in particular n-alkanes, are reviewed in next chapter, chapter 3. Experimental results and discussions from HB oligomer crystallization studies are reported in chapters 4–8, which serve as the original contribution to knowledge by this project.

Chapter 3 Oligomer Crystallization Studies

3.1 Introduction

In the past the polydisperse nature of all synthetic polymers made it complicated to study the crystallization of polymers. Recently a number of ultra-long chain and strictly monodisperse oligomers have been successfully synthesized. These oligomers have chain lengths that can bridge the gap between small molecules and polymers. Using these model materials, a range of aspects of polymer crystallization have been investigated so that the chain length dependent behaviour can be separated from that due to the 'mixed' nature of polydisperse systems. Previous research using oligomers as model systems to study polymer behaviour has already proved very valuable, and continues to offer great potential for clarifying some of the most fundamental questions about polymer behaviour.

The shorter chain component of a polydisperse polymer can be rejected during both crystallization and melting [Keith, 1963; Kawai, 1967; Sadler, 1971], which causes fractionation on crystallization and the smearing of the melting temperature on heating [Bassett, 1994]. Such tendency towards fractionation seemed to suggest that fractionation plays a dominant role in polymer crystal growth kinetics [Point, 1995] for the formation of complex crystal structures from the melt [Keith and Padden, 1964; Balijepalli *et al.*, 1996]. This makes it very difficult to model or theoretically explain the melting and crystallization behaviour of complex polymer systems. However, by using monodisperse samples it is possible to remove all the uncertainties present in even the sharpest fractions, and obtain an insight into the behaviour that is due purely to the long chain nature of the molecules and not a result of the inherently mixed nature of most polymer systems. There has in the last decade been a great deal of interest in the crystallization of long, precise length, oligomers of polyethylene (n-alkanes) and other short chain materials, such as low molecular weight PEO fractions and nylon oligomers, see e.g. [Ungar and Zeng, 2001]. These short chain oligomers of precisely defined chain length have provided excellent model materials for studying the complex processes involved in polymer crystal growth, thickening and melting, and could help to throw new light onto the old problems in polymer crystallization.

This chapter will start with a review of relevant previous research results with some close to monodisperse, or monodisperse oligomer materials such as sharp fractions of low molecular weight poly(ethylene oxide), PEO, and uniform ultra-long n-alkanes. A summary of the microbial functions of HB oligomers found in living cells will be presented, followed by the details of chemical synthesis strategy of monodisperse OHB production.

3.2 Early Studies on Crystallization of Short Chain Oligomers

Polymers usually have a distribution of chain lengths, giving polymer science a statistical basis rather than the more exact science of small molecules. Previous work on low molecular mass poly(ethylene oxide) PEO fractions has shown some interesting behaviour including a pattern of change of growth rate as the crystal form changes [Arlie *et al.*, 1965]. However, the oligomers used in those studies were not strictly of uniform length, but rather contained a small range of lengths. A set of extremely monodisperse short chain polyethylenes (with up to 390 carbon in the chain) was later developed by a strictly controlled step-by-step synthesis technique [Bidd and Whiting 1985; Lee and Wegner, 1985]. These n-alkanes with exactly the same length, i.e. monodisperse, can serve as a link between the sciences of small and long molecules. The study of alkanes has revealed a great deal about the behaviour of polyethylene crystallization. Similarly, the entirely monodisperse HB oligomers, which are the subject of this project, could also contribute to the whole field.

3.2.1 Short chain low molecular weight PEO fractions

Since PEO oligomers could be obtained with a narrow molecular weight distribution, their crystal morphologies and crystallization kinetics have been studied extensively. By measuring the small angle X-ray scattering (SAXS) spacings, l, given by materials with different chain lengths as crystallized at different temperatures, Skoulios and co-workers [Arlie *et al.*, 1965; Gilg *et al.*, 1967] found that l varied in discrete steps with crystallization temperature, T_c. The values of l corresponded to the average chain length and integer fractions of that length. For the highest T_c, l corresponded to the extended chain; with a decrease of T_c the values of l progressively decreased to $l/2$,

$l/3$, etc, corresponding to once, twice, etc. folded chain forms. Such behaviour indicates that the chain ends are at the surface of the crystalline lamellae in preferred crystallization modes. This is in contrast to the situation in polydisperse polymers where l was found to be proportional to $1/\Delta T$, ($\Delta T = T_m^0 - T_c$, is the supercooling) [Keller, *et al.*, 1968].

Further work concentrated on the morphology and growth of narrow PEO fraction crystals has been summarized by Kovacs and co-workers [Kovacs and Gonthier, 1972 and 1975; Buckley and Kovacs, 1984]. PEO fractions were crystallized from the melt over a wide range of supercooling ΔT. Single crystals were grown from the melt at low and moderate ΔT, and the crystal morphologies were observed to develop in a flat basal plane by optical microscopy. Thickening was observed from the centre of the first grown lamellae at some stage of growth. This thickening itself was accompanied by a multiple fraction of the chain length, i.e. if the crystal first grows as a once-folded form, then the thickened part will be extended form, and so on. The growth of the thickened portion could then be followed simultaneously with that of the original layer further out. The two growth rates are in general different, and the innermost thicker layer can catch up with the outer one [see Higgs and Ungar, 1994 for a review]. It can also take up different lateral habits and give a variety of crystal morphology effects. The crystal morphology differs dramatically as the crystal chain form changes [Kovacs *et al.*, 1975; Cheng and Chen, 1991]. The lateral growth rate (G) can be determined as a function of temperature for each thickness. Surprisingly, while the rate increases with decreasing temperature, there are several breaks in the slopes. It was found that the T values associated with these discontinuities correspond to the stability limit of the next shortest fold length. Figure 3.1 shows the temperature dependence of the growth rate (G) as a function of crystallization temperature for six PEO fractions. The breaks in the slope are more noticeable in low molecular weight fractions but are absent in the polymer. The existence of such sharp increases in $dG/d(\square T)$ is qualitatively, and entirely predicted by the secondary nucleation theory [Zerbi *et al.*, 1982].

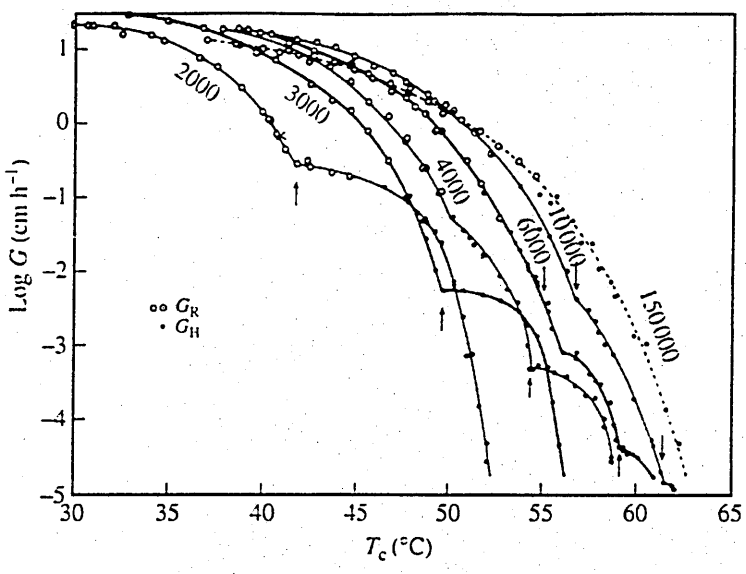

Figure 3.1 Growth rates (G) as a function of crystallization temperature of six PEO fractions. G_H is the growth rate of {010} faces, and G_R of the spherulites [Kovacs and Gonthier, 1972].

The later observation that melting temperatures varied in discrete steps further supported the quantization of lamellar thickness. It was suggested that integer folding in PEO fractions may be due to the specific nature of OH end groups and their hydrogen bonding tendency. The possibilities of hydrogen bonding between the HB oligomer chains are discussed in chapters 4–8.

3.2.2 Strictly uniform ultra-long n-alkanes

Short chain crystalline n-alkanes have been used as model chain molecules and studied for many years. Their crystal structure [Smith, 1953; Shearer *et al.*, 1956; Pieszek *et al.*, 1974], crystal growth and morphology [Dawson, 1952; Keller, 1957], melting temperature [Flory, 1963; Wunderlich, 1977], chain mobility [Yamanobe *et al.*, 1985], conformational defects [Zerbi *et al.*, 1981], self-diffusion [Ungar and Keller, 1979], and other properties were extrapolated to represent the crystalline phase of polyethylene. An early comprehensive review of the structural and thermodynamic data of n-alkanes was presented by Broadhurst [Broadhurst, 1962].

However none of these alkanes were long enough to fold. It was not until the 1980's that strictly monodisperse ultra-long n-alkanes, with chain lengths up to 390 carbons, became available [Bidd and Whiting, 1985; Lee and Wegner, 1985; Brooke *et al.*,

1996]. These materials, which are model substances for low molecular weight polymers, are sufficiently long to display some 'polymeric' properties such as chain folding. However, since they are strictly monodisperse, they are free from many of the complications inherent to polymers. Previous studies on these oligomers have already presented a wealth of information and new insights into polymer crystallization in general and polyethylene crystallization in particular [Ungar and Keller, 1986 and 1987; Organ *et al.*, 1990; Ungar and Organ, 1990]. Of special importance to this thesis are some observations relating to integer folding [Ungar *et al.*, 1985], transient non-integer states [Ungar and Keller, 1987, Zeng and Ungar, 1998], crystallization and nucleation rate minima [Organ *et al.*, 1996], morphologies changing and crystal thickening [Organ *et al.*, 1990; Ungar *et al.*, 2001] etc. It will be beneficial to compare these key findings with the results from the HB oligomer crystallization studies carried out in this project, and they are briefly described below.

3.2.3 Relevant key findings from alkanes and PEO fractions crystallization studies

3.2.3.1 Integer folded (IF) chain conformations

Crystallization experiments on long n-alkanes have been performed from both the melt and solution. A high regularity of lamellar stacking gave a clear SAXS diffraction pattern with many higher orders. This led to a more accurate measurement of lamellar spacing. Low frequency Raman spectroscopy using the longitudinal acoustic mode (LAM) also confirmed the length of straight chain segments at the same time. Studies of monodisperse alkane crystals grown from solution have shown that the chains did indeed fold, with the onset of folding being partly determined by the length of the chains and partly by the crystallization temperatures. The chains with less than 100 carbon atoms can form extended-chain crystals. Chains with more than about 100 or 150 carbon atoms form folded-chain crystals, with the precise value depending on the crystallization temperatures. The fold lengths in the final stages of crystallization were found to be integer fractions (IF) of the chain length. For instance, while alkane $C_{102}H_{206}$ could only be obtained in extended chain from, $C_{150}H_{302}$ can also be crystallized with once-folded form from solution or by quenching from the melt. The most folds (4 folds) were obtained at this stage in the longest alkane,

$C_{390}H_{782}$, with increasing supercoolings [Ungar *et al.*, 1985]. In the most regular crystals, the portion of the chain within the fold region is found to be no more than 2–4 carbon atoms [Ungar *et al.*, 1988]. Figure 3.2 shows the different integer folded forms obtained from n-alkanes.

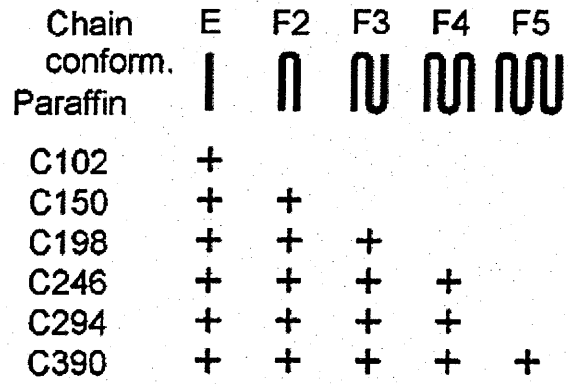

Figure 3.2 Integer folded (IF) forms observed in long n-alkanes [Ungar, 1988].

These results on alkanes suggest that the preference for integer folding is inherent in monodisperse oligomer systems, and is not due to the specific nature of the end groups, such as the OH end group, or the hydrogen bonding in low molecular weight distribution PEO. Later studies with methoxy terminated PEO fractions also exhibited a preference for integer folding at the stable stages of crystal growth [Cheng and Chen, 1991]. This integer folding (with extended and once-folded chain forms) has also been confirmed by our studies with monodisperse HB oligomers up to 32 repeat units long.

3.2.3.2 Noninteger folded (NIF) chain conformations

It was recognized by synchrotron SAXS that the folds in crystals of long n-alkanes were not always sharp (as shown in Figure 3.2) during crystallization from the melt [Ungar and Keller, 1986]. At temperatures below the extended chain growth region, the initial lamellar periodicity was a noninteger fraction (NIF) value of whole chain length, even after correcting for tilt [Ungar and Keller, 1986]. It corresponded to a fold length between the chain length and half that value, and was dependent on crystallization temperature and time. It was also observed that crystallization starts

with rather imperfect crystals, with significant disorder along the fold surface, where the fold length itself is not close to any integer fractional value. However the crystal can still perfect itself during its growth, i.e., these NIF lamellae can subsequently transform isothermally by thickening to extended-chain, or, at lower T_c, by thinning to once-folded chain lamellae with hairpin chain conformation.

Ungar *et al.* (1998) reconstructed the electron density profile normal to the lamellae by using SAXS intensities of a number of diffraction orders to reveal the nature of the NIF form in alkanes [Ungar and Zeng, 1998]. The results showed that NIF is up to one third amorphous, with some chains integrally folded in two and others not folded at all, but traversing the crystalline layer only once. These latter chains are only half-crystalline, their ends forming the amorphous layer. A tilt of 35° within the chains was also proposed from the electron density profile together with the time-resolved Raman spectroscopy measurements [Zeng *et al.*, 2000]. In contrast to the integer once folded chain form, NIF allows crystals to grow faster as not all chains need attach perfectly, giving their ends flush with the crystal surface. However, if the lamella is to grow, nearly half the chains have to be placed correctly and crystallize fully with a fold in the middle. Otherwise the overcrowding at the crystal amorphous interface would block the crystal growth. This explains the fact that lamellar crystals of flexible polymers must grow laterally with chain folding.

This NIF form and its transformation phenomenon were also found in PEO fractions [Song and Krimm, 1989; Cheng *et al.*, 1991]. However it is still not clear if the NIF form in PEO has the same structure as that proposed for the alkanes at this stage. More information about NIF can be found in [Ungar and Zeng, 2001]. More surprisingly, certain non-integer folded forms, in particular those producing crystal thicknesses of 2/3, 3/4 and 5/6 of the extended chain length, also exist in the mature HB oligomer crystals from our results. This could be associated with hydrogen bonding between the chain ends. Detailed discussion and suggested folded chain conformations of HB oligomers will be presented in chapters 4–8.

3.2.3.3 Fold surface and end surface

As discussed in chapter 2, it has been a controversy for many years whether the polymer chain fold is tight adjacently re-entrant (as shown in Figure 1.4), or random re-entry with loose loops as suggested by the 'switchboard' model. Even in the more perfect single crystals grown from solution, there is still an amorphous layer of cilia and probably adsorbed chains cover the fold surface [Hoffman and Davis, 1978].

The integer folded (IF) single crystals of monodisperse long alkanes grown from solution have the advantage that they do not contain cilia and hence leave the fold surface uncovered. Electron microscopy of surface decorated alkane crystals revealed tight fold conformations at the surface [Ungar and Organ, 1987; Wittmann and Lotz, 1985]. However, at low temperatures, a switchboard type fold surface occurred more easily, particularly at the first stage of the crystal growth. A mixture of tight adjacent re-entrant and switchboard type folds is now more commonly accepted in polymer crystals, as illustrated in Figure 2.2. More information on the fold and end surface can be learned from studies of cyclic compound models, see [Ungar and Zeng, 2001].

3.2.3.4 Stepwise growth rate and crystallization rate minima

Studies on PEO fractions with low molecular weight distributions between 1,500 and 12,000 have revealed the stepwise variations in growth rate as a function of crystallization temperature, Figure 3.1. The rate of change of crystal growth rate with supercooling $dG/d(\square T)$ increases sharply at a series of specific crystallization temperatures, marked by arrows in Figure 3.1. These indicate the transitions between the growth of crystals with different chain-folded conformations. Secondary nucleation theory can predict this behaviour once modifications have been introduced to allow for quantization of lamellar thickness [Zerbi *et al.*, 1982]. According to the secondary nucleation theory, polymer crystals grow by depositing layers of stems on the side surface of the lamella (see Figure 2.5). Each new layer can only spread easily once it has been secondarily nucleated. As described in section 2.3.2.1 in chapter 2, the main barrier to secondary nucleation is the side surface free energy $2b\sigma l$ needed to create the two new side surfaces of a single stem nucleus (here b is the chain width and σ the side surface free energy). For polymer crystals of fixed fold length l, a linear

relationship is expected between G and □T over the limited temperature range available experimentally [Hoffman, 1985]. In fact, the ln$G$ vs □T data plotted in Figure 3.1 does not deviate much for a given chain-folded form if plotted on a linear scale [Sadler, 1985]. This linear G vs □T relationship is also consistent with the alternative 'roughness pinning' theory of Sadler [1983, 1985]. According to this theory, there is no appreciable difference between nucleation and growth of molecular layers on the growth face and as a result the growth surface is rough rather than smooth [Ungar and Zeng, 2001].

Work with exact length n-alkanes has also shown pronounced effects with exact quantization of the crystal thickness into integral fractions of the chain length. More surprisingly, the growth rate G was found to reach a maximum value before decreasing into a sharp minimum and rising again thereafter, as the supercooling increases. This phenomenon has been observed in crystallization both from melt [Ungar and Keller, 1987] and solution [Organ *et al.*, 1989]. Also it applied to both crystal growth and primary nucleation [Organ *et al.*, 1996]. Figure 3.3 shows the linear growth rate (G) of crystals of $C_{246}H_{494}$ as a function of crystallization temperature (T_c) crystallized both from the melt and solution. The growth rates both pass through a maximum and reach a sharp minimum at the transition temperature from extended to once-folded chain forms [Organ *et al.*, 1997].

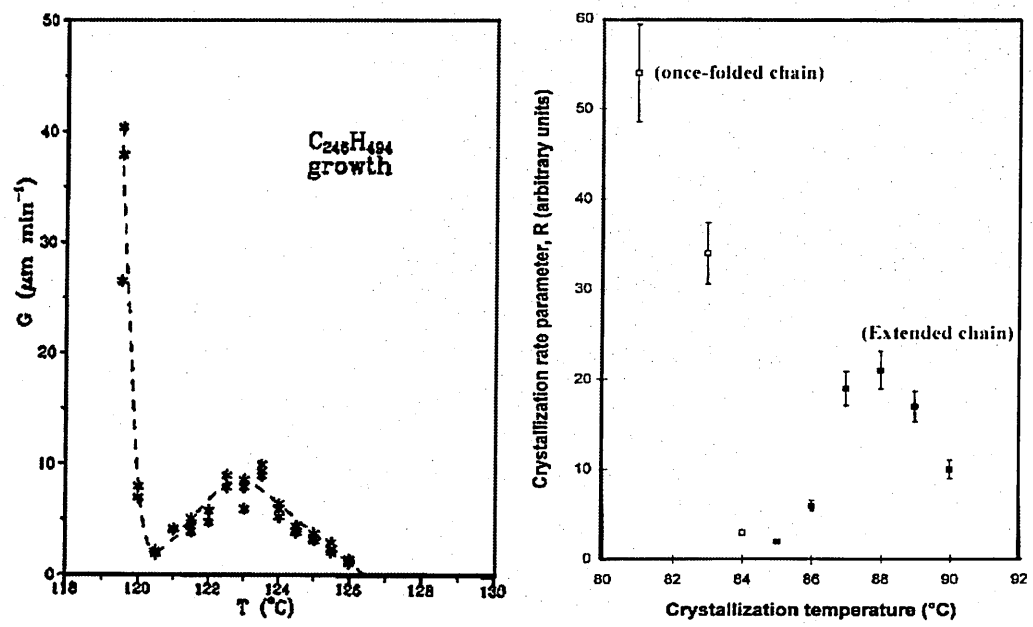

Figure 3.3 Crystallization rates of $C_{246}H_{494}$ (from melt and solution/toluene) as a function of crystallization temperature T_c [from Organ, 1997].

The rate minimum at the transition between extended and once-folded forms has been observed in a number of alkanes from $C_{162}H_{326}$ to $C_{294}H_{590}$ [Boda *et al.*, 1997; Sutton *et al.*, 1996; Organ *et al.*, 1997; Hobbs *et al.*, 2001]. A crystallization rate minimum between once-folded and twice folded growth intervals has been measured from solution grown alkane $C_{294}H_{590}$ [Morgan *et al.*, 1998]. A weak minimum between extended and once-folded growth has been reported in melt crystallization of methyl terminated PEO fractions [Cheng and Chen, 1991]. A less pronouced growth rate minimum has also been observed in melt-crystallization of n-alkanes mixtures with several different chain lengths, More details can be found in [Ungar and Zeng, 2001; de Silva, *et al.*, 2002]. In more recent work growth rates have been measured from direct optical observations of growing crystals of $C_{198}H_{398}$ in 1-phenyldecane and of $C_{162}H_{326}$ and $C_{198}H_{398}$ in octacosane [Ungar and Putra, 2001 and 2003]. Minima in growth rate at the transition from extended to folded chain growth were found both as a function of temperature and of concentration [Ungar *et al.*, 2000]. All these minima seem to show the same effect as the discontinuities observed in Figure 3.1. Indeed, crystallization rates obtained with HB oligomers of 24 and 32 repeat units both from melt and solution crystallization also show similar discontinuities (or kinks) in the rate gradient as a function of T_c, although the discontinuities in the latter cases are even weaker. Their growth rates and crystal morphologies will be discussed in detail in chapters 4 and 5.

The underlying causes of these growth rate minima have been the subject of some discussion. However various models generally agree that there is a competition between unstable growth (attachment) of the folded form and the growth of the stable extended (or less folded) form near the transition temperature, which is also termed as 'self-poisoning' [Ungar and Keller, 1987]. This explanation recognizes the fact that chains wrongly attached to the crystal surface may hinder further growth in the more stable form. This was also emphasized by the roughness-pinning crystallization theory of Salder. The blocking or pinning may not be obvious in polymers, but it becomes very pronounced in monodisperse oligomers.

The growth rate minima cannot be explained by standard secondary nucleation theory, where whole stems are assumed to be deposited in one step, because there is no allowance for competing attachments to the growth front in different conformations

[Sadler and Gilmer, 1987]. However, the minimum in growth rate can be at least qualitatively well reproduced by making small adjustments to the model, see e.g. [Ungar and Zeng, 2001]. Computing simulations have also reproduced the kinetics of the self-poisoning minimum and have provided some additional insight into the crystal morphology studies [Sadler and Gilmer, 1987; Higgs and Ungar, 1994].

3.2.3.5 Morphology changes

The crystal morphology changes at the transition temperature, i.e. at the growth rate minimum, from one form to another. The melt-grown single crystals of PEO fractions become rounded near the extended and once-folded chain growth transition [Cheng and Chen, 1991]. Above and below the transition temperature, the crystals have facets, which also show slight curvature. However, at and just above the transition, where self-poisoning appears to be pronounced, the crystal shapes changed to be circular. This may suggest that for PEO, the self-poisoning effect is associated with circular crystal habits [Ungar, 1993]. By re-examining the original growth rate data for polyethylene oxide (PEO) of Kovacs' work [Kovacs *et al.*, 1975], an anomalous retardation near the extended to folded chain growth transition has also been observed [Ungar, 1993]. This retardation was suggested to be accompanied by a change in crystal habit [Sadler, 1983; Cheng and Chen, 1991].

Crystals of long alkanes show more changes on morphology over a wide range of crystallization temperatures both from the melt and solution, see [Organ *et al.*, 1996; Ungar *et al.*, 2000; Ungar and Putra, 2001]. In the melt grown crystals, the banding of n-alkane spherulites becomes more widely spaced and less regular as the crystallization temperature is increased. The overall shape of the n-alkane sperulites changes from perfectly circular forms at the lower crystallization temperatures to less regular shapes at the higher temperatures. In the case of solution grown single alkane crystals, for instance $C_{198}H_{398}$, the crystal habit changes with decreasing T_c from perfect rhombic lozenges with {110} lateral facets through nearly hexagonal truncated lozenges, and leaf-shaped (or lenticular) crystals with curved {100} faces, and finally to needle-like crystals bounded by straight {100} faces just above the growth rate minimum. On lowering T_c, further chain-folded crystallization takes over and the habit reverts to that of truncated lozenges, at still lower T_c, the shape changes to

lenticular and the cycle is repeated [Ungar and Zeng, 2001]. The T_c dependence of crystal habit within one such cycle is the exact reversal of that in solution crystallized polyethylene [Toda, 1991; Organ and Keller, 1985]. The temperature dependencies of G_{100} and G_{110} are different, for all alkanes, the growth normal to {100} faces is more retarded by self-poisoning than the growth normal to {110} faces. This applies both to solution [Ungar and Putra, 2001] and to the melt crystallization [de Silva *et al.*, 2003].

3.2.3.6 Crystal lamellar thickening

The thin lamellar crystals of polymers are usually regarded as meta-stable, and have such shape due to kinetics rather than equilibrium thermodynamics. As higher temperatures are imposed, their mobility is usually increased, so the crystals often thicken. Two distinct situations exist in which this thickening effect occurs. The early studies on lamellar thickening were made on material which was already fully crystallized, both from the melt and dilute solution, before reheating to a high temperature and holding there [Keller and O'Connor, 1958; Fischer and Schmidt, 1962; Koening and Tabb, 1974]. This situation is known as annealing. The second situation is known as isothermal thickening and is the process whereby the lamellar thickness increases during isothermal crystallization [Weeks, 1963; Hoffman and Weeks, 1965 and Chivers *et al.*, 1982]. The thickening is normally continuous and linear with the logarithm of time [Fischer and Schmidt, 1962]. However, the earliest SAXS studies of PEO fractions have already shown that the lamellar thickness increases in a stepwise manner [Spegt, 1970]. Each step corresponded to one integer folded (IF) form. Thickening happens more readily when crystal lamellae are stacked on top of one another, as this reduces the need for chains to be transported to the thickening region. The quantized nature of lamellar thickening makes it easier to see the thickening process using different microscopy and calorimetric techniques, such as optical microscopy [Kovacs *et al.*, 1975], electron microscopy, differential scanning calorimetry (DSC) [Organ *et al.*, 1990; Hobbs *et al.*, 2000] and atomic force microscopy (AFM) [Winkel *et al.*, 2000] etc. More information can be found in the review of [Ungar and Zeng, 2001].

Clearly, it is important to understand the generality of processes such as those described above so that any implications for polymer crystallization may be more properly assessed.

3.2.4 Other uniform oligomer systems

The informative results on the uniform n-alkanes encouraged the synthesis and subsequent crystallization studies of similar monodisperse oligomers of other chemical species. Apart from n-alkanes, pure monodisperse nylon 6 [Brooke *et al.*, 1997] and nylon 6,6 [Brooke *et al.*, 1999] oligomers have also been successfully synthesized recently with sufficient length to form chain folded crystals. Once folded and twice folded crystals of nylon 6 and nylon 6,6 have been obtained from solution and studied by X-ray and electron microscopy [Cooper *et al.*, 1998; Atkins, *et al.*, 2000; Jones *et al.*, 2000]. Several other monodisperse models, such as proteins with repeating sequences of amino acid [McGrath *et al.*, 1992; Krejchi *et al.*, 1994]; poly(L-alanylaglycie), poly(AG), with alternating alanyl and glicyl units [Panitch *et al.*, 1997]; strictly uniform oxyethylene/methylene block oligomers [Yeates and Booth, 1985] etc. have also been synthesized and proved to be useful for crystallization studies.

Another type of strictly uniform oligomer model material, oligomers of poly(hydroxybutyrate), OHB, have also been recently successfully synthesized [Seebach, *et al.*, 1994]. While the original interest was biological as PHB is a bacterial polyester (which can also be used as a thermoplastic), the HB oligomers offer a brand new model material that proved very useful for the study of polymer crystallization [Barham *et al.*, 1984]. Sections below summarize some of the microbial functions of HB in living cells other than its role as an energy storage medium (described in chapter 1). The specific chemical synthesis strategy, to produce this strictly uniform oligomer used through out this project, is reported at the end of this chapter.

3.3 Hydroxybutyrate (HB) Oligomers

3.3.1 Introduction

Hydroxybutyrate oligomers (OHB) are short chain analogues of the polymer poly(3-R-hydroxybutyrate), PHB, which are synthesized via a sequential coupling process developed by Seebach and co-workers at ETH, Zurich. Details of the chemical synthesis will be given below in the later section. HB oligomers have several advantages over other oligomer model materials used in pervious studies. It gives a monomer unit larger and more chemically complex than other oligomer systems, which allows us to explore the generality of the behaviour in the alkanes and other oligomer systems. The molecules are capable of folding many more times in the thin HB crystals than in other oligomers used before. They give chain-folded single crystals with considerably shorter fold length than alkanes, down to a minimum of ~4 nm [Barham *et al.*, 1984; Sykes, 1996]. The range of crystallization temperature for PHB, and hence HB oligomer, is much wider. It may be crystallized from the melt over a large range of supercoolings ($40^{\circ}C \leq \Delta T \leq 120^{\circ}C$), while in other oligomer systems using conventional methods supercoolings of no more than 25–40°C can be achieved due to the prohibitively fast crystallization rates as the temperature is reduced [Kovacs *et al.*, 1975 and 1977; Ungar *et al.*, 1990; Organ *et al.*, 1996]. In contrast, PHB crystallizes much more slowly, hence making the full temperature range from the glassy state to the melt easily accessible. Therefore it offers a good opportunity to study crystallization over a wide range of temperatures using exact length HB oligomers as models for polymer crystallization. Furthermore, the chirality in PHB molecules has great potential to open up a whole new area of research. Finally, HB oligomers occur naturally in living cells and have been shown to facilitate ion transport across lipid membranes. Therefore the crystal structures formed by HB oligomers are of much wider interest.

3.3.2 Functions of HB oligomers in living cells

3.3.2.1 HB oligomer complex as a non-proteinogenic ion channel

Quantitatively, the most import role of poly(3-R-hydroxybutyrate), P(3-HB), is to store carbon-containing material in the cells of micro-organisms (up to 90% of cell dry weight) [Holmes, 1987] . Apart from its occurrence as a storage compound, PHB is also found, particularly at low molecular weight, in bacterial membranes and in the tissues of plants and animals [Reusch *et al.*, 1989 and 1992].

Rather surprisingly, traces of PHB were detected by Resuch and Sadoff in different types of bacteria when these bacteria were genetically transformable [Resuch and Sadoff, 1988] 'Genetically transformable' indicates the ability of a cell to take up DNA from the external medium, or in short, a competent cell. Resuch *et al.* also observed a major change in the lipid composition of the membranes by measuring the fluorescence intensity of N-phenyl-1-naphthylamine in the membranes of competent cells, no such changes could be found in non-competent cells.

The PHB detected in these bacteria showed a molecular weight corresponding to ~150 repeat units, and was predominantly accumulated in the inner cell membrane. Biological membranes are essentially lipid bilayers interspersed with proteins with thickness of ~5 nm [Stryer *et al.*, 1990]. Lipid bilayers are practically impermeable to ions and most polar molecules. However, these must to be able to pass through the membranes since they play an important role in many physiological processes. Proteins dispersed through the lipid bilayer are thought to be responsible for the interactions between the inside of the cell and the environment.

The HB oligomer extracted from a competent bacterial cell has been found to be always accompanied by calcium polyphosphate ($Ca{\cdot}PP_i$), with a length between 130 and 170 monomeric units [Reusch and Sadoff 1988]. This isolated complex has been shown to be very labile when removed from the natural environment. These findings led to the highly speculative postulation of a HB/$Ca{\cdot}PP_i$ complex, which may be located in the inner cell membrane. Figure 3.4 shows a model for the structure of an ion channel of such a complex model proposed by Reusch and Sadoff.

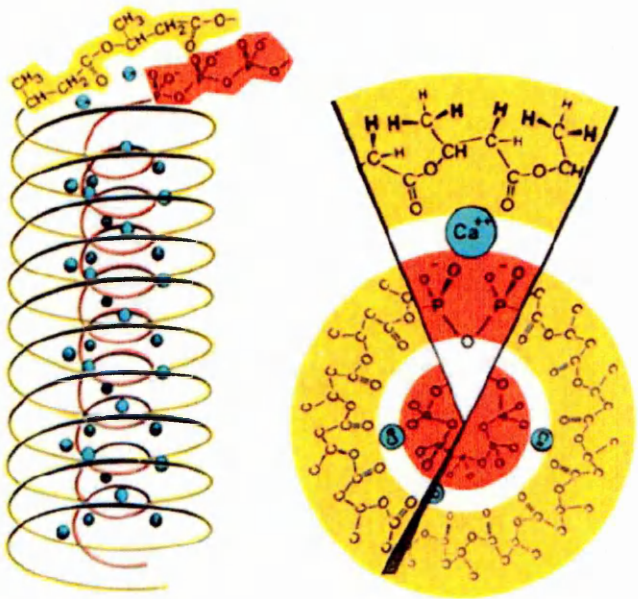

Figure 3.4 Structure of a HB/Ca·PP_i complex suggested by Reusch and Sadoff (1988). Colour yellow represents the HB oligomers, red the polyphosphate and blue the Ca^{2+} ions. The left view is perpendicular to the channel axis, right viewing down the channel axis.

Since the complex components could only be detected in genetically competent bacteria, it was suggested that this complex could act as a nonproteinogenic transmembrane ion channel, which is responsible for Ca·PP_i or even DNA uptake of the cell. However the mechanism of DNA uptake through the cell membranes of bacteria still remains unclear.

3.3.2.2 Alternative model for the HB oligomer ion channel

Seebach *et al.* proposed another model for the structure of a cellular ion channel, with the HB 2_1 helix of *M*-helicity and a pitch of ca. 0.6 nm [Seebach, 1995]. Since the HB oligomer has repeatedly been found to form a helix of pitch of 0.6 nm, it is unlikely that a helix of pitch of 2 nm could also exist as a low energy structure. The fact that oligo- and poly(3-HB) form crystal lamellae of ~5 nm thickness, when crystallized at temperature below 40°C, is intriguing when one considers that the sum of the lengths of two lipidic side chains of a phospholipid is also ~5 nm. Therefore, a chain of ca. 140 HB repeat units in a 0.6 nm pitch 2_1 helical conformation folded as in the lamellar crystals could form 8 folds assuming tight folds of two HB repeat units [Barham *et al.*, 1994]. Seebach *et al.* also showed that HB 32-mer could form ion channels in

lipid bilayers. A possible structure of HB oligomer with lipid membrane proposed by Seebach *et al.* is given in Figure 3.5; Figure 3.6 is a schematic diagram indicating the OHB ion-transport mechanisms.

Figure 3.5 Possible structure of HB/Ca·PP_i complex within lipid membrane, with 16 monomer units per stem (after Seebach, 1995).

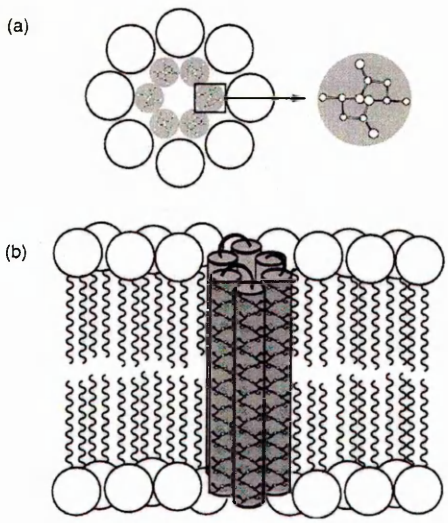

Figure 3.6 Schematic representation of the postulated pore formation for HB 32-mer in a lipid bilayer. One single pore is composed of three HB 32-mer once folded molecules. (a) Top view with enlargement of one helical string; (b) side view (after Seebach, 1999).

The problems with this alternative proposal are (A) the resulting HB/Ca·PP_i complex does not have the right charge distribution to suit a lipidic membrane bilayer

environment and (B) only few carbonyl oxygens may be available on the inside of the tube to coordinate the Ca^{2+} ions, this can be improved by the incorporation of water molecules. More information about the HB oligomer microbial functions in the cell can be found in [Reusch and Sodoff, 1988; Seebach *et al.*, 1995 and 1999] etc.

Although it is a fascinating topic to consider the biological functions of the HB oligomers involved in many living organisms (including human beings), it is outside the scope of this project. All the HB oligomer materials used in this work were synthesized in collaboration with Professor Seebach at ETH, Zurich. The whole synthesis strategy was produced and processed by Prof Seebach and his group at ETH, see a review by Seebach [Seebach *et al.*, 1995]. The author has been enormously grateful to them for providing her with an opportunity to learn the chemical synthesis for the production of the monodisperse HB oligomers at ETH in Feb 2002. The HB oligomers mainly used in this project are with 16, 24 and 32 repeat units, all in unprotected form or with a benzyl group at one end (stated in the text). Details of the development of the synthesis processes to produce the HB oligomers with exactly defined chain length are described below in a chronological order.

3.3.3 Chemical synthesis of monodisperse HB oligomers

3.3.3.1 The early stage of HB oligomers synthesis

To obtain HB oligomers of a defined chain length, the initial attempts laid in the partial depolymerization of PHB. Various mixtures of oligomers were formed by hydrolysis, alcoholysis, or by ester pyrolysis at temperatures higher than 175°C, where the average molecular weight is determined by the length of the heating period [Seebach *et al.*, 1994; Bürger, 1993]. The molecular weights of these oligomers have been measured by ^{1}H-NMR spectroscopy end group determination, gel permeation chromatography (GPC, polystyrene standard) and by plasma desorption mass spectroscopy (PDI-MS). All the measurements confirmed that there is a molecular weight distribution in these HB oligomers [Bürger *et al.*, 1993]. This proved that it was impossible to produce entirely monodisperse HB oligomers by the degradation of PHB due to the polydisperse characteristics of the polymer. Therefore a more precise method was needed.

3.3.3.2 Synthesis of nearly monodisperse HB oligomers

For the synthesis of HB oligomers with length up to 100–150 monomer units (repeat units), a possible method was the segment condensation strategy by selectively removing the two protecting end groups on an unsymmetrical oligomer. Initially, a benzyl ether protecting group was chosen for the OH terminus and a *t*-butyl ester for the COOH terminus. The unprotected portions were then coupled after activation of the acid with oxalyl chloride to double the molecule size. A dimer was chosen for the starting material in this procedure [Plattner *et al.*, 1993; Seebach *et al.*, 1994].

All the compounds were again characterized by ^{1}H-NMR, ^{13}C-NMR, IR and mass spectroscopy. The last method revealed unexpected results that a single 3-HB unit has been lost, after applying three MS techniques. The MS spectra showed that this loss is not caused by fragmentation in the mass spectrometer, since the measured mass include the protecting groups on both ends of the chain. As none of the purification methods could be chose to separate *n* mers from (*n*–1)mers on a preparative scale, it was clear that the oligomers, prepared by the above method, would also consist of mixtures, although these oligomers are very close to entirely monodisperse with $M_w/M_n \leq 1.0005$ [Seebach, 1995].

Some of the HB oligomers produced using the above synthesis method were offered by Prof Seebach to our polymer research group 10 years ago. Although these oligomers were not strictly monodisperse, they were the only OHB samples available at that time. Some preliminary experimental work was performed by a former PhD student to examine their structure and crystallization growth [Sykes, 1996]. Some of the results will be included in this thesis for a complete view of HB oligomer crystallization studies.

3.3.3.3 Synthesis of entirely monodisperse HB oligomers

To synthesize entirely monodisperse HB oligomers, the protecting group and the coupling procedures have to be changed. It was found that the loss of a HB unit during the de-benzylation is particularly apparent when *N,N*-dimethylformamide (DMF) is used as solvent and elevated temperatures are employed [Seebach *et al.*,

1994 and 1995]. This loss can be avoided by choosing trifluoroethanol (CF_3CH_2OH) instead of DFM as solvent. Trifluoroethanol and halogenated hydrocarbons (CH_2Cl_2, $CHCl_3$, $ClCH_2CH_2Cl$) are the only solvents in which the longer chain HB oligomers are soluble at room temperature. This limits the number of synthetic methods that could be used for their conversions. Finally, a benzylester protection group was chosen for the COOH terminus and a *t*-butyldiphenylsilylether (TBDPS ether) protection group for the OH terminus. This is the only (commercially available) silyl group stable in the presence of the HCl produced during the conversion of the acid to the acid chloride in preparation for the coupling steps.

The direct degradation of the PHB to get the starting monomers for the whole synthesis is given in Figure 3.7(a). The steps to give the monomers for synthesis of the dimer are outlined in Figure 3.7(b). The dimer is the starting material for the synthesis of longer chain HB oligomers.

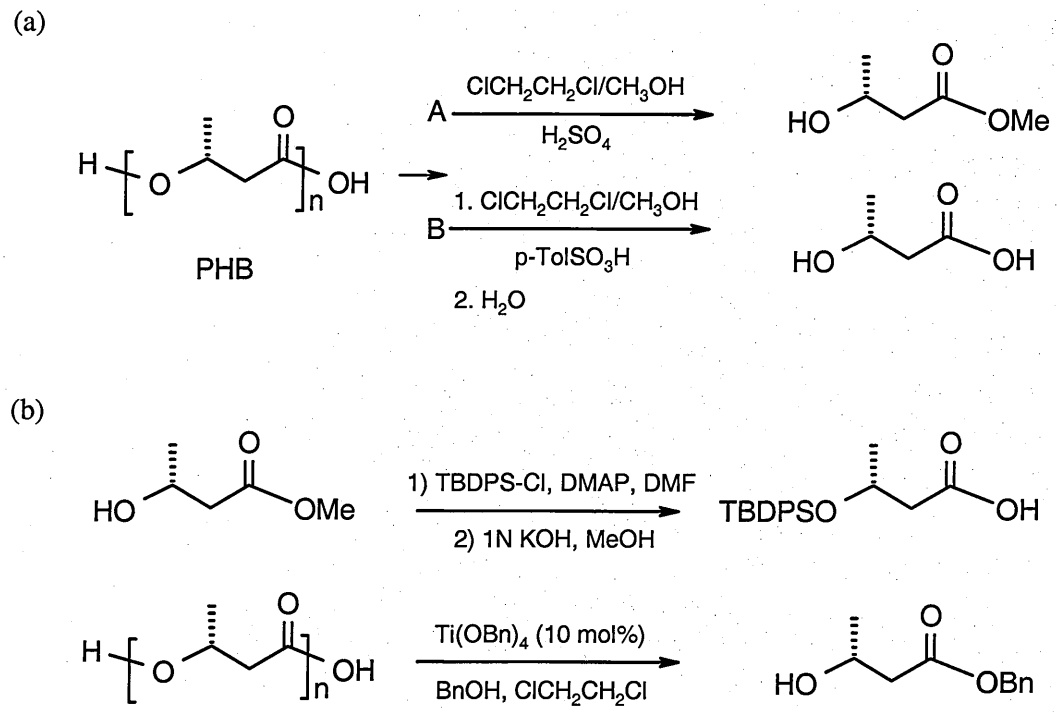

Figure 3.7 Synthesis of the starting materials for the new synthesis of monodisperse HB oligomers. (a) Direct degradation of the PHB for monomers; (b) steps to get the monomers for the starting material dimer.

Figure 3.8 gives a diagram showing the stages in the synthesis of entirely monodisperse HB oligomers. (a) is the segment coupling strategy algorithm, (b) is the de-protecting reaction formula which leads to an end product of HB oligomers without any protecting groups at both ends, also performed by the author at University of Bristol, and (c) presents the protecting end group symbols. Under pyridine catalysis, the acid chloride reacted with the corresponding alcohol at –78°C. At this temperature there was no loss of a single HB unit.

(a)

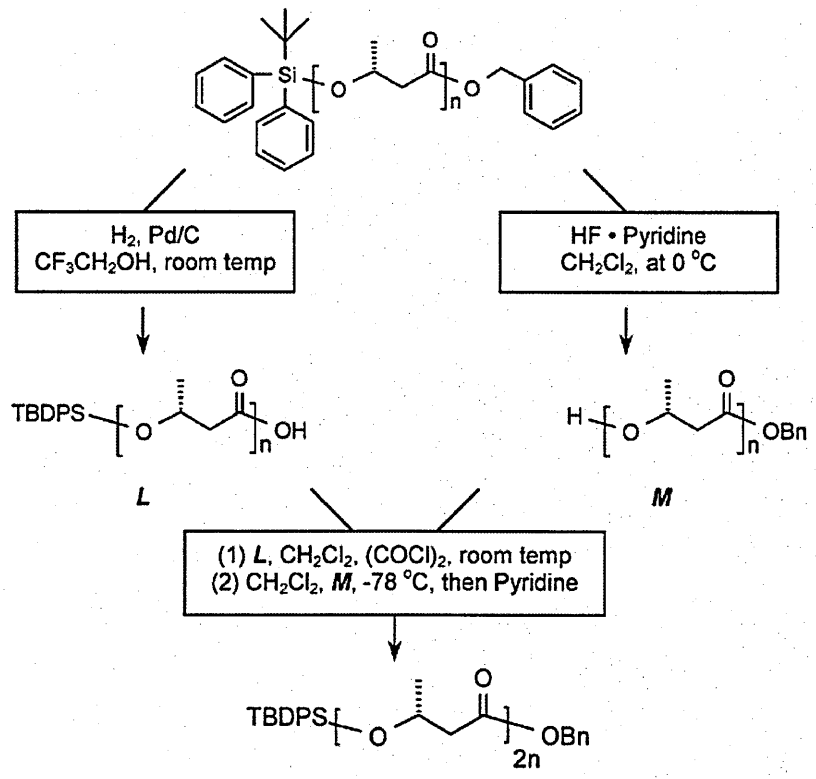

(b)

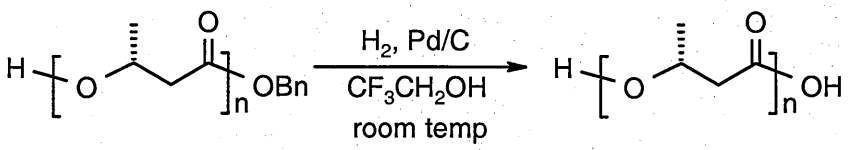

(c)

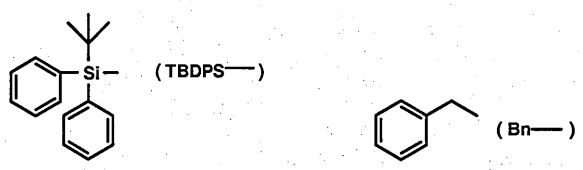

Figure 3.8 Diagram indicating the stages in the synthesis of entirely monodisperse HB oligomers. (a) Segment coupling synthesis strategy for entirely monodisperse HB oligomers; (b) De-protecting reaction formula; (c) Protecting end-group symbols (Courtesy of Seebach).

All the resulting compounds (containing 16, 32, 64 and 128 etc repeat units) were fully characterized by ^{1}H-NMR, ^{13}C-NMR and mass spectroscopy as before. From the NMR spectrum, the ratio of areas of peaks can be calculated and compared to what would be expected from pure compound. From the mass spectroscopy, observation of a single peak corresponding to the molecular weight of pure compound confirms the purity. Thus, the LSI-MS/MALDI-MS and NMR examinations of the HB oligomers confirmed that the materials produced by this synthesis method are completely monodiperse [Seebach, 1996; Waser, 2000; Rueping *et al.*, 2001; Albert *et al.*, 2002].

Using this latest synthesis strategy an entirely monodisperse HB oligomer model material was successfully produced, which provides a great opportunity to study the crystallization behaviour of this polymer. The HB oligomers used in this work are mainly with 24 and 32 repeat units (referred to as 24-mer and 32-mer). They are the only chain lengths available among the materials in this project that could exhibit chain folding. The HB 24-mer was provided by Professor Seebach, following the segment coupling strategy described as above. The HB 32-mer with benzyl protecting end group was synthesized by the author at ETH under the supervision of Prof Seebach and members of his group at the beginning of this project. The completion of the fully unprotected HB 32-mer samples and the measurements to confirm their purity by ^{1}H-NMR and mass spectroscopy were also performed by the author in the Department of Chemistry at Bristol University, following the same method used by the ETH group.

Chapter 4 Morphology and Growth from the Melt

4.1 Introduction

In practice a great deal has been learned from studies of n-alkanes, low molecular weight PEO fractions and other oligomer systems (see chapter 3). Although a wealth of information has been gathered from the previous studies on the short chain oligomer materials, the link from short exact length oligomers which form crystals with discrete thicknesses to long molecules which form crystals with a continuous spectrum of thicknesses still remains to be more established.

Using the sequential coupling strategy described in the last section of the previous chapter, 24-mer and 32-mer HB oligomers were successfully synthesized and they served as the sample materials mainly used in this project. All the experimental work and results analysis with these samples are reported in chapters 4–8, with each chapter focusing on specific areas of their crystallization behaviour. The studies from the HB oligomer growth both from the melt and solution show some fundamental differences in behaviour from other oligomers. It is hopeful that these differences could throw new light onto polymer crystallization studies.

This chapter reports the morphology and growth of HB 24-mer and 32-mer crystals crystallized from the melt. The chapter starts with a brief description of the sample preparation and experimental procedures. Then the spherulitic morphologies of HB 24-mer and 32-mer over a wide range of crystallization temperatures are shown. The band spacing and crystallization rates as a function of crystallization temperature are calculated and presented. Discussion and conclusions are given at the end of the chapter.

4.2 Experimental Method

4.2.1 Sample preparation

The HB 24-mer and 32-mer samples were synthesized using the segment coupling method developed by Professor Seebach and members of his group at ETH, Zurich. The HB 24-mer was kindly provided by Professor Seebach, and the 32-mer with benzyl protecting group was synthesized by the author at ETH Zurich. The detailed synthesis method to describe the coupling strategy is presented in section 3.3.3.3 in the previous chapter. The synthesis has been developed to produce an end product of 100% purity and more details can be found in [Lengweiler *et al.*, 1996; Fritz *et al.*, 1998; Seebach *et al.*, 1999].

Preparation of fully unprotected 32-mer sample was completed also by the author in the Department of Chemistry at the University of Bristol following the method used by the ETH group and the purity was confirmed by NMR and mass spectroscopy analysis. This reaction was shown in Figure 3.8 (b). Most samples used in the experiments described here were in the 'free' form, i.e. all protecting end groups had been removed. In some cases a HB 32-mer with a benzyl protecting group was used due to the limited availability of the 32-mer free sample. The 32-mer with the protecting group is referred to as 32-mer(p) in the text. The chemical structures of HB 24-mer, free and protected 32-mer are shown in Figure 4.1. The full structures for HB oligmers between 8 and 96 units will be given in chapter 6.

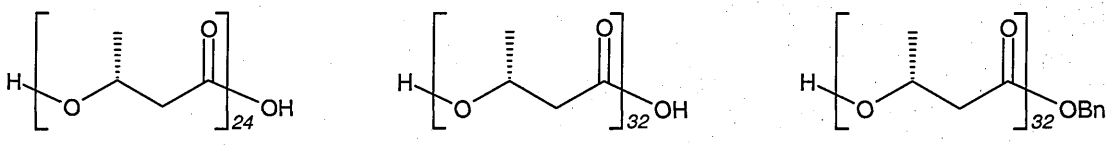

(a) (b) (c)

Figure 4.1 (a) 24-mer with no protecting end groups
(b) 32-mer with no protecting end groups
(c) 32-mer with benzyl protecting group, 32-mer(p)

4.2.2 Experimental procedure

The spherulitic morphologies of HB 24-mer and 32-mer crystals were observed directly in an optical microscope with crossed polarizers. Growth rates were then measured from observations of the growth of the chosen spherulites. Small samples of HB 24-mer, 32-mer and 32-mer(p) were prepared from the original as-received powders by melting them between two 6 mm diameter cover slips on a Linkam hot-stage. The typical conditions for melting were 0.5 minute held at ~170°C for HB 24-mer and ~180°C for 32-mer. The samples were then cooled at 80°C min^{-1} until they reached the required crystallization temperature, T_c. At this point a timer was started and digital photographs were taken at appropriate intervals as spherulites nucleated and grew at constant T_c, using a Pixelink digital camera attached to the top of the microscope.

The melting points of HB 24-mer and 32-mer powder samples were first measured using a Perkin-Elmer differential scanning calorimeter (DSC) 7. A small quantity (typically ~0.3 mg) of the HB oligomer solid powder was placed in an aluminium DSC pan and heated to melt the samples completely at 10°C min^{-1}, the melt temperatures for 24-mer and 32-mer are measured from the peak of the melting endotherms.

In order to extend the range of accessible crystallization temperatures it was often advantageous to use two hot stages:- melting the sample on the one and then rapidly transferring to a second, pre-set to the desired crystallization temperatures. A picture showing the two hot-stages used in this project is shown in Figure 4.2. This two hot-stage method could be used to avoid any complete crystallization during cooling at the higher supercoolings. Oligomer films (made between two cover slips) need to be transferred between the two hot-stages in the minimum possible time. Measurements were repeated using both one and two hot-stage methods where possible, and confirmed that the experimental set-up used here did not affect the results obtained.

It should be noted that the 'spherulites' grown from HB oligomer thin films referred to here are actually very thin two-dimensional 'disculites'. For convenience, the word spherulite will continue to be used in the text.

Figure 4.2 Photograph showing the two hot-stages used to grow HB oligomer spherulites from the melt in this project. Left hand side is a Linkam hotstage, right a thermal hotstage constructed for this project.

The growth rates were subsequently calculated from the increase in spherulite radius, r, with time t, during crystallization. A linear relationship will be seen until the spherulites start to impinge on each other. Each sample was used for several measurements, until degradation became apparent, which was indicated by a reduction in melting temperature. Since the HB oligomer spherulites have been observed to be all nucleated at around the same time, it suggests that the nucleation is primarily heterogeneous and hence it is not possible to measure the nucleation rates by counting the increase in number of spherulites growing over time.

4.3 Results

4.3.1 HB 24-mer spherulites grown from the melt

Figure 4.3 shows two sets of HB 24-mer spherulites growing at 63°C and 99°C with crystallization time indicated. The different morphologies will be discussed in a later section, where more spherulite morphologies over a wide range of crystallization temperatures will be presented.

(a)

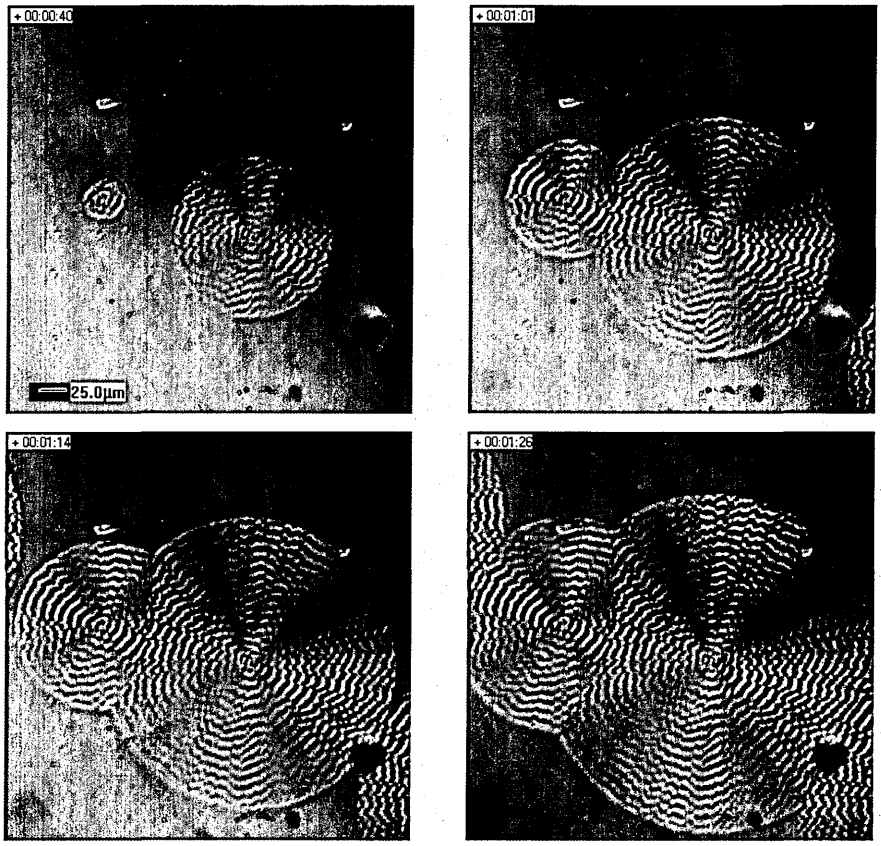

(b)

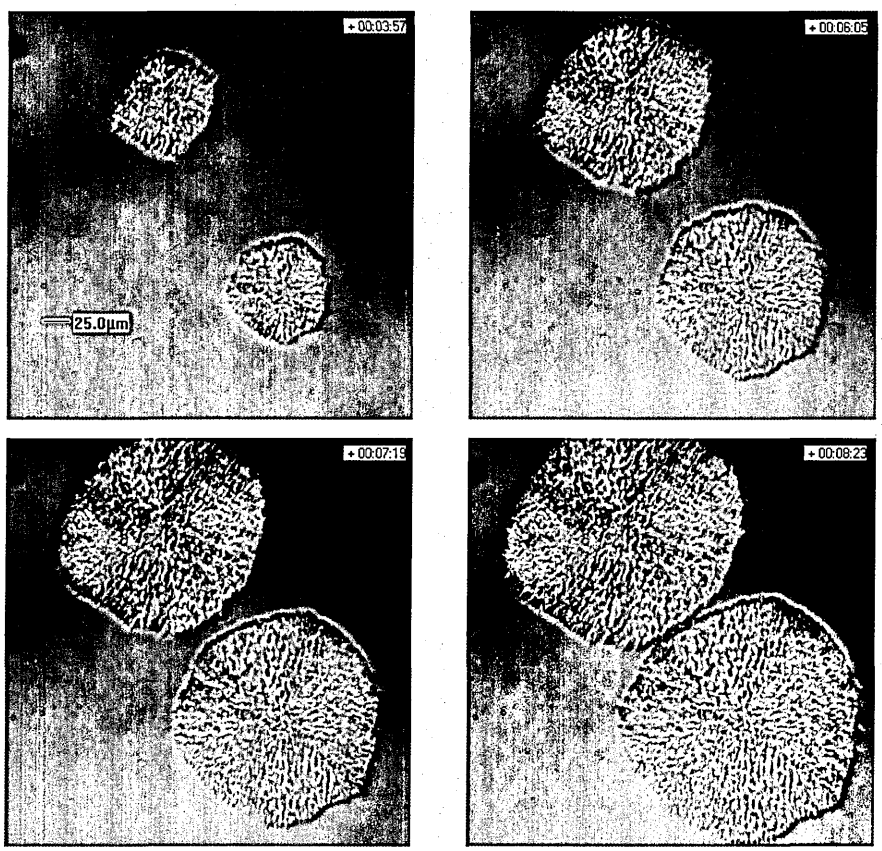

Figure 4.3 Examples of spherulites of HB 24-mer growing at (a) 63°C, (b) 99°C observed in optical microscope with crossed polarizers. The 25 µm scale bar applies to all figures. Crystallization times are as shown.

A typical set of data from which a growth rate was calculated is shown in Figure 4.4. Each set of points represents a different spherulite from the same sample, or, where very few spherulites were obtained, a different cross-section from the spherulite. In the few cases where the spherulites were not circular (as shown in Figure 4.3b) the longest dimension was always measured for consistency. The spherulite radius increased in a linear fashion as seen in Figure 4.4. A growth rate was then calculated from the gradient of each line and the average found. The values obtained from the individual spherulites within the same sample differ by less than 1%.

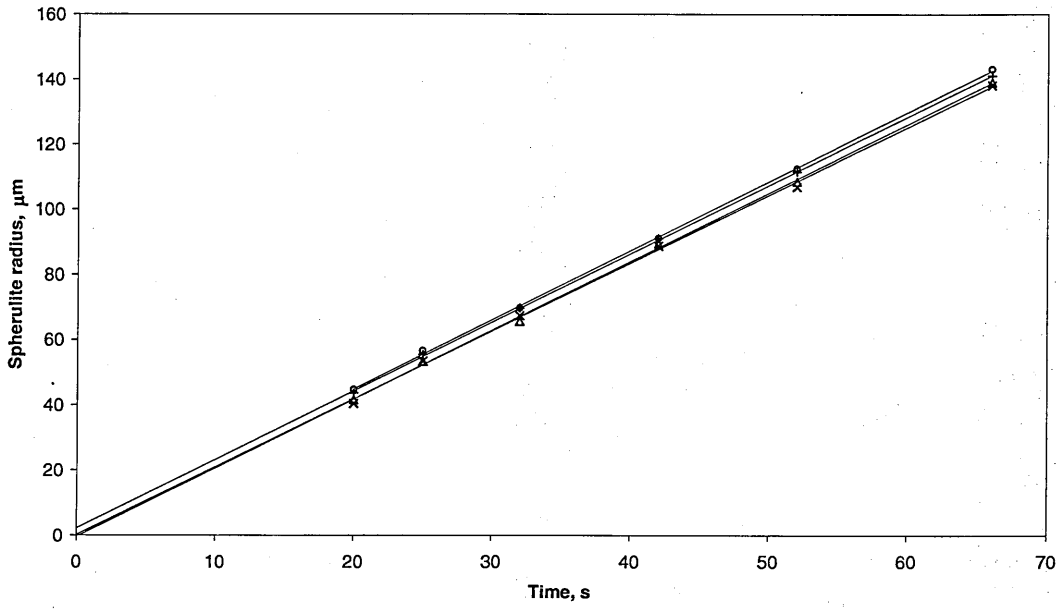

Figure 4.4 Spherulite radius as a function of crystallization time for four HB 24-mer spherulites growing at T_c = 82°C.

It is obvious from Figure 4.4 that the spherulites have all nucleated at around the same time – in this case close to $t_c = 0$. This was often (though not exclusively) found to be the case, and suggests that the nucleation is primarily heterogeneous. At the lower crystallization temperatures (and particularly where only one hotstage was used) spherulites often started to grow before T_c was reached (i.e. before $t_c = 0$). However, comparison of results from different spherulites and different samples confirms that this did not affect the subsequent rate of growth at T_c.

The growth rates of HB 24-mer spherulites as a function of crystallization temperature over the range of 40–120°C, is given in Figure 4.5. Each point is the average of

several measurements taken from different spherulites within the same sample, as described above. Where more than one point is plotted for a particular temperature these refer to independent measurements from different samples. The growth rate curve shown in Figure 4.5 has the distinctive form expected (but rarely fully accessible experimentally) from a crystallizable polymer. Similar curves have been obtained, for instance, from PHB and its co-polymers [Barham *et al.*, 1984; Organ and Barham, 1991], but this is believed to be the most complete curve obtained to date from an oligomer system.

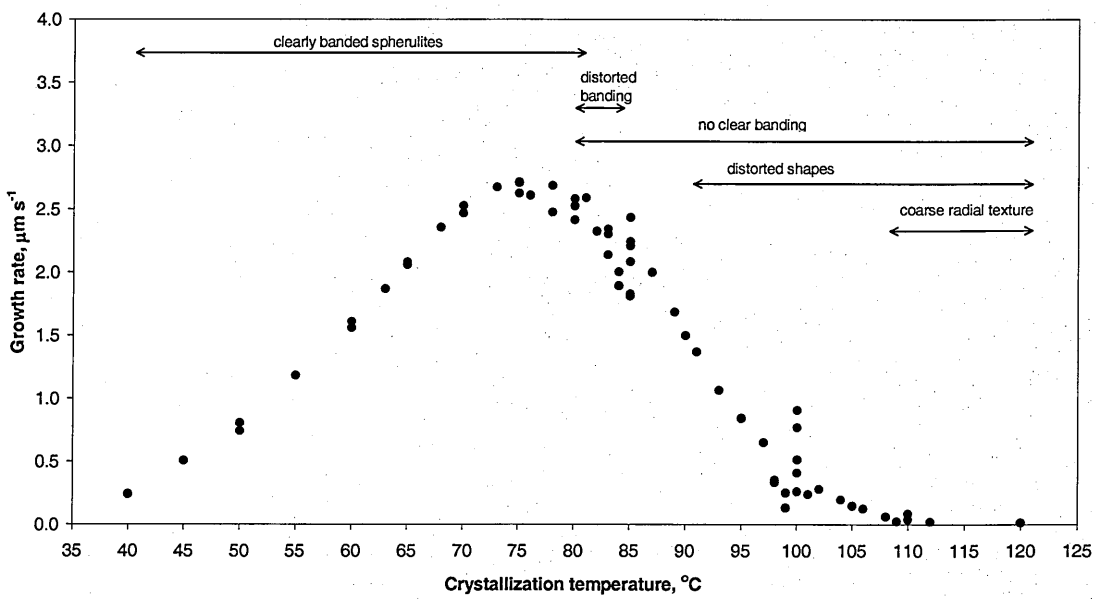

Figure 4.5 Growth rate as a function of crystallization temperature for HB 24-mer crystallized from the melt.

At the high temperature end of the curve, the growth rate rises as the crystallization temperature falls, due to the increase in thermodynamic driving force with supercooling. As the temperature is reduced further the growth rate passes through a maximum and then falls. This is due to reduced mobility of the chains as the viscosity of the melt increases: the crystallization rate is restricted to the rate at which chains can diffuse to the growing surface, and this falls with temperature. Apart from the very obvious peak in growth rate at T_c = 75°C there are two regions of the curve, at around 85 and 100°C, where the data is particularly scattered. These will be reserved to consider later in the discussion section.

Further examples of the HB 24-mer spherulite morphologies obtained over a wider range of temperatures are shown in Figure 4.6. These pictures have been chosen to illustrate spherulites of similar size to each other (the 25 μm marker shown in Figure 4.6a applies to all the pictures), but note that the corresponding crystallization times vary considerably, reflecting variations in both growth and nucleation rates. No attempt has been made to quantify nucleation rates, since most nucleation appears to be heterogeneous, but a general trend towards higher nucleation rates (and shorter incubation times) was observed as T_c was reduced.

(a) $T_c = 50°C$, $t_c = 1m\ 45s$

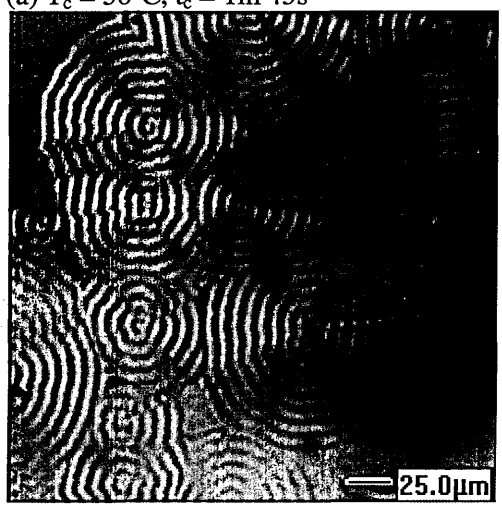

(b) $T_c = 55°C$, $t_c = 1m\ 37s$

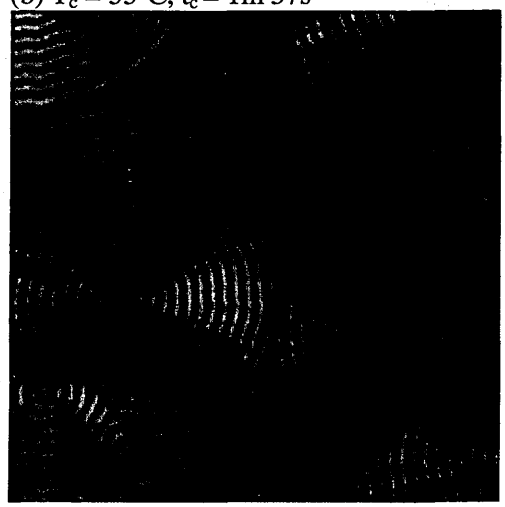

(c) $T_c = 75°C$, $t_c = 1m\ 11s$

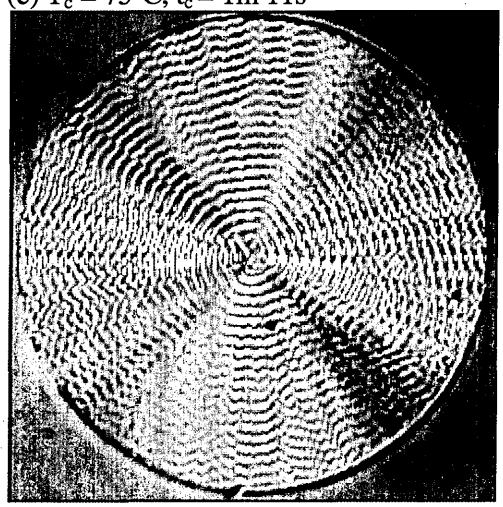

(d) $T_c = 85°C$, $t_c = 1m\ 27s$

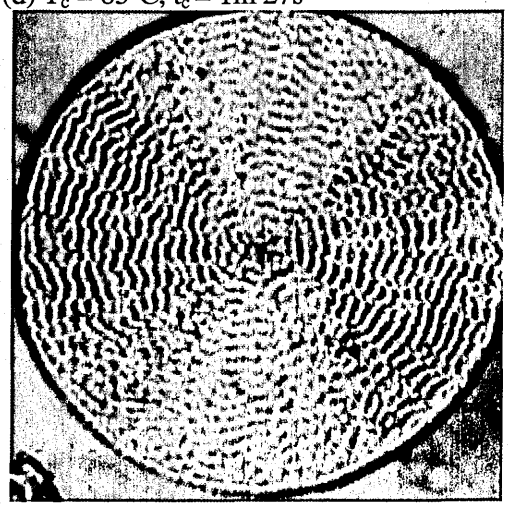

(e) $T_c = 90°C$, $t_c = 1m\ 6s$

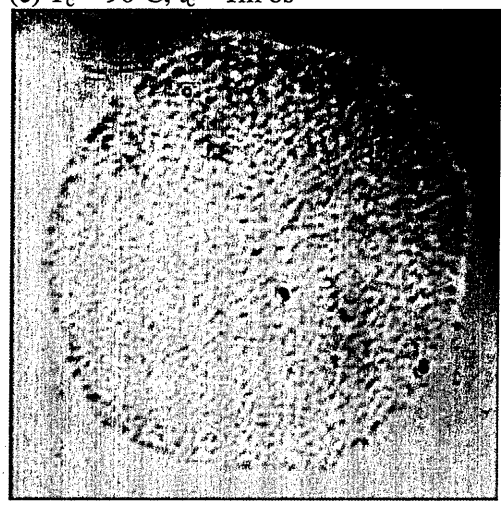

(f) $T_c = 98°C$, $t_c = 6m\ 46s$

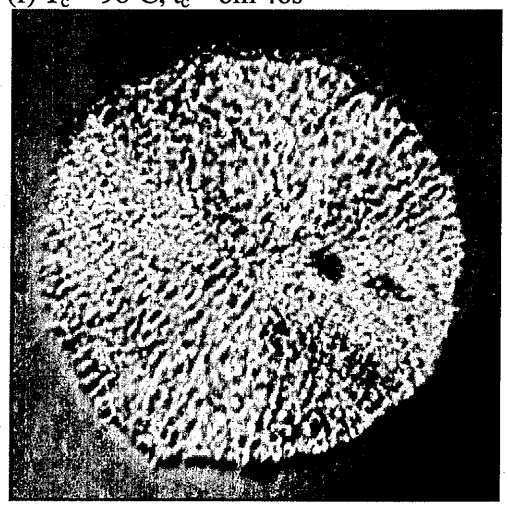

(g) $T_c = 100°C$, $t_c = 13m\ 41s$

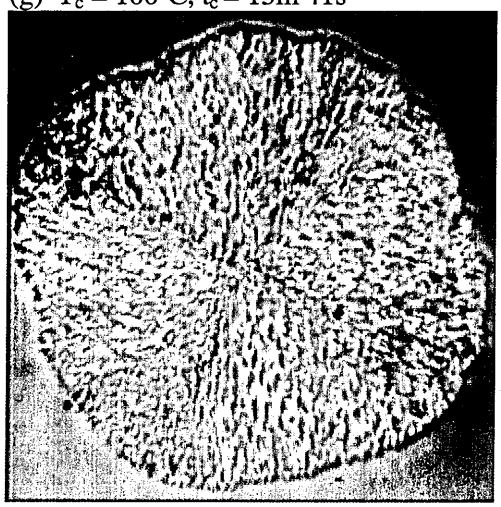

(h) $T_c = 101°C$, $t_c = 12m\ 32s$

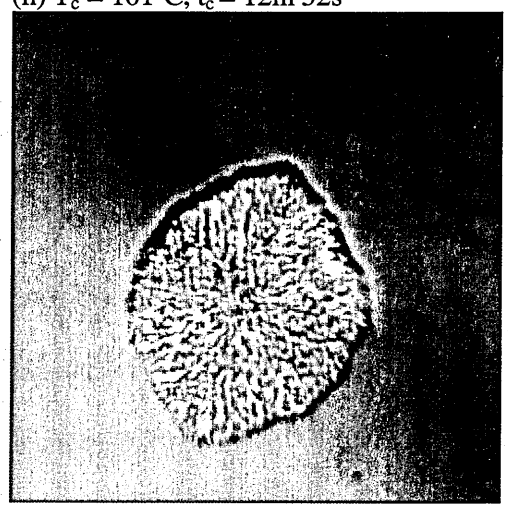

(i) $T_c = 112°C$, $t_c = 58m\ 18s$

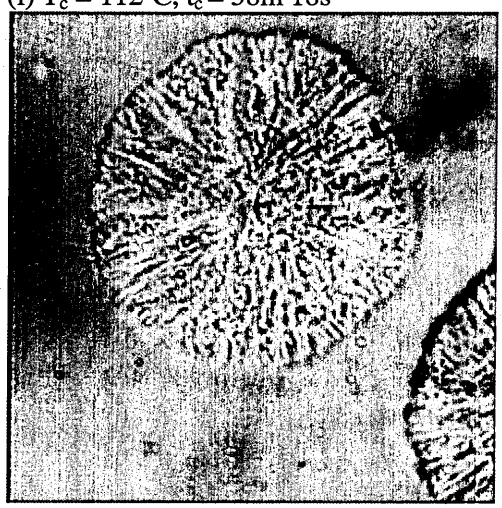

(j) $T_c = 120°C$, $t_c = 3hr\ 14m$

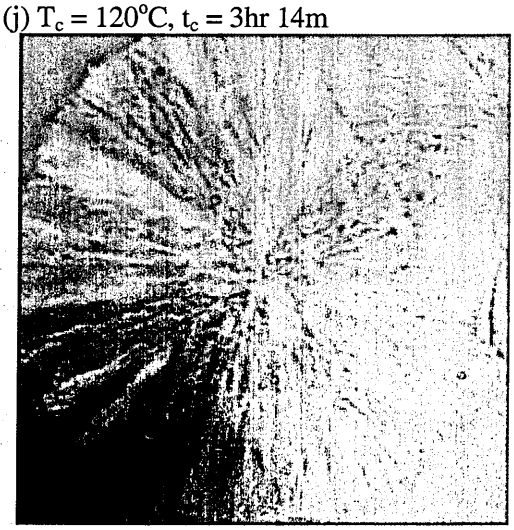

Figure 4.6 Examples of spherulite morphology obtained from HB 24-mer grown at different temperatures, T_c. Crystallization times (t_c) have been chosen so that the spherulites are of similar size. The 25 μm marker applies to all the frames.

The general types of spherulite morphology observed, and the temperature ranges over which they occur, are indicated by the text with the arrows in Figure 4.5. At crystallization temperatures of 80°C and below the spherulites are particularly distinctive, showing very clear and often extremely regular banding. Examples are shown in Figure 4.6 (a)–(c). The band spacing did not vary significantly with temperature, falling in the range 4–8 μm for the vast majority of samples. This is remarkably similar to the essentially constant band spacing observed in PHB over a similar temperature range [Barham *et al.*, 1984; Hobbs *et al.*, 2000]. Figure 4.7 shows band spacing as a function of crystallization temperature for HB 24-mer samples and includes PHB data from reference of Hobbs *et al.* [2000] for comparison. The sharp rise in band spacing seen at around 100°C in PHB was not observed in HB 24-mer samples. Instead, the regular banding begins to break down as the crystallization temperature is raised from 80 to 85°C. Some spherulites grown in this temperature range displayed a distorted band structure, such as that shown in Figure 4.6 (d), while in others no banding was visible at all. Above 85°C no clear banding was ever observed in the spherulites, see Figure 4.6 (e)–(j).

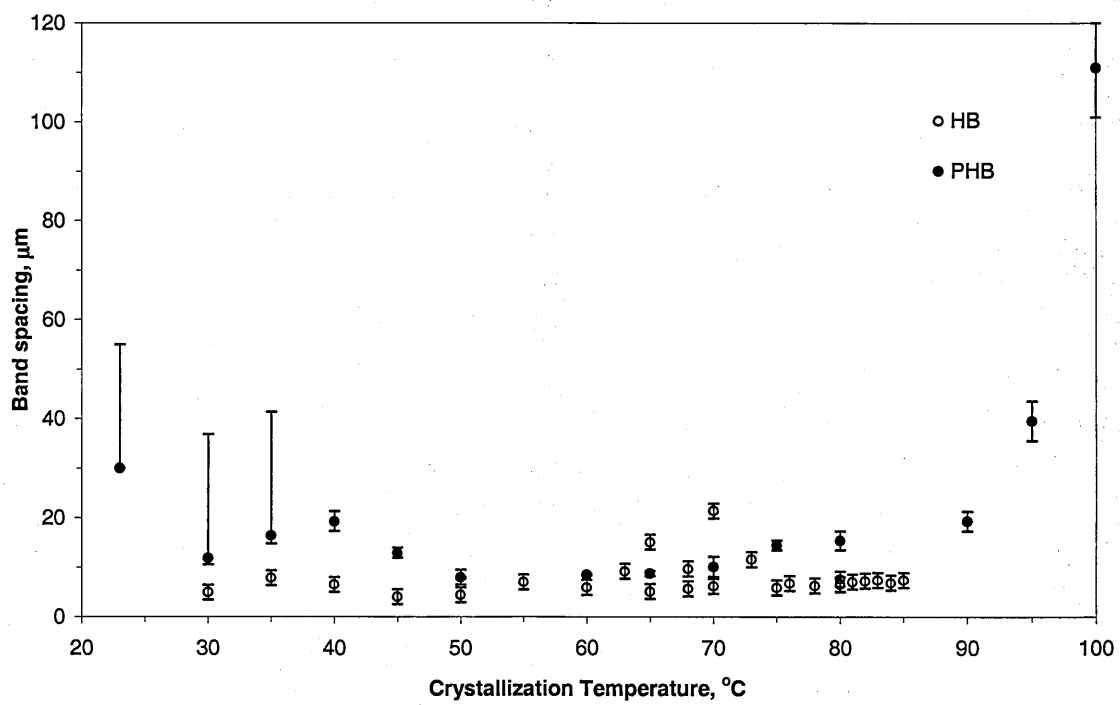

Figure 4.7 Band spacing in spherulites of 24-mer and PHB [PHB results from Hobbs, 2000].

At temperatures above 90°C the perfectly circular shapes began to look distorted and the outer edges less well defined. This is most apparent in Figure 4.6 (h) where the spherulites are distinctly asymmetrical. These entities are reminiscent of the structures described as hedrites, or axialites, sometimes observed in polymeric systems at high crystallization temperatures [Geil, 1960; Bassett *et al.*, 1963; Hoffman *et al.*, 1975] and believed to arise from large clumps of single crystals. A further, more subtle, change in morphology occurs at the highest temperatures (above ~110°C), where a coarse radial texture starts to appear. This is most clearly illustrated in Figure 4.6 (j). This coarse textured spherulite morphology was also observed in the 32-mer spherulites grown at high temperature given in next section. In fact, a clear morphological change from banded to coarse textured spherulites has been seen in PHB spherulites grown at the temperature range between 110 and 120°C, without any apparent discontinuity in the growth-rate gradient [Hobbs, 1996].

Significant differences in birefringence occurred in the non-banded spherulites. Figure 4.6 (e) shows an example of a spherulite grown at 90°C which displays very little contrast – indeed even the maltese cross is absent – while the spherulite grown at 98°C shown in Figure 4.6 (f) is much brighter. At crystallization temperatures up to ca. 80°C (where clear banding is seen) there is a general tendency for the magnitude of the birefringence to increase with increasing temperature. However, at higher crystallization temperatures the variations in birefringence showed no clear correlation with crystallization temperature, sample, or experimental method (use of one or two hot-stages). At the highest crystallization temperatures, where a change in crystal texture occurs, the birefringence was always low.

4.3.2 HB 32-mer spherulites grown from the melt

Experimental methods for growing and observing HB 32-mer spherulites are the same as those for the 24-mer. A few 32-mer crystals with no protecting ends were observed and captured for comparing with the 32-mer(p) samples, to look at any effect of a benzyl end group. A limited range of crystallization temperature between 100 and 128°C was chosen to perform all the experimental work with HB 32-mer, due to the accessibility of supercoolings with only one hotstage when these measurements were

made. In the case of 24-mer measurements, an improved two-hotstage method was developed to give a much wider range of supercoolings.

Figure 4.8 shows examples of a set of HB 32-mer(p) spherulites growing at 108°C with time indicated. The HB 32-mer(p) spherulites generally show circular spherulitic shape. There is no clear banding observed in these spherulites in the range of crystallization temperature described here. This absence of banding was also observed in the HB 24-mer spherulites grown at temperatures above ~90°C, see Figure 4.6 (e)–(j). Previous studies with HB 32-mer and 16-mer showed nice banding in the spherulites at lower crystallization temperature, as shown in Figure 4.9. Note that the HB oligomer samples used in Figure 4.9 are slightly different from those used in this work. The previous materials were synthesized by Seebach *et al* using a former coupling strategy (see section 3.3.3.2 in chapter 3), leading to two protecting end groups, benzyl at one end and 2-isobutyl at the other. Two examples of spherulites grown from 32-mer free samples at 107°C and 110°C with time indicated are given in Figure 4.10.

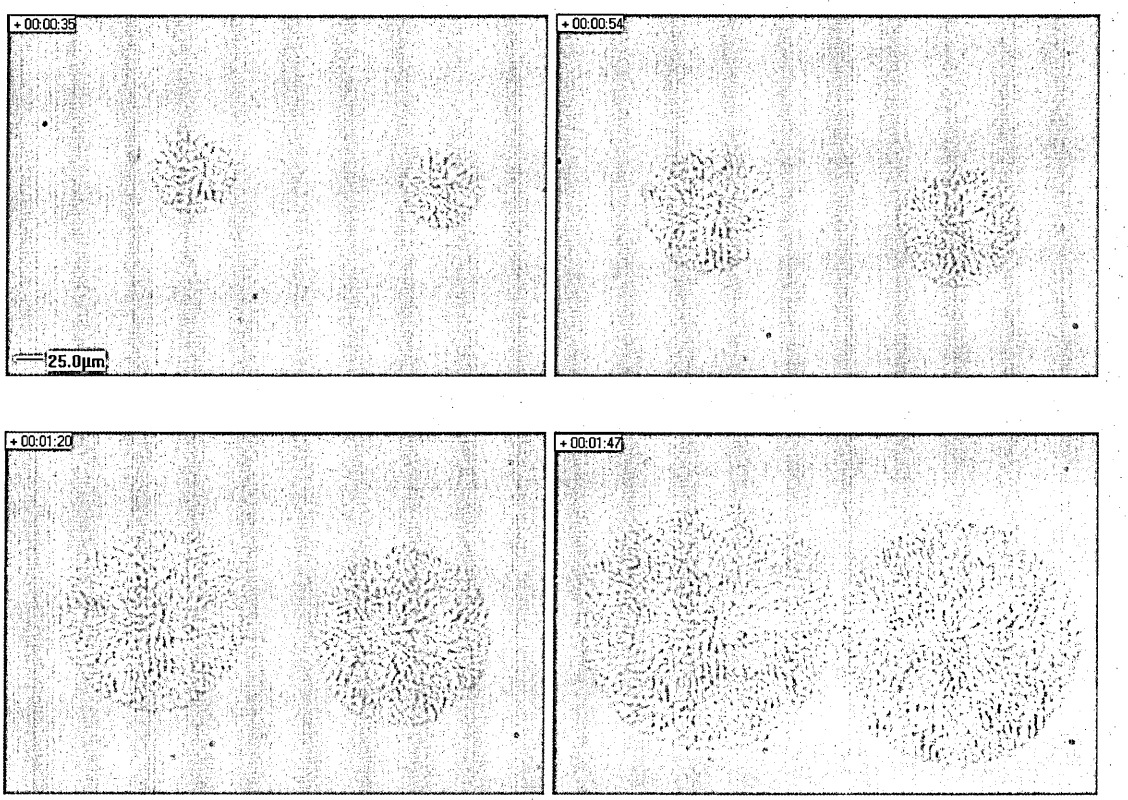

Figure 4.8 Examples of spherulites of HB 32-mer(p) grown at 108°C observed in the optical microscope with crossed polarizers. The 25 µm scale bar applies to all the figures. Crystallization times are as shown.

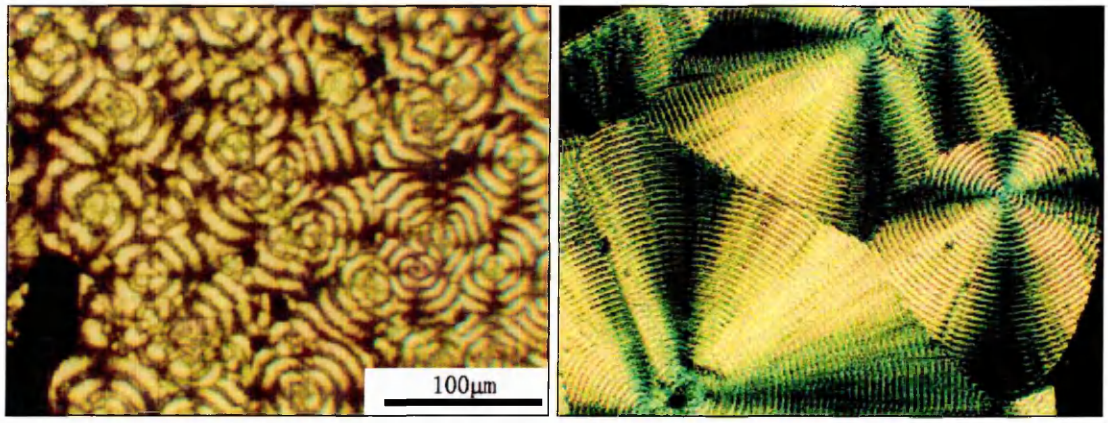

Figure 4.9 Micrographs of spherulites of HB 32-mer and 16-mer fully protected samples grown at 30°C [from Sykes, 1996]. The 100 μm scale bar applies to both pictures.

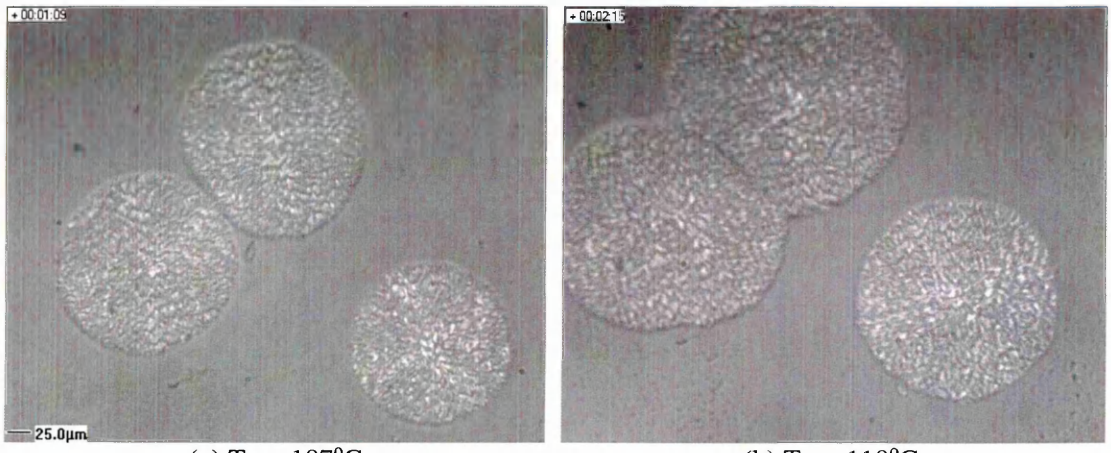

(a) Tc = 107°C (b) Tc = 110°C

Figure 4.10 spherulites of HB 32-mer(free) grown at (a) 107°C, (b) 110°C at time indicated.

The spherulite morphologies of 32-mer(free) crystals do not vary from the protected ones. Overall, they all have a circular spherulitic shape, without clear banding at crystallization temperature presented here. However, at the lower temperatures they do show clear banding, like those seen in Figure 4.9 (a) and PHB (see Figure 2.3a). This similar spherulitic shape from both free and protected 32-mer samples suggests that a benzyl protecting end group does not affect the crystal morphology. Hence, most of the later experiments chose the HB 32mer(p) instead of 32-mer free samples, due to the limited quantity of the solid powder available in the free form. More discussions on the effect of the benzyl end group on the behaviour of the 32-mer crystal growth during thickening and unfolding will be given in chapter 7.

Figure 4.11 gives some examples of spherulite morphologies obtained from 32-mer(p) grown at a range of crystallization temperatures between 102 and 128°C. Crystallization times have been chosen to give similar sized spherulites. The 25 μm scale bar in Figure 4.11 (a) applies to all the pictures. Again, no attempt has been made to measure the nucleation rates, since most spherulites appear to start growing at the same time, as mentioned for the 24-mer.

(a) T_c = 102°C, t_c = 22s

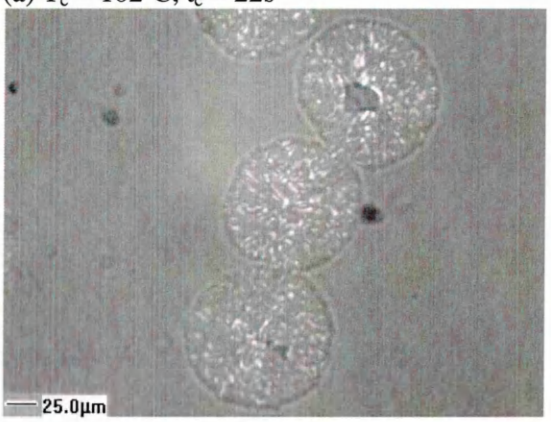

(b) T_c = 110°C, t_c = 1m 25s

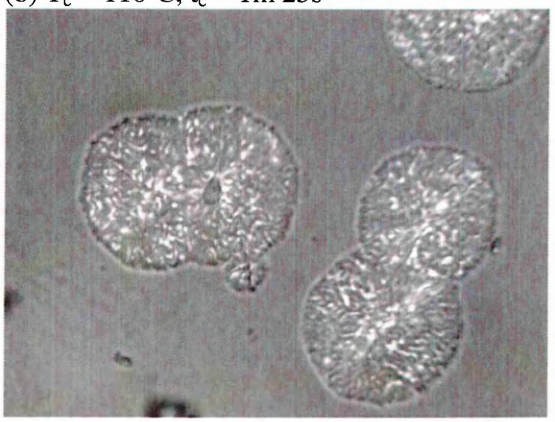

(c) T_c = 113°C, t_c = 1m 30s

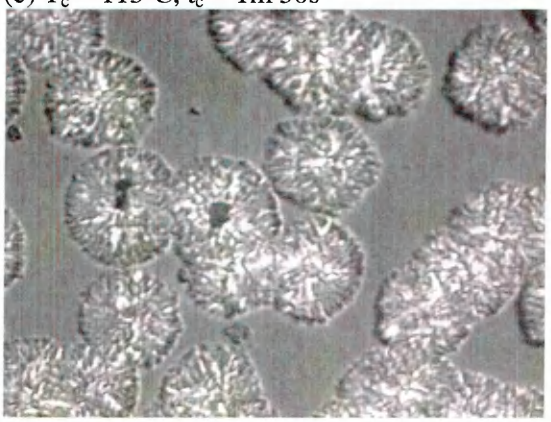

(d) T_c = 114°C, t_c = 2m 17s

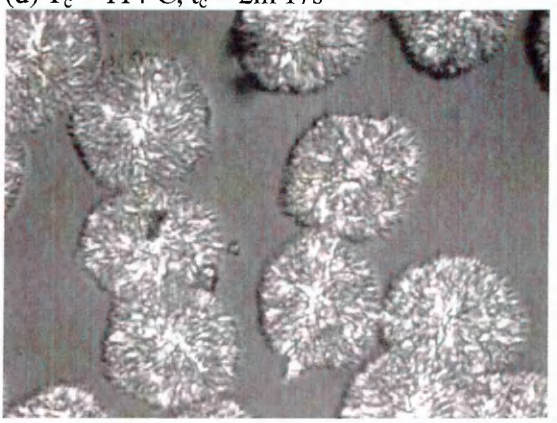

(e) T_c = 115°C, t_c = 3m 15s

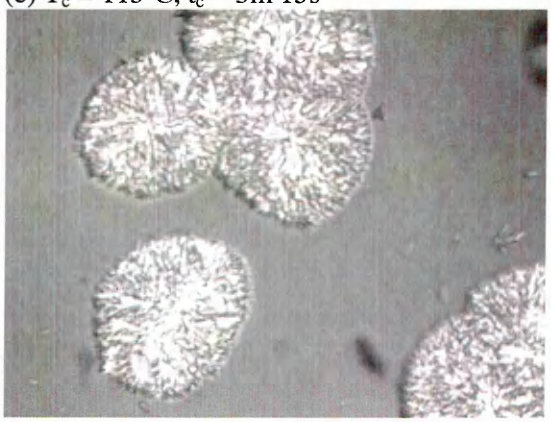

(f) T_c = 116°C, t_c = 3m 51s

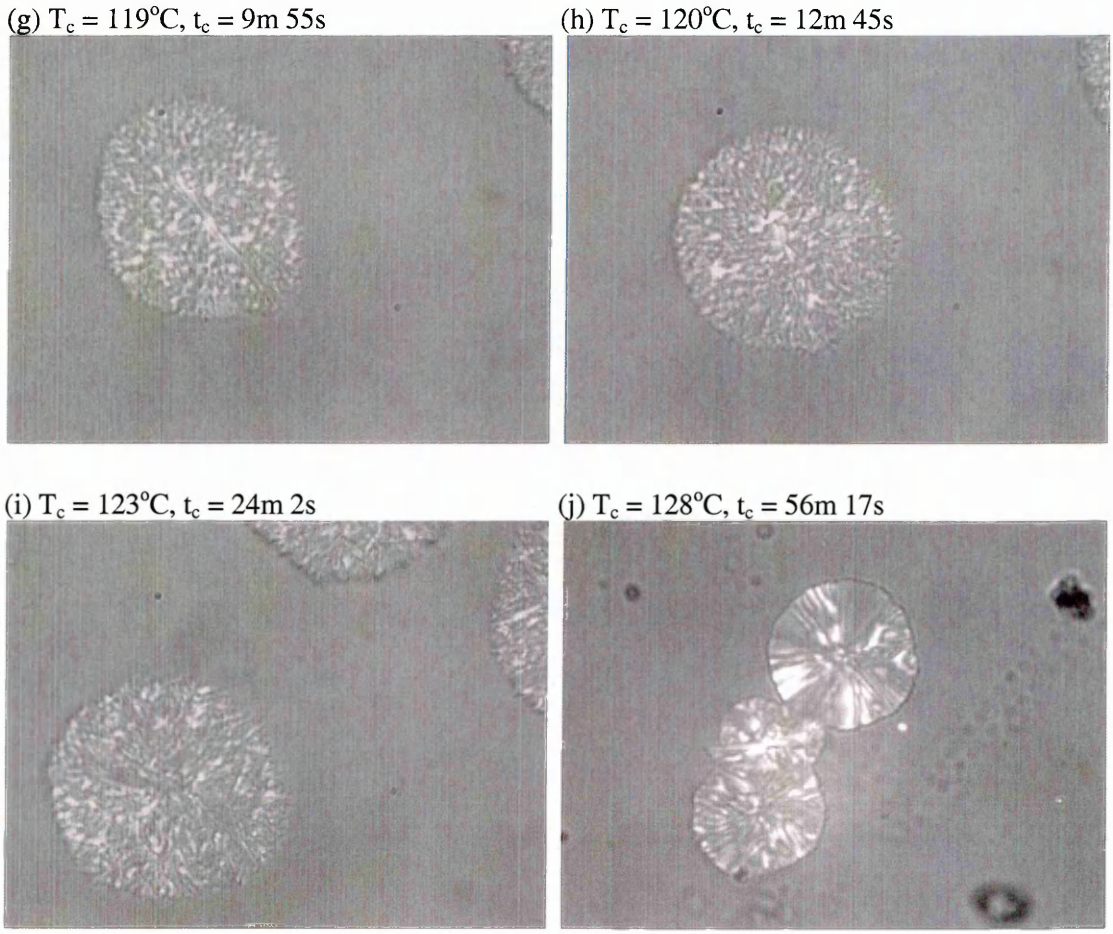

Figure 4.11 Examples of spherulite morphology obtained from HB 32-mer(p) grown at different temperatures. The 25 μm scale bar applies to all the frames.

All the 32-mer crystals show generally spherulitic growth as well. The spherulites grown at lower temperatures show circular shapes, a tendency to a less well-defined circular, or truncated lozenge shape, was seen at around 113°C to 119°C (Figure 4.11d–g). This shape change was more pronounced in HB 24-mer spherulites growth at above ~90°C (see Figure 4.6e–h). At the highest temperature, coarse textured spherulites were also observed in 32-mer (Figure 4.11j).

The growth rates measured directly from spherulites of both HB 32-mer(free) and 32-mer(p) samples are shown in Figure 4.12. Once again, the growth rate data from 32-mer free samples (as shown by crosses) show little difference to that of the protected ones. This suggests that the benzyl end groups have no effect on crystal growth rates as well as morphology. Since only limited supercoolings were accessible due to the

one hotstage method, the curve for 32-mer samples in Figure 4.12 only shows the right handed side of the full growth rate curve (see Figure 4.5) for 24-mer.

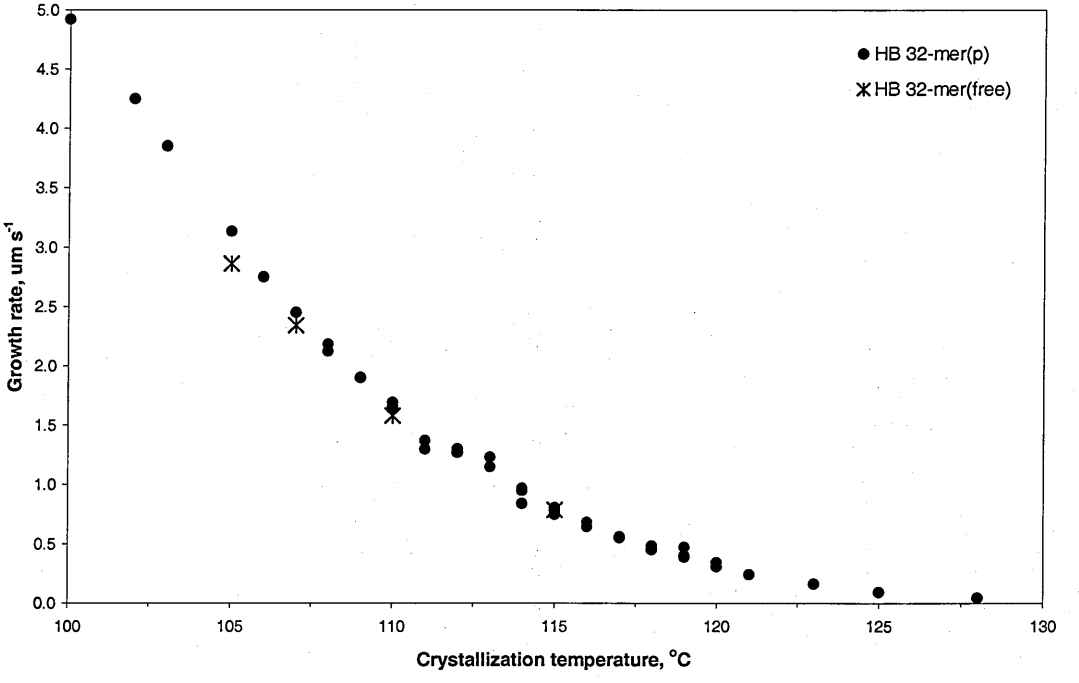

Figure 4.12 Growth rates as a function of crystallization temperature for HB 32-mer samples crystallized from the melt.

In the case of 24-mer growth, distorted banding or non-clear banding appeared at above ~80°C as arrowed in Figure 4.5, while in the 32-mer sample, no clear banding was observed in the range of crystallization temperature used here, i.e., above 100°C. According to the DSC results, the melting point for 24-mer is ~145°C and for 32-mer is ~160°C. This ~15°C interval in the melting points is comparable to the difference of temperatures at which the spherulite banding started to disappear for the two samples. Further experiments to examine the crystal thickness dependence (mainly from 24-mer) on the crystallization temperature will be given in chapter 6.

More interestingly, like the two scattered regions found in 24-mer growth rate curve at around 85 and 100°C, a very similar result has been showed in the 32-mer growth curve, Figure 4.12. At temperatures about 113 and 119°C, two subtle but notable discontinuities (or kinks) could be seen in the growth-rate gradient, although they are less pronounced than those found in the 24-mer.

4.4 Discussion

The results presented above provide complementary sets of data describing crystal growth rates and morphologies for HB 24-mer and 32-mer spherulites grown from the melt over a wide range of crystallization temperatures. To compare their behaviour to other oligomer system, in particular n-alkanes, some extended discussions are given as below.

4.4.1 Crystal growth rates

In previous work on n-alkanes and some of the PEO fractions, large changes in growth rate were seen near the temperatures at which the crystal growth changed between different integer folded (IF) chain forms. In many cases these changes were so pronounced that the growth rate passed through a minimum at, or close to, the transition temperature. At high temperatures only the thicker crystal form is stable, as the temperature is reduced it becomes possible for a thinner form to grow. The rate of growth of both forms increases with decreasing temperature, but they do not actually increase at the same rate so that at some temperature the thinner form can become the faster growing one. This on its own would lead to a graph of growth rate vs temperature with a number of branches, one for each thickness. In general, one would then expect the growth rate to follow the highest possible growth rate since the faster growing crystals would tend to dominate. Various explanations for the deviations from this behaviour with minima in growth rate at the transitions have been given, but essentially all are similar. If a thin crystal starts to form at the surface of a thicker one at a temperature where the thicker crystals still have a higher growth rate then growth is actually retarded, leading to a reduction in growth rate. The phenomenon is also referred to as self-poisoning, see section 3.2.3.4 in the previous chapter.

The data shown here do show some apparent discontinuities in growth-rate gradient of HB oligomers, particularly, for HB 24-mer at temperatures around 85 and 100°C. Similar but much weaker kinks were also found in the 32-mer at around 113 and 119°C. But all these discontinuities are less pronounced than the minima found in the alkanes. However, the small angle X-ray data and the unfolding transitions seen

during heating suggest that there may well be changes in the crystal thicknesses of the growing crystals near these discontinuous temperature regions. This specific aspect will be discussed in detail in chapter 7. The full set of crystal thickness data, obtained with HB 24-mer and 32-mer samples grown both from the melt and solution will be presented and discussed in chapter 6, where the growth rate curves will be considered further.

4.4.2 Spherulitic morphologies

It could be noted that, as already established for n-alkanes, the purity and monodispersity of the HB oligomer material does not prevent the formation of spherulites. This provides further evidence that theories of spherulite formation based on the segregation of impurities are not applicable to this system and, given the similarity in behaviour to PHB, are also unlikely to be the primary cause of spherulite growth in the polymer. Comprehensive review of this topic can be found in [Bassett, 2003].

The very distinctive band spacing of HB 24-mer spherulites obtained at crystallization temperatures of 80°C and below is remarkably similar to that observed in PHB, despite the fact that the crystals are somewhat thinner and the chains are substantially shorter. This implies that the band spacing is linked more to the nature of the chain than to its length. However, rather than the sudden increase in band spacing seen in PHB above 90°C, the banding in the HB 24-mer simply disappears, suggesting that a certain proportion of folds are necessary for banding to occur at all. Similar behaviour has been observed for n-alkanes, where banding has been reported in spherulites of $C_{294}H_{590}$ quenched rapidly from the melt but not in those grown isothermally at higher temperature [Bassett *et al.*, 1996].

Regular spherulitic growth continues up to temperatures of about 98°C in the case of the 24-mer, although at the higher temperatures the growth fronts become increasingly ragged in appearance. Figure 4.6 (e) shows one of several examples of spherulites with very low birefringence. This topic is not in the range of the research area here, but probably will lead to an interesting subject for future work. In brief it can be suggested that the low birefringence is due to a peculiar growth where the

spherulites grow from a cooler side of the cell towards the centre so that the optic axis moves towards the perpendicular to the slides. The actual temperature gradient across the cell and the overall growth rate allow the angle made by the optic axis to the cell to vary continuously with growth temperature so that low birefringence spherulites will grow at different crystallization temperatures depending on the precise experimental conditions. Similar variations in birefringence have been studied in PHB previously [Hobbs *et al.*, 2000].

The change in shape of spherulites, from circular to hedritic, at the higher crystallization temperatures follows that seen both in some polymer systems and in the n-alkanes [Bassett, 2003]. In general, a change to a hedritic morphology at higher crystallization temperatures has been attributed, phenomenologically, to reduced branching, possibly linked to a change in growth regime. It is also noted here that the most irregular spherulite shapes, particularly for the HB 24-mer, coincide with the temperatures where the discontinuities in the growth-rate gradient have been located. So it is also conceivable that different lamellae within the aggregate are growing with different thicknesses and hence at different rates.

The change in texture towards a coarser, more fibrillar nature at higher temperatures, seen both from 24-mer and 32-mer, can also be linked to the absence of branching. This has been clearly demonstrated by TEM studies of n-alkanes; indeed in that case spherulites do not form at all when crystals grow in the extended chain form [Bassett *et al.*, 1996]. Figures 4.6 (j) and 4.11 (j) show crystals of 24-mer and 32-mer grown at 120°C and 128°C respectively, which are believed to contain extended chains. While these crystals do have the general appearance of a spherulite, the much coarser texture and the clear linear radii produce a quite different texture to that observed at lower temperatures and suggest that branching is also greatly reduced, if not completely absent, here. More discussions on HB oligomer crystal morphologies associated with the crystal thicknesses and the chain conformation will be presented in detail in chapter 6.

4.5 Conclusions

From complementary observations of HB 24-mer and 32-mer spherulites grown from the melt over a wide range of crystallization temperatures, the spherulitic crystal morphologies were well defined using optical microscopy. The spherulites grown at lower temperatures are banded and look remarkably similar to those grown from the polymer, PHB. The band spacings are also very similar to those observed in PHB. As the crystallization temperature increased the banding disappeared, the shape of the spherulites became less regular, and a coarser texture associated with reduced branching developed.

Spherulites of HB 32-mer with and without protecting end group were observed and compared. Little difference has been found between these two types of 32-mer either in crystal morphologies or growth rates. This suggests that a benzyl protecting end group has no effect on spherulite morphology and growth. Further measurements to check the effect of the benzyl group when heating the 32-mer samples will be presented and discussed in chapter 7.

Spherulite growth rates have been measured over a very wide range of crystallization temperature. In 24-mer, the growth rates pass through a maximum at 75°C, and show a very similar curve to that measured from PHB. However, the measurements were unusually scattered at around 85 and 100°C for 24-mer, giving two noticeable kinks during the spherulite growth. A much weaker tendency for discontinuities in growth-rate gradient has also been observed for 32-mer at around 113 and 119°C. The features seen here, although less pronounced, could correspond to the growth rate minima found in the alkanes, where they have been linked to a change between preferred crystal chain conformations. Crystal thickness data associated with unfolding transitions on heating followed in real time using X-rays will provide more evidence for these claims, and will be reported and discussed in detail in chapters 6 and 7.

Chapter 5 Morphology and Growth from Solution

5.1 Introduction

A full set of morphology and growth rate data of HB 24-mer and 32-mer spherulites grown from the melt over a wide range of crystallization temperatures has been reported in the previous chapter, chapter 4. These results are very similar to those found in the n-alkanes and PEO fractions grown from the melt. More experiments with crystals grown from solution would provide an extended insight for comparing the crystallization behaviour of HB oligomers to other oligomer systems.

This chapter presents PHB and HB oligomer single crystal morphologies grown from solution, mainly from propylene carbonate, at different temperatures. Crystallization rates over a wide range of supercooling were measured by real time wide angle X-ray scattering at the ESRF Grenoble. The data will be reported and discussed in detail below.

5.2 Early Work on Growing PHB Single Crystals

Polymer single crystals were first inferred from the electron diffraction of *Gutta Percha* [Storcks, 1939]. However, this discovery was ignored until single crystals of polyethylene were grown from dilute solution in 1957 [Till, 1957; Keller, 1957 and Fisher, 1957]. Subsequently, single crystals of many other polymers were grown, e.g. [Geil, 1963]. As previously mentioned in section 2.2.1 in chapter 2, the electron diffraction patterns of the polyethylene crystals grown from dilute solution have revealed that the polymer chains are lying perpendicularly to the platelet, and therefore chain folding occurred [Keller, 1957]. Figure 5.1 (a) shows a well defined single crystal of polyethylene together with its electron diffraction pattern, (b) shows typical multi-layered polyethylene single crystals grown from dilute solution obtained by the author at the very beginning of this project.

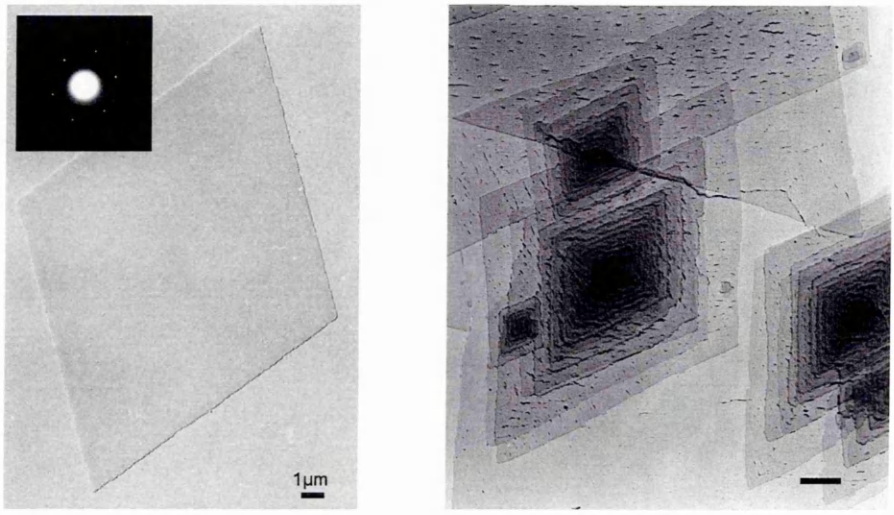

(a) (b)

Figure 5.1 Electron micrographs of (a) a well defined single crystal of polyethylene together with its electron diffraction patter (courtesy of SJ Organ); (b) typical multi-layered single crystals of polyethylene grown from xylene solution. The scale bars represent 1 μm.

PHB crystals were first grown from dilute solution in chloroform [Alper *et al.*, 1963]. They were seen to be thin, flexible lath shape with a distinct lamellar morphology, crystal thicknesses being ~5 nm. Wide angle X-ray and electron diffraction showed the chain direction to be perpendicular to the lamellar surface (Figure 1.3 in chapter 1). In 1957, Lundgren *et al.* observed that crystals grown from samples of PHB produced by different bacteria gave similar crystal morphologies. Marchessault *et al.* (1981) grew PHB crystals from dilute solution in a mixture of chloroform and ethanol, and the electron diffraction pattern from these crystals also confirmed the same *a* and *b* dimensions of the PHB unit cell found previously from X-ray diffraction [Cornibert and Marchessault, 1972; Yokouchi *et al.*, 1973]. The crystal structure of PHB is given in Figure 1.2 in chapter 1 at the beginning of this thesis. Later, more solvents to grow PHB crystals were tried and reported: propylene carbonate [Barham *et al.*, 1984; Welland *et al.*, 1989; Seebach *et al.*, 1994]; poly(ethylene glycol) [Marchessault *et al.*, 1988; Revol *et al.*, 1989]; toluene [Revol *et al.*, 1989]; octanol [Revol *et al.*, 1989] and triacetin [Lauzier *et al.*, 1992]. More information on PHB single crystals grown from a variety of solvents, molecular weights, concentrations and crystallization temperatures under similar conditions can be found in [Otun, 1985; Birley *et al.*, 1995; Sykes, 1996 etc].

Although PHB crystals could be grown from some solvent mixtures, such as chloroform/ethanol and dichloroethane/ethanol mixtures, it was considered preferable to use a single solvent as such a system can be better controlled. Propylene carbonate, being a poor solvent for PHB, was found to be the most suitable solvent. Crystals could be precipitated from dilute solution in propylene carbonate at temperatures up to ~90°C. For a full list of solvents to grow PHB single crystals, refer to [Otun, 1985 and Sykes, 1996].

To obtain crystals of a roughly uniform size, and in single layer rather than multi-layers, a technique called 'self-seeding' was used [Blundell *et al.*, 1966]. The process of self-seeding involves heating a crystal suspension to a seeding temperature, T_s, just above its visual clearing point. Minute particles, thought to consist of crystalline high molecular weight polymer which was stabilized by refolding, remain un-dissolved. The un-dissolved materials can act as nuclei for more crystals to grow on cooling the solution. The number of nuclei and hence the crystal size can be controlled by varying T_s over a small range [Organ, 1983; Otun, 1985; Sykes, 1996].

Once the crystals have grown, for most purposes, it is more convenient to suspend them in a volatile solvent rather than in the one in which they have been grown. The second solvent will be referred to as the 'new' solvent, while the first solvent will be called the 'old' solvent. The new solvent needs to be a non-solvent for PHB at room temperature, it also needs to be miscible with the old solvent. The whole procedure is usually referred to as 'solvent exchanging'. First the suspension is filtered at the crystallization temperature in order to remove any un-crystallized polymer from the crystal suspension, new solvent is then added. If cold solvent is added before hot-filtering, the crystal edges will become ragged as the polymer remaining in the solvent quickly crystallizes at the lower temperature. Traditionally, acetone, ethanol or methylated spirits have been used as the new solvents.

5.3 Experimental

PHB single crystals grown from propylene carbonate and a few other solvents, following the same self-seeding strategy, were first repeated at the beginning of this

project. Examples of electron micrographs will be presented later in this chapter for a review of PHB single crystal morphology. Only propylene carbonate was chosen as the solvent for all the HB oligomer solution crystallization experiments.

The same HB 24-mer and 32-mer (both free and protected) powders were used for solution grown experiments. The details of chemical synthesis and the sample preparation of the HB oligomer samples were described earlier in section 3.3.3.3 in chapter 3. Their full chemical formulae were given in Figure 4.1 in chapter 4.

5.3.1 Growing the single crystals

The PHB single crystals were grown from dilute solution following the same single crystal recipe described above, for more details see [Organ, 1983; Otun, 1985; Sykes, 1996]. The procedures mainly consisted of several stages: finding the right solvents; making up the solution ready for crystal growing; 'self-seeding' the solution then cooling to the crystallization temperature and holding for an appropriate crystallization time to obtain a suspension of single crystals; exchanging the solvents if necessary and finally observing by transmission electron microscopy (TEM). Propylene carbonate, octanol and toluene solvents were used to grow PHB single crystals for preliminary experiments in this work. When propylene carbonate was used as the solvent, the solvent was exchanged with acetone at room temperature after hot filtering with propylene carbonate since propylene carbonate has a low volatility at room temperature. The sample grids for TEM observation were then made.

Single crystals of the HB oligmers were grown from dilute solution with a concentration of ~0.1% (w/v) in propylene carbonate at the temperatures required. The self-seeding and hot solvent exchanging were not applicable to HB oligomer samples due to the limited availability of HB oligomer powders. In this case, the oligomer sample grids were left in the vacuum for a couple of days to evaporate off the solvent, propylene carbonate.

5.3.2 Transmission electron microscopy (TEM)

Crystals were prepared for Transmission Electron Microscopy (TEM) by placing a drop of the crystal suspension directly onto a carbon coated electron microscope grid, the solvent then being allowed to evaporate off in the vacuum. Some crystal grids were then shadowed by vacuum evaporation of a ~2 mm platinum/palladium alloy wire, at a distance over 6 cm and with an angle of approximately 30°, to enhance the contrast. This shadowing technique is especially necessary to observe the PHB/OHB crystals in the electron microscope, as they are relatively thin, with thickness only about 5 nm compared to 25 nm of polyethylene crystals. A Phillip 400 transmission electron microscope was used in this project with an operating voltage of 100 kV.

PHB and OHB crystals are susceptible to beam damage in the electron microscope. This takes the form of the disappearance of both the image and the diffraction pattern of the crystals. Under beam conditions such that the bright field image of the crystals is just visible, the diffraction pattern only lasts for about 3 seconds. Diffraction patterns were obtained from unshadowed crystals by reducing the brightness of the beam as much as possible so that the crystals were not visible in bright field. The specimen was then searched in diffraction mode until suitable crystals were found. The two dimensional shapes of the crystal will not be seriously altered by irradiation as the carbon film acts as an effective constraint to any dimensional changes [Grubb *et al.*, 1972]. Finally, a very short exposure time (~2 seconds) was chosen to minimize any beam damage while taking the photos and allow observation of electron diffraction patterns.

5.3.3 Atomic force microscopy (AFM)

AFM was first applied to polymers in 1988 [Albrecht *et al.*, 1988] and has since found many applications in polymer science. It can visualize objects on an atomic scale under the right conditions. The main principle of the AFM is the fact that with a spring of an appropriately small spring constant and mass, the atomic forces would be able to displace it in a detectable way. Consequently, the AFM does not measure forces directly, it rather measures the deflection of a cantilever caused by a force exerted on it. The cantilever possesses a sharp tip near its free end used to sense the

surface. A schematic view of the AFM operation is showing in Figure 5.2. The AFM can image polymer or oligomer specimens without the need for staining or etching.

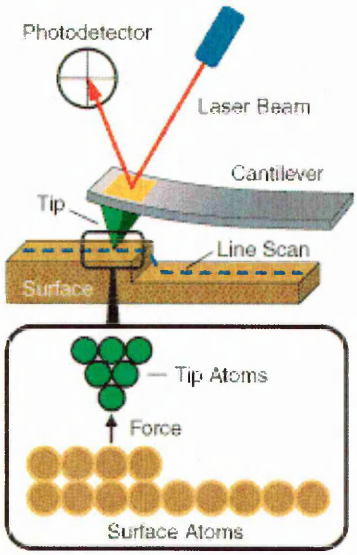

Figure 5.2 Schematic drawing illustrates how the AFM works [from Molecular Imaging Website, 2003].

AFM works by bringing a cantilever tip in contact with the surface to be imaged. An ionic repulsive force from the surface applied to the tip bends the cantilever upwards. The amount of bending, measured by a laser spot reflected on to a split photo detector, can be used to calculate the force. There are a number of different possible ways of controlling the cantilever-sample interaction during imaging. The most commonly used of these are contact mode and tapping mode. In contact mode the tip is kept within the repulsive regime of the inter-molecular force curve. The main drawback of this is that large lateral forces are exerted on the sample as the tip is 'dragged' over its surface. This frequently causes extensive damage to soft samples and can make imaging virtually impossible. In tapping mode the cantilever is oscillated at its resonant frequency and positioned above the sample so it only interacts with the surface for a small fraction of its oscillation period. This significantly reduces the lateral forces exerted on the sample, and has been successfully utilized in imaging soft, biological samples [Wawkuschewski *et al.*, 1995].

AFM was used here to observe the HB oligomer crystal morphologies to compare with the crystals observed under TEM. The crystal lamellar thicknesses were also measured with AFM to compare with the thickness data obtained by small angle X-ray scattering (SAXS). HB 24-mer and 32-mer powders were dissolved in propylene carbonate (with a concentration of ~0.02% w/v) in 1.5 ml test tubes, and the solutions left to crystallize for several days at the chosen temperatures in an oil bath. A drop of the crystal suspension was then put onto a freshly cleaned cover-slip or mica, and put under vacuum to evaporate off the solvent. The samples were observed in a Digital Instruments 'Veeco Dimension D3100' AFM, operated in a 'tapping mode' using silicon cantilevers with a nominal spring constant of 50 Nm^{-1} and resonant frequency of ~300 kHz at room temperature. Thicknesses measured with AFM are of an individual crystal, rather than the average over many crystals as measured by X-ray scattering. The AFM work presented here was kindly carried out by Dr JK Hobbs. The sample preparation was performed by the author, who was also present and helped to choose the crystals during the whole experimental work. AFM pictures of HB 32-mer single crystals and the thickness data will be presented and discussed in the results section.

5.3.4 X-ray scattering

Both wide and small angle X-ray scattering (WAXS & SAXS) were applied to HB oligomer samples grown from solution at the European Synchrotron Radiation Facilities (ESRF) Grenoble, France. The WAXS was used to follow crystal growth during crystallization from solution at desired temperatures and the results will be reported below. The SAXS was used to measure the crystal thicknesses, the experimental data and discussion will be given in the next chapter, chapter 6.

5.3.4.1 Wide angle X-ray scattering/diffraction (WAXS/WAXD)

The wide angle scattering measurements were carried out at the Materials Science beamline, ID 11, at the ESRF Grenoble. The X-ray wavelength was of 0.0496 nm, and the beam size was 300μm×300μm. Each two dimensional diffraction pattern was collected for 3 seconds using a Bruker Smart CCD detector, which in its high resolution mode has a sensitive area of 16×16 mm^2 consisting of 2000×2000 pixels

each of size 78×78 μm^2. The read-out time is necessarily slow and total dead time between exposures was 12 seconds. The sample detector distance was 0.2 m and was calibrated using a silicon standard. The resulting two dimensional patterns were corrected for spatial distortions prior to integration. After subtraction of the solvent (and glass tube) background, a pseudo-Voigt function was fitted to the one dimensional integrated data to produce values for the peak positions, full width at half-maximum (FWHM) and total intensity. No correction for thermal lag has been applied, although independent calibration available in a previous experiment suggests that this may be up to 2°C using the same experimental set-up [Terry *et al.*, 2003].

A measured amount of HB oligomers (typically ~0.3 mg) were placed in 2 mm diameter Lindemann tubes and sufficient propylene carbonate was added to give a concentration of approximately 3% (w/v). The Lindemann tubes were then shortened and flame sealed to prevent any evaporation of solvent during the experiments. For exposure to the X-ray beam the samples were mounted in a modified silver block Linkam hotstage (see Figure 5.3), with the tubes at an angle of about 45°C to the horizontal. The samples were positioned such that the X-ray beam passed through the tubes a few millimetres from their end and adjusted so that the solvent scatter was at a maximum, i.e. through the thickest available section of the tube. A metal cover was used to hold the sample tubes against the silver block, this ensured good thermal contact and allowed accurate positioning of the Lindemann tubes after changing the samples. The temperature of the silver block was recorded using the internal platinum resistor and the temperature at the start of collecting a diffraction pattern was recorded alongside the pattern.

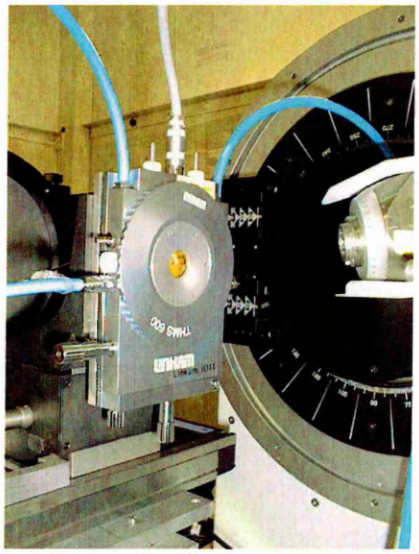

Figure 5.3 Picture showing a modified silver block Linkam hotstage mounted within the detector set-up at ID11 beamline at ESRF Grenoble [from ESRF official website].

Each sample was first heated to completely dissolve the HB oligomers, as evidenced by the disappearance of the diffraction pattern. The resultant solution was then cooled at 40°C per min until the desired crystallization temperature T_c was reached. The sample was then held isothermally at this T_c for certain time t_c until the crystallization was thought to be completed. The range of temperatures used was based on previous DSC measurements which, although not sufficiently well defined to allow growth rate measurements to be made, gave a good idea of the temperature range over which crystals would grow within a reasonable time scale. Crystallization temperatures for HB 32-mer were in the range 10–55°C. Most samples were used for several sets of measurement but were discarded as soon as they showed any anomalies in either dissolution behaviour (cross-linking due to beam damage eventually leads to an increase in dissolution temperature) or in background intensity level (due to solvent escaping from the tubes).

X-ray diffraction patterns were collected every 12 seconds with an exposure time of 1 second. The beam was turned off between exposures to minimize any radiation damage to the samples (bearing in mind the ease of degradation of PHB). The onset of crystallization could be clearly seen from the initial appearance of the diffraction pattern. Crystallization was allowed to proceed until a maximum intensity appeared to have been reached.

5.3.4.2 Small angle X-ray scattering (SAXS)

SAXS measurements with HB oligomer samples to obtain a full set of crystal thicknesses data over a wide range of crystallization temperatures were performed both at beamline ID2 ESRF and at Bristol University with a Bruker NanoSTAR X-ray system. Detailed results associated with the growth rate and crystal morphologies presented in chapter 4 will be given and discussed in chapter 6.

5.4 Results

5.4.1 Crystal morphologies grown from solution

5.4.1.1 PHB single crystals

PHB single crystals grown from dilute solution with different solvents were prepared during the first stage of this project following the same self-seeding strategy described above (see section 5.3.1). Examples of a set of electron micrographs of PHB single crystals grown from different solvents are given in Figure 5.4. Two types of molecular weight PHB powder were used here. One is PHB batch G04, with a polydispersity (M_w/M_n) of ~2, and a weight-average molecular weight (M_w) of 159,000. Another PHB sample is G08, with polydispersity of ~4 and M_w of 25,500.

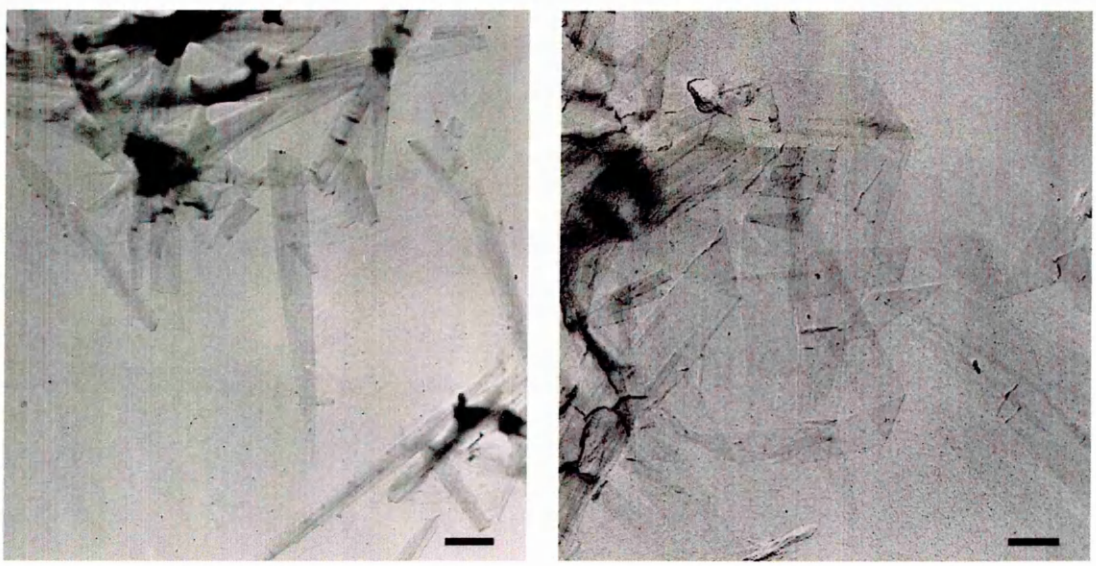

(a) (b)

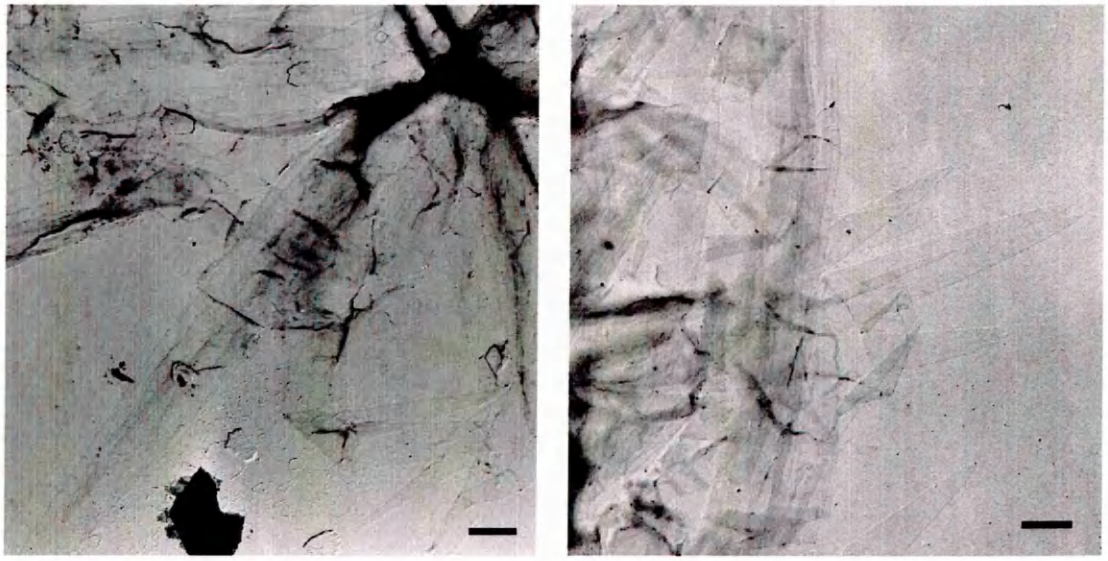

(c) (d)

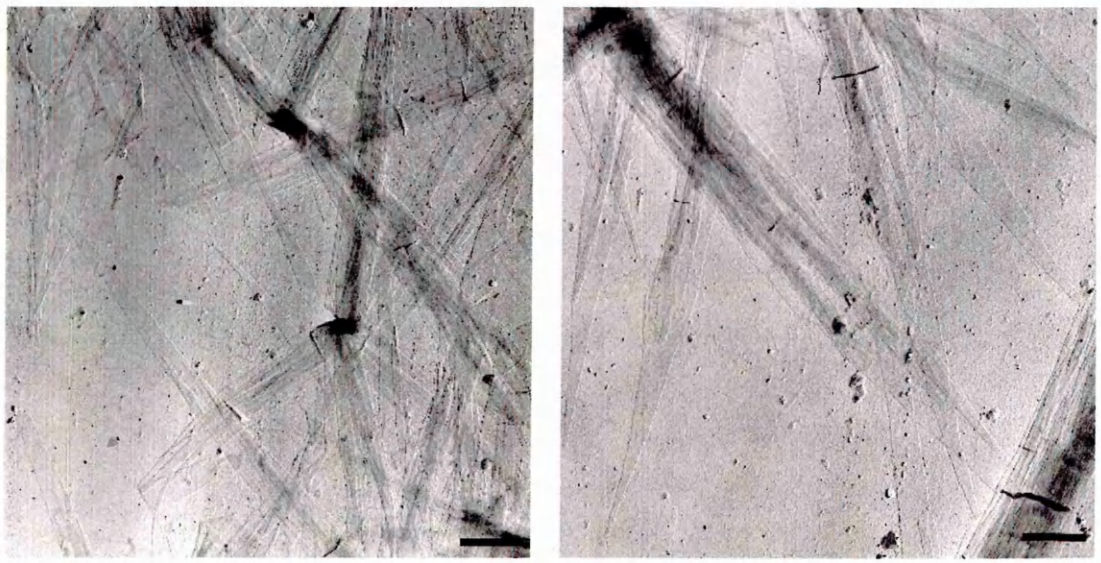

(e) (f)

Figure 5.4 Electron micrographs for PHB single crystal grown from different solvents at certain crystallization temperatures, scale bars represent 1μm.

(a) PHB (G04) single crystals grown from octanol at 80°C
(b) PHB (G04) single crystals grown from octanol at 97°C
(c) PHB (G04) single crystals grown from propylene carbonate at 60 °C
(d) PHB (G04) single crystals grown from propylene carbonate at 82 °C
(e) and (f) Low molecular weight PHB (G08) single crystals grown from toluene at room temperature

Electron micrographs in Figure 5.4 show typical examples of the morphology of PHB crystals grown from dilute solution. In general, crystals grown from all solvents were elongated lath-like shape crystals similar to polypropylene single crystals [Sauer *et*

al., 1965]. These crystals also showed some evidence of a flat surface at the growing tip. In all the preparations, there was considerable aggregation of crystals, which are visible in each picture as the dark colour centres. The appearance of the crystals varies a little depending on several factors, such as crystallization temperature, solvent and molecular weight. More detailed information has been reported in previous work on PHB [Otun, 1985; Sykes, 1995; Birley *et al.*, 1995], and is not the main focus within this project.

5.4.1.2 HB oligomer single crystals

The HB oligomer single crystals grown from dilute solution had an appearance very similar to those grown under similar conditions from the whole polymer, PHB. Example electron micrographs taken from typical HB 24-mer and 32-mer crystals grown from solution, together with the electron diffraction pattern are shown in Figure 5.5. AFM images of 32-mer crystals grown from propylene carbonate solution at different temperatures with height scans are given in Figure 5.6 and 5.7.

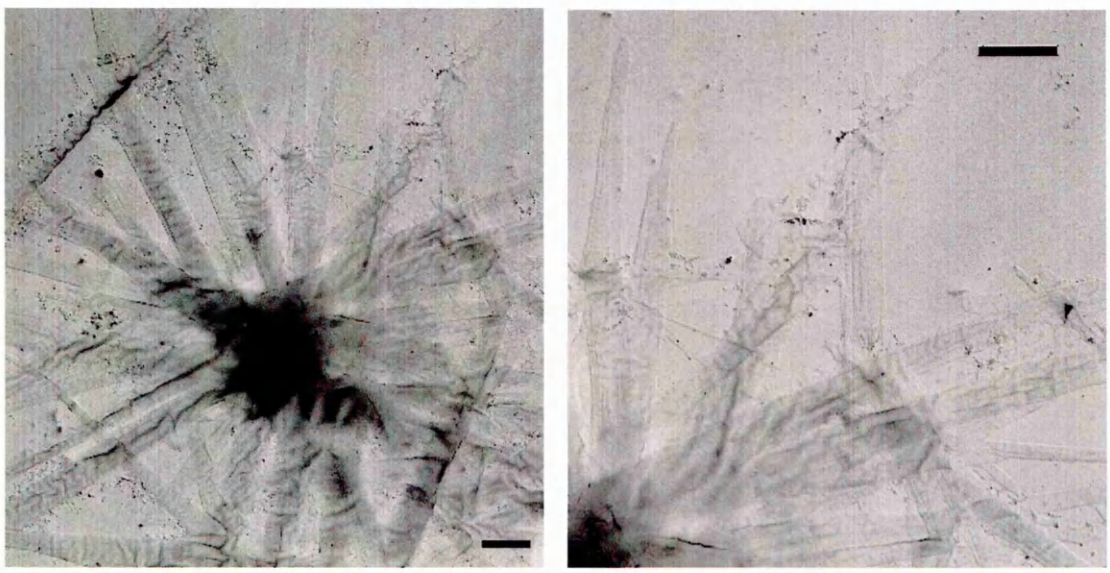

(a) (b)

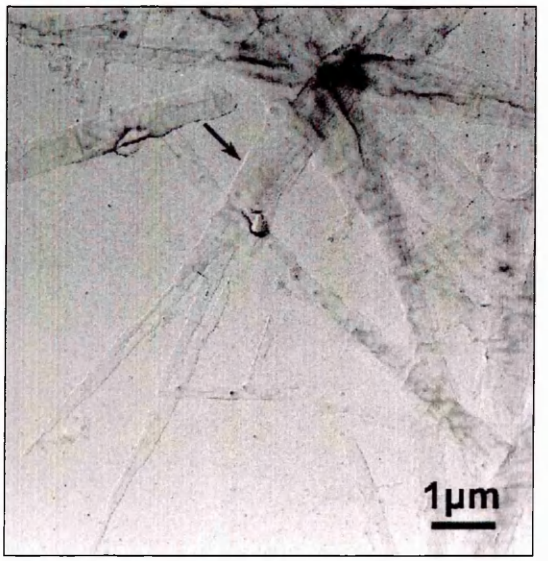

(c)

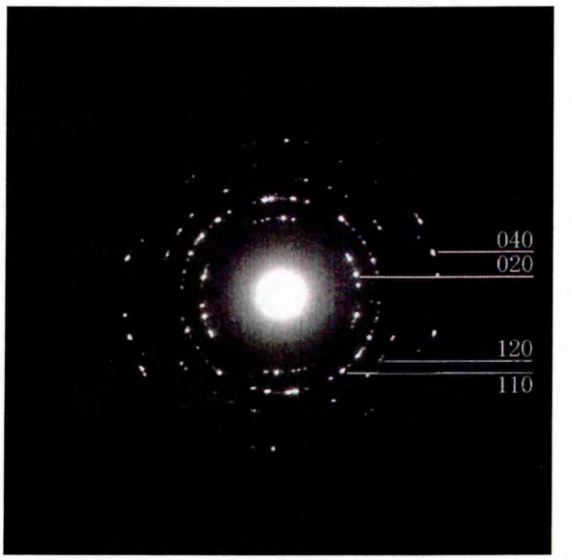

(d)

Figure 5.5 Electron micrographs of HB oligomer crystals grown from 0.1% (w/v) solution in propylene carbonate: (a) and (b) HB 24-mer crystals quenched at 10°C; (c) HB 32-mer at room temperature; (d) Electron diffraction pattern of 32-mer single crystals with reflections indexed taken from the area in (c) as the arrow indicated. Note the clear spots in this diffraction pattern suggest that several crystals are overlapping in the selected area from which the diffraction pattern was taken. Scale bars represent 1 μm.

Again, the electron diffraction pattern from HB 32-mer crystals indicates that the chains are perpendicular to the crystal lamellar planes, as in PHB (see Figure 1.3 in chapter 1). All the diffraction spots can be indexed as being *hk0* reflections, albeit from several different crystals lying with their long axes pointing in different directions within the plane of the sample. It should be also noted that the diffraction pattern of the HB oligomers is almost identical to that of the PHB crystals so that the indexing is based on the known unit cell of the polymer.

The AFM images of HB 32-mer crystals grown in propylene carbonate show similar morphology to the electron micrographs. Two possibly overlapping layers can be seen at the growth front in the right bottom of Figure 5.6 (a), suggesting a single layer of lamellar thickness of ~4.1 nm. At higher crystallization temperatures, the crystals have more smooth edges as shown in Figure 5.7, and are similar to those found in PHB single crystals see Figure 5.4 and [Sykes, 1996].

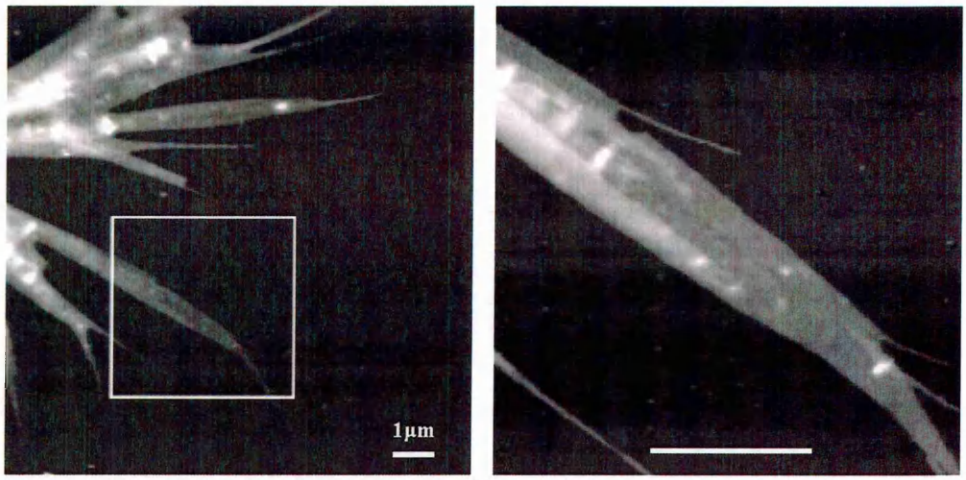

(a)

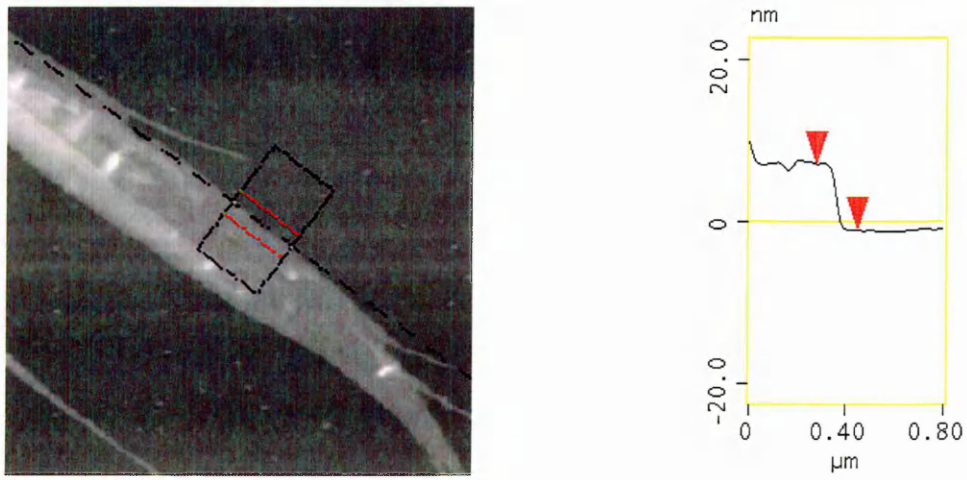

(b)

Figure 5.6 AFM images of HB 32-mer crystals grown in ~0.02% (w/v) propylene carbonate solution at room temperature. (a) Images of a crystal aggregate, scale bars represent 1 µm; (b) Image of the magnified area showing with a height scan of ~8.21 nm (possibly with two layers of single crystals).

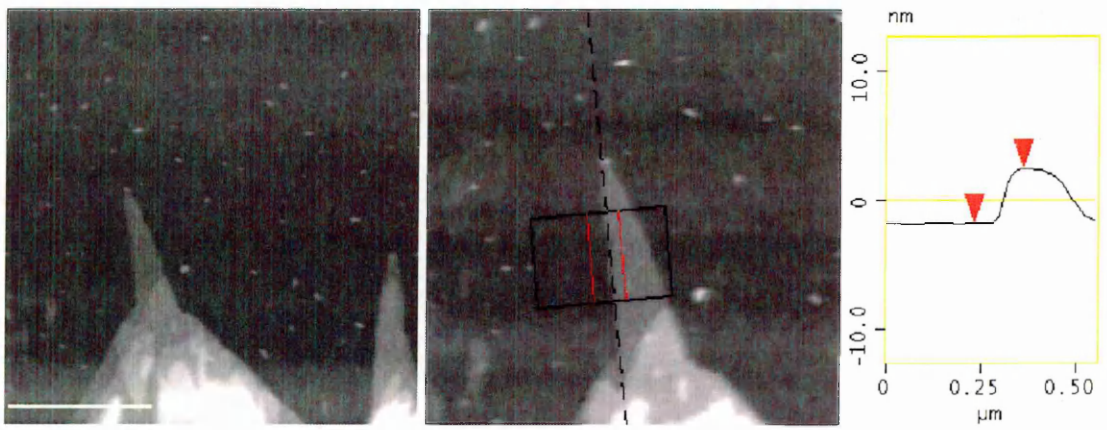

Figure 5.7 AFM images of HB 32-mer crystals grown in ~0.03% (w/v) propylene carbonate solution at 50°C. The height scan gives a single crystal thickness of ~4.21 nm. Scale bar represents 1 µm.

5.4.2 Crystallization rates from solution

Crystallization rates have been measured in solution grown n-alkanes by following the development of dissolution endotherms over time in the DSC. Attempts to apply the DSC method for measuring crystallization rates on the HB oligomers grown from solution were unsuccessful. Dissolution endotherms were typically very broad, making both the peak position and the peak area difficult to measure precisely. An alternative method based on the use of synchrotron X-ray radiation has recently been reported for n-alkanes [Terry *et al.*, 2003] in which the growth rate is determined from measurements of the area of the crystalline diffraction peaks over time as the crystals are grown in situ. This method, originally developed to allow measurements of growth rates too fast to be followed by DSC, was successfully applied to the HB 32-mer and 24-mer crystallized from solution and the results are reported here. The high intensity of the synchrotron radiation allows clear diffraction patterns to be obtained for crystal concentration as low as 0.1% (w/v) and the high resolution of the detector employed permits very small changes to the lattice parameters to be observed and measured.

5.4.2.1 HB 32-mer

A typical example of wide angle diffraction data obtained from a ~3% (w/v) suspension of HB 32-mer crystals grown in propylene carbonate after subtraction of solvent background is shown in Figure 5.8. Some amorphous halo arising from the solvent is still visible, but the main crystal reflections stand out clearly. An additional background subtraction was carried out for each peak individually based on curve fitting to sections of the spectrum on either side of the peak: this enabled peak positions and areas to be calculated to a high degree of accuracy. Figure 5.9 shows a series of plots showing how the intensity of the (020) reflection increases over time during crystallization at different crystallization temperatures, T_c. Similar results were obtained using the (110) reflections. The time is measured from the onset of crystallization: in practice there was occasionally an incubation time before crystallization began but, in contrast to the rate, this varied depending on the thermal history of the sample and was not considered reliable. In particular, the incubation time was considerably longer the first time a sample was used which suggests that

some sort of seeding mechanism was involved for subsequent crystallizations which affected the onset of crystallization but not the growth rate. A crystallization rate can be measured from the maximum gradient of the linear portion of the graph. The decrease in rate as the crystallization temperature increased is very apparent. The intensity reaches a plateau as the material in solution is exhausted, as can be seen at the lower crystallization temperatures in Figure 5.9. This maximum intensity (T_c = 10°C) is taken to represent 100% crystallinity.

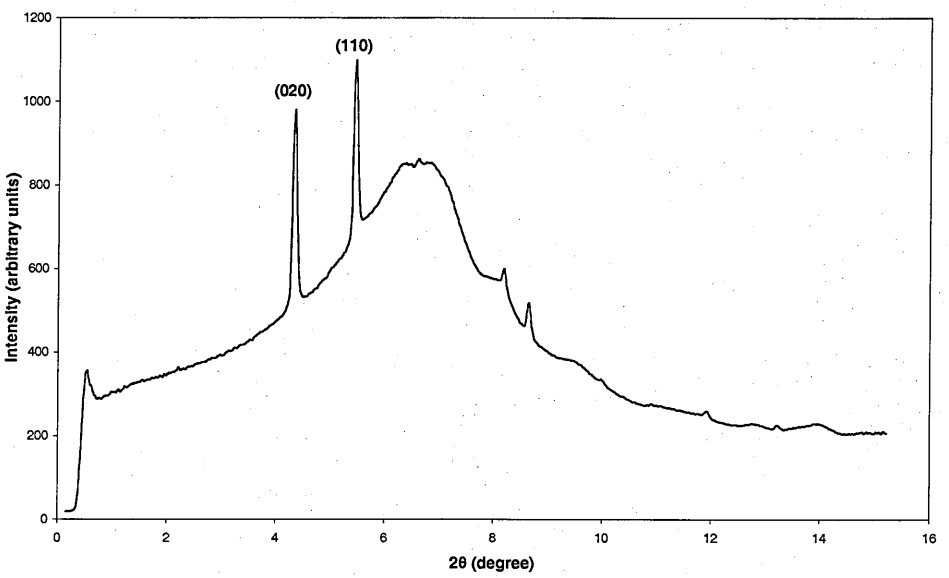

Figure 5.8 Typical wide angle diffraction data obtained from a 3% (w/v) suspension of 32-mer crystals in propylene carbonate during crystallization at 10°C after partial subtraction of solvent background. Two strongest diffraction peaks with main crystalline reflections (020) and (110) are indicated.

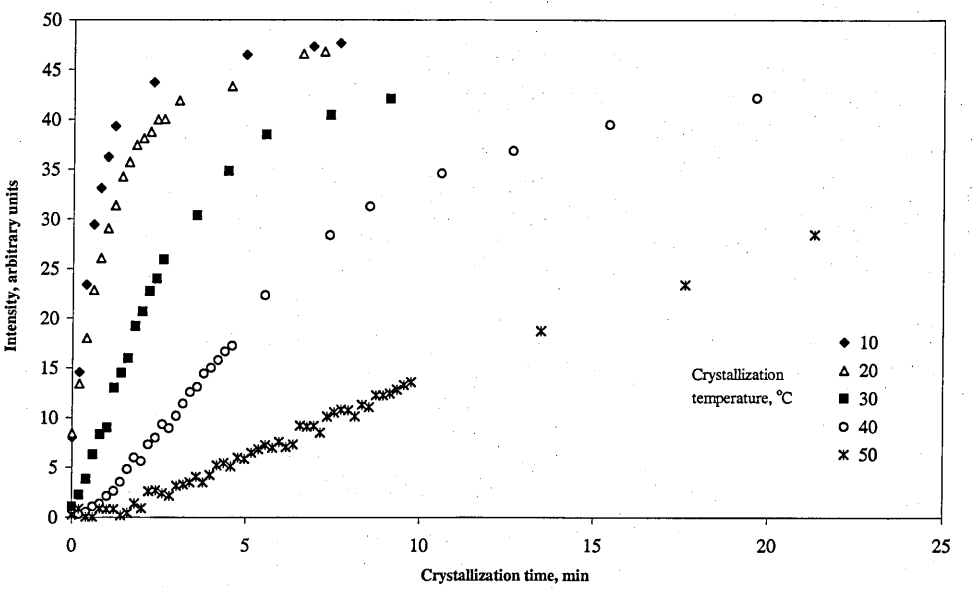

Figure 5.9 Intensity of the (020) reflection as a function of time during crystallization of 32-mer at the temperature shown. Crystallization rate is measured from the maximum gradient of the initial linear portion of the graph.

All the curves in Figure 5.9 were obtained from consecutive measurements on the same fixed sample. No more than five sets of measurements were made on a single sample to avoid possible discrepancies arising from radiation damage. Measurements were occasionally repeated to ensure consistency. Crystallization rates were measured over a range of temperatures using three different samples, by measuring the maximum slope of the linear portion of the intensity vs time at each temperature. Since the quantity of sample exposed to the beam is not known the results are in arbitrary units, which are consistent for a given sample but differ between samples. When combining the three sets of results it was necessary to normalize them and this posed some difficulties. Small differences in concentration or in the position of the sample in the beam could lead to substantial variations between samples in both the absolute intensity and the maximum intensity after background subtraction. Figure 5.10 (a) shows the raw data from the three sets of crystallization rate of the (020) reflection measurements. Each set of measurements is internally self-consistent, but it is clear that some scaling is required in order to combine them in a meaningful way. It was decided to take a pragmatic approach and to scale samples 1 and 3 to sample 2 by assuming that where a measurement had been made at (or close to) the same temperature in two different samples, the rate should be the same. The scaling factors were calculated at 40°C for sample 1 and 37°C for sample 3 and applied to all the data in that series. The result is shown in Figure 5.10 (b). In the raw data from sample 1 alone there appears to be a discontinuity in growth-rate gradient in the range 30–40°C and later results confirm that there is a transition from extended chain growth at 40°C to folded chain growth at 30°C (this will be presented in chapter 8). If the normalization is accepted then the discontinuity is revealed more clearly at around 36–37°C: this tentative suggestion is backed up by other evidence, considered further in the discussion section in chapter 8.

All temperatures quoted here are those recorded from the hotstage and are internally self-consistent. However, in similar experiments on n-alkanes using the same equipment, a 2°C thermal-lag below those recorded temperatures was inferred using an independent calibration [Terry *et al.*, 2003].

(a)

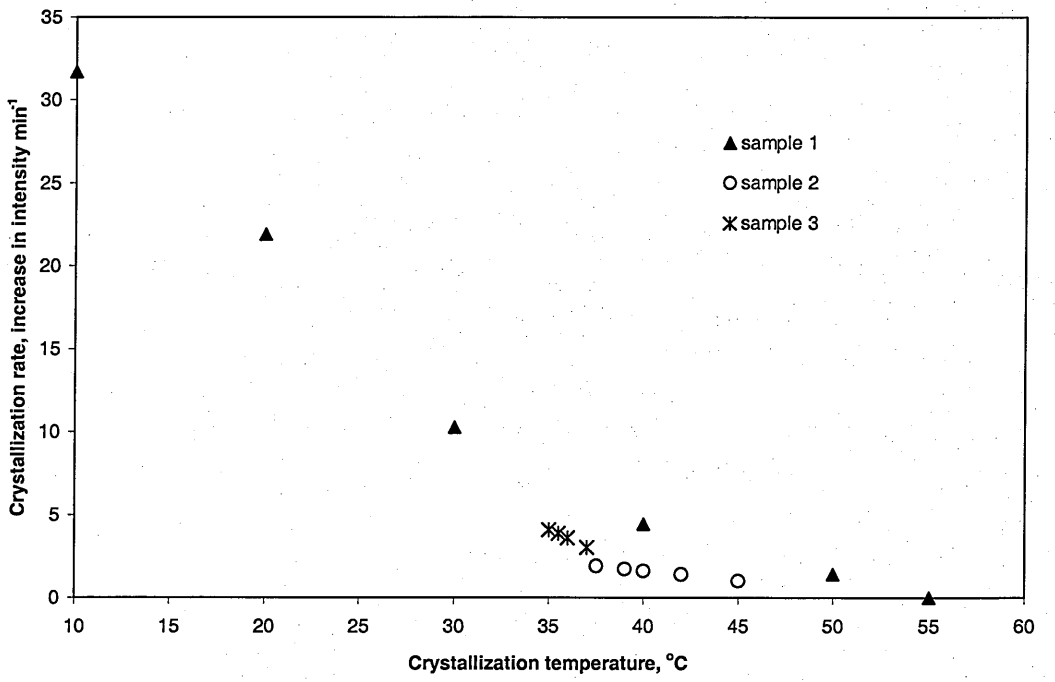

(b)

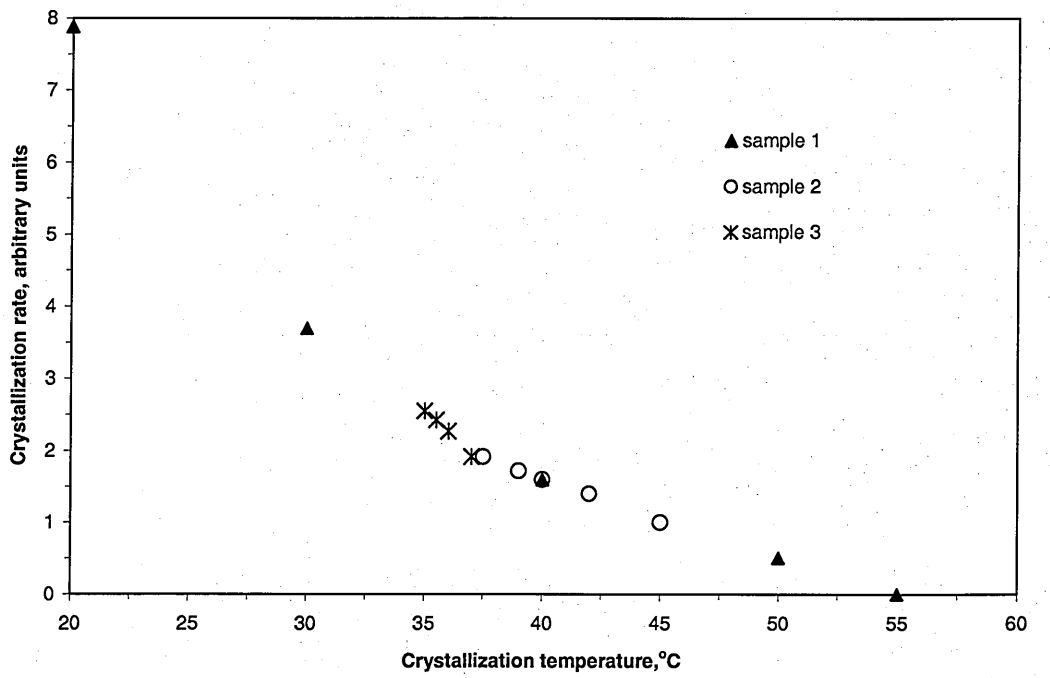

Figure 5.10 Variation of crystallization rate of (020) reflection with temperature for HB 32-mer grown from ~3% (w/v) solution in propylene carbonate. (a) raw data; (b) after normalization as described in the text. The point at 10°C has been omitted from (b) so that the region of interest can be seen more clearly. The data in Figure 5.9 corresponds to sample 1.

The high-resolution detector employed here allows very small changes in lattice spacing, *d*, with either temperature or time to be measured. Slightly different values of *d* were observed at different crystallization temperatures due to thermal expansion, which will be discussed later in chapter 8. There was no visible change in lattice spacing over time during isothermal crystallization, once crystallization was established.

The variation in intensity and hence crystallization rate of the (110) reflections with temperature are not presented here, but they showed identical trends in behaviour.

5.4.2.2 HB 24-mer

More limited experiments were carried out using HB 24-mer samples and there was insufficient data to compile a complete set of growth rate measurements. The growth rates measured were in a similar range to, but slightly higher than, those obtained from the 32-mer. Figure 5.11 shows typical wide angle diffraction data obtained from a 2.7% (w/v) suspension of HB 24-mer crystals in propylene carbonate after subtraction of solvent background. The two strongest crystal reflection peaks (020) and (110) are exactly the same as those in 32-mer (Figure 5.8).

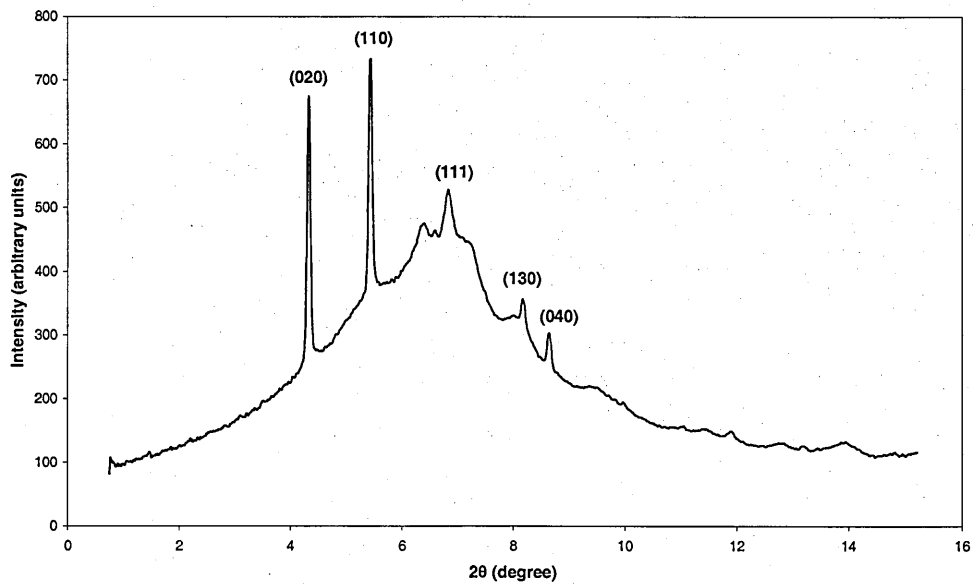

Figure 5.11 Typical wide angle diffraction data obtained from a 2.7% (w/v) suspension of HB 24-mer crystals in propylene carbonate during crystallization at 35°C after partial subtraction of solvent background.

Figure 5.12 gives a very limited range of crystallization rate data from the (020) reflection for HB 24-mer grown from 2.7 % (w/v) solution in propylene carbonate at a few temperatures. Only two samples were used in the experiment. Due to the insufficient data, Figure 5.12 shows no convincing evidence for a discontinuity in the growth-rate gradient or any rate minima, although there appears to be a possible feature at around 30–35°C. Further unfolding results on heating the 24-mer crystals suggest a change from folded to extended chain growth is between 35–40°C, the data will be present in chapter 8.

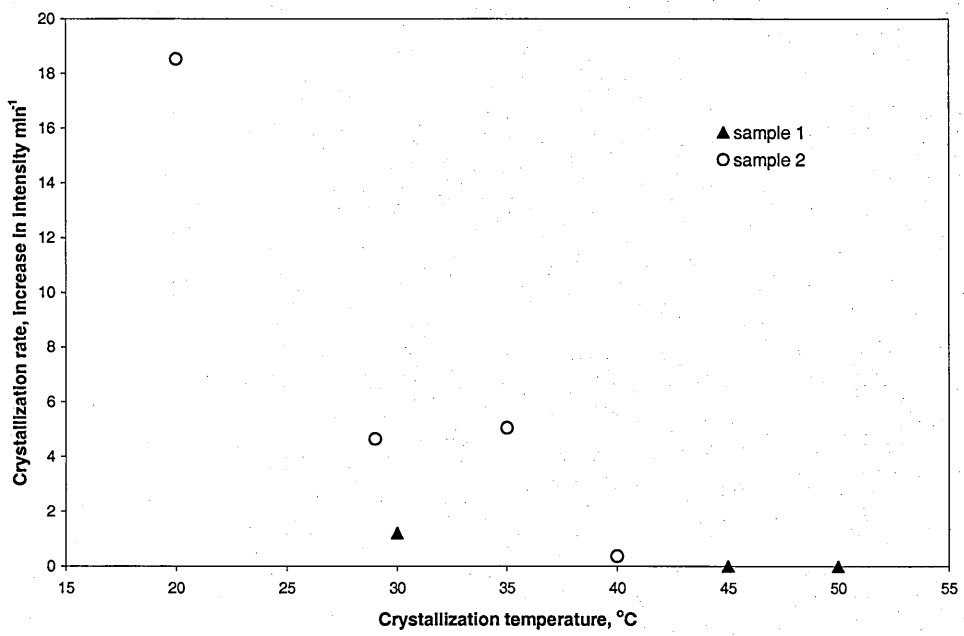

Figure 5.12 Variation of crystallization rate of (020) reflection with temperature for HB 24-mer grown from 2.7 % (w/v) solution in propylene carbonate. The data was insufficient to compile a complete set of growth rate measurements.

5.5 Discussion

The X-ray diffraction patterns obtained from both HB 24-mer and 32-mer oligomers are comparable with those previously reported for the polymer PHB, from which an orthorhombic unit cell with lattice parameters of a=0.576 nm, b=1.32 nm and c=0.596 nm (at room temperature) was deduced [Barham *et al.*, 1984; Mitomo *et al.*, 1987]. The chains are believed to fold in a zig-zag fashion along the (110) lattice direction (see Figure 1.5 in chapter 1). WAXS data from melt crystallized samples which will be reported in chapter 7 displays many more clear reflections, but the presence of the

solvent background in these solution samples restricted the analysis to consideration of the strongest reflections, corresponding to (020) and (110).

Crystals were grown over a range of 10–55°C for the 32-mer and 20–40°C for the 24-mer. Above these temperatures crystallization was prohibitively slow. Lower temperatures require higher cooling rates to ensure that no significant crystallization occurs during cooling. A comprehensive set of growth rate data was obtained for the 32-mer, but the results for the 24-mer were more limited.

The tentative discontinuity in 32-mer growth-rate gradient seen at around 36–37°C in Figure 5.10 is somewhat similar to those found in the 24-mer and 32-mer growth rates from the melt crystallization at higher temperatures (Figure 4.5 and 4.12) presented in chapter 4. But it is much less pronounced than those obtained from long n-alkanes grown from solution [Organ *et al.*, 1989 and 1997; Morgan *et al.*, 1998; Hobbs *et al.*, 2001], where they are associated with a transition from one stable crystal form to another. In separate experiments, thickness measurements have been made on crystals of HB 24-mer and 32-mer with a benzyl end group on one end of the chain, and the results indicate that the 32-mer grows with extended chains at high crystallization temperatures and with folded chains at lower temperatures. Different chain conformations are possible but for solution grown crystals the thickness is consistent with chains that are folded in half. In the AFM thickness measurements on crystals of 32-mer grown at 65°C, the crystals were consistent with once-folded chains too. The solution concentration in that case was 0.018%. The full sets of thicknesses data on HB 24-mer and 32-mer crystals grown form both the melt and solution are given in the following chapter, chapter 6.

A further insight into the conformation of chains within the crystals grown at different temperatures is obtained when the crystals in suspension are heated. In general, partial dissolution and re-crystallization have been observed during heating in both HB 24-mer and 32-mer samples crystallized at the lower temperatures, which corresponds to chain extension in crystals which were initially folded. This unfolding transition is accompanied by a small increase in lattice spacing along the (110) direction. More comprehensive data from HB 24-mer and 32-mer on crystal thickening, lattice

parameter changes and chain unfolding behaviour during heating will be presented and discussed in detail in chapter 8.

5.6 Conclusions

Oligomers of hydroxybutyrate containing 24 or 32 monomer units can crystallize from solution in propylene carbonate over a wide range of temperature. Overall, the single crystals have an appearance very similar to those of PHB grown under similar conditions. Results to be presented in the following chapters suggest that the crystals grown at the higher temperature contain extended chains, while in those grown at lower temprerature the chains are folded. Electron diffraction indicates that the chains are closely perpendicular to the basal planes of the crystals. Wide angle X-ray diffraction suggests that all crystals, no matter what their thicknesses, have the same crystal structure.

The 32-mer crystallization rate from solution in propylene carbonate has been measured as a function of temperature by following the intensity increase of the (020) reflections in real time using WAXS. Limited growth rate data were obtained for the 24-mer. A possible discontinuity in the rate gradient could be located at 36–37°C for the 32-mer, and an even weaker indication of a discontinuity for 24-mer at 30–35°C. These discontinuities in growth-rate gradient, if they exist, are similar to those found in the melt growth, but much less pronounced than similar effects seen in long n-alkanes. This tentative suggestion of discontinuities is supported by other much more compelling evidence based on whether or not the crystals thicken on heating, and will be considered further in chapter 8.

Chapter 6 Crystal Thickness and Chain Conformation

6.1 Introduction

Studies on crystallization of alkanes and other oligomer model materials, as described in chapter 3, have revealed that crystals have distinct thicknesses, which are integer fractions (IF) of the length of underlying molecules, with thinner crystals being grown at lower temperature. Also the growth rates of the crystals exhibit clear minima when the growth temperature is near the transition between different folded forms. In some studies of crystallization from the melt, non-integer folded forms have been found as transient states which may thicken (or thin) to form the more stable integer folded chain forms.

By studying the crystallization behaviour of HB oligomers, comprehensive results have been presented in the previous two chapters on crystal morphologies and growth rates both from the melt and solution. The crystal morphologies have been well defined, and discontinuities are observed in the HB 24-mer and 32-mer growth-rate gradients both from melt and solution crystallization, although they are less pronounced than the rate minima found in the alkanes. Using small angle X-ray scattering, the thicknesses of HB oligomer crystals were measured and correlated with the growth rate data, which leads to a corresponding chain conformation model.

This chapter reports data on HB oligomer crystal thicknesses both from the melt and solution crystallization. To examine the possible links between the crystal growth rates, morphologies and thicknesses, a different chain conformation model is suggested and discussed.

6.2 Experimental

HB 24-mer and 32-mer crystal thicknesses were measured by small angle X-ray scattering (SAXS). The samples were made from both the melt and solution at various

crystallization temperatures. The sample preparation method was reported in the previous chapters. The thicknesses of all the HB oligomer as-received powder, together with some preliminary results obtained by a former PhD student with one shorter and one longer HB oligomer (8-mer and 96-mer) provided previously by Prof Seebach, are presented here for a complete view on HB oligomer crystallization studies.

6.2.1 Small angle X-ray scattering (SAXS)

If a crystalline sample is placed in an X-ray beam, then the X-rays will be scattered in accordance with Bragg's Law, given by Equation 6.1

$$n\lambda = 2d\sin\theta \qquad (6.1)$$

Where n is the order of the diffraction peak, λ is the wavelength of the X-rays, d is the periodicity in the sample and 2θ is the scattering angle from the incident beam. X-ray diffraction is usually used to obtain information about unit cell dimensions in crystals, but can also detect periodicity on a larger scale if 2θ is relatively small. A regular stack of crystal lamellae will have a periodicity corresponding to the crystal thickness and this will produce a peak in the small angle region (usually $2\theta < 6^{o}$) of the X-ray diffraction pattern. SAXS can therefore be used to measure crystal thicknesses.

6.2.1.1 Bruker NanoSTAR small angle X-ray machine

Two small angle X-ray systems were used to measure the crystal thicknesses in this study. At first, Bruker NanoSTAR small angle X-ray scattering equipment from the University of Bristol was chosen to measure the crystal thicknesses on the original as-received HB oligomer powders and some of the melt-grown HB oligomer crystals. The newly developed Bruker NanoSTAR machine is based on a combination of the latest X-ray optics technology, with cross-coupled Göbel Mirrors for parallel incident beam conditions (0.1 mm or 0.3 mm pinhole collimator), high precision mechanics (high-resolution pinhole chamber with sample changer and sample scanning device), a 2-dimensional, zero background, high-resolution area detector (Bruker AXS Hi-STAR) and a powerful software package controlling the system (SAXS NT). In a

reasonably short measuring time, the size, orientation and nano-structure of the oligomer samples can be easily determined. A photograph of the detector part from the Bruker NanoSTAR X-ray system is shown in Figure 6.1.

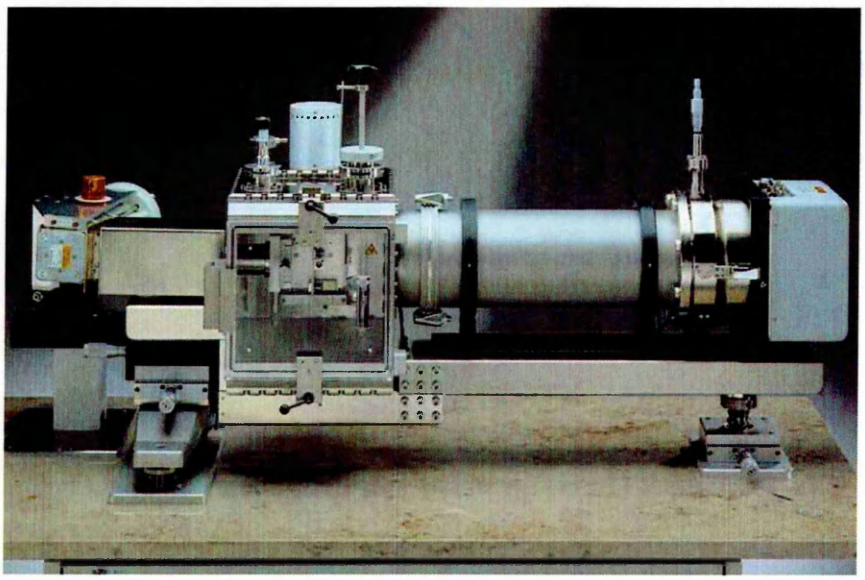

Figure 6.1 Photograph of the detector part from the Bruker NanoSTAR X-ray system.

Both the original HB oligomer powders and the melt-grown crystals made on two hot-stages (as described in section 4.2.2 in chapter 4), were scraped into 1.5 mm diameter Lindemann tubes and flame sealed. The samples were then exposed to the X-ray beam at room temperature. The running voltage in this case is 40 kV with an anode current of 35 mA, using CuK□ radiation wavelength of 0.1541 nm. While the as-received powder samples were left overnight for a longer exposure time to get a high intensity diffraction spectrum, the re-crystallized HB oligomer samples only need several hours for exposure. The usual corrections for intensity, such as unwarping correction in the spatial dimension and the subtraction of the background noise etc, were applied before locating the peak positions from which the crystal long periods could be determined by Bragg's Law.

If the sample contains an un-oriented set of lamellae (e.g. bulk crystallized material as grown from the melt) the small angle scattering pattern is circularly symmetric, which is the case in our experiments. If there is some orientation in the crystals (e.g. sedimented single crystal mats), there will be an orientation in the diffraction pattern.

The sedimented crystal mats are usually made following a certain single crystal recipe, which involves self-seeding, growing single crystals from dilute solution and hot-filtering procedures [Organ, 1983; Otun, 1985 and Sykes, 1996]. Considering the limited quantity of the HB oligomer powders available for this project, it is not feasible to make sedimented single crystal mats from solution grown crystals in this work.

The SAXS pattern obtained from the Bruker NanoSTAR small angle X-ray system showed an exactly circularly symmetric pattern. Typical SAXS patterns for a melt grown HB 24-mer crystals and 16-mer(p) as-received powder are shown in Figure 6.2. The peak intensity in Figure 6.2(b) is much higher than (a), also a clear second order peak can be seen in (b), suggesting that more well-defined crystals exist in HB 16-mer(p) as-received powders than in 24-mer crystals crystallized at 70°C.

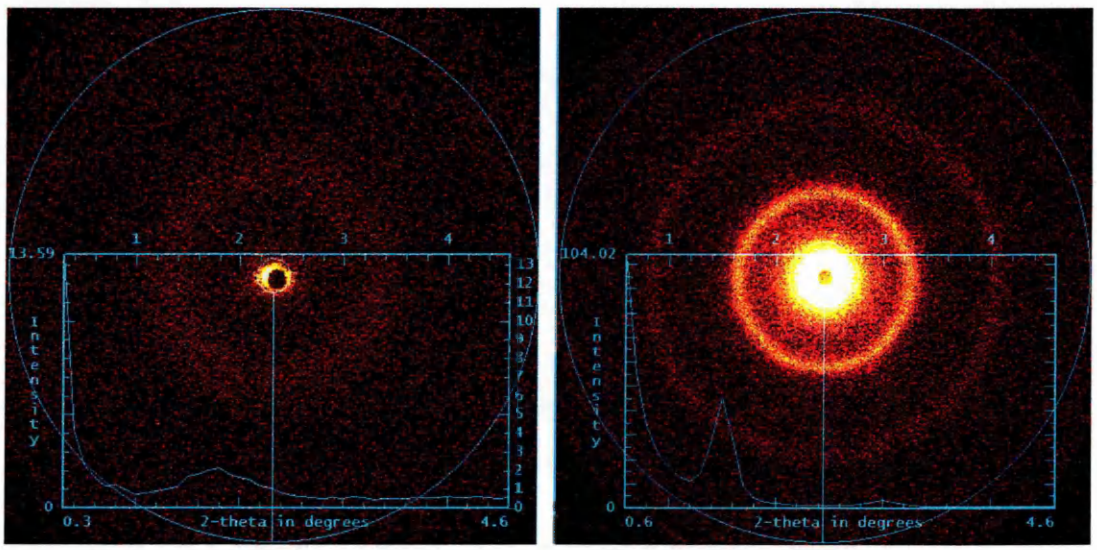

(a) (b)

Figure 6.2 SAXS pattern together with its integration intensity distribution as a function of the scattering angle 2θ from (a) HB 24-mer sample grown from the melt at 70°C; (b) 16-mer(p) as-received powder sample.

6.2.1.2 The synchrotron X-ray radiation

The first use of synchrotron radiation in X-ray scattering [Rosenbaum *et al.*, 1971] opened new possibilities in scientific investigation in polymer science [Elsner *et al.*,

1985]. The intensity of the synchrotron radiation is extremely high compared to that available using a conventional source, which makes the measurement more efficient.

Some of the melt-grown OHB crystal thickness experiments were performed by SAXS using the high brilliance beamline ID2 at the European Synchrotron Radiation Facility (ESRF), Grenoble. Thin sample films were again grown isothermally between cover slips on two-hotstages from the melt, and then scraped off into 1.5 mm diameter Lindemann tubes. For exposure to the X-ray beam the sample tubes were mounted in a modified sliver block Linkam hotstage (for in-situ heating, cooling and isothermal crystallization). The samples were exposed at room temperature with only one or two exposures (of no more than 3 seconds each) to reduce the damage and degradation due to the high radiation intensity. The wavelength is 0.0995 nm and the detector distance in this case was 5 m. Data were collected using the Frelon CCD camera attached to an image intensifier. The resulting 2-D data were corrected for spatial distortions prior to integration.

Another advantage of the high brilliance ID2 beamline is that it can collect WAXS and SAXS data at the same time. The WAXS and SAXS detectors have been specially designed and set-up to give more scattering information on the same crystal sample. A photograph taken from ESRF ID2 beamline is given in Figure 6.3. Further details of the experimental set-up, the detector characteristics and the procedure used for data collection and analysis have been reported elsewhere, see [Terry *et al.*, 2003; ESRF official website]. Raw pictures showing SAXS and WAXS pattern simultaneously taken at the ID2 beamline at ESRF are given in Figure 6.4. A few samples were heated and crystallized in-situ in the beam with up to 5 minutes total exposure to the X-rays. More data obtained at ID11 beamline at ESRF using in-situ WAXS to reveal thickening and unfolding during heating will be presented and discussed in chapter 7.

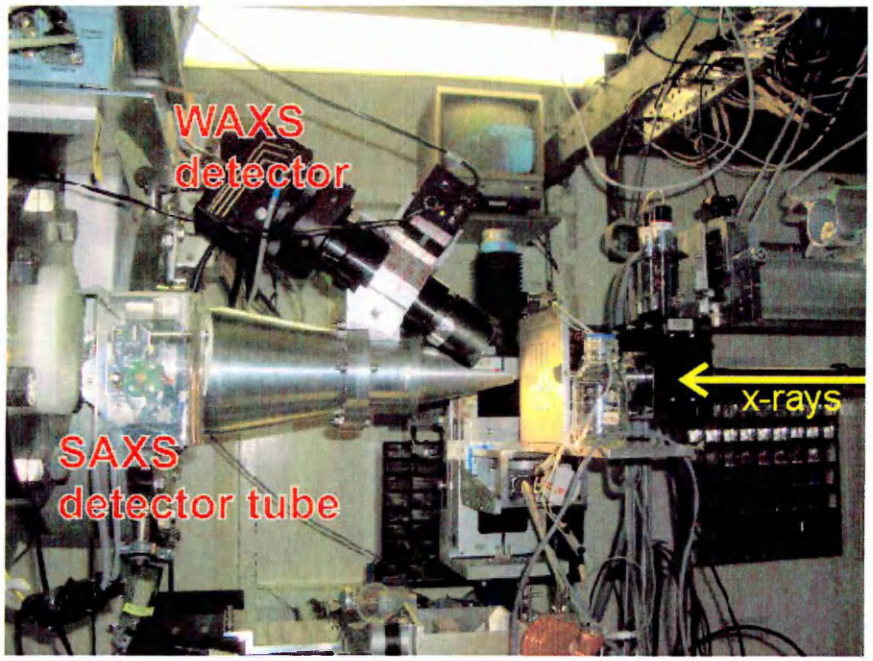

Figure 6.3 Photograph of ID2 beamline detectors with WAXS and SAXS set-up at ESRF Grenoble [from ESRF official website].

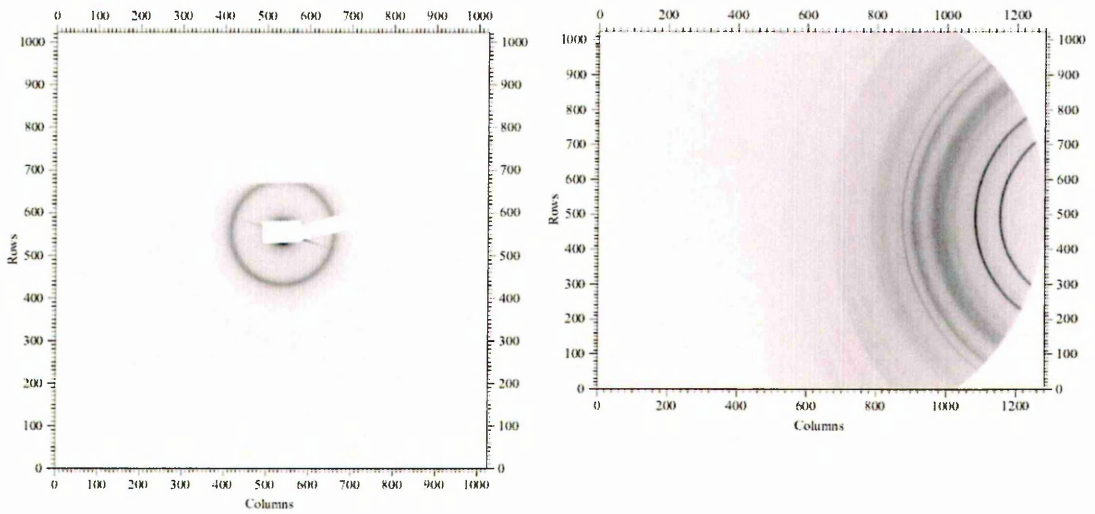

(a) (b)

Figure 6.4 Raw pictures showing (a) SAXS and (b) WAXS pattern of a HB 32-mer(p) sample grown from the melt at 121°C. The two pictures are simultaneously taken using synchrotron radiation at the ID2 beamline at ESRF.

6.2.2 Atomic force microscopy (AFM)

A few thickness measurements of HB 32-mer crystals grown from solution were also made by AFM, in collaboration with Dr JK Hobbs. The 32-mer samples were dissolved in propylene carbonate with a concentration of ~0.2% (w/v) in 1.5 ml test tubes, and the solutions were then left in an oil bath at the chosen crystallization temperatures for several days. A drop of the crystal suspension was put onto a freshly cleaned cover-slip, put under vacuum to evaporate the solvent, and observed in a Veeco Dimension D3100 AFM. The AFM was operated in 'tapping mode' using silicon cantilevers with a nominal spring constant of 50 Nm^{-1} and resonant frequency of ~300 kHz at room temperature. More information on the AFM and its operation has been presented in the previous chapter, chapter 5. Thicknesses measured with the AFM are of an individual crystal rather than the average over many crystals as measured by X-ray scattering.

6.3 Results

6.3.1 Thicknesses from HB oligomer as-received powders

Preliminary studies on the thicknesses of some shorter and longer HB oligomers have been performed by Sykes in 1995. These data are complementary to the data obtained in this work and are included for a complete view in Table 6.1, along with the data for a PHB sample that was re-crystallized in a similar way to the oligomers. All the data in Table 6.1 were obtained using a conventional X-ray system at Bristol, and all the materials (except that for PHB) are as received, in the form of crystalline powders. The data indicate that the crystals are either grown from extended chains or, for the longer oligomers, from folded chains. The majority of 32-mer crystals contain once folded chains. The 96-mer with a crystal thickness of ~4.83 nm (compared to an extended chain length of 28.6 nm) is folded several times and probably has 5 folds. The molecule length is based on two HB units of 0.596 nm, ignoring the length of all the protecting end groups.

OHB/PHB	Molecule length (nm)	Suggested conformation	Crystal thickness (nm)	
			Extended	Once Folded
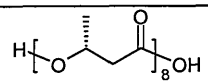 **8-mer (free)**	**2.38**	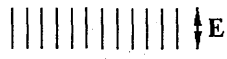	**2.52 ± 0.02**	
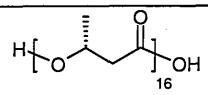 ***16-mer (free)**	**4.77**		**4.80 ± 0.04**	
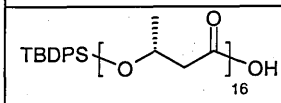 ***16-mer (protected)**	**4.77**	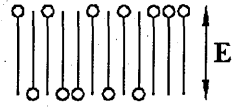	**5.92 ± 0.04**	
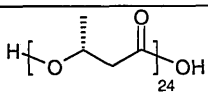 ***24-mer (free)**	**7.15**	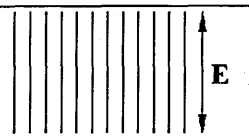	**7.30 ± 0.04**	
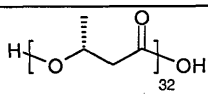 ***32-mer (free)**	**9.54**	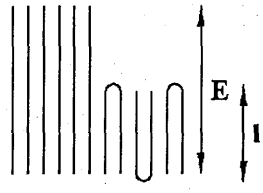	**9.81 ± 0.05**	**4.93 ± 0.03** (majority)
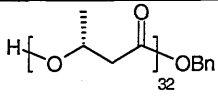 ***32-mer (protected)**	**9.54**	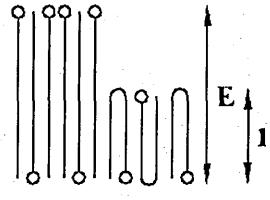	**9.92 ± 0.05**	**4.99 ± 0.02** (majority)
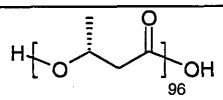 **96-mer (free)**	**28.61**	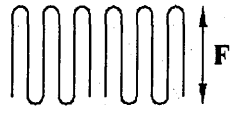		**4.83 ± 0.03**
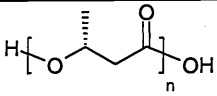 ***PHB**	**0.596 × n/2**	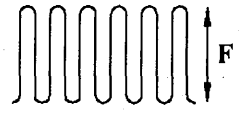		**5.58 ± 0.05**

Table 6.1 Crystal thicknesses of 'as-received' HB oligomer materials. Samples marked with asterisks were measured in this work, the others are form Sykes [Sykes, 1996]. Molecule length is based on two HB units of 0.596 nm, ignoring the length of all the protecting end groups.

In the as-received 24-mer samples only very low intensity and very broad diffraction peaks, at angles corresponding to fully extended chains, were observed. This suggests that in the HB 24-mer original as-received powders the crystals (if they exist at all) are almost entirely extended. In the case of HB 32-mer and 32-mer(p) original powders, diffraction peaks corresponding to both folded and extended chains were observed, but the proportions differed. The intensity of the peak at wider angles was much higher, suggesting that the HB 32-mer samples contained a mixture of very small proportion of extended chain crystals (and possibly an even smaller proportion of 2/3 length of the extended chain crystals, which are not shown in Table 6.1) and a majority of once folded chain crystals. Figure 6.5 shows the SAXS integration peaks for HB 24-mer and 32-mer as-received powders as a function of scattering angle 2θ, after the usual corrections and background subtraction are applied. The exposure time for 24-mer and 32-mer scattering was 12 hours, 3 hours in the case of 32-mer(p).

(a)

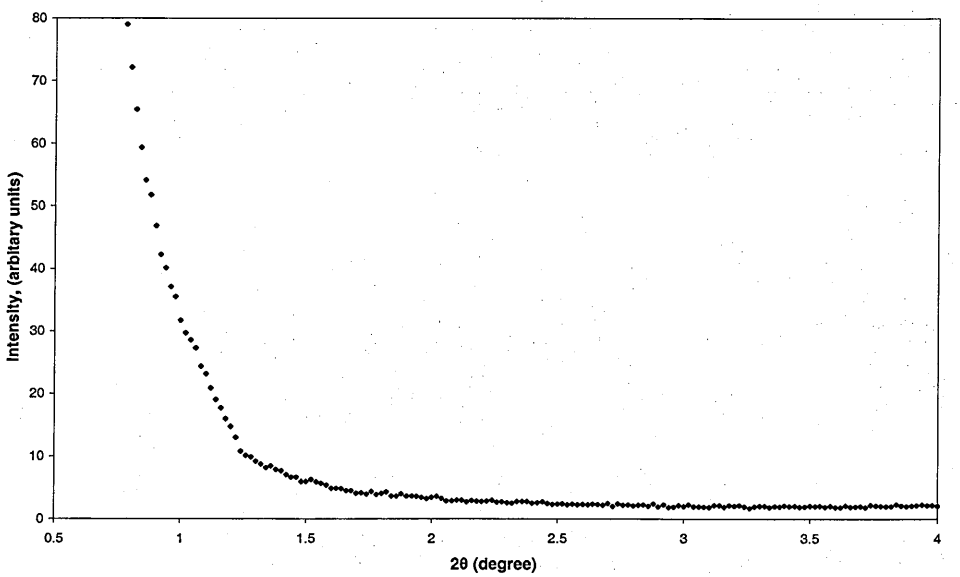

(b)

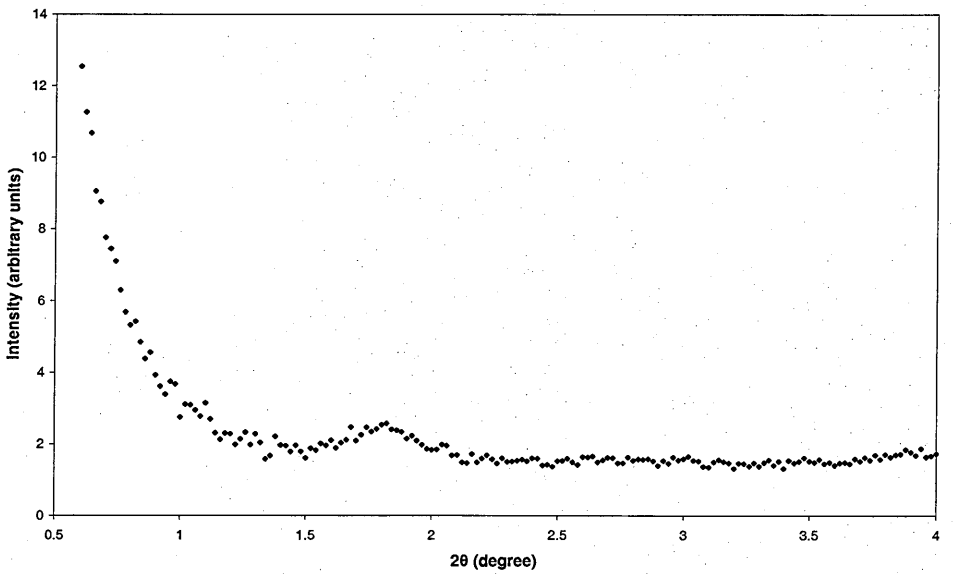

(c)

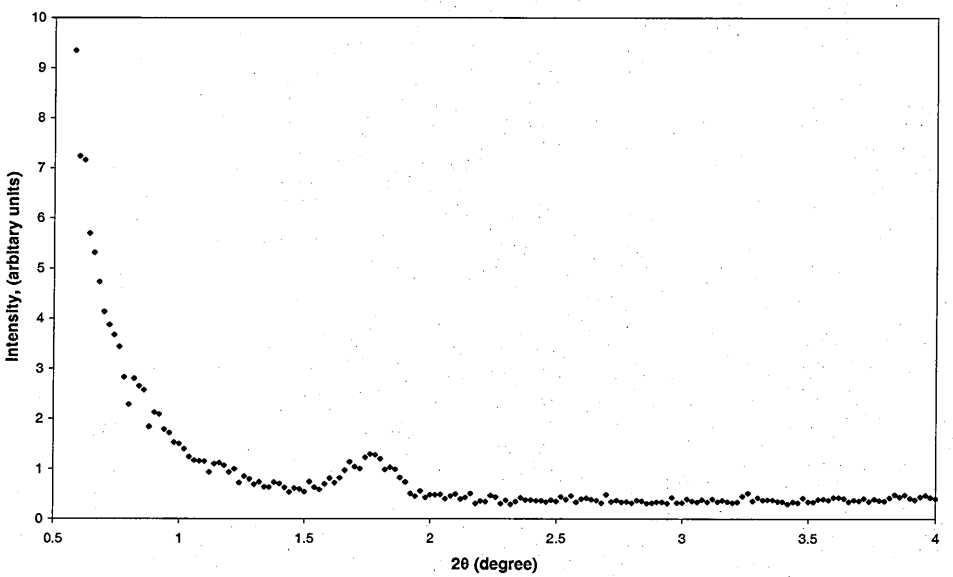

Figure 6.5 SAXS integration peaks of (a) HB 24-mer, (b) 32-mer and (c) 32-mer(p) as-received powders as a function of scattering angle 2θ.

6.3.2 Thicknesses from HB 32-mer re-crystallized samples

SAXS thickness data were also measured on HB oligomer samples re-crystallized under better controlled conditions. The experimental procedures for preparing the melt and solution grown HB oligomer samples are given in previous chapters. SAXS data obtained from various melt and solution crystallized HB 24-mer and 32-mer samples are summarized in Table 6.2. All the spectra were recorded at room

temperature, apart from the reheated samples of A, B and F, which were recorded in-situ with the synchrotron X-rays at the higher temperatures at the ESRF. The AFM thickness data of HB 32-mer crystal grown from propylene carbonate solution are given in Table 6.3. It should be noted that the quenched samples may well have crystallized over a range of temperature during cooling.

OHB sample	Crystallization temperature (°C)	SAXS long period (nm)
A 32-mer (p)	Room temp (quenched)	4.31 ± 0.02
A 32-mer (p)	Reheated to 150	10.21 ± 0.02
B 32-mer (p)	107	5.90 ± 0.02
B 32-mer (p)	Reheated to 150	10.07 ± 0.02
C 32-mer (p)	112	6.04 ± 0.02
D 32-mer (p)	113	6.09 ± 0.02
E 32-mer (p)	121	6.10 ± 0.02
F 24-mer (free)	Room temp (quenched)	3.86 ± 0.02
F 24-mer (free)	Reheated to 140	7.65 ± 0.02
G 24-mer (free)*	90	5.32 / 3.71 ± 0.02
H 32-mer (fr) in 3.5% PC soln	Room temp (quenched)	5.4 ± 0.1
J 32-mer (fr) in 3.2% PC soln	42	5.9 ± 0.1
K 24-mer (fr) in 3.2% PC soln	10 (quenched)	4.27 ± 0.02
L 24-mer (fr) in 2.9% PC soln	38	4.34 ± 0.05

Table 6.2 Data of SAXS thicknesses (after correction) for re-crystallized HB 24-mer and 32-mer samples. For 24-mer sample G (marked with an asterisk), two populations of crystals exist simultaneously.

Sample	Concentration in propylene carbonate (w/v)	Crystallization temp (°C)	AFM thickness (nm) ± 0.4
32-mer (fr)	0.021% in PC	Room temp (quenched)	8.21 / 4.10*
32-mer (fr)	0.018% in PC	65	4.84
32-mer (p)	0.023% in PC	65	5.03
32-mer (fr)	0.028% in PC	50	4.21

Table 6.3 Data of AFM thicknesses for re-crystallized 32-mer samples. *Two overlapping layers can be seen in the bottom picture in Fig 5.6b, giving a single layer thickness ~4.10 nm.

Figure 6.6 shows some typical SAXS spectra for HB 32-mer samples from which the data in Table 6.2 were derived (samples A and B). Second or higher order peaks were only occasionally seen in the chain folded samples, but were more common for

extended chain crystals. All the thicknesses obtained for HB 32-mer and a few initial measurements from HB 24-mer (from Tables 6.1–6.3) are gathered together in Figure 6.7. More comprehensive thickness data subsequently obtained for 24-mer crystals grown from the melt over a wide range of crystallization temperatures will be presented and discussed in detail in a later section in this chapter.

(a)

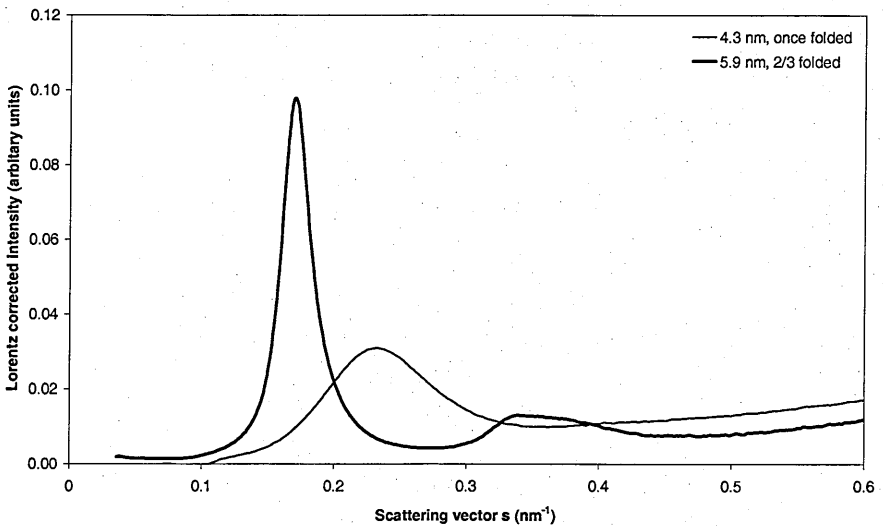

(b)

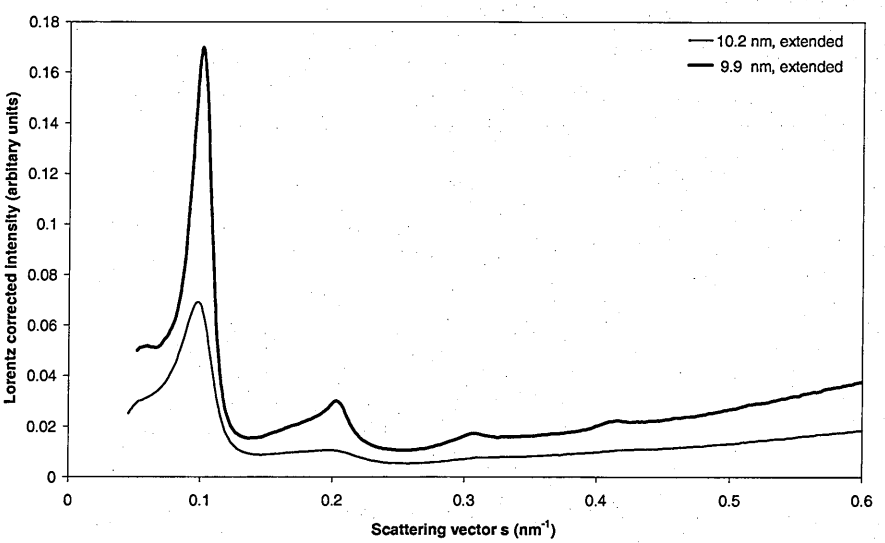

Figure 6.6 Typical SAXS spectra for HB 32-mer(p) samples A and B. The spectra were recorded at (a) 31°C (b) after heating to 160°C. The data have had the Lorentz correction applied and the background scattering subtracted. The light curve is from sample A, crystallized at room temperature, and the bold curve is for sample B, crystallized at 107°C. The crystal thicknesses calculated from the peak positions are as shown.

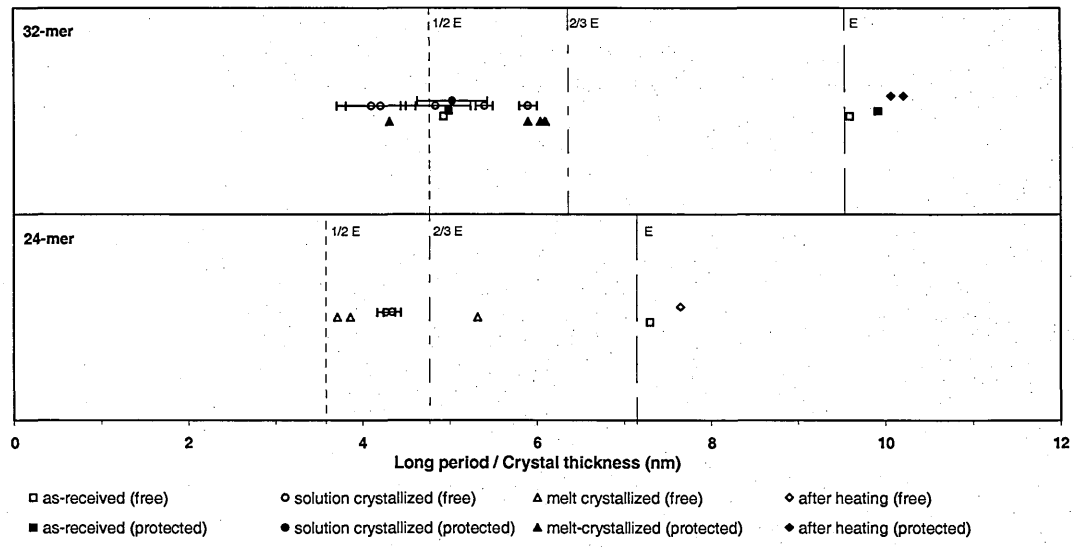

Figure 6.7 Chart summarizing the crystal thicknesses data of HB 32-mer and 24-mer presented in Tables 6.1–6.3. The chain lengths are calculated based on two HB units of 0.596nm, ignoring the length of protecting end groups and any chain length involved in the fold for simplification.

Consider first the melt-crystallized samples of HB 32-mer(p), shown as solid triangles on the upper part of Fig 6.7. Here, only two distinct crystal thicknesses have been seen. The quenched sample (A) gives a value close to that for once-folded chain forms. At the higher crystallization temperatures, similar values have been measured in all the samples, which lie between the once-folded and extended chain lengths. Indeed, the value obtained here is very close to 2/3 of the extended chain length. One of the samples from which a thickness close to 2/3E was recorded is sample B, for which the SAXS spectra is shown in bold in Figure 6.6(a). Interestingly, the broad lower intensity peak visible in this trace is in fact a doublet, suggesting a mixed population of crystals. The shape and the position of this peak could be explained by a combination of a second order peak from the crystals of 2/3E, together with a first order peak from a small population of thinner crystals, possibly containing twice folded chains. Extended chain crystals were never obtained directly, but on heating the crystals a transformation occurred during which the initially folded chains became extended. This process will be described in more detail in the next chapter, chapter 7.

The values obtained from solution grown crystals are more scattered, and also subject to larger uncertainties. The experimental error associated with the AFM

measurements is relatively large, and all the 32-mer crystals measured had thicknesses within the range expected from once-folded chains. The SAXS measurements were obtained from crystals in suspension, so although the intrinsic error in the measurements is smaller, the stacking between layers is likely to be very poor and the measured periodicity may not be a good reflection of the actual crystal thickness.

The crystal thickness values were calculated based on two HB units of 0.596 nm, ignoring the length of protecting end group and any chain length involved in the fold for simplification. These values are for chains that are arranged exactly perpendicular to the basal plane, any chain tilt would of course lead to smaller thicknesses. According to these calculations, many of the recorded crystal thicknesses are indeed close to that of a crystal containing chains folded to 2/3 of their full length.

The initial results from melt-crystallized 24-mer also yielded thickness values close to those of the once-folded chain, extended chain length (as-received power and after heating) and to a value in between, which is again close to 2/3 of the extended chain length as shown in Figure 6.7. Further thicknesses measurements from 24-mer melt grown crystals over a wide range of crystallization temperature were subsequently obtained to complement the growth rate curve presented in chapter 3. These thickness data confirmed a preference for the 2/3E thickness value. Even more surprisingly, more non-integer folded (NIF) forms have been found. The data are given below.

6.3.3 Thicknesses from HB 24-mer re-crystallized samples

The full set of crystal thicknesses measured from HB 24-mer melt grown crystals over the same range of the temperature as its growth rates (see Figure 4.5 in chapter 4) are shown in Figure 6.8. The different experimental methods are distinguished. A few data points from Table 6.2 and Figure 6.7 are included in Figure 6.8 for completeness. The 'ESRF, crystallization in situ' data were recorded at the crystallization temperature and a correction for thermal expansion has been applied using the data calculated from heating experiments followed by real time WAXS at ID11 ESRF (details will be given in chapter 7). Where two such points are shown at the same temperature they refer to different crystallization times and this will be explained in the discussion section. All the other results were measured at room temperature with

the exception of the 'previous results' point at 120°C, which refers to material that has thickened on heating and for which no reference is available. Some samples showed a very small secondary population of crystals of a distinctly different thickness: these crystals are likely to have grown on quenching, at a lower temperature than the initial crystallization.

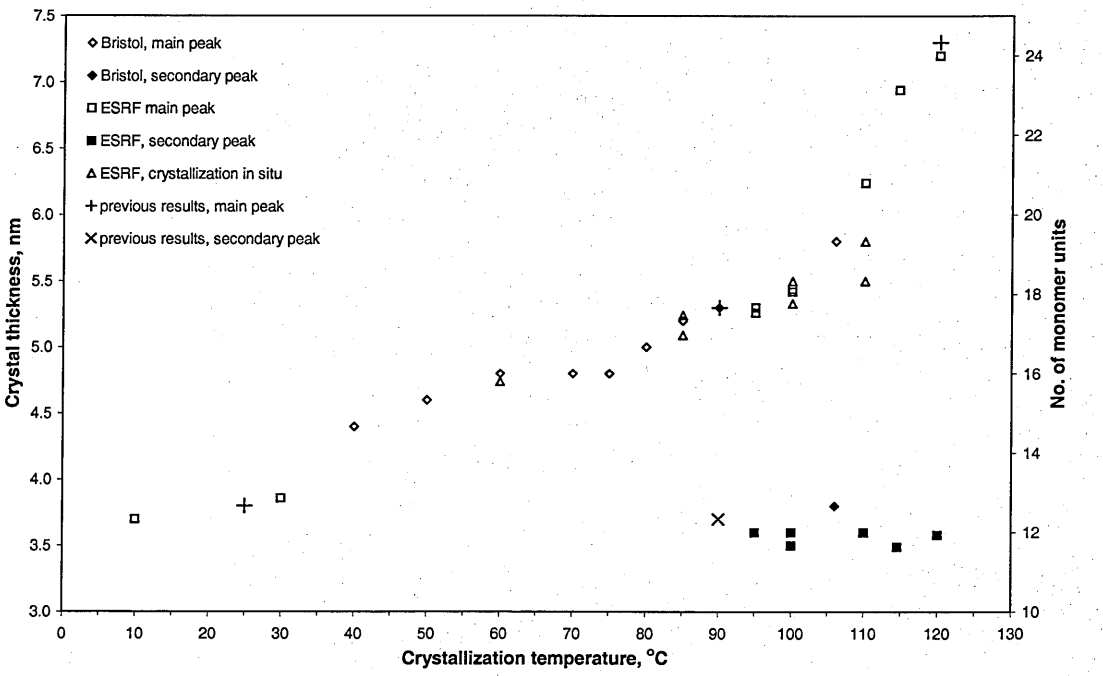

Figure 6.8 Crystal thicknesses of HB 24-mer samples as a function of crystallization temperature. See text for details.

6.4 Discussion

In common with other oligomer systems, it is possible to grow crystals from HB oligomers containing chains which are either extended or folded in half. However, crystals with intermediate thicknesses have also been produced. Most notably, a strong tendency for HB 32-mer crystals to form with a thickness equal to 2/3 of the extended chain length has been observed. Even more surprisingly, in the case of 24-mer crystals grown from the melt over a wide range of crystallization temperatures, more thicknesses equal to non-integer folded (NIF) chain length, such as 2/3, 3/4, 5/6 of the extended chain length have been observed.

The fact that these NIF crystal thicknesses occur begs the question why? The initial HB oligomer samples are all monodisperse, and there is no evidence for significant degradation either during these experiments or from DSC. Surprisingly, these materials appear to show even less preference for integer folding than non-monodisperse PEO fractions [Cheng *et al.*, 1991]. To examine a possible explanation and explore possible links between the crystal growth rates, morphologies and thicknesses, a model based on different chain conformations has been proposed.

6.4.1 HB 32-mer

The first questions that arise from looking at the thickness results from HB 32-mer measurements are: Are the chains folding with non-integer fold lengths? Are the chains tilted relative to the basal planes of the crystals? Are there thick amorphous layers, or are these results due to the co-existence of different crystal forms? Could hydrogen bonding between chains influence behaviour? The discussion below will concentrate primarily on the common occurrence of crystals with thickness close to 2/3 of the extended chain length, while acknowledging that these results do not conclusively exclude other intermediate values.

Firstly, look at the electron diffraction pattern shown in Figure 5.5 (d) in chapter 5, taken from the 32-mer single crystals grown under similar conditions to the 32-mer samples presented here. The electron diffraction pattern indicates that there is only little if any chain tilt, so the large tilt that would be necessary to account for the observation of crystals of thickness ~2/3 of the chain length can be ruled out, at least in the case of the solution crystallized samples (samples H, J, K and L in Table 6.2). Also, as will be shown in detail in chapter 7, on heating crystals which are thinner than the fully extended length they thicken to that length. It seems improbable that this behaviour could arise simply from changes in chain tilt. If the crystals of 1/2 the extended chain length contained tilted extended chains they would be tilted at an angle of 60° to the basal plane – which would be an extraordinary degree of tilt. Thus, it seems clear that these crystals containing once folded chains are approximately perpendicular to the basal plane. Now if these crystals thicken, in a steady fashion, up to the thickness corresponding to fully extended chains perpendicular to the basal plane, then it seems much more probable that they do so by 'dragging' chain ends

through the crystals and keeping the chains approximately normal to the basal plane than that they should, on heating, both change the angle of tilt and unfold at the same time. Given the above, the argument that chain tilt alone can offer an explanation of the observation of 32-mer crystals with a thickness of 2/3 the extended chain length does not seem plausible.

A second explanation is that there is a low crystallinity providing crystals with a 'core' thickness of approximately 1/2 the chain length and a thick amorphous zone. Such a model has been suggested to explain the appearance of transient non-integer (NIF) states in n-alkanes. The sketch in Figure 6.9 [taken from the work of Ungar *et al.*, 2000] illustrates how this model could lead to the impression of a crystal with a thickness of 2/3 the chain length. In such a model half of every other chain is excluded from the crystal giving a thick amorphous layer so that an overall thickness approaching 2/3E could be achieved (provided the chains are normal to the basal plane of the crystals). The overall crystallinity of such samples would be around 75% of the crystallinity of crystals formed from extended or once folded chains.

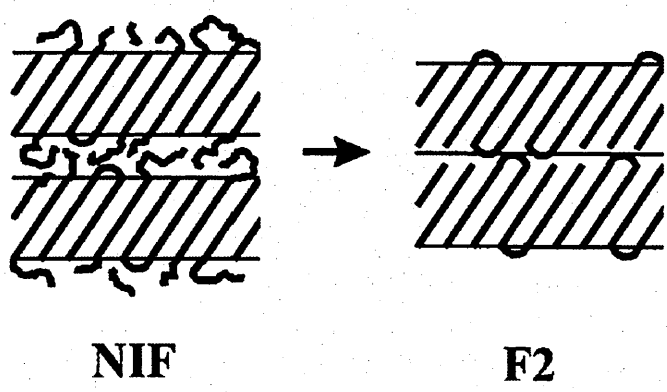

Figure 6.9 Schematic drawing [from Ungar *et al.*, 2000] of the non-integer (NIF) form in n-alkanes and the transformation to the once folded form. The NIF form must involve folded chains and chains that have a single traverse with a total cilium length of one half the chain length. The resulting repeat distance is then approximately 2/3 the extended chain length. Such crystals will have an amorphous content of approximately 25%.

Figure 6.10 shows wide angle diffraction patterns (after background subtraction) from samples of 32-mer(p) with thicknesses close to 1/2 and 2/3 the extended chain length, taken at room temperature. These do not show any significant difference in crystallinity: indeed a quick glance at the diffractograms suggests that, if anything, the

sample with a thickness of 2/3 the chain length has a slightly higher crystallinity than the crystals grown from once folded chains. The SAXS patterns in Figure 6.6 also suggest a higher degree of order in the 2/3E crystals although the broad, and possibly double, second order peak seen in this sample hints at a more complex distribution.

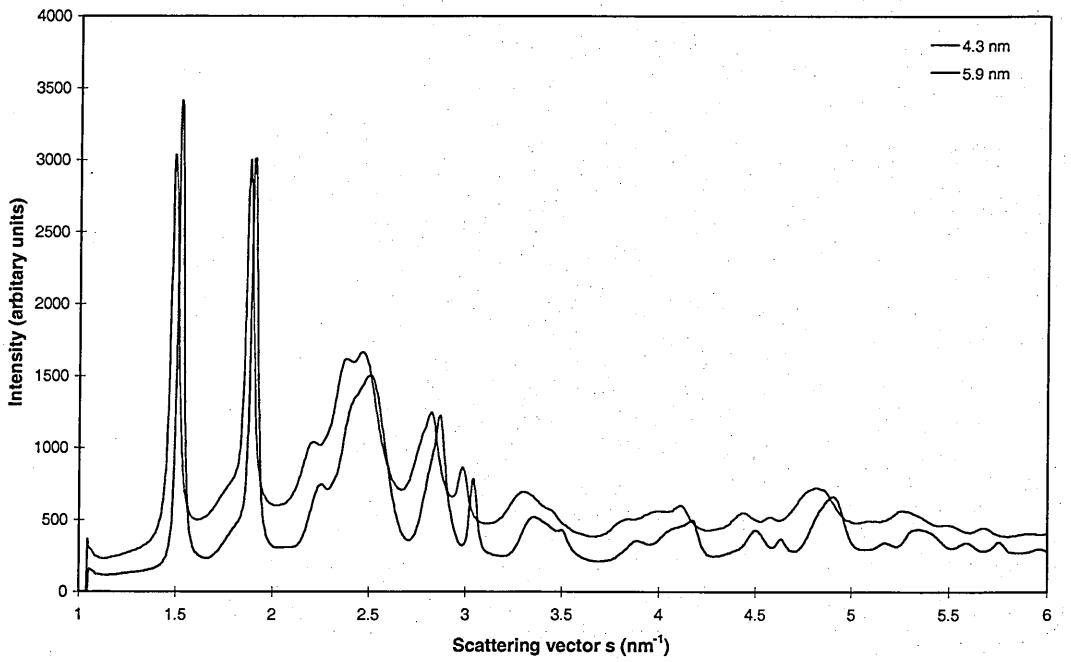

Figure 6.10 Wide angle diffractograms for two HB 32-mer(p) preparations, both recorded at 31°C. An amorphous background from a completely melted sample has been subtracted. The purple line corresponds to sample A, which contains crystals with thickness 4.3 nm. The blue line corresponds to sample B, with crystals of thickness 5.9 nm.

NIF states have of course been seen in alkanes [see e.g. Ungar *et al.*, 2000] and in sharp low molecular weight fractions of poly (ethylene oxide), PEO [e.g. Cheng *et al.*, 1991 and 1992]. But in the alkanes (and most of the PEO cases) the NIF states are transient: the crystals will change thickness to an integer folded form during crystallization. However, in PEO, there have been reports of NIF states that are more stable than the integer folded forms and it appears that these NIF states can have a high crystallinity as judged by the heat evolved as they crystallize [Cheng *et al.*, 1991]. Indeed Cheng *et al* have proposed a 2/3 folded structure with the ends incorporated in the lattice for these states.

Hence, based on the argument above, a possible arrangement of two chains within a crystal of 2/3 the thickness of the extended chain of 32-mer is sketched in Figure 6.11. The 2/3E fold model is based on two HB units of 0.596 nm, ignoring the length of protecting end group and any chain length involved in the fold. Also any chain tilt would lead to a smaller value of crystal thicknesses. Two of the chain ends lie within the crystal: in these HB oligomers these ends must be different due to the directional nature of the HB chain. In the case of the unprotected HB oligomers one end is a hydroxyl group and the other a carboxylic acid. It is therefore likely that hydrogen bonding will occur between the chain ends, effectively forming a dimer. Strong evidence for the formation of such dimers in a long alkanoic acid has been reported by Ungar and Zeng [Zeng and Ungar, 1999] who observed bilayer structures made up from extended chain doublets. If such doublets occur here then this proposed 2/3 folded structure could in fact be regarded as the once folded form of the doublet. Other intermediate crystal thicknesses might be similarly explained as integer fraction thicknesses of longer entities (triplets, quads etc). It should be noted that no direct evidence has been seen for doublet structures in the HB oligomer experiments here. Unusual behaviour during the later stage of melting, which will be reported in chapter 7, may indicate their presence and will be discussed later.

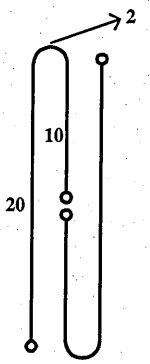

2/3 E

Figure 6.11 Sketch indicating how the chains could be arranged in a crystal of 2/3 the thickness of the extended chain length in 32-mer. The circles represent the OH groups (or protecting end groups) at the chain ends. The digits indicate the number of monomer repeat units, giving an approximately 2 monomers involved in the folds, and ignoring any chain tilt.

In the protected 32-mer(p) sample the carboxylic acid end is capped by a benzene ring. This is small enough to fit into the lattice of the shallow 2_1 helix, and the similarity in behaviour between the capped and uncapped chains suggests that any

association between chains is only slightly reduced by the presence of the end group. So it is at least plausible that the ends of the chains may be inside the crystals as is implied by the model for 2/3 integer folding in Figure 6.11.

Based on the HB 32-mer data, a plausible model has been proposed to explain these NIF crystals with 2/3E chain length. A more detailed study with HB 24-mer crystals grown over a wide range of crystallization temperatures, including a greater range of accurate measurements of crystal thickness gives more insight into the links between the chain conformation, crystal morphologies and growth rates. The discussion is given below.

6.4.2 HB 24-mer

6.4.2.1 Chain conformation

Two 24-mer melt grown samples (sample F and G, in Table 6.2) were first measured with SAXS at ESRF. Crystals of sample F, which were grown at room temperature, contain folded chains. When heated to around 140°C, they unfolded to produce extended chain crystals. The thicknesses of these crystals, before and after heating, have been included in Figure 6.8 (labelled by 'previous results') for completeness. In that case the folded chain form had a thickness close to half of the extended chain length (E/2), implying that the chains were folded exactly in half. Other thickness measurements for both 24-mer and 32-mer suggested that a crystal form with thickness close to 2/3 of the extended chain length (2/3E) was also common. This is in contrast to the results found in long n-alkanes, where stable crystal thicknesses have been found to correspond only to integer fractions of the extended chain length (E/2, E/3 etc). It is suggested that, in the HB oligomers, hydrogen bonding between chain ends can effectively link chains together into longer units, making a wider range of chain conformations possible.

Subsequently a wider range of thickness measurements were made on the 24-mer. These more comprehensive results are also shown in Figure 6.8. They demonstrate clearly that a wide range of thicknesses can be obtained between the values E/2 and E, although the relationship between crystal thickness and crystallization temperature is

not straightforward. It is known that the samples are highly crystalline from wide-angle X-ray scattering results. Assuming a simple model in which the oligomer chains are linked together by hydrogen bonds to create pseudo-polymers, which crystallize via adjacent re-entry at the crystal surface, a series of discrete values of crystal thickness are possible corresponding approximately to the length of n repeat units where n lies between 12 and 24. The length of each repeat unit corresponds to half the *c* (*c*=0.596 nm) spacing in the unit cell, i.e. 0.3 nm, based on the same unit cell parameters in PHB [Barham *et al.*, 1984].

At the lowest crystallization temperatures, a value of thickness close to E/2 has been obtained. A small proportion of crystals with this thickness were also detected in samples grown at much higher temperatures, consistent with some secondary crystallization on quenching to room temperature. Once folded crystals of 24-mer begin to melt at around 105°C, so it is extremely unlikely that these crystals could have grown at the crystallization temperature. At the highest temperature of 120°C, a thickness very close to the extended chain length has been measured, both from primary crystallization and from folded chain crystals that have been heated subsequent to growth. Between these extremes a range of values are obtained, but the points are clustered particularly around values corresponding approximately to chains with 16 and 18 repeat units (see Figure 6.8).

The small plateau at a thickness corresponding to 16 repeat units confirms the earlier suggestion from HB 32-mer that a crystal thickness of 2/3 E is a preferred value, although the preference is not strong. It can be argued that this thickness is energetically favoured because the arrangement of chains results in a relatively high proportion of chain ends on the crystal surface (and hence a lower surface energy). Now the model can be extended further by calculating the proportion of chain ends that would lie on the surface of a perfect crystal for each value of n between 12 and 24: this is shown on the chart in Figure 6.12. Using this simple model, chain conformations with 12 and 24 repeat units can be seen as particularly favourable (as expected) followed by 16 (2/3 E), 18 (3/4 E) and 20 (5/6 E). The chain conformations corresponding to these values are sketched in Figure 6.13.

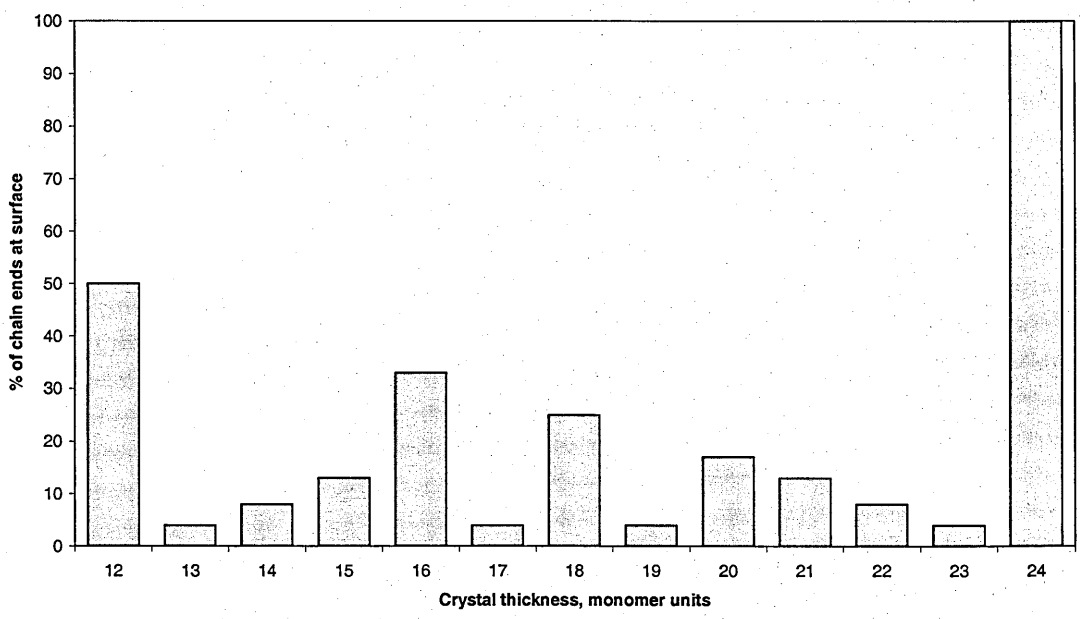

Figure 6.12 Chart showing the percentage of chain ends in the 24-mer crystal surface for different crystal thicknesses; see text for an explanation of the assumptions made.

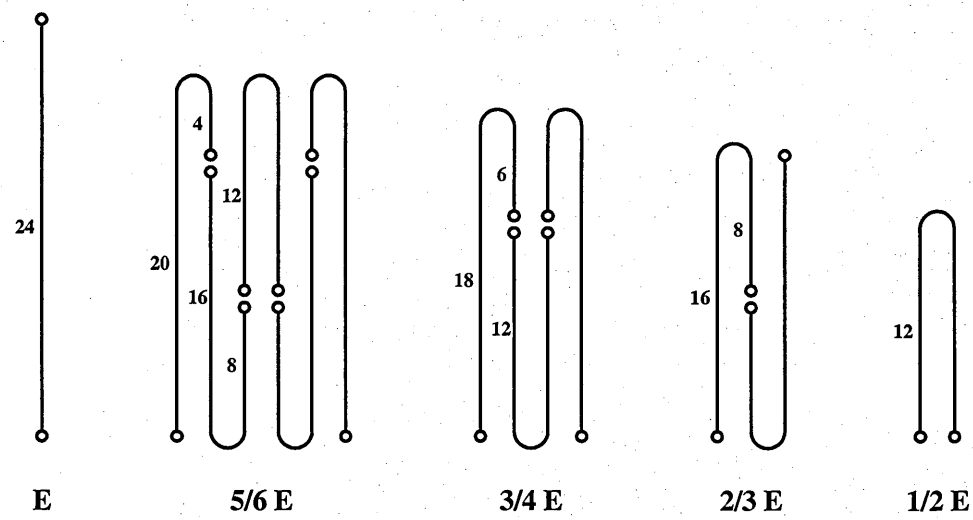

Figure 6.13 Schematic drawing showing the favourable chain conformations corresponding to extended (E), 5/6E, 3/4E, 2/3E and 1/2E chain forms, ignoring the chain length involved in the folds for simplification. The circles represent the OH groups (or protecting end groups) at the chain ends and the numbers indicate the monomer repeat units in each section.

The experimentally observed preference for crystals with thickness close to 16 and 18 monomer units is thus consistent with the prediction from this simple model for the most energetically favourable thicknesses. The actual measured thicknesses are slightly less than the exact fractional values, as would be expected due to the length of

chain involved in the fold. A preference for a thickness corresponding to 20 repeat units is less clear, although crystals grown at 106 and 110°C both yielded results quite close to this value, see Figure 6.8.

Two different X-ray systems were used to obtain the results, as shown in Figure 6.8. The nominal beam size for both X-ray systems is comparable at about 0.3 mm diameter, so that in these experiments several spherulites were generally sampled simultaneously. The two systems use different types of X-ray source, optics and detectors, which result in significantly better resolution in the ESRF system. If crystals are growing within the same sample with different, but similar, thicknesses this will be particularly difficult to resolve using the 'Bristol' set-up and the possibility of mixed crystal populations in these samples cannot be easily ruled out.

A second complication is that crystals can, and do, thicken during growth. The pairs of points recorded in-situ at ESRF at 85, 100 and 110°C were each obtained during a single crystallization run, the lower point coming from the initial growth and the upper point taken after crystallization was complete. This is an aspect that requires further investigation and will form the subject of a subsequent project. Apart from the points described above, crystallization times were relatively short; chosen to allow most of the sample to crystallize, while minimising the time available for annealing.

6.4.2.2 A reconsideration of crystal growth rates associated with the chain conformation

The growth rate vs crystallization temperature curve of HB 24-mer in Figure 4.5, given previously in chapter 4, reveals particularly scattered growth rate measurements at 85 and 100°C. For convenience, the growth rate curve is repeated here in Figure 6.14. By comparison with the thicknesses data in Figure 6.8, it is interesting to note that 85°C corresponds to the point at which the crystal thickness changes from 16 to 18 monomer units and 100°C marks the end of the temperature region where values close to 18 monomer units are favoured. At both these temperatures a number of slightly different crystal thicknesses were measured. Since each growth rate measurement corresponds to an individual spherulite, while the SAXS measurements are likely to encompass several different spherulites, it seems plausible that the result

observed here is a competition between two similarly stable crystal forms. An individual spherulite might grow in either form, depending on the initial nucleation conditions, while the SAXS result would be skewed towards the thickness of the majority population.

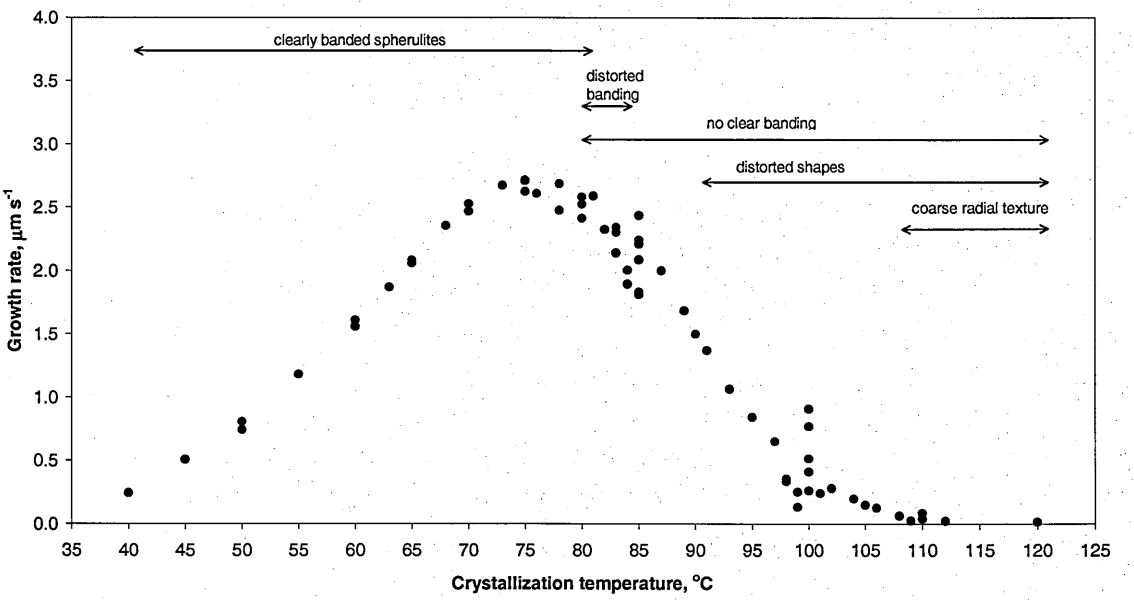

Figure 6.14 Growth rate as a function of crystallization temperature for HB 24-mer crystallized from the melt.

Crystals with different thicknesses have different melting points; the thicker the crystal the higher the melting point. Similarly, the supercooling at which a crystal grows will depend not only on the temperature, but also upon the actual crystal form (thickness) in which it grows ($l \propto 1/\Delta T$). This leads to an interesting phenomenon: at a higher crystallization temperature only a thick crystal can grow; as the temperature is reduced, so the supercooling for that crystal thickness increases and hence its crystallization rate also increases. Eventually the temperature falls below the melting point of a thinner crystal form, so it may start to grow. But the supercooling for that form is still low and it will only grow slowly; however, as the temperature falls further the growth rate increases and it can become the faster growing crystal, so it dominates.

As shown previously in chapter 4, there are some apparent discontinuities in the growth-rate gradient of 24-mer, particularly at temperatures around 100 and 85°C,

although they are not as pronounced as the minimum found in the n-alkanes. The SAXS measured thickness data shown in Figure 6.8 suggest that there may well be changes in the thickness of the growing crystals near these temperatures; from 16 to 18 repeat units at around 85°C and from 18 to 20 repeats near 100°C. Unfortunately, these thickness data are not directly measured from the crystals on which the growth rate measurements were made. However, an attempt can still be made to look in greater detail at the variation of growth rate with temperatures to see whether there are differences that may be attributed to changes in crystal thickness. It is conventional to plot ln$G$ against $1/T_c\Delta T$ and expect to see a linear graph (see section 2.3.2.2 in chapter 2), rather than the highly curved graph obtained when G is plotted against T_c in polymer crystallization. In the case of 24-mer growth, it is known that different crystals are growing with different thicknesses and hence at different supercoolings, therefore a more general plot can be made.

It is important to recognize that it is dealed here with oligomers rather than polymers. In polymer systmem the equilibrium melting temperature, T_m^0 is usually taken as the melting point of an infinitely thick crystal made up from infinitely long molecules. In the case of oligomers this is, of course, not appropriate. The melting temperatures corresponding to different chain lengths are taken from the graph of T_m vs n shown in Figure 6.15, and the supercoolings are thus calculated by $\Delta T = T_m - T_c$. The melting points of different crystal forms of 24-mer and 32-mer of known thickness in Figure 6.15 were derived from data obtained in heating experiments described in the following chapters, chapter 7 and 8.

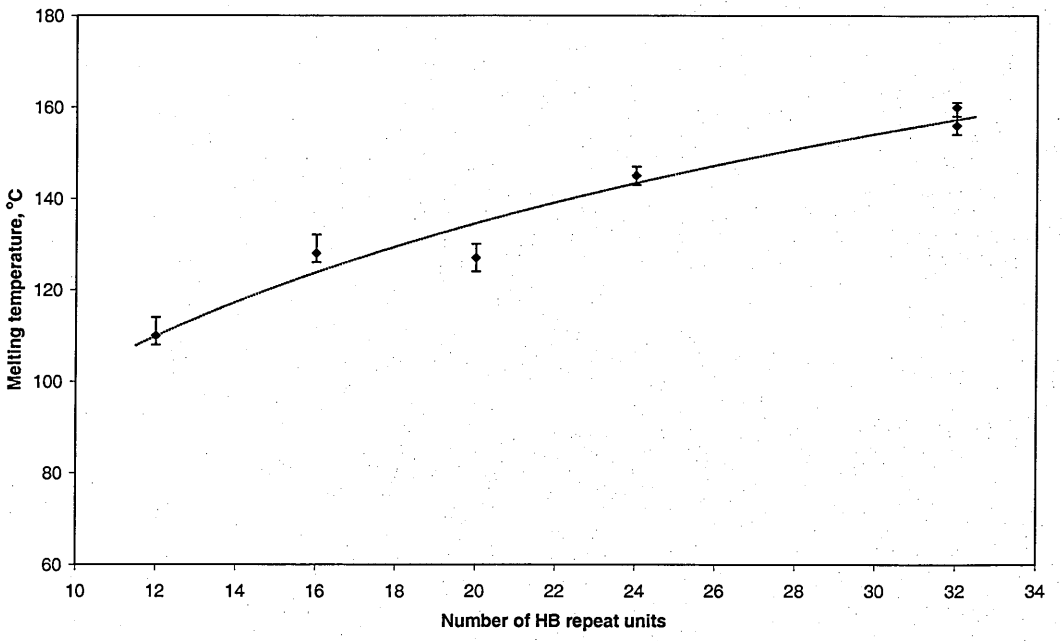

Figure 6.15 Variation in melting temperatures with crystal thicknesses, expressed in number of monomer units.

To construct the graph of ln$G$ against $1/T_c\Delta T$ from the growth rate data in Figure 6.14 a small subset of temperatures for which (by comparison with Figure 6.8) the crystal thicknesses are reasonably credible was first selected. These were at 78°C, 90–95°C, 106–110°C and 120°C. The corresponding thicknesses are 16, 18, 20 and 24 monomer repeat units respectively. These points are circled on Figure 6.16 (a), and were used to generate the best-fit line shown on the graph. Then an attempt has been made to plot the remaining points, taking the range of possible thicknesses into account. For example, for crystallization between 79 and 89°C, 16 or 18 repeat units should be considered, while between 97 and 105°C 18 or 20 repeat units are possible. These different possibilities are shown on Figure 6.16 (a) by the uncircled points corresponding to each value of n. In most cases it is clear that only one of the different possible thicknesses produces a data point near the expected line. In that case it is assumed that the crystals actually grew with that thickness: those points, together with the points used to generate the original line, are plotted in Figure 6.16 (b).

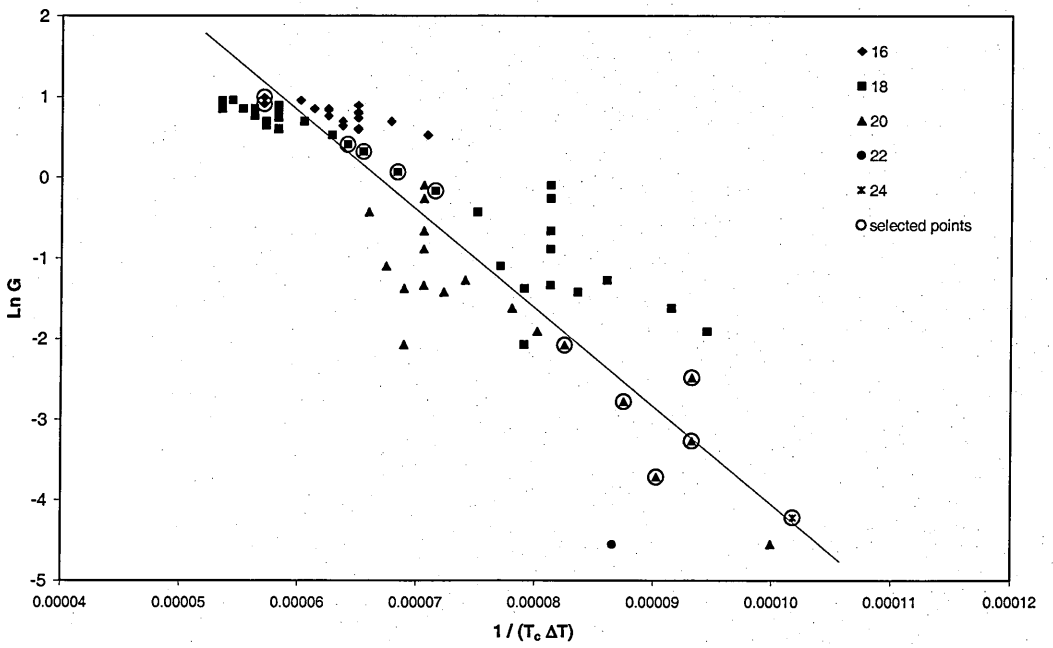

Figure 6.16 (a) Plot of ln$G$ vs $1/T_c\Delta T$ used to deduce the most likely thickness corresponding to each growth rate. The line was constructed from the circled points, where the crystal thicknesses are reasonably credible. For other points two possible values are shown.

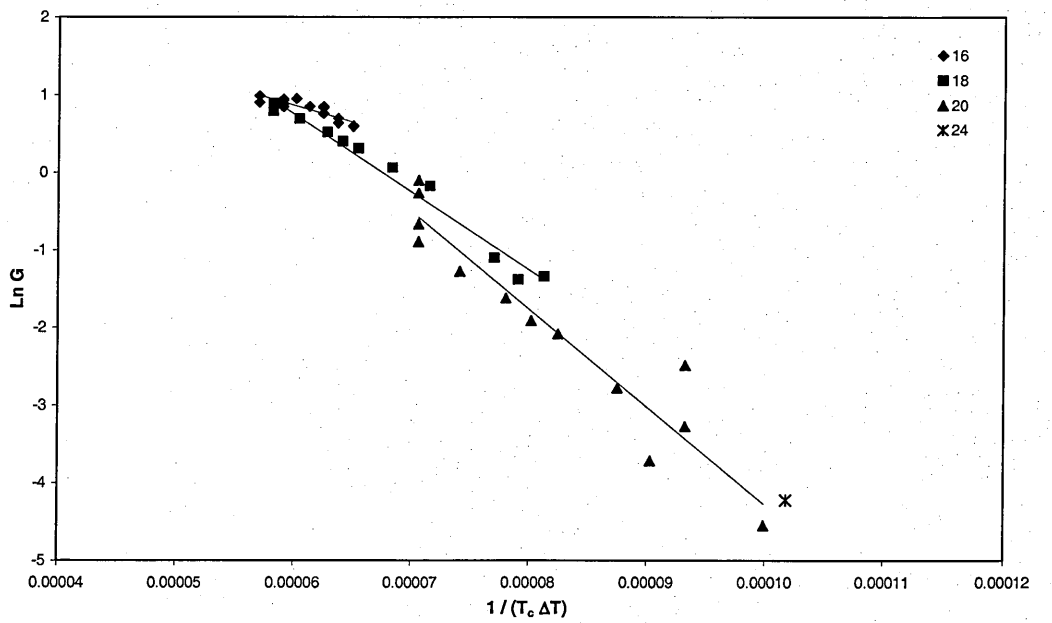

Figure 6.16 (b) Separate best fit lines calculated for each set of data from Figure 6.16 (a), each line corresponding to a different crystal thickness. On this graph only the points closest to the line from Figure 6.16 (a) are included.

Of course, this procedure is at best a crude approximation. The 'equilibrium melting temperature', T_m^0, for each thickness comes from measurements of actual melting

temperatures (T_m) and these values are subject to significant error. Furthermore, in practice it should not be expected that all the data lie on a single straight line but rather there should be a separate line for crystals of each thickness, due to differences in the surface free energies and other terms. In Figure 6.16 (b) a separate best fit line has been included for each of the three sets of data corresponding to thicknesses of 16, 18 and 20 repeat units. This technique shows that the data are best interpreted as coming from crystals growing with different thicknesses and gives a most likely thickness to each growth rate measurement. Figure 6.17 shows all the replotted data in the form of G vs T_c, now using different symbols to show the assumed crystal thickness of each sample. The open symbols represent points which did not fit well to either value.

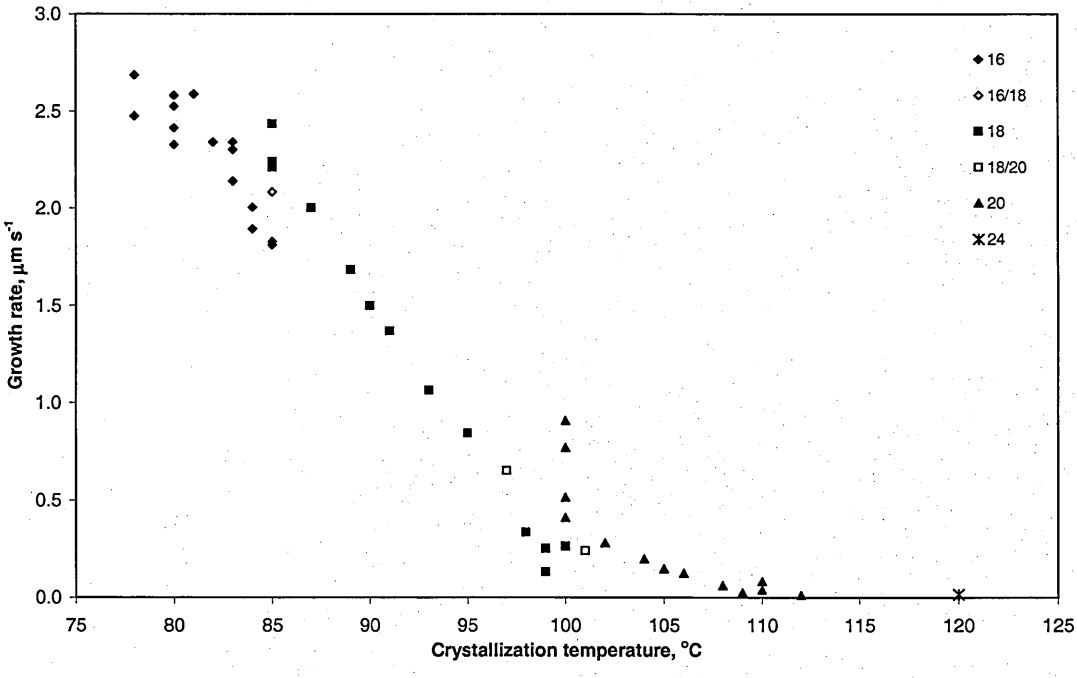

Figure 6.17 Growth rate as a function of crystallization temperature for the 24-mer, showing the most likely crystal thickness (in monomer repeat units) as deduced from Figure 6.16.

The origin of the discontinuities at 85 and 100°C now become much clearer. In each case two superimposed curves can effectively be seen. At 100°C one curve (black triangles) corresponds to crystals with a thickness of 20 repeat units, and shows a sharp rise in G as ΔT increases; the other (black squares) correspond to crystals with a thickness of 18 repeat units. These crystals are at a lower effective supercooling and therefore grow more slowly. However, it is known that in alkanes the nucleation rate

passes through a minimum with decreasing crystallization temperature which corresponds to a change of growth in one folded form to a thinner folded form; this is best explained as the thinner form having a higher nucleation rate then the thicker form [Organ *et al.*, 1996]. Accordingly, it may be expected that in the case of HB oligomers grown at lower temperatures, nucleation of the thinner crystals is more likely to occur and they therefore should become the dominant form as the temperature is reduced further. The intermediate values are likely to arise from competition between these two competing crystal types, which may also be a factor in the particularly distorted crystal shapes that occur in this temperature range, see Figure 4.6 (g) and (h) in chapter 4. A similar situation is evident at 85°C, where curves corresponding to crystals with thickness 16 (black diamonds) and 18 (black squares) repeat units are superimposed.

Figure 6.16 (b) shows clearly that there is a decrease in 'slope' with decreasing crystal thickness. At first sight this may seem surprising. The 'slope', d, in this plot, in the terms of the simple models is given by

$$d = -\frac{Kb\sigma\sigma_e T_m^{\,0}}{k\Delta H} \qquad (6.2)$$

where K is a constant (usually 2 or 4 depending on the growth mechanism), b is the lattice parameter in the growth direction, σ is the crystal side surface free energy, σ_e is the crystal end surface free energy, ΔH the enthalpy of fusion, k is Boltzman's constant and $T_m^{\,0}$ is taken from actual melting temperatures for different thicknesses, in this case, equals to T_m–T_c. Equation (6.2) is derived from Equations (2.8)–(2.10) in chapter 2. From Figure 6.12 one might expect σ_e to increase with decreasing crystal thickness, and ΔH to decrease with decreasing thickness. Furthermore, the viscosity of the melt will increase with decreasing temperature (decreasing thickness) so that an overall decrease in overall slope with decreasing thickness is at least reasonable.

6.5 Conclusions

Measurements on crystal thicknesses of HB 24-mer and 32-mer crystals grown both from the melt and solution over a range of crystallization temperatures have been performed using small angle X-ray scattering.

Overall, the HB oligomers form thin crystals with a range of thicknesses between extended and half of the extended chain length, although some thicknesses are possibly preferred over others. This is in contrast to the long n-alkanes, where a clear preference for thicknesses which are an integer fraction of the extended chain length has been observed. The difference in HB oligomer behaviour is likely to be due to the presence of hydrogen bonding between chain ends, which enables the oligomers to exhibit a more polymeric behaviour.

The results can be interpreted in terms of a model where crystal thicknesses which result in a relatively higher proportion of chain ends in the surface are slightly preferred over others. For the 24-mer, these correspond to E/2, 2/3E, 3/4E and 5/6E chain length. The suggested discontinuities previously observed in the gradient of the growth-rate vs crystallization temperature curve (at ~85 and 100°C) for the 24-mer can then be interpreted in terms of changes from one preferred chain conformation to another, i.e. from 2/3E to 3/4E and from 3/4E to 5/6E respectively. Whether such behaviour is a phenomenon limited to HB oligomers or is more general and can occur in other systems remains an open question still to be addressed.

Chapter 7 Unfolding Transitions during Heating of HB Oligomer Crystals Grown from the Melt

7.1 Introduction

Previous work on long *n*-alkanes crystallized from the melt has demonstrated that stable crystal forms have thicknesses equal to integer fractions (IF) of the extended chain length. Transient non-integer fraction (NIF) forms are often formed during initial crystallization but these rapidly transform into IF crystals (see section 3.2.3 in chapter 3). A structure has been proposed for the NIF crystal form which contains a mixture of folded and extended chains, with a thick amorphous region composed of long cilia from the extended chain portions [Ungar *et al.*, 2000]. Folded chain crystals thicken when heated to higher temperature, successively passing through thicker IF conformations until they melt completely. Published examples include the once-folded to extended chain transition in $C_{198}H_{398}$ [de Silva *et al.*, 2002] and transitions from four times folded to three, two, then once-folded chains in $C_{390}H_{782}$ [Ungar and Zeng, 2001]. A high resolution WAXS study of chain folded $C_{198}H_{398}$, $C_{246}H_{494}$ and $C_{294}H_{590}$ [Terry *et al.*, 2003] has shown that each thickening event is preceded by an increase in disorder, as measured by the change in peak width, and that each thickening step is accompanied by a contraction of the crystal lattice.

A preference for certain more stable crystal thicknesses is also found for the HB oligomers but these are not always integer fraction forms. Presented in this chapter are the results from heating HB oligomer original as-received powders, melt-grown crystals of HB 24-mer and 32-mer with the chains folded in half, and crystals of 32-mer with a thickness corresponding to 2/3 of the extended chain length which are believed to correspond to a stable NIF form. There are both similarities and differences between the behaviour of these materials and the long n-alkanes: clear thickening transitions are seen, but the thickening can occur in discrete steps or gradual stages depending on the sample. Lattice distortions associated with chain unfolding produce an expansion in the fold direction when the chain extends. The effects of heating rate and of the benzyl protecting group on the thickening process are also investigated here.

7.2 Experimental Procedure

High resolution real time wide angle X-ray scattering (WAXS) has been used to follow changes in crystallinity and lattice parameter which occurred on heating HB oligomer crystals grown from the melt. These effects can be correlated with changes in crystal thickness detected by small angle X-ray scattering (SAXS). The samples used in this study have 16, 24 or 32 repeat units (to be referred to as 16-mer, 24-mer and 32-mer respectively here) and most research effort was concentrated on the 32-mer, both with or without a benzyl protecting end group. The structures of the free and protected HB 32-mer powder samples are given in Figure 7.1.

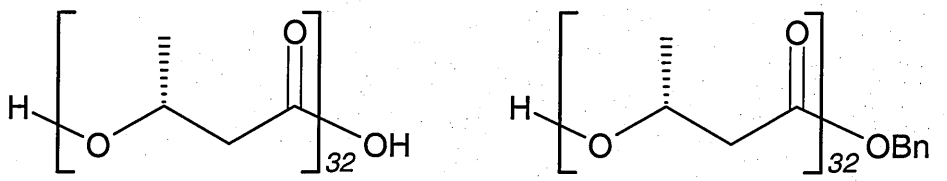

(a) (b)

Figure 7.1 Chemical structures of (a) HB 32-mer with no protecting end groups; (b) HB 32-mer with benzyl protecting end group.

For the initial WAXS measurements powders of 16-mer, 24-mer, 32-mer and 32-mer(p) were packed into 0.5mm diameter Lindemann tubes and mounted in a modified silver block Linkam hotstage placed in the X-ray beam. The samples consisted of as-received powders, which originally crystallized rapidly during solvent evaporation in the final stages of preparation. WAXS and SAXS measurements were made at the ESRF Grenoble, using beamlines ID11 and ID2 respectively.

The samples were heated at a rate of 2 or 4°C min^{-1} from a temperature well below the melting point and X-ray diffraction patterns were collected every 12 seconds with an exposure time of 1 second. The beam was turned off between exposures to minimize radiation damage to the sample. Samples can be used several times before any serious degradation could be detected, but all the results reported here correspond to the first melting run. Further details of the experimental set-up and the detector characteristics have been given in chapters 5 and 6. Temperatures quoted here are as recorded from

the hotstage and are internally self-consistent. No correction for thermal lag has been applied, although independent calibration available in a previous experiment suggests that this may be up to 2°C using the same experimental set-up.

7.3 Results and Discussion

A WAXS pattern obtained from the HB 32-mer at room temperature with the main reflections indexed is given in Figure 7.2. This is typical of those from all the HB oligomers and corresponds very well to the patterns obtained from the polymer PHB [Barham *et al.*, 1984; Mitomo *et al.*, 1987]. Data analysis has been carried out using the two strongest reflections, arising from the crystallographic planes (020) and (110). After appropriate background subtraction the positions of the peaks were calculated together with the intensity (equal to the area of the peak) and the peak width, which is quoted as full width at half-maximum height (FWHM).

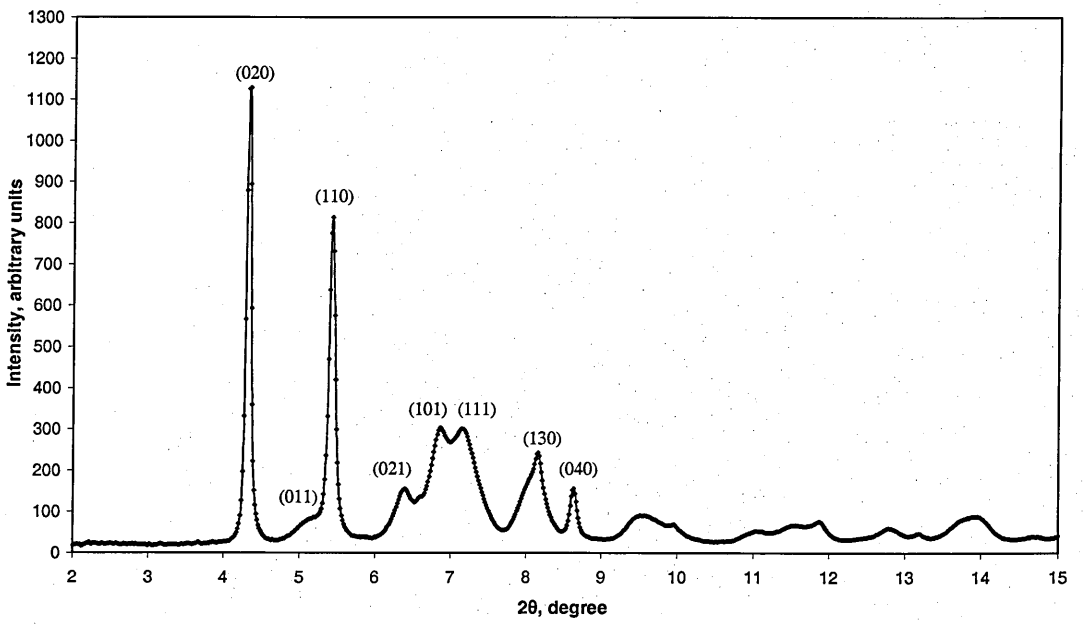

Figure 7.2 Wide angle X-ray diffraction pattern from HB 32-mer (original as-received powder) taken at room temperature, with the main crystalline reflections indexed.

7.3.1 Unfolding transitions in the HB 32-mer

Figure 7.3 shows typical results from a 32-mer with free ends heated at 4°C min^{-1}. In Figure 7.3(a) the change in intensity as the sample is heated is shown alongside the variation in d-spacing, for the (020) reflection. Equivalent data for the (110) reflection is given in Figure 7.3(b). The variation in peak width with temperature was similar in both crystallographic directions and is shown for (020) in Figure 7.3(c), superimposed on the intensity data so that the behaviour at key temperatures can be compared.

(a)

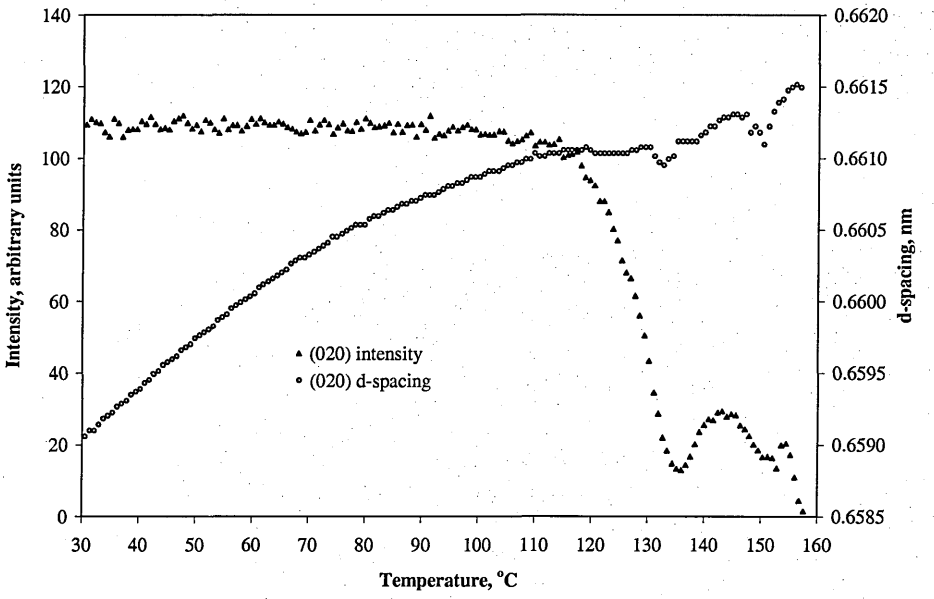

(b)

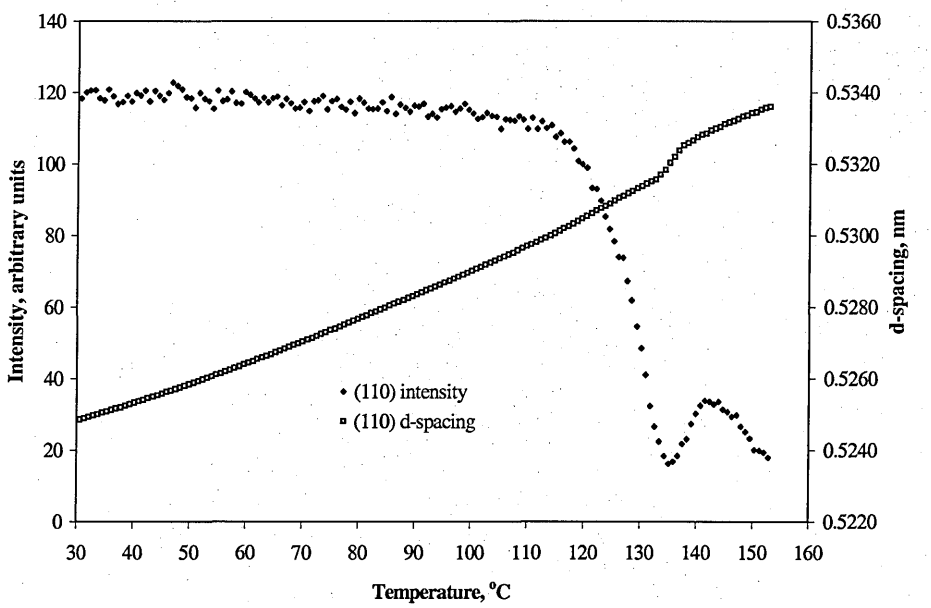

(c)

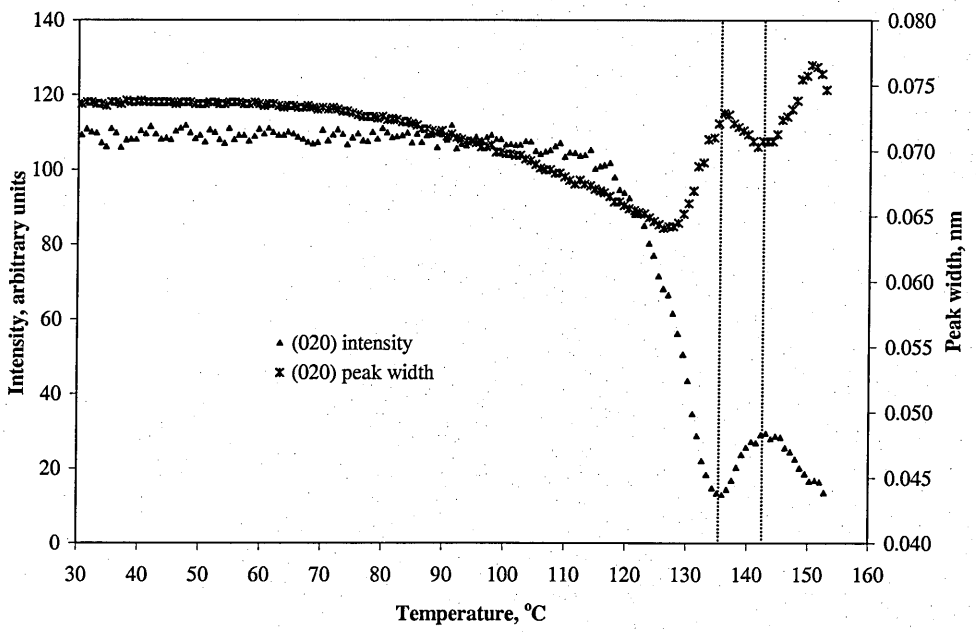

Figure 7.3 Wide angle X-ray results from HB 32-mer, heated at 4°C min^{-1}.
(a) Variation in intensity and lattice spacing with temperature in the (020) direction.
(b) Variation in intensity and lattice spacing with temperature in the (110) direction.
(c) Variation in peak width with temperature for the (020) reflection. This is superimposed onto the intensity data so that the behaviour at the key temperatures of 136 and 143°C, shown by dotted lines, can be compared.

From previous SAXS measurements on the as-received powders, it is known that these crystals contain folded chains, the exact nature of the folded chain conformations that can occur has been discussed earlier in chapter 6. Crystal thicknesses have been measured in different samples corresponding to chains which are folded exactly in half (integer fraction, IF) or to non-integer fraction (NIF) folded forms, most often with thickness equal to approximately two thirds of the extended chain in HB 32-mer. For the purposes of the present discussion the chains are simply referred to as folded or extended. Crystal thickness data will be considered with the SAXS results in the later section.

The intensity data shown in Figure 7.3 shows a very pronounced transition during melting, similar to those observed previously in long n-alkanes [Terry *et al.*, 2003] and in solution grown crystals of these oligomers, which will be reported in the next chapter, chapter 8. SAXS measurements have confirmed this to be associated with chain unfolding. The initial drop in intensity beginning at approximately 120°C

represents melting of folded chains. Extended chain crystals then begin to form and the intensity starts to rise again at 136°C, reaching a peak at 143°C. Above this temperature the extended chain crystals melt. While the main peak was obtained consistently from sample to sample, the small subsidiary peak in the intensity curve between 152 and 156°C shown in Figure 7.3(a) was not reproducible and this data has been omitted from subsequent traces. Similar small but non-reproducible effects were occasionally seen in other samples, always towards the end of the melting process. These may be artefacts arising from slight movement of sample in the X-ray beam, or could represent some real but secondary structural feature. One possibility could be the formation of a double layer structure made up of dimers linked by hydrogen bonding. Such structures have been observed in a long chain alkanoic acid [Zeng and Ungar, 1999]. At present there are not sufficient data to pursue this possibility further.

Further insights into the re-crystallization are obtained from the peak width data shown in Figure 7.3(c), where lines have been drawn at 136 and 143°C to aid comparison between the two curves. The peak width begins to decrease even before the apparent onset of melting of folded chain crystals, and continues to fall up to 130°C. This behaviour can be explained by the initial removal of less ordered folded chain crystal, so that the crystals remaining at 130°C, although smaller, are more perfect. Although the intensity is still falling from 130–136°C the peak width increases, and this is believed to be indicative of the onset of chain unfolding, causing disruption to the regular lattice packing. As extended chain crystals begin to form and the intensity rises, the peak width once again decreases, with 143°C representing the maximum extent of extended chain crystallization. Finally, as the newly formed extended chain crystals begin to melt the peak width first rises as the regular lattice becomes disrupted, and then starts to fall as the crystalline intensity decreases to zero. The changes in *d*-spacing on heating are discussed later.

7.3.2 Influence of heating rate

In Figure 7.4 the previous results are compared with a second sample of 32-mer heated at a slower rate of 2°C min^{-1}. Figure 7.4(a) shows the change in intensity with temperature: the basic pattern of behaviour is the same and the transition temperatures are virtually unchanged. The slower heating rate allows more time for unfolding to

take place and a higher proportion of material is transformed into the extended chain form. This result emphasises the relatively slow rate of unfolding in this sample. By increasing the time spent in the critical temperature range of 135–143°C from 2 minutes (at 4°C min^{-1}) to 4 minutes (at 2°C min^{-1}) the amount of re-crystallized material (as judged from the relative areas of the diffraction peaks) has risen from ~28% to ~65% of its initial value. Corresponding data for the (020) *d*-spacing and peak width at the slower heating rate are shown in Figure 7.4(b). The peak width data, which is plotted on an arbitrary *y* scale to facilitate temperature comparisons, shows a similar pattern to that seen at the higher heating rate.

(a)

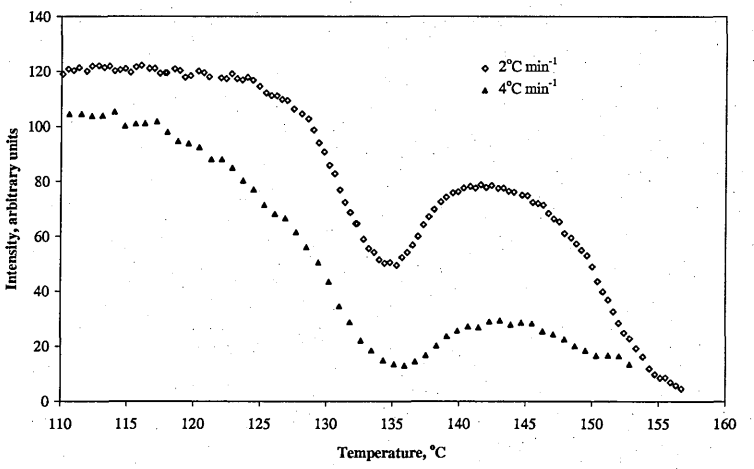

(b)

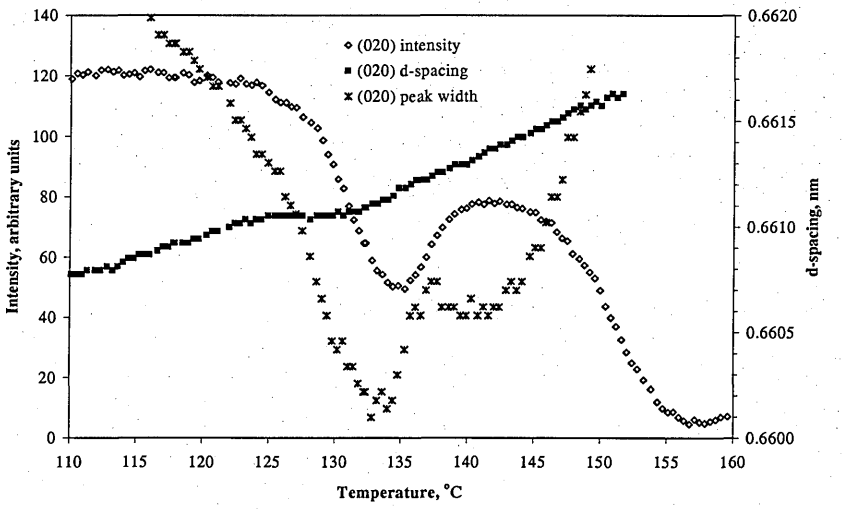

Figure 7.4 Effect of heating rate on the unfolding transition for HB 32-mer. (a) Change in intensity with temperature during heating at 2 and 4°C min^{-1}; (b) Variation of (020) lattice spacing and peak width with temperature during heating at 2°C min^{-1}, with intensity data included for comparison. The peak width is plotted on an arbitrary scale.

7.3.3 Changes in lattice spacing accompanying chain unfolding

The principal fold direction in PHB has been shown to be along the (110) direction [Barham *et al.*, 1984] and it is assumed to be the same in these HB oligomers. In this direction, where there is connectivity along the chain, a very clear change in lattice spacing is observed during chain unfolding and an example can be seen in Figure 7.3(b). The lattice expands in a regular way during heating, as would be expected from thermal expansion. In addition, there is a discontinuous increase of 0.001 nm (or ~0.2%) associated with chain unfolding, identical to that seen in solution grown crystals of HB oligomers, which will be given in chapter 8, but opposite in direction to that observed during unfolding in n-alkanes [Terry *et al.*, 2003]. In this case, it appears that the folds serve to pull adjacent oligomer stems closer together along the (110) fold direction. Thermal lattice expansion is also seen in the (020) direction, and a somewhat irregular decrease in the rate of expansion accompanying partial dissolution and re-crystallization can be seen in Figure 7.3(a). A much clearer pattern of behaviour is apparent when the slower heating rate is employed, as seen in Figure 7.4(b). As the folded chain crystals begin to melt the thermal expansion is reduced, but the original rate of expansion resumes once extended chain crystals start to form. Overall, there is a discontinuous decrease in (020) lattice parameter of approximately 1.5×10^{-4} nm, or 0.02%, in this direction, which is considerably smaller than the increase along the fold direction. If the crystal lattice were truly orthorhombic both before and after chain extension, these differing expansion factors would imply a large increase in (100) lattice spacing, which was not observed in the diffraction patterns. It therefore appears that the lattice is in fact slightly skewed in at least one of the crystal types observed here. It could suggested that the extended chain crystal lattice represents a 'perfect' HB lattice, which is evidently disrupted by the chain folds in a manner which pulls the chains closer together in the fold direction.

7.3.4 Effect of benzyl protecting end group

Figure 7.5(a) compares the (020) intensity data from a sample of 32-mer with no protecting end groups to that of 32-mer(p) which has a protecting benzyl group attached to one end of the chain. The heating rate was $4^{o}C\ min^{-1}$ in both cases. The corresponding changes in *d*-spacing on heating are shown in Figure 7.5(b). The

samples give similar initial intensity, melting occurs over a very similar range of temperature, and the extent of the initial melting is virtually the same. Therefore the samples are believed to have a very similar initial composition.

(a)

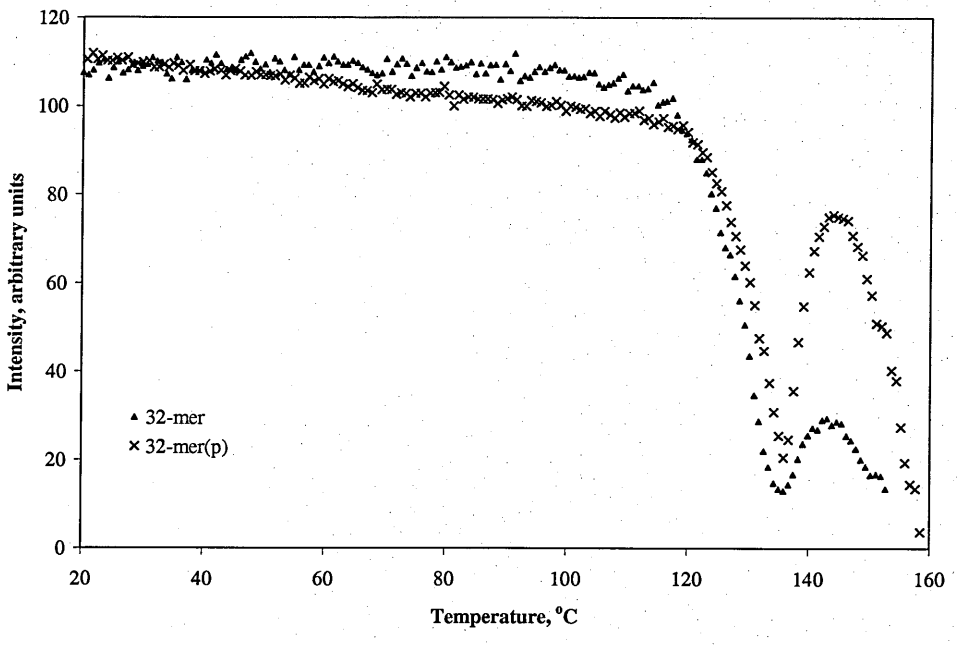

(b)

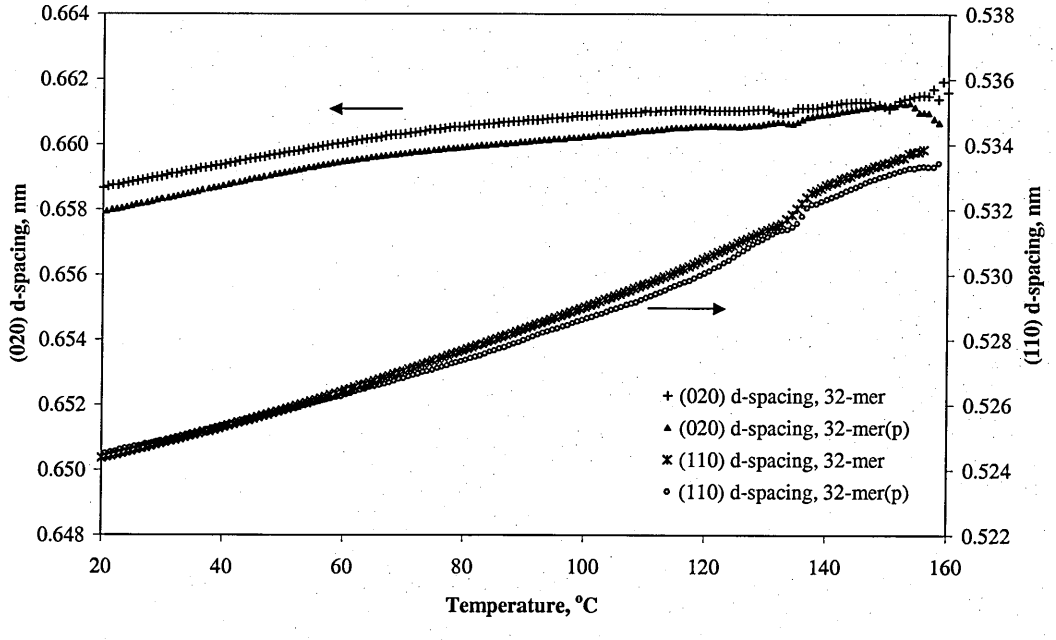

Figure 7.5 Effect of benzyl end group on the unfolding transition. (a) Variation in (020) intensity with temperature for HB 32-mer samples. (b) The corresponding changes in *d*-spacing on heating. The 32-mer has no protecting end group, while the 32-mer(p) has a protecting benzyl group attached to one end of the chain. Heating rate is 4°C min^{-1}.

The temperature range over which chain unfolding and re-crystallization occurs is not affected by the presence of the benzyl end group, but the extent of re-crystallization is much greater in the sample with the protecting end. This rather surprising result implies that rather than impeding the unfolding process, the presence of the benzene ring facilitates unfolding. One possible explanation, that the presence of the benzene ring weakens the forces of attraction between neighbouring chains, does not seem to be borne out by the lattice-spacing measurements. Figure 7.5(b) shows that there is a small but consistent difference in the (020) spacing when the chains are folded, with the benzyl-terminated chains packing more closely than the unprotected chains. This difference is reduced when the chains extend. In the (110) direction the spacing is initially the same, but the lattice containing benzyl-terminated chains expands slightly less during heating. A more likely explanation for the increased rate of chain unfolding is that the capped oligomers have higher mobility due to reduced hydrogen bonding between the ends of chains, so that the potential for formation of dimers, trimers etc is reduced. A full explanation of these small but genuine differences requires a detailed analysis of the precise crystal structure, which is beyond the scope of this study. For the current purposes it suffices to note that unfolding transitions are clearly seen in samples of 32-mer, whether or not the benzyl protecting end group is present, and the transition temperatures are not affected by the end group. The benzyl protecting end group had no apparent effect on either crystal morphologies or growth.

The co-efficient of thermal expansion, calculated from the unprotected samples between 20 and 80°C, is 3.1×10^{-5} nm $^{\circ}C^{-1}$ in the (020) direction and 5.5×10^{-5} nm $^{\circ}C^{-1}$ in the (110) direction. Very similar data has also been obtained from PHB polymer and is given in other publication [Martinez-Salazar *et al.*, 1989]. However, it should be noted that the *a* and *b* axes are assigned differently in that publication. No obvious jumps were observed during the heating of PHB, over a temperature range where the chains are unfolding, but did not approach the extended chain length.

7.3.5 A return to the crystal thicknesses in the HB 32-mer

Having established that the unfolding transitions occurred in both protected and unprotected samples, the 32-mer(p) was used for subsequent SAXS experiments since it showed clearer transitions and was available in larger quantity. In this section,

studies of unfolding transitions followed by real time WAXS, and the associated changes in HB 32-mer crystal thickness and chain conformation, will be presented in detail.

Figure 7.6 shows crystal thickness data for two samples of 32-mer(p) as a function of temperature, collected during heating at 4°C min^{-1}. The horizontal lines correspond to the extended chain length of 32-mer (E), and to half and two thirds of that value. These lengths are included for guidance only. They make no allowance for the length of the benzene ring (which adds approximately 0.5 nm to the total length of the chain, but which can take up different positions within the crystals), nor for the length of the fold itself, nor for thermal expansion of the lattice during heating.

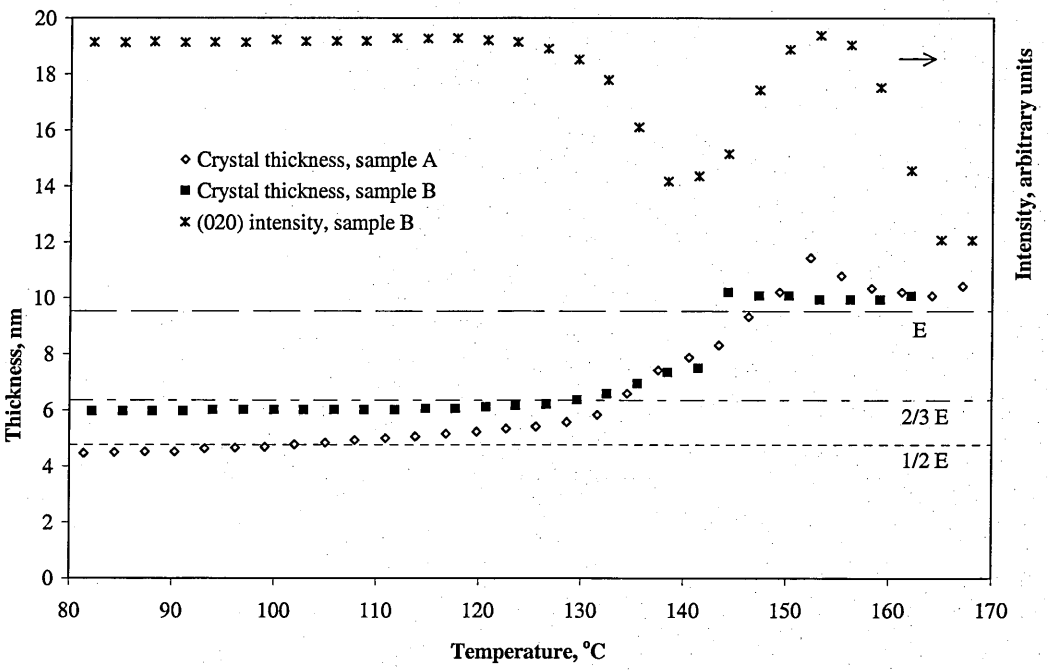

Figure 7.6 Crystal thickness measured from SAXS for 32-mer(p) as a function of temperature, collected during heating at 4°C min^{-1}. The horizontal lines correspond to the extended chain length of 32-mer (*E*), and to half and two thirds of that value (1/2E and 2/3E). Sample A crystallized during rapid cooling to room temperature; sample B was crystallized isothermally at 107°C. WAXS data collected simultaneously is included for sample B for ease of comparison.

Sample A crystallized during rapid cooling to room temperature and has an initial thickness slightly less than E/2. Sample B was crystallized isothermally at 107°C and has an initial thickness close to 2/3E. The possible chain conformation in this sample is discussed earlier in section 6.4.1 in chapter 6. WAXS data collected simultaneously

showed a clear transition in both samples, and the data for sample B is included in Figure 7.6 for comparison. This data provides convincing evidence that the transition in crystallinity observed using WAXS is indeed associated with chain unfolding to produce the change in crystal thickness revealed using SAXS.

The changes in crystal thickness which occur during heating for both samples confirm the proposed model of partial melting of folded chains, followed by re-crystallization in an extended chain form. There are, however, some subtle differences in behaviour between the two samples, which will now be examined in more detail. Figures 7.7 and 7.8 show a series of Lorentz corrected SAXS spectra corresponding to representative temperatures selected from the range of data summarized in Figure 7.6. The vertical lines in Figures 7.7 and 7.8 indicate the value corresponding to the thickness of extended chains of 32-mer (E) at room temperature and to one half and two thirds of that value, with the same qualifications as before. Note that the crystals of sample B (which have thickness close to 2/3E in Figure 7.6) give much sharper SAXS peaks than those of A (close to 1/2E) and that the small second order peak just visible in Figure 7.8 is actually a doublet. Room temperature spectra from these samples are shown in Figure 6.5 in chapter 6 and the differences are discussed there.

In both samples, an initial rise in intensity with temperature has been seen as would be expected as the density difference between the crystalline and amorphous phase increases, see Figures 7.7(a) and 7.8(a). In the once-folded IF sample represented by Figure 7.7, there is a gradual shift in peak position during reorganization, towards higher crystal thicknesses, see Figure 7.7(b). This is accompanied by a decrease in intensity and a broadening of the peak, suggesting that a range of thicknesses may be present at any one time. Finally, the crystals stabilize at a thickness close to the extended chain value and the intensity rises once more, Figure 7.7(c). In the final trace at 167.1°C the crystals have almost completely melted.

The intensity variations are similar for the 2/3 folded NIF sample represented by Figure 7.8, but in this case there is a much sharper transition between folded and extended chain crystals. This contrasting behaviour suggests that unfolding is essentially a single stage process for this sample.

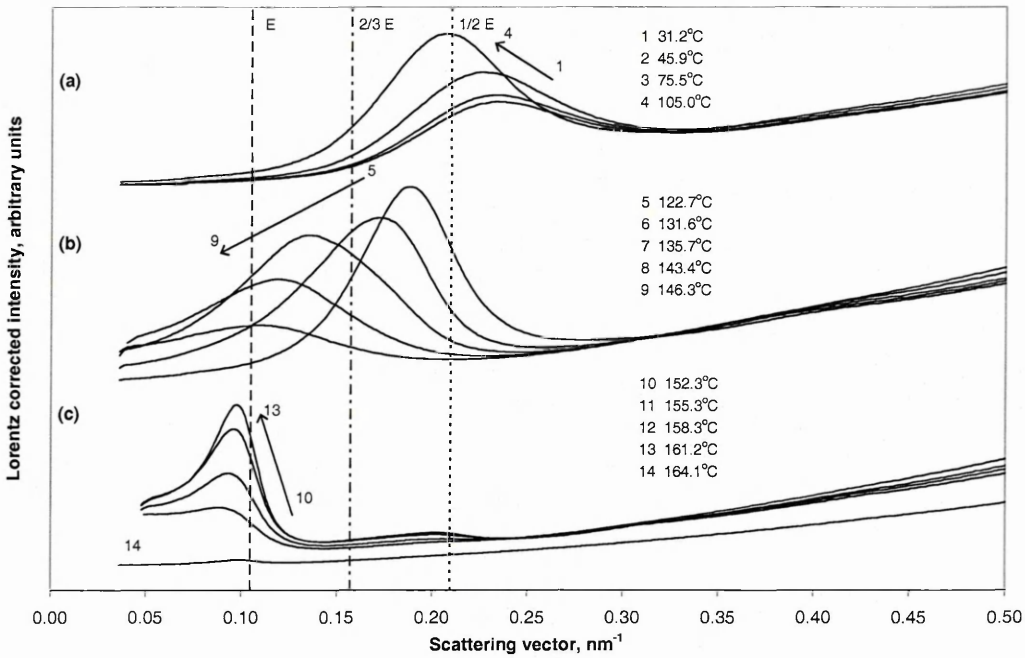

Figure 7.7 (a)–(c) SAXS spectra obtained at the temperatures shown from 32-mer(p) sample A. The vertical lines indicate the scattering vectors corresponding to the thickness of the extended chain length of the 32-mer (*E*) at room temperature and to 1/2 and 2/3 of that value.

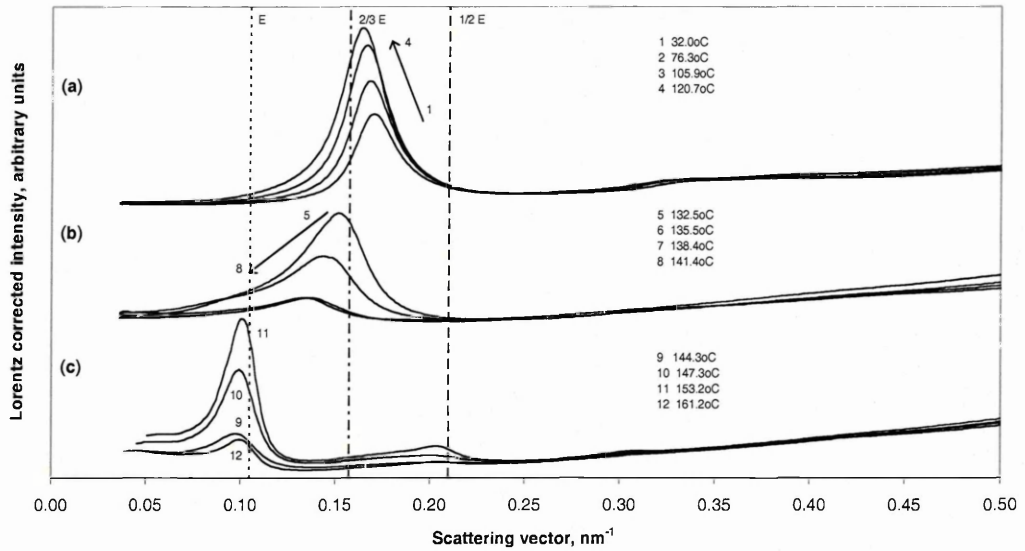

Figure 7.8 (a)–(c) SAXS spectra obtained at the temperatures shown from 32-mer(p) sample B. The vertical lines indicate the scattering vectors corresponding to the thickness of the extended chain length of the 32-mer (*E*) at room temperature and to 1/2 and 2/3 of that value.

7.3.6 Shorter chains: HB 24-mer and 16-mer behaviour

SAXS measurements from 16-mer powder give a crystal thickness of 4.80 nm, which compares well with the extended chain length of 4.77 nm, Table 6.1 in chapter 6. Figure 7.9 shows the WAXS intensity of the (110) reflection as a function of

temperature during heating at 4°C min^{-1}. No clear transition is apparent. The small discontinuity between 127 and 129°C may be due to movement of sample within the beam during melting, or could again indicate the presence of thicker crystals made up from dimers formed by chain association through hydrogen bonding between chain ends. The behaviour is consistent with extended chain crystals that do not re-organize during heating.

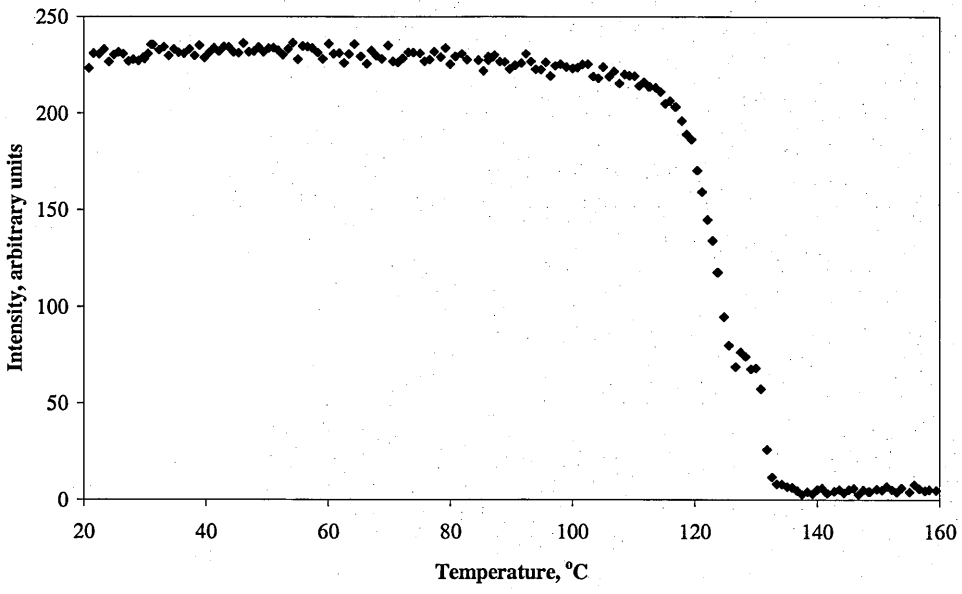

Figure 7.9 (110) WAXS intensity as a function of temperature for 16-mer, heated at 4°C min^{-1}

Results from simultaneous SAXS and WAXS measurements from a sample of 24-mer are shown in Figure 7.10. This sample was crystallized from the melt by rapid cooling to room temperature (sample F in Table 6.2). The measurements were taken during subsequent heating at 4°C min^{-1}. The initial crystal thickness changes from ~3.9 nm at low temperature to ~7.7 nm at high temperatures. By comparison with the extended chain length of 7.2 nm it is clear that once-folded chains initially existed, close to the IF value, which unfold on heating. The unfolding behaviour bears some similarity to that observed in the 32-mer but the transition is more rapid and occurs at a much earlier stage in the melting of the folded-chain crystals. Because extended chain crystals start to form before the majority of folded chain crystals have melted, the SAXS patterns collected during unfolding often show a double population of crystals. This is illustrated in Figure 7.11, which shows a selection of SAXS profiles collected at temperatures before (Figure 7.11a), during (Figure 7.11b) and after (Figure 7.11c)

the unfolding transition. As before, the lengths of the extended chain (E) and of half that value are included for comparison. Unlike the 32-mer IF sample shown in Figure 7.6 and 7.7, no crystal thicknesses were detected in the intermediate range between E/2 and E.

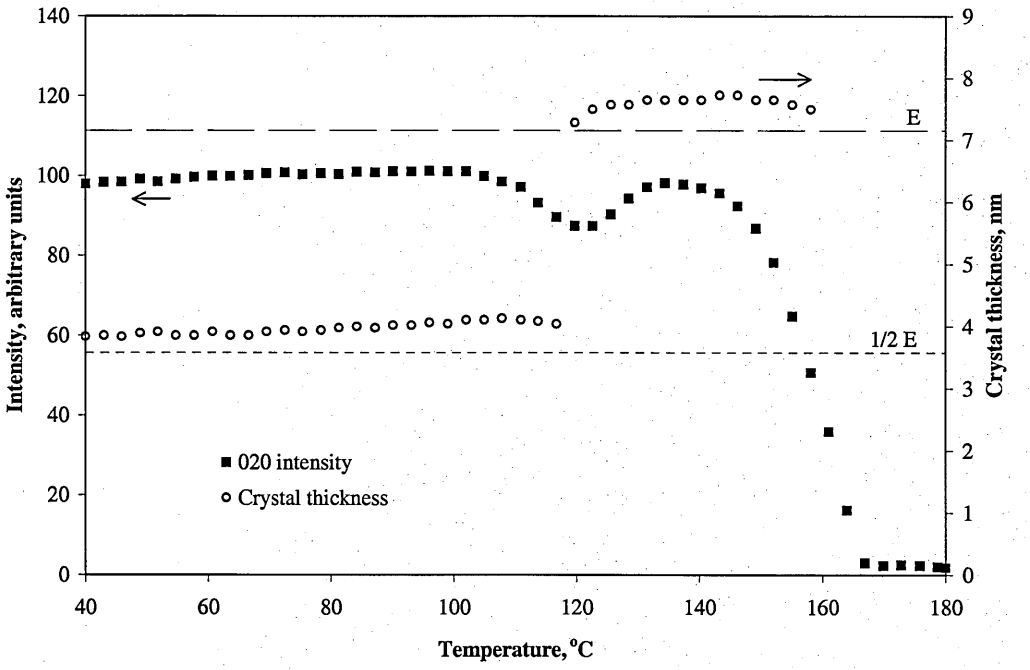

Figure 7.10 Simultaneous SAXS and WAXS measurements from a sample of 24-mer crystallized from the melt by rapid cooling to room temperature and subsequently heated at 4°C min^{-1}. The dashed lines correspond to the extended chain length (E) and 1/2 of that value.

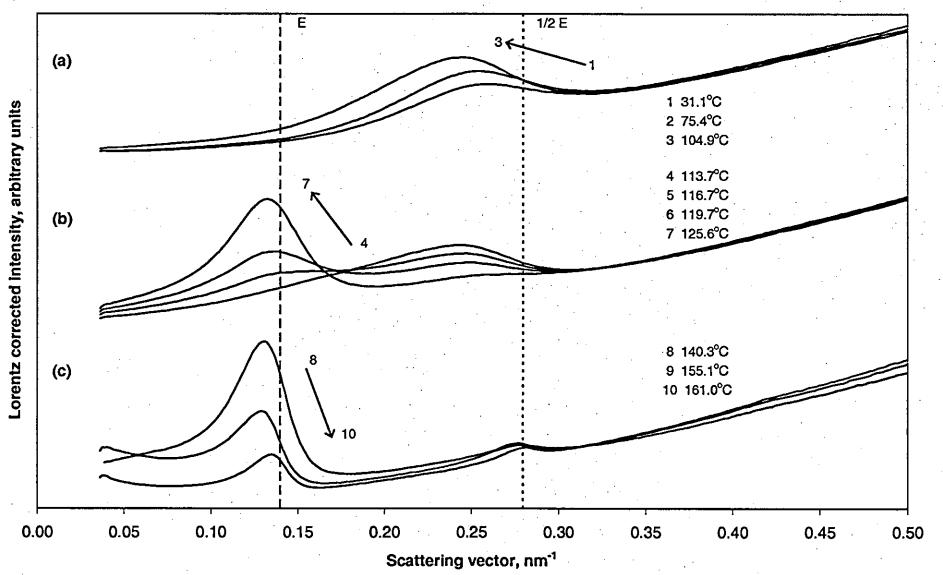

Figure 7.11 (a)–(c) SAXS spectra obtained at the temperatures shown from 24-mer crystallized from the melt by rapid cooling to room temperature and subsequently heated at 4°C min^{-1}. The vertical lines correspond to the thicknesses of the extended chain length (E) and to 1/2 of that value.

Ungar and co-workers have published SAXS results showing the once-folded to extended chain transition in $C_{198}H_{398}$ [de Silva *et al.*, 2002] and transitions from four times folded to three, two then once folded chains in $C_{390}H_{782}$ [Ungar and Zeng, 2001]. In both cases the thickening proceeds via discontinuous jumps from one integral folded form to another, as seen here for the 24-mer. In the $C_{198}H_{398}$ example chain tilt is invoked to account for a gradual decrease in thickness with temperature in both the folded and extended chain forms, with the tilt reaching a maximum value of 35° just below the melting point of the extended chain crystals. There is no evidence here for appreciable chain tilt in the HB samples. Polyethylene crystals can be grown with a wide range of lamellar thicknesses and, when heated, have been shown under certain conditions to rearrange initially via a discontinuous doubling in thickness. This is followed by a further gradual increase in thickness, the final extent of which depends on the heating rate (or annealing time) employed [Barham *et al.*, 1981; Martinez-Salazar *et al.*, 1985].

The behaviour of the 32-mer is rather different to that of the 24-mer, since there are examples both of stable NIF states and of transitory crystals with thicknesses between the stable forms. The latter may be partly a consequence of the slow thickening rate, which enables intermediate forms to be detected. It also seems that the effects of chain association through hydrogen bonding between ends would lead to a more 'polymeric' behaviour. However, the fact that the two different samples of 32-mer behave differently from each other is puzzling and suggests that the explanation is more complex.

7.4 Conclusions

High resolution wide angle X-ray scattering has been used to follow changes in crystallinity and lattice parameter which occur on heating hydroxybutyrate oligomers. These effects can be correlated with changes in crystal thickness detected by small angle X-ray scattering. Melt-grown crystals from HB oligomers with 24 and 32 repeat units that initially contain once folded chains transform during slow heating to produce extended chain crystals. This chain unfolding occurs via a process of partial melting and re-crystallization, and is accompanied by an expansion in the crystal

lattice of approximately 0.2% in the (110) fold direction and a much smaller contraction in the (020) direction. The rate of transformation is slow and is affected by the length of chain and the nature of the end groups. For the samples examined here complete extension took approximately 3 minutes in the 24-mer, 4 minutes in the protected 32-mer, and was not achieved within 4 minutes in the free 32-mer. The presence of a benzyl protecting group on one end of the chain does not affect the transformation temperature but reduces the (020) and (110) lattice spacings very slightly, as well as increasing the rate of transformation.

The variation in crystal thickness during chain unfolding depended both on the length of the chain and on the initial crystal thickness (which in turn depended on the crystallization temperature). In the 32-mer(p) examples were seen of a gradual increase in thickness from IF folded chains to extended chains, and of a discontinuous jump in thickness from NIF folded chains to extended chains. In the 24-mer a dual population of IF folded and extended chains was observed during transformation. In all cases examined here the stable crystal forms displayed specific crystal thicknesses simply related to the extended chain length, but the intermediate stages of thickening vary between samples.

Chapter 8 Thickening and Unfolding on Heating of HB Oligomer Crystals Grown from Solution

8.1 Introduction

Studies of n-alkane single crystals grown from dilute solution in toluene have shown that stable crystal forms have thicknesses equal to exact integer fractions of the extended chain length, the same as those found from melt-grown crystals. Under some conditions crystals can thicken from one stable form to another at a constant crystallization temperature, and characteristic crystal morphologies have been observed during this process [Organ *et al.*, 1990]. Rates of crystallization and thickening in solution have been measured using a method based on differential scanning calorimetry (DSC). These have revealed minima in crystallization rate where primary crystallization changes from one chain folded form to another. The growth rate dependence and associated changes in crystal morphology are explained using a simple theoretical model based on self-poisoning of a growing extended (or less folded) chain surface by almost-stable more times folded chain conformations.

A much wider range of preferred crystal thicknesses have been observed for the HB oligomers as presented in chapter 6. The growth rate data on HB oligomer crystals grown from the melt, in particular HB 24-mer, has revealed apparent discontinuities in growth-rate gradient at 85 and 100°C, but less pronounced than the minima found in the alkanes. These discontinuities associated with the thickness data and unfolding transitions followed by real time SAXS have confirmed the change between different crystal conformations at each point. A discontinuity has also been observed in solution-grown HB 32-mer growth-rate gradient at 36–37°C and limited data from 24-mer gives a weak indication of a discontinuity at 30–35°C. These discontinuities could correspond to the change from folded to extended chain forms.

This chapter concentrates on the crystal thickening and chain unfolding behaviour of HB 24-mer and 32-mer grown from dilute solution in propylene carbonate, followed in real time using synchrotron X-ray radiation. The growth rate data have been

successfully measured by in-situ synchrotron wide angle X-ray scattering (WAXS) and reported earlier in chapter 5. The changes to crystals of 24-mer and 32-mer that occur on heating in suspension will be described in detail here. These can be understood in terms of chain unfolding and provide further insight into whether the crystals grown at a particular temperature contained folded or extended chains. The high intensity of the synchrotron radiation allows clear diffraction patterns to be obtained for crystal concentrations as low as 0.1% (w/v) and the high resolution of the detector employed permits very small changes to the lattice parameters to be observed and measured.

8.2 Experimental Procedure

Samples were prepared from HB 24-mer and 32-mer. The 32-mer was also used for growth rate studies; both samples were used for heating experiments. The samples used in the experiments described in this chapter are all in the 'free' form.

A measured amount of oligomer (typically 0.3 mg) was placed in a 2mm diameter Lindemann tube and sufficient propylene carbonate was added to give a concentration of approximately 3% (w/v). The Lindemann tubes were then shortened and flame sealed to prevent evaporation of solvent during the experiment. For exposure to the X-ray beam the samples were mounted in a modified silver block Linkam hotstage. The wide-angle diffraction data were collected at the Materials Science beamline, ID11 at the ESRF Grenoble. Further details of the experimental set-up, the detector characteristics and the procedures used for data collection and analysis have been reported in section 5.3.4.1 in chapter 5.

Each sample was first crystallized isothermally as described previously in chapter 5. After crystallization was complete, the samples were heated at $8^{o}C\ min^{-1}$ until they had completely re-dissolved. Diffraction data were collected so that any changes occurring prior to dissolution could be examined. In one experiment the heating was stopped midway and the sample annealed for some time before resuming heating.

8.3 Results

8.3.1 HB 32-mer

Further insight into the conformation of chains within the crystals grown at different temperatures is obtained when the crystals are heated. Figure 8.1 shows the variation in intensity of the (020) reflection as HB 32-mer crystals are heated, in suspension in propylene carbonate, to the point where they dissolve. Results are shown for five different crystallization temperatures that span the range of interest and correspond to the same range shown in Fig 5.9 in chapter 5. The curves have been staggered along the *y* axis for ease of comparison: the final intensity was zero in each case.

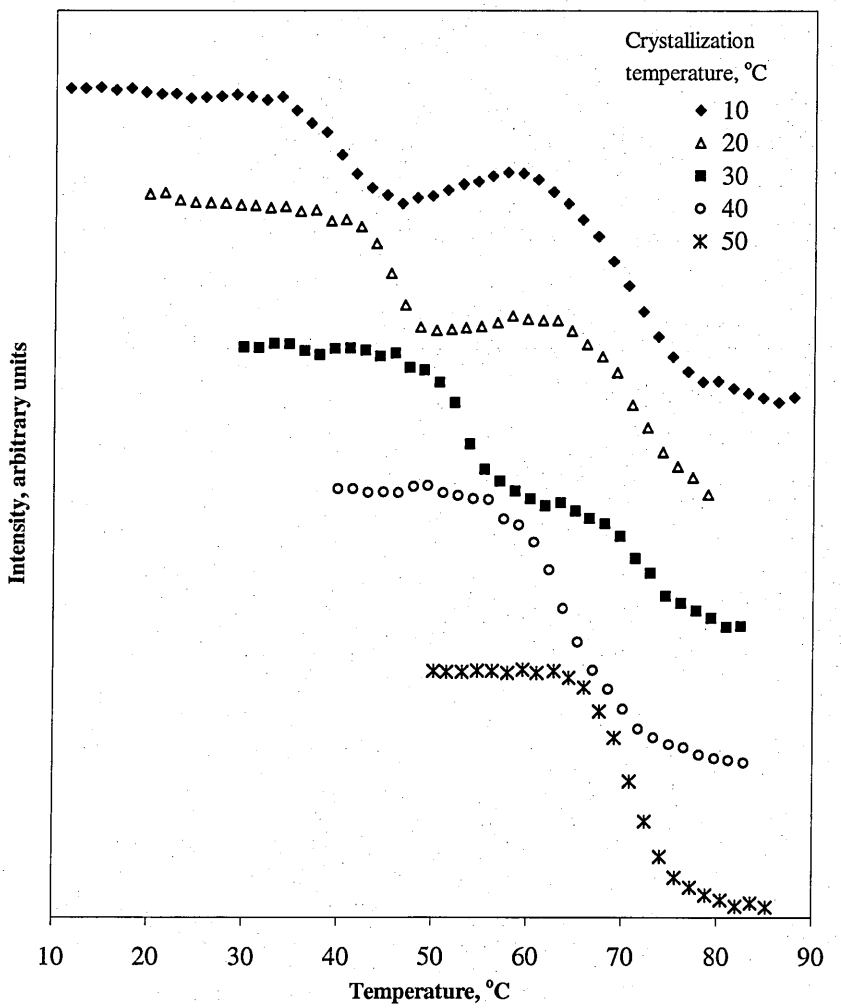

Figure 8.1 Variation in intensity of the (020) reflection as crystals of HB 32-mer, grown at the crystallization temperatures shown, are heated in suspension at 8°C min^{-1} to the point where they dissolve. The curves have been staggered along the intensity axis for ease of comparison: the final intensity in each case is zero.

The subtleties of the observed behaviour will be discussed later, but the main features can be summarised as follows:

- The initial drop in intensity, corresponding to the onset of dissolution, increases with crystallization temperature.
- The temperature at which the crystalline intensity falls to zero is similar for all samples and in the range 82–86°C.
- A two stage dissolution process is evident for crystals grown at 10, 20 and 30°C, i.e. at temperatures below the discontinuity (36–37°C) in crystallization-rate gradient seen in Figure 5.10 in chapter 5. This indicates partial dissolution and re-crystallization during heating.
- A single dissolution process occurs for crystals grown at 40 and 50°C, i.e. at temperatures above the discontinuity in crystallization-rate gradient.

The variation in intensity of the (110) reflection with temperature is not shown, but it showed identical trends in behaviour.

Figure 8.2(a) shows the variation in (020) lattice spacing with temperature, for the same 5 samples as shown in Figure 8.1. The lattice spacing increases with temperature, as would be expected. If the maximum values are taken to represent an 'ideal' behaviour then the expansion is linear (as shown by the dotted line on the graph) and yields a co-efficient of thermal expansion of $2.5 \pm 0.3 \times 10^{-5}$ nm $^{\circ}C^{-1}$. There is some deviation from this linear behaviour, particularly for the samples grown at the lower crystallization temperatures: the point at which the thermal expansion deviates from linear behaviour is comparable to the onset of dissolution seen in Figure 8.1.

The effect of heating on the (110) lattice parameter is illustrated in Figure 8.2(b). For the samples crystallized at 40 and 50°C there is a simple linear relationship between lattice spacing and temperature. The samples grown at lower temperatures begin to expand at a similar rate, giving an average co-efficient of thermal expansion (□) of $5.3 \pm 0.3 \times 10^{-5}$ nm $^{\circ}C^{-1}$ although the absolute values differ slightly according to the original crystallization temperature. These samples experience an increased rate of lattice expansion over the temperature range where it is seen that partial dissolution and re-crystallization is taking place. The additional shift in lattice spacing, over and

above that expected from thermal expansion, introduced during this process can be up to 0.001 nm as indicated by □*d* on Figure 8.2(b).

(a)

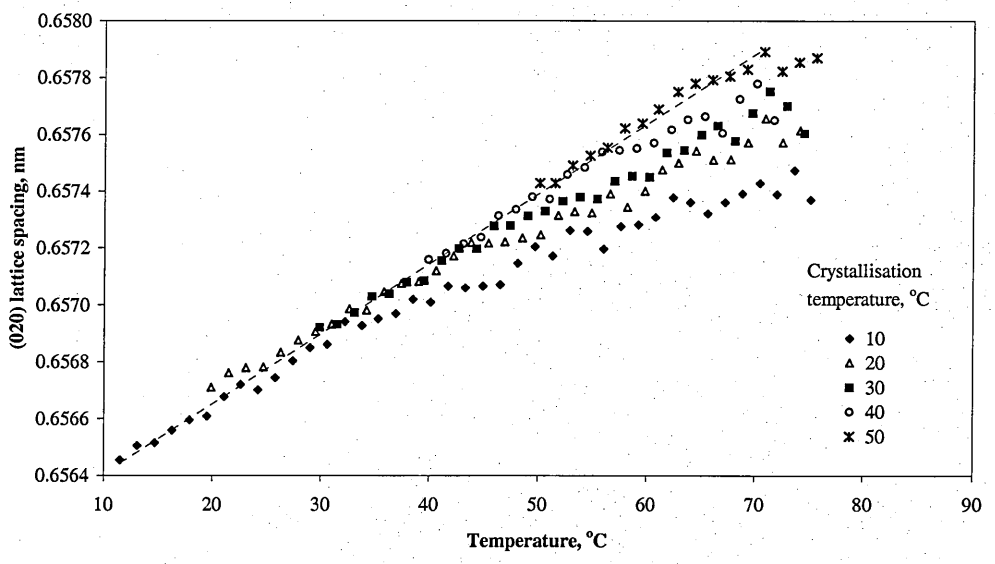

(b)

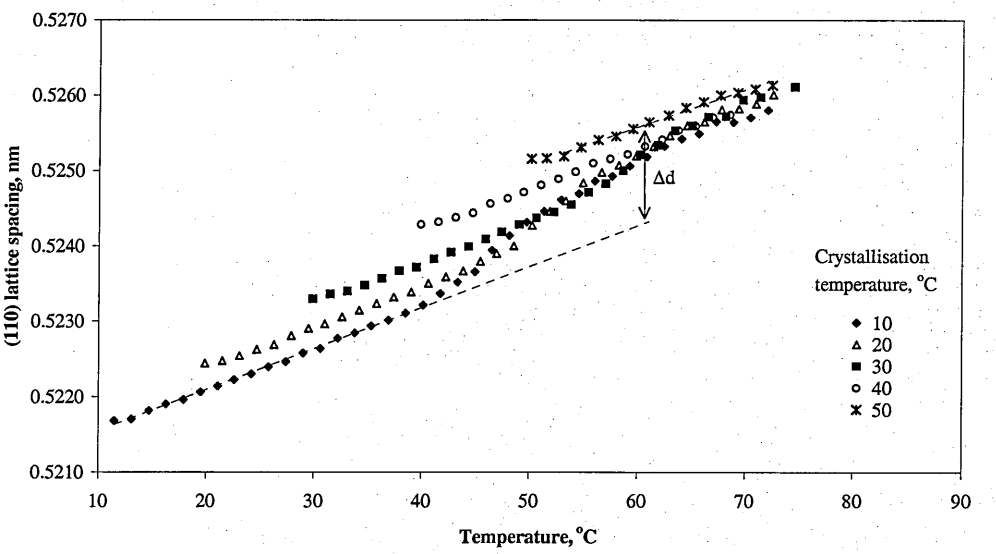

Figure 8.2 (a) Increase in (020) lattice spacing with temperature for the 32-mer. (b) Increase in (110) lattice spacing with temperature for the 32-mer. The dotted lines show the data from which the co-efficient of thermal expansion calculations were made.

In Figure 8.3(a) the variations in lattice spacing during heating are plotted alongside the intensity curve for the sample crystallized at 10°C. The lattice spacings are plotted on the same scale, but have been displaced along the *y* axis for ease of comparison. It

is clear that deviations from linear behaviour are linked to the partial dissolution/re-crystallization process, and that the (110) lattice spacing is affected much more than the (020). Changes in peak width also occur over this temperature range, as shown for the same sample in Figure 8.3(b). The peak width is a measure of the full width at half the maximum height (FWHM) and gives an indication of the degree of order in the corresponding crystallographic direction. An increase in FWHM occurs during the transition stage, which persists until dissolution sets in once more. Similar behaviour was observed for the crystals grown at 20 and 30°C.

(a)

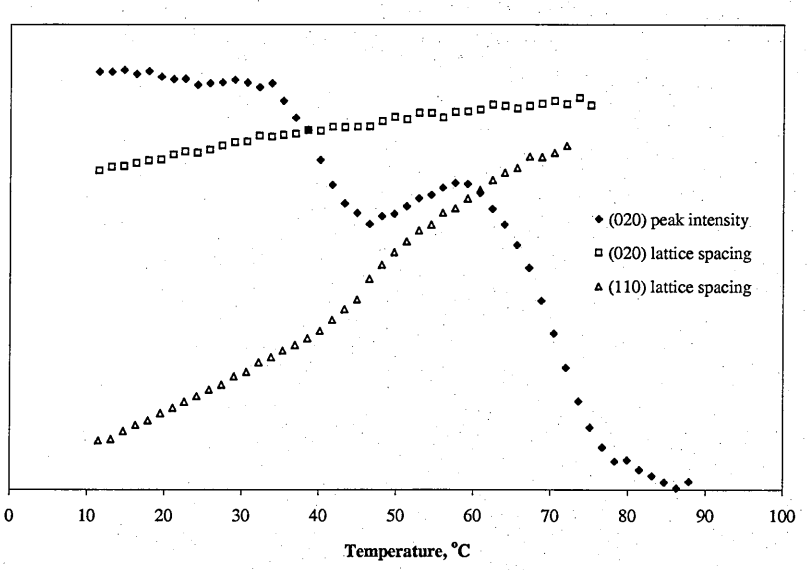

(b)

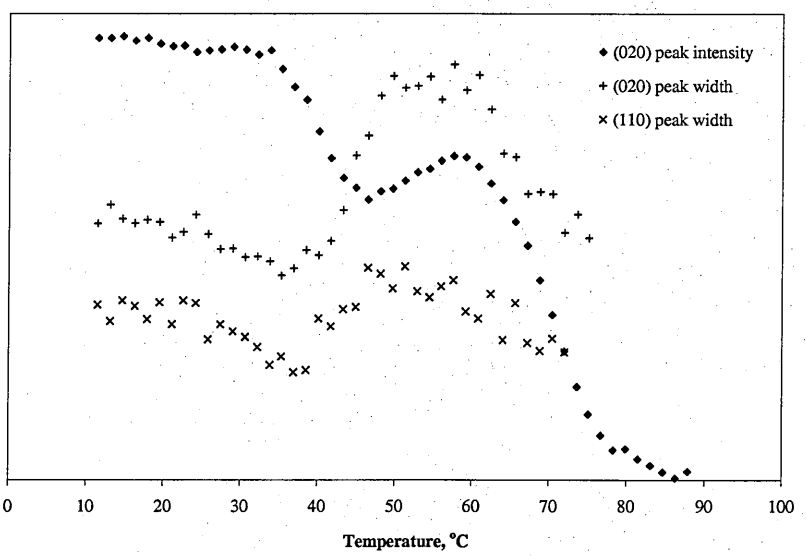

Figure 8.3 (a) Variation in peak intensity and lattice spacings with temperature. (b) Variation in peak intensity and peak widths with temperature. Both sets of data are from a sample of HB 32-mer crystallized at 10°C. The data have been plotted using different (arbitrary) *y* axis scales to facilitate comparison. The temperature axis is the same in each case.

8.3.2 HB 24-mer

More limited experiments were carried out using the 24-mer and growth rate measurements have been presented previously in Fig 5.12 in chapter 5. On heating the crystals in suspension in solvent, similar effects were observed as for the 32-mer. Figure 8.4 shows a set of intensity vs temperature curves for 24-mer crystals grown at four different temperatures, which have been staggered along the *y* axis for ease of comparison. Again there is evidence for partial dissolution and re-crystallization, more limited in extent than for the 32-mer, for the crystals grown at the lower T_cs. For $T_c = 40^{\circ}C$ a single dissolution process was observed. The temperature of the onset of dissolution does not vary greatly with initial crystallization temperature in the range 29–40°C.

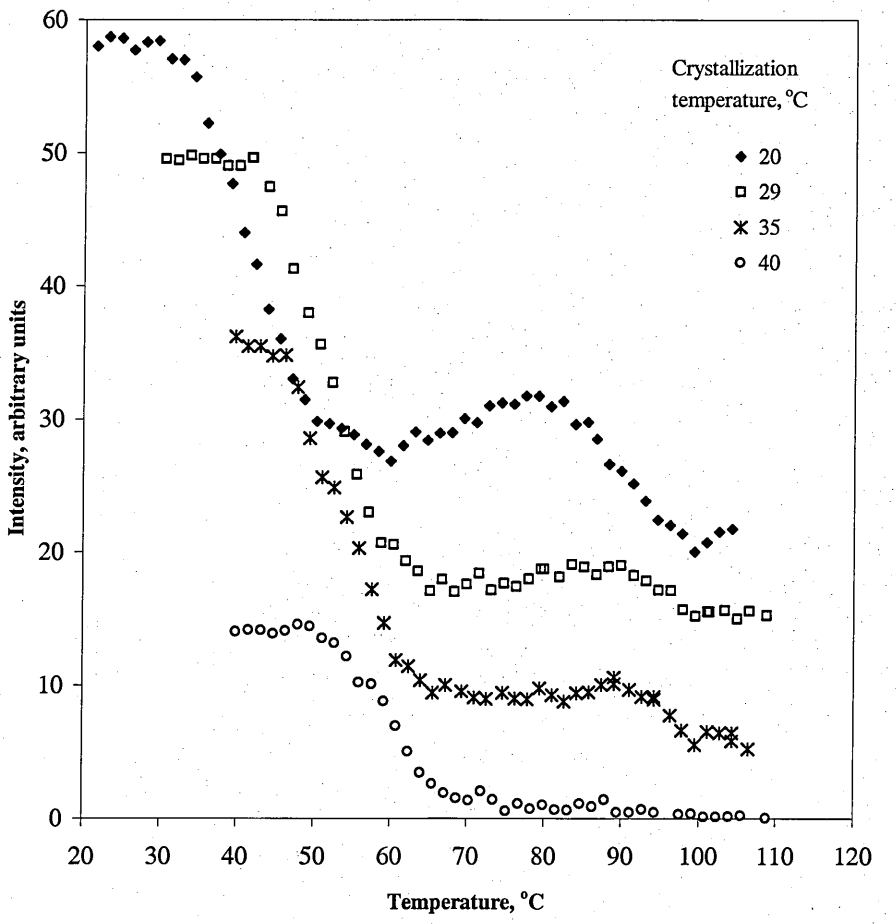

Figure 8.4 Intensity of the (020) reflection as a function of temperature during crystallization of HB 24-mer at the temperatures shown. The curves have been staggered along the intensity axis for ease of comparison: the final intensity in each case is zero.

Figure 8.5(a) superimposes the data for T_c = 29°C onto that for a second sample, which was crystallized at a very similar temperature but interrupted during heating and held at 60°C for approximately 15 minutes to investigate the effect of annealing. At this point more than 80% of the original intensity has been lost. 60°C is well above the temperature range where samples will crystallize from solution in a reasonable time scale. However, annealing in the presence of a small amount of crystalline material appears to have induced a self-seeding effect as the intensity rises within a relatively short time to a value higher than that in the original sample. The increase in intensity over time during the annealing period is shown in Figure 8.5(b).

(a)

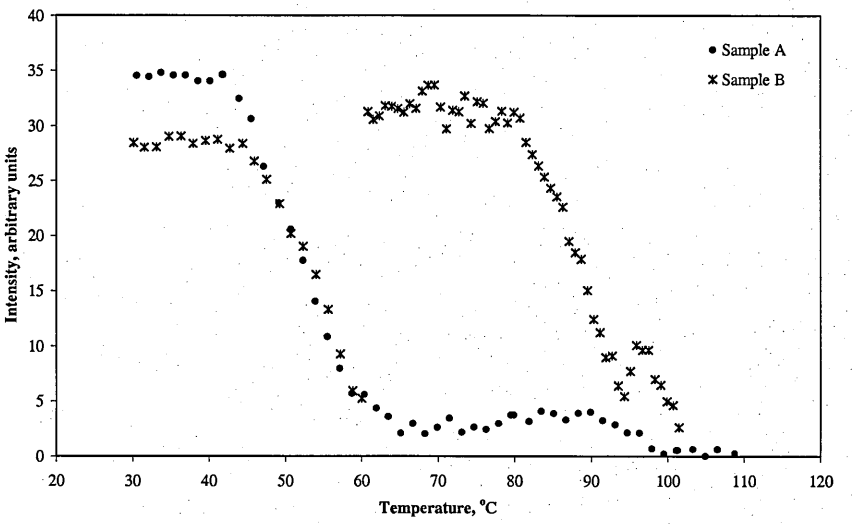

(b)

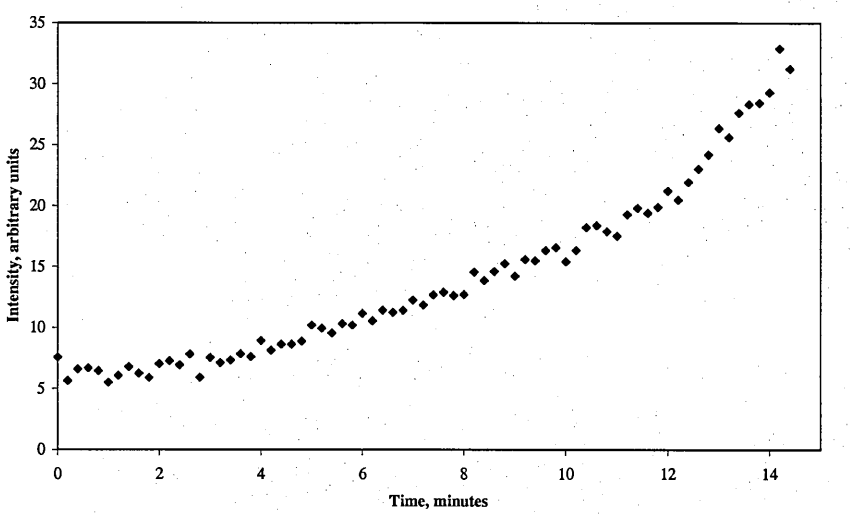

Figure 8.5 (a) Intensity of the (020) reflection as a function of temperature for two samples of 24-mer. Sample A was crystallized at 29°C and heated at 8°C min^{-1} until it dissolved. Sample B was crystallized at 30°C and annealed for 15 minutes at 60°C during heating; (b) Change in intensity of the (020) reflection with time for sample B, during annealing at 60°C.

The small upturn in intensity just before final dissolution in Figure 8.5a, seen also to a lesser extent in the traces for $T_c = 20$ and 35°C in Figure 8.4, is curious. Examination of the WAXS patterns in this range show no change in crystal structure. Similar effects were also occasionally seen in melt crystallized samples, see Figure 7.3(a), and may simply be the result of the movement of sample within the beam, or possibly an indication of double layer crystals formed from dimers. Such structures have been reported by Zeng and Ungar [Zeng and Ungar, 1999] using a long-chain 1-alkanoic acid in which hydrogen bonding can occur between chain ends.

The variations in both *d* spacing and peak width on heating followed similar patterns in the 24-mer to those described above for the 32-mer. The clearest effects were seen in the (110) lattice spacing and the (020) peak width and examples of each of these are shown in Figure 8.6 for the sample crystallized at 20°C. The corresponding intensity vs temperature is included for comparison. This data yields a shift in (110) spacing accompanying chain unfolding of approximately 0.001 nm, in line with that measured for the 32-mer, and is identical to that seen in melt grown HB crystals. The coefficients of thermal expansion in the (110) and (020) lattice directions were also within the range given for the 32-mer. The peak width increases and then decreases during partial dissolution and re-crystallization in a similar manner to that seen in Figure 8.3 for the 32-mer.

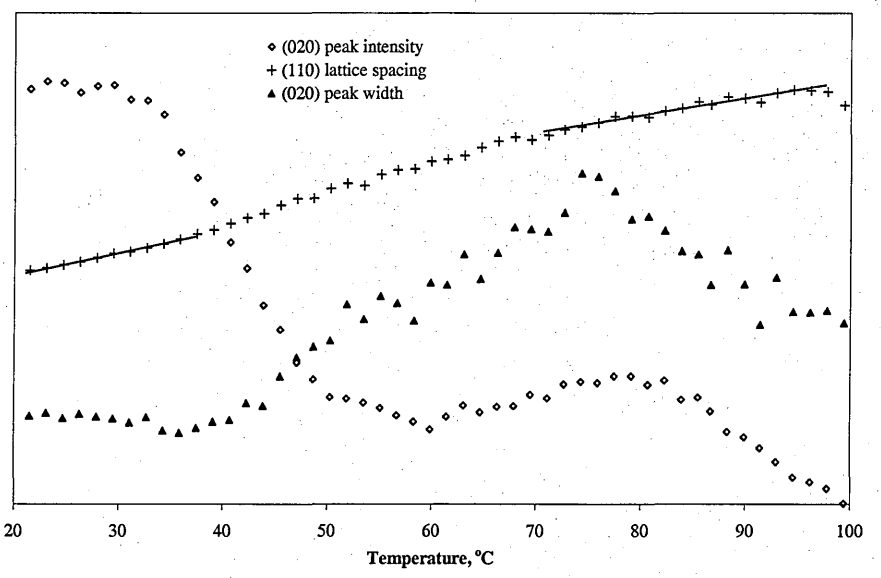

Figure 8.6 Peak intensity, lattice spacing, and peak width for a sample of 24-mer crystallized at 20°C. The three sets of data have been plotted using different (arbitrary) *y* axis scales to facilitate comparison. The temperature axis is the same in each case. The lines show the data from which the co-efficient of thermal expansion calculations were made.

As before, it is believed that the partial dissolution and re-crystallization observed during heating in samples crystallized at the lower temperatures corresponds to chain extension in crystals which were initially folded. The small increase in lattice spacing along the (110) direction which results from this chain unfolding can be seen clearly by comparing the diffraction patterns taken at the same temperature from samples just before and just after annealing at 60°C. Intensity data for this sample is shown in Figure 8.5 and the diffraction patterns taken before and after annealing for 15 minutes are superimposed in Figure 8.7. The increase in intensity resulting from annealing is clearly apparent and the peak position of the (110) reflection has shifted from 0.525 to 0.526 nm.

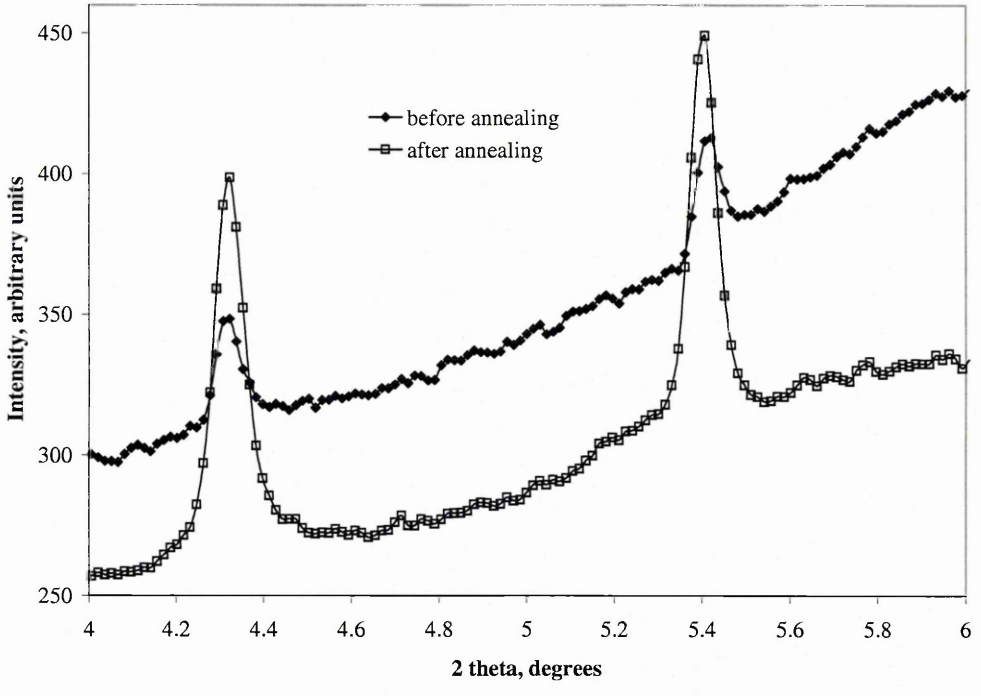

Figure 8.7 X-ray diffraction patterns from the 24-mer (sample B) taken before and after annealing at 60°C.

8.4 Discussion

The growth rate data for crystals grown over a range of 10–55°C for the 32-mer and 20–40°C for the 24-mer have been given in chapter 5. Above these temperatures crystallization was prohibitively slow, although it is apparent from the single annealed sample of 24-mer that there may be some scope for extending the range using a self-seeding procedure. Lower temperatures require higher cooling rates to ensure that no

significant crystallization occurs during cooling. A comprehensive set of growth rates was obtained for the 32-mer, but the results for the 24-mer were more limited.

The tentative discontinuity in 32-mer growth-rate gradient suggested at around 36–37°C presented earlier in chapter 5 is much less pronounced than those obtained from long n-alkanes grown from solution, where they are associated with a transition from one stable crystal form to another. It is now clear from the dissolution behaviour seen in Figure 8.1, however, that crystals from sample 1 grown below the discontinuity are able to reorganize into a more stable form on heating while those grown above the discontinuity are not. Thickness measurements made on crystals of a 32-mer with a benzyl end group on one end of the chain, which have been reported in chapter 6, also indicate that the 32-mer grows from the melt with extended chains at high crystallization temperatures and with folded chains at lower temperatures. Different chain conformations are possible but for solution grown crystals the thickness is consistent with chains that are folded in half.

Crystals of 32-mer grown at 10, 20 and 30°C show clear transitions on heating that can be associated with chain unfolding. In other sample (sample 3 in Figure 5.10), much smaller discontinuities were observed in a similar temperature range for the crystals grown at 35 and 35.5°C, which suggest that chain unfolding either happened very quickly, or had already occurred to some extent before the crystals were heated. Isothermal thickening at the crystallization temperature is known to occur rapidly in solution grown crystals of n-alkanes close to the temperature where primary growth changes from folded to extended chains [Ungar and Organ, 1990]. No discontinuity was visible for crystals grown at 36°C or above, consistent with these crystals containing extended chains. It should be noted that the temperature of the transition from folded chain to extended chain growth will vary with solution concentration [Ungar *et al.*, 2000; Terry *et al.*, 2003]. In earlier reported AFM thickness measurements on crystals of 32-mer grown at 65°C, the crystal thicknesses were consistent with once-folded chains. The solution concentration in that case was 0.018% (w/v).

From examination of the dissolution behaviour of the 24-mer, transitions for crystallization temperatures up to 35°C, but not at 40°C, have been seen. This suggests

a change from folded to extended chain growth between 35 and 40°C for the 24-mer. This is slightly higher than the position of the minimum tendency in growth rate suggested by Figure 5.12 in chapter 5, which is at 30–35°C. Further measurements would be necessary to look at the transition point more precisely.

Similar changes in intensity during heating (i.e. an initial decrease, followed by an increase, then by final melting) have been observed for melt crystallized samples of HB oligomers (presented in chapter 7) and long n-alkanes containing folded chains. In the case of the alkanes the unfolding was accompanied by a rapid contraction of the crystal lattice in both the (110) and (200) directions, which was attributed to the removal of lattice distortion introduced by the folds [Terry *et al.*, 2003]. By contrast, in the HB oligomers, a discontinuous increase in (110) spacing of typically 0.001 nm (or approximately 0.2%) results from chain unfolding. This is in addition to a small and regular increase in lattice spacing during heating due to thermal expansion. It should be remembered that (110) is the fold direction in PHB, and this result suggests that in this case the folds are causing the lattice to skew slightly. The same behaviour was seen in the annealed sample, where the (110) lattice spacing increased by 0.001nm at constant temperature as new, extended chain, crystals grew from folded chain seeds. The effect of unfolding in the (020) direction, where there is no physical link between the chains, is seen more clearly in melt crystallized samples and has been described in the previous chapter, chapter 7.

The increase in peak width accompanying thickening correlates well with the changes in lattice spacing. This is most probably due to the superposition of the thickened lattice and the un-thickened lattice and reaches a maximum in the region where both lattices would be expected to be present. An alternative explanation put forward for the alkanes [Terry *et al.*, 2003] invoking the transitory introduction of defects into the lattice during the unfolding process could also contribute.

The initial onset of dissolution depends strongly on crystallization temperature and falls in the range 40–70°C for the 32-mer. In contrast to the behaviour of the alkanes [Organ and Keller, 1987], there do not appear to be discretely different values corresponding to folded and extended chain crystals and this is consistent with the possibility of a wider range of crystal thicknesses, as discussed in chapter 6. This

more polymeric behaviour in the HB oligomers may arise from associations between chain ends caused by hydrogen bonding, which could reduce the tendency of the oligomer chains to act as independent units. However, the end point of dissolution is the same for all crystals regardless of their original conformation, and gives the dissolution temperature of extended chain crystals as approximately 85°C. For the 24-mer the onset of dissolution fell in the range 40–50°C and the end point was at approximately 100°C. The fact that this value is higher than that measured for the 32-mer is surprising and suggests that the degree of perfection achievable in the extended chain crystals during their limited lifetime is greater in the shorter chain oligomer. The high dissolution point in the 24-mer could also be further evidence for the formation of a double-layer structure, as mentioned previously. Experiments using differential scanning calorimetry (DSC) might be helpful in this respect and need further investigation in the future.

8.5 Conclusions

Synchrotron X-ray radiation has been used to observe the crystallization and study the chain unfolding behaviour during heating in HB 24-mer and 32-mer crystals grown from solution. The suggestions made concerning discontinuities in crystallization-rate gradient of the 32-mer and 24-mer are supported by the chain unfolding transitions on heating.

The folded chain crystal forms grow at lower crystallization temperatures, i.e. below 36–37°C for 32-mer and below 35°C for 24-mer, and transform during heating to the more stable extended chain form. Crystals grown above the transition temperature contain extended chains that do not rearrange during heating. This transformation occurs via a process of partial dissolution and re-crystallization, which can be followed in-situ from measurements of X-ray crystallinity as the samples are heated at constant rate. Unfolding is accompanied by a thermal expansion of the lattice in the range of $5.3 \pm 0.3 \times 10^{-5}$ nm $^{\circ}C^{-1}$, with an additional discontinuous increase of 0.001nm in the fold direction (110) and by associated changes in peak width. Chain unfolding may also be achieved by annealing folded chain crystals at temperatures above the initial crystallization temperature.

Chapter 9 Conclusions and Future Work

This thesis aims at investigating the crystallization behaviour in 3-hydroxybutyrate (HB) oligomers with exact length between 8 and 96 repeat units, which are short chain analogues of the polymer poly(3-R-hydroxybutyrate), PHB. These materials, synthesized via a sequential coupling process developed by Seebach and co-workers at ETH Zurich, are very useful to explore the generality of the crystallization behaviour observed previously in the n-alkanes, since they have the larger and more chemically complex monomer unit. The main objective of this work is to gain a more comprehensive understanding of HB oligomer crystal chain folding, crystal growth and thickening, and morphological changes at different crystallization conditions, both from the melt and solution. This final chapter will summarize the main findings presented in this thesis, and suggest general areas in which further work may be profitable.

9.1 Conclusions

The original contributions to knowledge by this study are summarized as follows:

9.1.1 Crystal morphology

Spherulitic crystals grown from the melt over a wide range of crystallization temperatures and observed using polarizing optical microscope were well defined. The spherulites grown at lower temperatures are nicely banded and look remarkably similar to those grown from the polymer, PHB. The band spacings are also very similar to those observed in PHB. As the crystallization temperature increased the banding disappeared, the shape of the spherulites became less regular, and a coarser texture associated with reduced branching developed at the highest temperatures.

Single crystals of HB 24-mer and 32-mer were grown from dilute solution in propylene carbonate, and observed in the transmission electron microscope (TEM) and atomic force microscope (AFM). Overall, the single crystals have an appearance

very similar to those from PHB grown under similar conditions. Electron diffraction indicates that the chains are closely perpendicular to the basal plane of the crystals. Wide angle X-ray diffraction suggests that all crystals, no matter what their thicknesses are, have the same crystal structure. Crystals of HB 32-mer with free ends and with a protecting benzyl group at one end were observed and compared. Not much difference was found between the two types of 32-mer on crystal morphologies.

9.1.2 Crystallization rates

Crystal growth rates have been measured over a wide range of crystallization temperature for HB 24-mer and 32-mer grown both from the melt and solution. The complementary growth rate data for 24-mer and 32-mer spherulites grown from the melt were measured in real time using optical microscopy. A two-hotstage method gives a much wider supercooling range over which the growth rates were recorded for 24-mer. In the 24-mer grown from the melt, the growth rates pass through a maximum at 75°C, and show a very similar curve to that measured from PHB. However, the measurements were unusually scattered at around 85 and 100°C, giving two discontinuities in the growth-rate gradient. Similar but less pronounced phenomena have also been observed at around 113 and 119°C for 32-mer grown from the melt.

Crystallization rates of HB 32-mer grown from solution in propylene carbonate have been measured in-situ as a function of crystallization temperature, following the intensity increase of the (020) reflection as a function of time using high resolution synchrotron wide angle X-rays diffraction at the ESRF Grenoble. More limited data were obtained for the 24-mer grown from solution. A tentative discontinuity in the crystallization-rate gradient was observed at 36–37°C for the 32-mer and possibly ~30°C for the 24-mer. These discontinuities could possibly correspond to the growth rate minima found in the n-alkanes, although the effect is much less pronounced here. The discontinuities are suggested to be linked to a change between different chain conformations within crystals. The presence of a benzyl protecting group on one end of the 32-mer chain showed no effect on either crystal morphologies or growth.

9.1.3 Crystal thickness and chain conformation

Comprehensive measurements of crystal thickness from HB oligomer crystals grown both from the melt and solution have been performed using small angle X-ray scattering (SAXS). The HB oligomers can form thin crystals with a range of thicknesses between extended and half of the extended chain length, but with some preference for particular values. The preferred crystal thicknesses are those which result in a relatively higher proportion of chain ends in the surface, in particular, for the 24-mer those corresponding to E/2, 2/3E, 3/4E, 5/6E. The occurrence of such stable noninteger folded (NIF) chain forms is in contrast to the results from long n-alkanes where stable crystal thicknesses have been found to correspond only to integer fractions (IF) of the extended chain length (E, E/2, E/3 etc). It is suggested that in the HB oligomers, hydrogen bonding between chain ends could effectively link chains together into longer units, which enables the oligomers to exhibit a more polymeric behaviour and makes a wider range of chain conformations possible.

9.1.4 Thickening and unfolding transitions during heating

The crystals grown at the higher temperatures contain extended chains, while in those grown at lower temperatures, the chains are folded and can transform during heating to the more stable extended chain form. High resolution wide angle X-ray scattering (WAXS) has been used to follow the changes in crystallinity and lattice parameter which occur on heating the HB oligomers. These effects can be correlated with changes in crystal thickness detected by small angle X-ray scattering (SAXS).

Melt-grown crystals from HB 24-mer and 32-mer that initially contain once folded chains transform during slow heating to produce extended chain crystals. This chain unfolding occurs via a process of partial melting and re-crystallization and is accompanied by an expansion in the crystallographic lattice of approximately 0.2% in the (110) fold direction and a much smaller contraction in the (020) direction. The rate of transformation is slow and is affected by the length of the chain and the nature of the end groups. The presence of a benzyl protecting group on one end of the chain does not affect the transformation temperature but reduces the (020) and (110) lattice spacings very slightly, as well as increasing the rate of transformation. The variation

in crystal thickness during chain unfolding depended both on the length of the chain and on the initial crystal thickness (which in turn depended on the crystallization temperature). In the 32-mer(p) examples were seen of a gradual increase in thickness from IF folded (1/2E) chains to extended chains, and of a discontinuous jump in thickness from NIF folded (2/3E) chains to extended chains. In the 24-mer a dual population of IF folded (1/2E) and extended (E) chains was observed during transformation. In all cases examined here the stable crystal forms displayed specific crystal thicknesses simply related to the extended chain length, but the intermediate stages of thickening vary between samples.

The chain unfolding during heating of HB 24-mer and 32-mer grown from dilute solution in propylene carbonate has been followed in situ using Synchrotron X-ray radiation. A similar partial dissolution and re-crystallization to form extended chain crystals has also been observed during heating for the crystals grown at lower crystallization temperatures. Unfolding is accompanied by an expansion of the lattice in the fold direction (110) and by associated changes in peak width, in the similar range with those found in melt-grown samples. Chain unfolding can also be achieved by annealing folded chain crystals at temperatures above the initial crystallization temperature.

9.1.5 Summary

The work on HB oligomer crystallization presented here has revealed a great deal about the fundamentals of their crystallization behaviour, especially about the way in which the chains fold and how they re-arrange themselves from one folded form to another. Combined with previous results from crystallization studies of PHB, it is hoped that the new findings from this study will contribute towards a more complete view of the whole polymer crystallization process.

9.2 Suggestions for Further Work

Based on the work already undertaken in this study, the areas that could benefit from further investigation are suggested as following.

9.2.1 Longer chain HB oligomers

It has been suggested that the crystals of HB 24-mer and 32-mer studied in this project have a range of thicknesses between extended and half of the extended chain length. The most folded chain form is the once-folded form, and the possible NIF thicknesses are 2/3E, 3/4E and 5/6E. It is hoped that longer chain monodisperse HB oligomers with 48, or up to 128 repeat units, synthesized following the same segment strategy, could fold many more times under similar crystallization conditions. This would give a further insight into the whole range of crystal thicknesses, as well as the nature of the fold surface. The ability to form a possible greater diversity of thicknesses in HB oligomer system could promise the potential to provide a better bridge to polymer crystallization.

9.2.2 More studies on crystal morphologies

Spherulitic crystal morphologies of HB oligomers grown from the melt over a wide range of crystallization temperature, together with single crystals grown from dilute solution have been presented in this study. However, there are no significant morphology changes observed near the transition temperatures, like those rounded facet crystals found in n-alkanes and PEO fractions. Further observation on well defined longer chain HB oligomer crystals grown from both the melt and solution, associated with the thicknesses, could throw new light onto this issue.

Further interesting questions, e.g. the degree to which the oligomer crystals themselves are twisted and whether any such twist reflects the chirality of the molecules themselves, could be helpful to look at any link between chain folding and spherulite banding. This is an area which has recently received attention, following the observation that the molecular chirality of a polymer can have a deterministic influence over the chirality of the resultant morphology, in particular on the handedness of the lamellar twist. As PHB does not have a liquid crystalline phase, it is a good candidate molecule for further investigations on these phenomena with the added benefit in the oligomers of strict uniformity of molecular length.

9.2.3 Ageing studies

The stable NIF states observed in HB oligomers in this work, could help to bridge the gap between the behaviour of short chain oligomer and polymer further. A number of small but significant changes in the lattice parameters as the different folded forms grow and transform from one to another, could be associated with differences in the detailed fold structure and the strain that the folds place on the chain stem in the crystals themselves. These subtle changes, especially the changes in the stress placed on crystals, may be related to the ageing effect seen in the whole PHB polymer. Accordingly, further studies of the fold structures in oligomers, sharp fractions and whole polymer respectively could throw new light on the ageing process and finally on understanding the underlying causes of the loss of mechanical properties in PHB.

9.2.4 Application to surface modification

Once the crystallization conditions required to produce different types of crystals have been established, it will be possible to produce samples with very well defined chain composition. For example, a single crystal mat could be produced where virtually every chain has the same length, the same number of folds, the same orientation with respect to the surface, and where the position of functional groups relative to the surface is precisely known. Such samples could be used to carry out exploratory investigations using low pressure plasmas to induce changes at the sample surface and to assess the nature and extent of the changes. Such studies may provide information relevant to the effect of plasma treatment on all polyesters. OHB, hence, PHB, as a biocompatible polymer with much potential for specialized medical applications, is of special interest. Finally, a new line of investigation could lie in HB oligomers being used as model materials for studies of surface modification.

These are just a few of the possible directions in which future research could be considered, building on the results from this work.

References

Akhtar, S., Pouton, C.W., Notarianni, L.J., (1992), *Polymer*, **33**, 117.

Albert, M., Seebach, D., Duchardt, E. and Schwalbe, H., (2002), *Helv. Chim. Acta*, **85**, 633.

Anderson, A.J. and Dawes, E.A., (1990), *Microbiol. Rev.*, **54**, 450.

Albrecht, T.R., Dovek, M.M., Lang, C.A., Grutter, P., Quate, C.F., Kuan, S.W.J., Frank, C.W. and Pease, R.F.W., (1988), *J. Appl. Phys.*, **64(3)**, 1178.

Alper, R., Lundgren, D.G., Marchessault, R.H., Coté, W.A., (1963), *Biopolymers*, **1**, 545.

Arlie, J.P., Spegt, P., Skoulios, A.C.R., (1965), *Acad. Sci. Paris*, **260**, 5774.

Armistead, K.A. and Goldbeck-Wood, G., (1992), For a review of polymer crystallization theory, *Adv. Polym. Sci.*, **100**, 219.

Atkins, E.D.T., Hill, M.J., Jones, N.A., Sikorski, P., (2000), *J. Mater. Sci.*, **35**, 5179.

Balijepalli, S., Schultz, J.M., (1996), *Macromolecules*, **29**, 2095.

Barak, P., Coquet, Y., Halbach, T.R. and Molina, J.A.E., (1991), *J. Environ. Qual.*, **20**, 173.

Barham, P.J., Keller, A., (1977), *J. Mat. Sci.*, **12**, 2141.

Barham, P.J., Chivers, R.A., Jarvis, D.A., Martinez-Salazar, J., Keller, A., (1981), *Polym. Lett.*, **19**, 539.

Barham, P.J., Keller, A., Otun, E.L., Holmes, P.A., (1984), *J. Mater. Sci.*, **19**, 2781.

Barham, P.J., (1984), *J. Mat. Sci.*, **19**, 3826.

Barham, P.J., Chivers, R.A., Keller, A., Martinez-Salazar, J., Organ, S.J., (1985), *J. Mater. Sci.*, **20**, 1625.

Barham, P.J., Keller, A., (1986), *J. Poly. Sci.: Polym. Phys. Ed.*, **24**, 69.

Barham, P.J., Barker, P.A., Organ, S.J., (1992), *FEMS Microbiol. Rev.*, **103**, 289.

Barham, P.J., (1993), in *"Materials Science and Technology - A comprehensive treatment: Structure and properties of polymers"*, Cahn, R.W., Haasen, P., Kramer, E.J., Ed., VCH publisher, **12**, 153-212.

Barham, P.J. and Organ, S.J., (1994), *J. Mater. Sci.*, **29**, 1676.

Bassett, D.C., Keller, A., Mitsuhashi, S., (1963), *J. Polym. Sci.*, **A1**, 763.

Bassett, D.C., Patel, D., (1994a), *Polymer*, **35**, 1855.

Bassett, D.C., (1994b), *Phil. Trans. R. Soc. Lond.*, **A348**, 29.

Bassett, D.C., Olley, R.H., Sutton, S.J., Vaughan, A.S., (1996), *Macromolecules*, **29**, 1852.

Bassett, D.C., Olley, R.H., Sutton, S.J., Vaughan, A.S., (1996), *Polymer*, **37**, 4993.

Bassett, D.C., (2003), *J. Macromol. Sci.*, **B42**, 227.

Bidd, I. and Whiting, M.C., (1985), *J. Chem. Soc. Chem. Commun.*, 543.

Bidd, I., Holdup, D.W., Whiting, M.C., (1987), *J. Chem. Soc.*, Perkin Trans., **1**, 2455.

Billingham, N.C., Henman, T.J., Holmes, P.A., (1987), *Dev. Polym. Degrad.*, **7**, 81.

Binsbergen, F.L., (1972), *J. Crystal Growth*, **131**, 501.

Birley, C., Briddon, J., Sykes, K.E., Barker, P.A., Organ, S.J., Barham, P.J., (1995), *J. Mater. Sci.*, **30**, 633.

Black, S.N., Dobbs, B., Dempsey, P.S., Davey, R.J., (1990), *J. Mat. Sci Lett.*, **9**, 51.

Blundell, D.J., Keller, A., Kovacs, A., (1966), *J. Polym. Lett.*, **4**, 481.

Blundell, D.J., Keller, A., Ward, I.M., and Grant, I.J., (1966), *J. Polym. Sci.*, **B4**, 781.

Blundell, D.J., Keller, A. and Connor, T., (1967), *J. Polym. Sci.*, A2, **5**, 991.

Boda, E., Ungar, G., Brooke, G.M., Burnett, S., Mohammed, S., Proctor, D., Whiting, M.C., (1997), *Macromolecules*, **30**, 4674.

Brandl, H., Gross, R.A., Lenz, R.W., Lloyd, R., Fuller, R.C., (1991), *Arch. Microbiol.*, **155**, 337.

Broadhurst, M.G., (1962), *J. Res. Natl. Bur. Stand. Sect.*, **A66**, 241.

Brooke, G.M., Burnett, S., Mohammed, S., Proctor, D., Whiting, M.C., (1996), *J. Chem. Soc., Perkin Trans*, **1**, 1635.

Brooke, G.M., Mohammed, S., Whiting, M.C., (1997), *J. Chem. Soc., Perkin Trans.* 1, **22**, 3371.

Brooke, G.M., Mohammed, S., Whiting, M.C., (1999), *Polymer*, **49**, 773.

Brückner, S., Meille, S.V., Malpezzi, L., Cesàro, A., Navarini, L., Tombolini, R., (1988), *Macromolecules*, **21**, 967.

Buckley, C.P. and Kovacs, A.J., (1984), in *"Structure of Crystalline Polymers"*, Hall, I.H., Ed., Elsevier Applied Science: London, pp261-307.

Bürger, H.M., Müller, H.M., Seebach, D., Bornsen, K.O., Schar, M., Widmer, H.M., (1993), *Macromolecules*, **26**, 4783.

Bunn, C.W. and Alcock, T.C., (1945), *Trans. Faraday Soc.*, **41**, 317.

Bunn, C.W., (1953), in *"Fibres from Synthetic Polymers"*, by Hill, R., Elsevier, Amsterdam.

Cheng, S.Z.D., Wunderlich, B., (1986a), *J. Polym. Sci., Polym. Phys. Ed.*, **24**, 557.

Cheng, S.Z.D., Wunderlich, B., (1986b), *J. Polym. Sci., Polym. Phys. Ed.*, **24**, 595.

Cheng, S.Z.D., Cao, M.-Y., Wunderlich, B., (1986c), *Macromolecules*, **19**, 1868.

Cheng, S.Z.D., Chen, J.H., (1991), *J. Polym. Sci. Polym. Phys. Ed.*, **B29**, 311.

Cheng, S.Z.D., Zhang, A., Barley, J.S., Chen, J., Habenschuss, A., Zschack, P.R., (1991), *Macromolecules*, **24**, 3937.

Cheng, S.Z.D., Zhang, A., Chen, J., Heberer, D.P., (1991), *J. Polym. Sci., Polym. Phys. Ed.*, **29**, 287.

Cheng, S.Z.D., Zhang, A., Chen, J.H., Zhang, A.Q., Barley, J.S., Habenschuss, A., Schack, P.R., (1992), *Polymer*, **33**, 1140.

Chivers, R.A., Barham, P.J., Martinez-Salazar, J. and Keller, A., (1982), *J. Polym. Sci: Polym. Phys. Ed.*, **20**, 1717.

Chowdhury, A.A., (1963), *Arch. Microbiol.*, **47**, 167.

Cooper, S.J., Atkins, E.D.T., Hill, M.J., (1998), *Macromolecules*, **31**, 5032.

Cooper, S.J., Atkins, E.D.T., Hill, M.J., (1998), *Macromolecules*, **31**, 8947.

Cornibert, J., Marchessault, R.H., (1972), *J. Mol. Biol.*, **71**, 735.

Cornibert, J., Marchessault, R.H., (1975), *Macromolecules*, **8**, 296.

Dawson, I.M., (1952), *Proc. R. Soc.*, London, **A214**, 72.

de Koning, G.J.M. and Lemstra, P.J., (1992), *Polymer*, **33**, 3292.

de Koning, G.J.M., Lemstra, P.J., Hill, D.J.T., Carswell, T.G. and O'Donell, J.H., (1992b), *Polymer*, **33**, 3295.

de Koning, G.J.M., (1993), Prospects of bacterial poly[(r)-3-hydroxyalkanoates], *PhD Thesis*, Technische Universiteit Eindhoven.

de Koning, G.J.M., Lemstra, P.J., (1993), *Polymer*, **34**, 4089.

Delafield, F.P., Cooksey, K.E., Doudoroff, M., (1965a), *J. Biol. Chem.*, **240**, 4023.

Delafield, F.P., Doudoroff, M., Palleroni, N.J., Lusty, C.J., Contopoulos, (1965b), *J. Bacteriol.*, **90**, 1455.

de Silva, D.S.M., Zeng, X.B., Ungar, G., Spells, S.J., (2002), *Macromolecules*, **35**, 7730.

de Silva, D.S.M., Zeng, X.B., Ungar, G., Spells, S.J., (2003), *J.Macro. Sci. Phys.*, **B42** (3-4), 915.

DiMarzio, E.A., Guttman, C.M., (1982), *J. Appl. Phys.*, **53**, 6581.

Doi, Y., Kanesawa, Y., Kawaguchi, Y., Kunioka, M., (1989), *Makromol. Chem. Rapid Commun.*, **10**, 227.

Doi, Y., Kawaguchi, Y., Nakamura, Y., Kunioka, M., (1989), *Appl. Environ. Microbiol.*, **55**, 2932.

Doi, Y., (1990), *"Microbial Polyesters"*, VCH Publishers, UK Ltd.

Doi, Y., Kanesawa, Y., Kunioka, M., Saito T., (1990), *Macromolecules*, **23**, 26.

Doi, Y., Kanesawa, Y., Tanahashi, N., (1992), *Polym. Degrad. Stab.*, **14**, 173.

Ellar, D., Lundgren, D.G., Okamura, K., Marchessault, R.H., (1968), *J. Mol. Biol.*, **35**, 489.

Elsner, G., Riekel, C. and Zachmann, H.G., (1985), *Adv. Polym. Sci.*, Kausch, H.H. and Zachmann, H.G., Ed., Springer-Verlag, Berlin, Heidelberg, **67**, 3.

The European Synchrotron Radiation Facility (ESRF) offical website, (2005), 'X-ray Source' data.

Fisher, E.W., (1957), *Z. Naturforsch*, **12a**, 753.

Fisher, E.W. and Schmidt, G.F., (1962), *Angew Chem.*, **74**, 551.

Fisher, E.W. and Schmidt, G.F., (1962), *Angew Chem. Internat. Edit.*, **1**, 488.

Flory, P.J., Vrij, A., (1963), *J. Am. Chem. Soc.*, **85**, 3548.

Frank, F.C. and Tosi, M., (1961), *Proc. R. Soc. (London)*, **A263**, 323.

Frank, F.C., (1979), *Disc. Faraday Soc.*, **68**, 7.

Fritz, M.G., Seebach, D., (1998), *Helv. Chim. Acta.*, **81**, 2414.

Fritz, M.G., Walde, P. and Seebach, D., (1999), *Macromolecules*, **32(3)**, 574.

Gedde, U.W., (1995), *"Polymer Physics"*, Chapman and Hall.

Geil, P.H., (1960), *J. Polym. Sci.*, **47**, 65.

Geil, P.H., (1963), *"Polymer Singel Crystals"*, Wiley: Interscience, New York.

Gilg, B., Spegt, P., Terrisse, J. and Skoulios, A., (1967), *Makromol. Chem.*, **107**, 39.

Gilmore, D.F., Antoun, S., Lenz, R.W., Goodwin, S., Austin, R., Fuller, R.C., (1992), *J. Ind. Microbiol.*, **10**, 199.

Goldbeck-Wood, G., (1993), in *"Crystallization of Polymers"*, Dosière, M., Ed., Kluwer, Dordrecht, 249.

Goldbeck-Wood, G., (1994), *Makromol. Chem., Macromol. Symp.*, **81**, 221.

Grassie, N., Murray, E.J., Holmes, P.A., (1984a), *Polym. Degrad. Stabil.*, **6**, 47.

Grassie, N., Murray, E.J., Holmes, P.A., (1984b), *Polym. Degrad. Stabil.*, **6**, 95.

Grassie, N., Murray, E.J., Holmes, P.A., (1984c), *Polym. Degrad. Stabil.*, **6**, 127.

Grubb, D.T., Keller, A. and Groves, G.W., (1972), *J. Mat. Sci.*, **7**, 131.

Grubb, D.T., Dlugosz, J. and Keller, A., (1975), *J. Mat. Sci.*, **10**, 1826.

Hay, I.L., Keller, A., (1967), *J. Mater. Sci.*, **2**, 538.

Hay, I.L., Keller, A., (1968), *J. Mater. Sci.*, **3**, 646.

Heck, B., Hugel, T., Iijima, M., Strobl, G., (2000), Polymer, **41**, 8839.

Higgs, P.G. and Ungar, G., (1994), *J. Chem. Phys.*, **100**, 640.

Higgs, P.G. and Ungar, G., (2001), *J. Chem. Phys.*, **114**, 6958.

Hikosaka, M., (1990), *Polymer*, **31**, 458.

Hobbs, J.K., (1996), *PhD Thesis*, University of Bristol.

Hobbs, J.K., McMaster, T.J., Miles, M.J., Barham, P.J., (1996), *Polymer*, **15**, 3241.

Hobbs, J.K., Sykes, K.E., McMaster, T.J. and Barham, P.J., (1996), *J. Environ. Polym. Deg.*, **4**, 235.

Hobbs, J.K., Binger, D.R., Keller, A., Barham, P.J., (2000), *J. Poly. Sci.: Poly. Phys. Ed.*, **38**, 1575.

Hobbs, J.K., Hill, M.J., Barham, P.J., (2000), *Polymer*, **41(25)**, 8761.

Hobbs, J.K., Hill, M.J., Barham, P.J., (2001), *Polymer*, **42**, 2167.

Hoffman, J.D., Lauritzen, J.I., (1961), *J. Res. Natl. Bur. Stand., Sect.*, **A65**, 73.

Hoffman, J.D. and Weeks, J.J., (1965), *J. Chem. Phys.*, **42**, 4301.

Hoffman, J.D., Frolen, L.J., Ross, G.S., Lauritzen, J.I., (1975), *J. Res. Natl. Bur. Stand, A: Phys. And Chem.*, **79A**, 671.

Hoffman, J.D., Lauritzen, J.I., Davis, G.T., (1976), in *"Treatise on Solid State Chemistry"*, Hannay, N.B. Ed., Plenum Press: New York, **Vol 3**, Chapter 7, 497-614.

Hoffman, J.D., Davis, G.T., (1978), in *"Polymer Surfaces"*, Clark, D.T., Feast, W.J., Ed., John Wiley & Sons: Chichester, pp 259-268.

Hoffman, J.D., Guttman, C.M., DiMarzio, E.A., (1979), *Disc. Farad. Soc.*, **68**, 177.

Hoffman, J.D., (1983), *Polymer*, **24**, 3-26.

Hoffman, J.D., (1985), *Macromolecules*, **18**, 772.

Hoffman, J.D. and Miller, R.L., (1988), *Macromolecules*, **21,** 3038.

Hoffman, J.D. and Miller, R.L., (1989), *Macromolecules*, **22,** 3038.

Hoffman, J.D., (1992), *Polymer*, **32**, 2828.

Holland, S.J., Holly, A.M., Yasin, M., Tighe, B.J., (1987), *Biomaterials,* **8**, 289.

Holmes, P.A., Wright, L.F., Collins, S.H., (1981), *Eur. Patent Appl.*, EP 0 052 459.

Holmes, P.A., Wright, L.F., Collins, S.H., (1981), Copolyesters and process for their production, *Eur. Patent Appl.*, EP 0 069 497.

Holmes, P.A., (1982), *Eur. Patent Appl.*, EP 0 046 335.

Holmes, P.A., (1985), *Phys. Technol.*, **16**, 32.

Holmes, P.A., Lim, G.B., (1985), Separation process, *Eur. Patent Appl.*, EP 0 145 233.

Holmes, P.A., (1987), Biologically produced (R)-3-hydroxyalkanoate polymers and copolymers, in *"Developments in Crystalline Polymers"*, Bassett, D.C. Ed., **vol2**, London: Elsevier, 1-65.

Jones, N.A., Sikorski, P., Atkins, E.D.T., Hill, M.J., (2000), *Macromolecules*, **3**, 4146.

Kawai, T., (1967), *Die. Mak. Chem.*, **102**, 125.

Keith, H.D. and Padden, F.J., (1963), *J. Appl. Phys.*, **34**, 2409.

Keith, H.D. and Padden, F.J., (1964a), *J. Appl. Phys.*, **35**, 1270.

Keith, H.D. and Padden, F.J., (1964b), *J. Appl. Phys.*, **35**, 1286.

Keller, A., (1957), *Phil. Mag.*, **2**, 1171.

Keller, A. and O'Connor, A., (1957), *Nature*, Lond., **180**, 1289.

Keller, A. and O'Connor, A., (1958), *Disc. Faraday Soc.*, **25**, 114.

Keller, A. and Bassett, D.C., (1960), *J. Royal Micro. Soc.*, **79**, 243.

Keller, A. and Priest, D.J., (1968), *J. Macromol. Sci., Phys.*, **B2**, 479.

Keller, A. and Sadler, D.M., (1973), *J. Macromol. Sci., Phys.*, **B7(2)**, 263.

Keller, A., (1991), Contribution to *"Sir Charles Frank OBE, FRS – An Eightieth Birthday Tribute"*, Chambers, R.G., Enderby, J.E., Keller, A., Lang, A.R., Steeds, J.W., Ed., Adam Hilger ISBN 0 7503 0100, **7**, 265-306.

Keller, A. and Goldbeck-Wood, G., (1996) in *"Comprehensive Polymer Science, 2nd Supplement"*, Aggarval, S.L., and Russo, S., Ed., Elsevier Scientific Publishers, **7**, 241-302.

King, P.P., (1982), *J. Chem. Tech. Biotechnol.*, **32**, 2.

Knowles, J.C., Mahmud, F.A., Hastings, G.W., (1991), *Clinical Mat.*, **8**, 211.

Koening, J.L. and Tabb, D.L., (1974), *J. Macromol. Sci.*, **B9**, 141.

Kovacs, A.J. and Gonthier, A., (1972), *Kolloid Z. Z. Polym.*, **250**, 530.

Kovacs, A.J., Gonthier, A., Straupe, C., (1975), *J. Polym. Sci., Symp.*, **50**, 283.

Kovacs, A.J., Straupe, C., Gonthier, A., (1977), *J. Polym. Sci., Symp.*, **59**, 31.

Krejchi, M.T., Atkins, E.D.T., Waddon, A.J., Fournier, M.J., Mason, T.L., Tirrel, D. A., (1994), *Science*, **265**, 1427.

Krupp, L.R. and Jewell, W.J., (1992), *Environ. Sci. Technol.*, **26**, 193.

Lafferty, R.M., Korsatko, B., Korsatko, W., (1988), Rehm, H.J., Ed., *Biotechnol.* Vol **6b**, VCH Publishers, pp 135.

Lauritzen, J.I. and Hoffman, J.D., (1960), *J. Res. Nat. Bur. Stand, A: Phys. and Chem.*, **64**, 73.

Lauritzen, J.I., Hoffman, J.D., (1973), *J. Appl. Phys.*, **44**, 4340.

Lauzier, C., Marchessault, R.H., Smith, P., Chanzy, H., (1992a), *Polymer*, **33**, 823.

Lauzier, C., Revol, J.-F., Marchessault, R.H., (1992b), *FEMS Microbiol. Rev.*, **103**, 299.

Lee, K.S. and Wegner, G., (1985), *Macromol. Chem. Rapid Commun.*, **6**, 203.

Lemoigne, M., (1925), *Ann. Inst. Pasteu. Paris*, **39**, 144.

Lemoigne, M., (1927), *Ann. Inst. Pasteu. Paris*, **41**, 148.

Lengweiler, U.D., Fritz, M.G., Seebach, D., (1996), *Helv. Chim. Acta*, **79**, 670.

Liggat J., (1996), PHB and hydroxyalkanoate polymers, *Polym. Int.*, **39**, 167.

Lundgren, D.G., Alper, R., Schnaitman, C. and Marchessault, R.H., (1965), *J. Bacteriol.*, **89**, 245.

Marchessault, R.H., Coulombe, S., Morikawa, H., Okamura, K. and Revol, J.F., (1981), *Canad. J. Chem.*, **59**, 38.

Marchessault, R.H., Bluhm, T.L., Deslandes, Y., Hamer, G.K., Orts, W.J., Sundararajan, P.R., Taylor, M.G., (1988), *Makromol. Chem. Macromol. Symp.*, **19**, 235.

Martinez-Salazar, J., Barham, P.J., Keller, A., (1985), *J. Mater. Sci.*, **20**, 1616.

Martinez-Salazar, J., Sanchez-Cuesta, M., Barham, P.J., Keller, A., (1989), *J. Mat. Sci. Letters*, **8**, 490.

McGrath, K.P., Fournier, M.J., Mason, T.L., Tirrell, D.A., (1992), *J. Am. Chem. Soc.*, **114**, 727.

Merrick, J.M., Doudoroff, M., (1961), *Nature*, **189**, 890.

Mitomo, H., Barham, P.J., Keller, A., (1987), *Polym. Comm.*, **19**, 1241.

Molecular Imaging, (2003), at *http://www.molec.com/what_is_afm.html*.

Morgan, R.L., Barham, P.J., Hill, M.J., Keller, A., Organ, S.J., (1998), *J. Macromol. Sci: Phys.*, **B37**, 319.

Müller, H.-M. and Seebach, D., (1993), *Angew. Chem. Int. Ed., Engl.*, **32**, 477.

Okamura, K. and Marchessault, R.H., (1967), in *"Conformation Aspects of Biopolymers"*, Vol. II, Ramachandran, G.N. Ed., Academic Press, London and New York.

Organ, S.J., (1983), *PhD Thesis*, University of Bristol.

Organ, S.J., Keller, A., (1985), *J. Mat. Sci.*, **20**, 1571.

Organ, S.J., Keller, A., (1987), *J. Poly. Sci.: Poly. Phys. Ed.*, **25**, 2409.

Organ, S.J., Barham, P.J., (1989), *J. Mat. Sci. Lett.*, **8**, 621.

Organ, S.J., Ungar, G., Keller, A., (1989), *Macromolecules*, **22**, 1995.

Organ, S.J., Ungar, G., Keller, A., (1990a), *J. Poly. Sci.: Poly. Phys. Ed.*, **28**, 2353.

Organ, S.J., Ungar, G., Keller, A., (1990b), *J. Poly. Sci.: Poly. Phys. Ed.*, **28**, 2365.

Organ, S.J. and Barham, P.J., (1991), *J. Mat. Sci.*, **26**, 1368.

Organ, S.J., Barham, P.J., (1992), *J. Mat. Sci.*, **27**, 3239.

Organ, S.J., Barham, P.J., (1993), *Polymer*, **34**, 459.

Organ, S.J., Barham, P.J., (1993), *Polymer*, **34**, 2169.

Organ, S.J., (1993), *Polymer*, **34**, 2175.

Organ, S.J., Keller, A., Hikosaka, M., Ungar, G., (1996), *Polymer*, **37**, 2517.

Organ, S.J., Barham, P.J., Hill, M.J., Keller, A., Morgan, R.L. (1997), *J. Poly. Sci.: Polym. Phys. Ed.*, **35**, 1775.

Outn, E.L., (1985), *PhD Thesis*, University of Bristol.

Panitch, A., Matsuki, K, Cantor, E.J., Cooper, S.J., Atkines, E.D.T., Fournier, M.J., Mason, T.L., Tirrell, D.A., (1997), *Macromolucles*, **30**, 42.

Pieszek, W., Strobl, G.R., Makahn, K., (1974), *Acta Crystallogr. Sect.*, **B30**, 1278.

Plattner, D.A., Brunner, A., Dobler, M., Müller, H-M., Petter, W., Zbinden, P., Seebach, D., (1993), *Helv. Chim. Acta*, **76**, 2004.

Point, J.J., (1978), *Disc. Farad. Soc.*, **68**, 167.

Point, J.J., (1979), *Macromolecules*, **12**, 770.

Point, J.J., (1979), *Discuss. Faraday Soc.*, **68**, 167.

Point, J.J., Kovacs, A.J., (1980), *Macromolecules*, **13**, 399.

Point, J.J., (1995), *J. Chem. Soc., Faraday Trans.*, **91**, 2565.

Putra, E.G.R., Ungar, G., (2003), *Macromolecules*, **36(11)**, 3812.

Reusch, R.N. and Sadoff, H.L., (1988), *Proc. Natl. Acad. Sci.* USA, **85**, 4176.

Reusch, R.N., (1989), *Proc. Soc. Exp. Biol. Med.*, **191**, 377.

Reusch, R.N., (1992), *FEMS Microbiol. Rev.*, **103**, 119.

Reusch, R.N., Sparrow, A., Gardiner, J., (1992), *Biophys. Biochim. Acta*, **1123,** 33.

Reusch, R.N., Huang, R.P., Bramble, L.L., (1995), *Biophys. J.*, **69**, 754.

Reusch, R.N., (1996), at *Int. Symp. on Bact. PHAs*, Davos, Switzerland.

Revol, J.F, Chanzy, H.D., Deslandes, Y., Marchessault, R.H., (1989), *Polymer*, **30**, 1973.

Riis, V., (1989), *Plaste Katsche*, **36**, 148.

Rosenbaum, G., Holmes, K.C. and Witz, J., (1971), *Nature*, London, **230**, 434.

Rueping, M., Dietrich, A., Bushmann, V., Fritz, M.G., Sauer, M., and Seebach, D., (2001), *Macromolecules*, **34**, 7042.

Ryschenkow, G. and Faivre, G., (1988), *J. Cryst. Growth*, **87**, 221.

Sadler, D.M., (1971), *J. Polym. Sci.: Part A2*, **9**, 779.

Sadler, D.M. and Keller, A., (1976), Polymer, **17**, 37.

Sadler, D.M. and Keller, A., (1977), *Macromolecules*, **10**, 1128.

Sadler, D.M. and Keller, A., (1979), *Science*, **203**, 263.

Sadler, D.M., (1983), *Polymer*, **24**, 1401.

Sadler, D.M. and Gilmer, G.H., (1984), *Polymer*, **25**, 1446.

Sadler, D.M., (1985), *J. Polym. Sci., Polym Phys. Ed.*, **23**, 1533.

Sadler, D.M., (1987a), *Nature*, **326**, 174.

Sadler, D.M., (1987b), *J. Chem. Phys.*, **87**, 1771.

Sadler, D.M., (1987c), *Polymer*, **28**, 1440.

Sadler, D.M. and Gilmer, G.H., (1987), *Polym. Commun.*, **28**, 243.

Sadler, D.M. and Gilmer, G.H., (1988), *Phys. Rev.*, **B38**, 5684.

Sanchez-Cuesta, M., Martinez-Salazar, J., Barker, P.A. and Barham, P.J., (1992), *J. Mater. Sci.*, **27**, 5335.

Sauer, J.A., Morrow, D.R. and Richardson, G.C., (1965), *J. Appl. Phys.*, **36**, 3017.

Seebach, D., Bürger, H.M., Müller, H-M., Lengweiler, U.D., Beck, A.K., Sykes, K.E., Barker, P.A., Barham, P.J., (1994), *Helv. Chim. Acta*, **77**, 1099.

Seebach, D., Brunner, A., Bürger, H.M., Schneider, J., Reusch, R.N., (1994), *Eur. J. Biochem.*, **224**, 317.

Seebach, D., Brunner, A., Bachmann, B.M., Hoffman, T., Küknle, F.N.M., Lengeiler, U.D., (1995), in *"Biopolymer and -oligomers of (R)-3-Hydroxybutyrate Acids – Contributions of Synthetic Organic Chemists"*, Ernst Schering Research Foundation Publishing, 28.

Seebach, D., Brunner, A., Bürger, H.M., Reusch, R.N., Bramble, L.L., (1996), *Helv. Chim., Acta*, **79**, 507.

Seebach, D. and Fritz, G.F., (1999), *Int. J. Biol. Macromol.*, **25**, 217.

Shearer, H.M.M. and Vand, V., (1956), *Acta Crystallogr.*, **9**, 379.

Smith, A.E., (1953), *J. Chem. Phys.*, **21**, 2229.

Song, K., Krimm, S., (1989), *Macromolecules*, **22**, 1504.

Spegt, P., (1970), *Makromol. Chem.*, **139**, 139.

Strocks, K., (1939), *J. Am. Chem. Soc.*, **60**, 1753.

Stryer, L., (1990), *Biochemie*, **3** Auflage, Spectrum der Wissenschaften, Heidelberg.

Sudesh, K., Abe, H., Doi, Y., (2000), *Prog. Polym. Sci.*, **25**, 1503.

Sutton, S.J., Vaughan, A.S., Bassett, D.C., (1996), *Polymer*, **37**, 5735.

Sykes, K.E., (1996), PhD Thesis, *"Crystallization and Degradation of a Biodegradable Plastic – Polyhydroxybutyrate"*, University of Bristol.

Sykes, K.E., McMaster, T.J., Miles, M.J., Barker, P.A., Barham, P.J., Seebach, D., Müller, H-M., Lengweiler, U.D., (1996), *J. Mater. Sci.*, **30**, 623.

Terry, A.E., Hobbs, J.K., Organ, S.J. and Barham, P.J., (2003), *Polymer*, **44**, 3001.

Terry, A.E, Phillips, T.L., Hobbs, J.K., (2003), *Macromolecules*, **36**, 3240.

Till, P.H., (1957), *J. Polym. Sci.*, **24**, 301.

Toda, A., (1991), *Polymer*, **32**, 771.

Toda, A., Keller, A., (1993), *Colloids and Pol. Sci.*, **271**, 328.

Ungar, G., Keller, A., (1979), *Colloid Polym. Sci.*, **257**, 90.

Ungar, G., Stejny, J., Keller, A., Bidd, I., Whiting, M.C., (1985), *Science*, **299**, 386.

Ungar, G., (1986), *Macromolecules*, **19**, 1317.

Ungar, G., Keller, A., (1986), *Polymer*, **27**, 1835.

Ungar, G., Keller, A., (1987), *Polymer*, **28**, 1899.

Ungar, G., Organ, S.J., (1987), *J. Polym. Commun.*, **28**, 232.

Ungar, G., (1988), in *"Integration of Fundamental Polymer Science and Technology"*, Vol 2, Lemstra, P.J., Kleintjens, L.A., Ed., Elsevier Applied Sci., London, pp 342-362.

Ungar, G., Organ, S.J., Keller, A., (1988), *J.Poly. Sci., C: Poly. Letts.*, 258.

Ungar, G. and Organ, S.J., (1990), *J. Polym. Sci.: Polym. Phys. Ed.*, **28**, 2353.

Ungar, G., in *"Polymer Crystallization"*, (1993), Dosiere, M., Ed., NATO ASI Series, Kluwer: Dordrecht, pp 63-72.

Ungar, G., Zeng, X.B., Brooke, G.M., Mohammed, S., (1998), *Macromolecules*, **31**, 1875.

Ungar, G., Zeng, X.B., (1999), *Macromolecules*, **32**, 3543.

Ungar, G., Mandal, P.K., Higgs, P.G., de Silva, D.S.M., Boda, E., Chen, C., (2000), *Phys. Rev. Lett.*, **85**, 4397.

Ungar, G., Putra, E.G.R., (2001), *Macromolecules*, **34**, 5180.

Ungar, G. and Zeng, X., (2001), *Chem. Rev.*, **101**(12), 4157, and references therein.

Waser, P., (2000), PhD Thesis, *"Synthese unterschiedlich markierter Oligomerer der 3-Hydroxybuttersäure mit dem Ziel von Strukturbestimmungen"*, ETH, Switzerland.

Wawkuschewski, A., Cramer, K., Cantow, H.-J., Magonov, S.N., (1995), *Ultramicroscopy*, **58**, 185.

Weeks, J.J., (1963), *J. Res. Nat. Bur. Std.*, **A67**, 441.

Welland, E.L., Stejny, J., Halter, A., Keller, A., (1989), *Polym. Commun.*, **30**, 302.

Winkel, A.K., Hobbs, J.K. and Miles, M.J., (2000), *Polymer*, **41(25)**, 8791.

Winkel, A.K. and Miles, M.J., (2000), *Polymer*, **41(6)**, 2313.

Wittmann, J.C., Lotz, B., (1985), *J. Polym. Sci.: Polym. Phys. Ed.*, **25**, 205.

Wunderlich, B., (1973), *"Macromolecular Physics Volume 1: Crystal Structure, Morphology, Defects"*, Academic Press, New York and London.

Wunderlich, B., (1976), *"Macromolecular Physics Volume 2: Crystal Nucleation, Growth, Annealing"*, Academic Press, New York and London.

Wunderlich, B., Czornyj, G., (1977), *Macromolecules*, **10**, 906.

Yamanobe, T., Sorita, T., Komoto, T., Ando, I., Sato, H., (1985), *J. Mol. Struct.*, **131**, 267.

Yeates, S.G. and Booth, C., (1985), *Makromol. Chem.*, **186**, 2663.

Yokouchi, M., Chatani, Y., Tadokoro, H., Teranishi, K., Tani, H., (1973), *Polymer*, **14**, 267.

Young, R.J. and Lovell, P.A., (1991), *"Introduction to Polymers"*, Chapman and Hall, Second Edition.

Zeng, X.B., Ungar, G., (1998), *Polymer*, **39**, 4523.

Zeng, X.B., Ungar, G., (1999), *Macromolecules*, **32**, 3543.

Zeng, X.B., Ungar, G., Spells, S. J., (2000), *Polymer*, **41**, 8775.

Zeng, X.B., Ungar, G., (2001), *Phys. Rev. Lett.*, **86**, 4875.

Zeng, X.B., Ungar, G., (2001), *Macromolecules*, **34**, 6945.

Zeng, X.B., Ungar, G., (2002), *J. Macromol. Sci. Phys.*, **B41** (4-6): 1305.

Zeng, X.B., Ungar, G., (2003), *Macromolecules*, **36** (13), 4686.

Zerbi, G., Magni, R., Gussoni, M., Moritz, K.H., Bigotto, A., Dirlikov, S., (1981), *J. Chem. Phys.*, **75**, 3175.

Zerbi, G., Piazza, R., Holland-Moritz, K., (1982), *Polymer*, **23**, 1921.

Appendix

List of publications arising directly from this work:

- Li, J., Organ, S.J., Hobbs, J.K., Terry, A.E., Barham, P.J. and Seebach, D., (2004), "Crystallization of Hydroxybutyrate Oligomers: 1. Morphology and folding", *Polymer*, **45**, 8913-8923.

- Organ, S.J., Li, J., Terry, A.E., Hobbs, J.K., Barham, P.J., (2004), "Crystallization of Hydroxybutyrate Oligomers: 2. Growth and thickening of solution grown crystals observed in-situ using synchrotron radiation", *Polymer*, **45**, 8925-8936.

- Li, J., Organ, S.J., Terry, A.E., Hobbs, J.K., Barham, P.J., (2004), "Crystallization of Hydroxybutyrate Oligomers: 3. Unfolding transitions followed in real time using SAXS and WAXS", *Polymer*, **45**, 8937-8947.

- Organ, S.J., Li, J., Terry, A.E., Barham, P.J., (2005), "Morphology and Growth of a Hydroxybutyrate Oligomer with 24 Repeat Units", *Polymer*, by invitation for a special issue dedicated to Professor David Bassett, in press.